

University of Warwick institutional repository: <http://go.warwick.ac.uk/wrap>

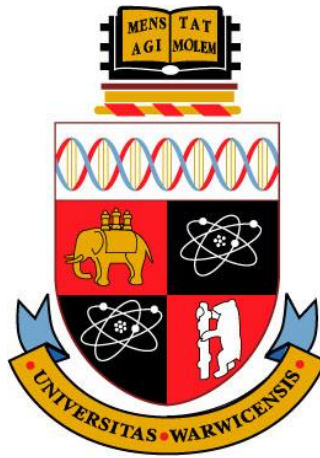
**A Thesis Submitted for the Degree of PhD at the University of Warwick**

<http://go.warwick.ac.uk/wrap/66188>

This thesis is made available online and is protected by original copyright.

Please scroll down to view the document itself.

Please refer to the repository record for this item for information to help you to cite it. Our policy information is available from the repository home page.



# **Continuous Flow Processes for Catalytic Upgrading of Biofeedstocks**

by

**Dorota Danuta Plaza**

A thesis submitted in partial fulfilment of the requirements for the degree of  
Doctor of Philosophy in Engineering

University of Warwick, Department of School of Engineering

October 2014

<b>Contents</b>	
<b>List of Figures</b> .....	<b>v</b>
<b>List of Schemes</b> .....	<b>xii</b>
<b>List of Tables</b> .....	<b>xiv</b>
<b>Acknowledgements</b> .....	<b>xv</b>
<b>Declaration</b> .....	<b>xvi</b>
<b>Abstract</b> .....	<b>xvii</b>
<b>List of Symbols</b> .....	<b>xviii</b>
<b>1 Introduction</b> .....	<b>1</b>
<b>2 Literature Review</b> .....	<b>7</b>
2.1 Flow Chemistry .....	7
2.1.1 Reaction Classification under Flow Conditions	7
2.1.2 Advantages of Continuous Flow Processes	10
2.1.3 Process Intensification	14
2.1.4 Semi-Permeable Membranes	16
2.2 Biofeedstocks .....	18
2.2.1 Biorefinery	18
2.2.2 Biofuels	20
2.2.3 Oleochemistry	22
2.2.4 Secondary Metabolites	24
2.3 Epoxidation of Long-Chain Olefins .....	26
2.4 Sequential Reaction in the Synthesis of Artemisinin to Final API Products under Flow Conditions .....	29
2.4.1 Stoichiometric Reduction of Artemisinin	30
2.4.2 Etherification of Dihydroartemisinin	31
2.5 Olefin Metathesis .....	34
2.5.1 Catalysts	34
2.5.2 Applications of Metathesis	37
2.5.3 Types of Olefin Metathesis	38

<b>3</b>	<b>Experimental .....</b>	<b>46</b>
3.1	Epoxidation of Cocoa Butter .....	46
3.1.1	Materials and Chemicals	46
3.1.2	Procedures of Epoxidation of Cocoa Butter in Batch and Flow Reactors	46
3.1.3	Viscosity	49
3.1.4	Interfacial Tension	49
3.1.5	Analytical Methods	50
3.2	Reduction of Artemisinin .....	61
3.2.1	Materials and Chemicals	61
3.2.2	Reduction of Artemisinin with NaBH <sub>4</sub>	61
3.2.3	Reduction of Artemisinin with LiBHET <sub>3</sub>	61
3.2.4	Flow Synthesis Procedure	62
3.2.5	Reduction of 9-epi Artemisinin	62
3.2.6	Analytical Protocols	63
3.2.1	Mass Spectrometry	66
3.3	Etherification of Dihydroartemisinin to Artemether .....	69
3.3.1	Materials and Chemicals	69
3.3.2	Batch Etherification of Dihydroartemisinin	69
3.3.3	Flow Etherification of Dihydroartemisinin	71
3.3.4	Analytical Protocols	71
3.4	Ethenolysis of Cocoa Butter .....	78
3.4.1	Reagents	78
3.4.2	Batch Reactions	78
3.4.3	Flow Experiments	79
3.4.4	Analytical Methods	81
<b>4</b>	<b>Results and Discussion .....</b>	<b>87</b>
4.1	Epoxidation of Cocoa Butter .....	87
4.1.1	Reaction Calorimetry under Batch Conditions	99
4.2	Determination of Critical Parameters Controlling Epoxidation of Cocoa Butter .....	104
4.3	Reduction of Artemisinin .....	125
4.4	Etherification of Dihydroartemisinin .....	136

4.4.1	Batch Etherification of Dihydroartemisinin	136
4.4.2	Flow Etherification Reaction	141
4.5	Ethenolysis of Cocoa Butter.....	157
4.5.1	Batch Experiments	157
4.5.2	Flow Experiments	158
<b>5</b>	<b>Conclusions and Future Work .....</b>	<b>166</b>
5.1	Epoxidation of Cocoa butter.....	166
5.1.1	Conclusions	166
5.1.2	Future Work	167
5.2	Reduction of Artemisinin .....	167
5.2.1	Conclusions	167
5.2.2	Future Work	168
5.3	Etherification of Dihydroartemisinin .....	168
5.3.1	Conclusions	168
5.3.2	Future Work	169
5.4	Ethenolysis of Cocoa Butter.....	169
5.4.1	Future Work	169
	<b>Appendix.....</b>	<b>170</b>
	<b>References .....</b>	<b>177</b>

## List of Figures

Figure 1-1. Schematic diagram of conversion of biomass into valuable products. Adapted from <sup>5</sup> .....	2
Figure 2-1. Flow patterns observed in capillary channels: (a,b) bubble flow, (c,d) Taylor flow, (e) transitional slug/churn flow, (f) churn flow, (g) film flow (down flow only), (h) annular flow. Adapted from <sup>28</sup> .....	9
Figure 2-2. Hydrodynamics of a segmented flow pattern.....	10
Figure 2-3. Heat and mass distribution recorded during a simulation of neutralisation exothermic reaction HCl and NaOH. Adapted from <sup>44</sup> .....	12
Figure 2-4. Comparison of temperature distribution of a batch reactor and a microreactor with ideal temperature distribution in the process of formation side products. Adapted from <sup>37</sup> .....	13
Figure 2-5. The concept of Process Intensification and its elements. Adapted from <sup>50</sup> . .....	15
Figure 2-6. A scheme of biomass conversion processes, adapted from <sup>66</sup> .....	19
Figure 2-7. Scheme of production process of biofuels from biomass, adapted from <sup>72</sup> . Legend: FAME – fatty acid methyl esters, HVO – hydrotreated vegetable oil, FT – Fisher Tropsch, CNG – compressed natural gas.....	20
Figure 2-8. A scheme of production of valuable chemicals from vegetable oils and fatty acids, adapted from <sup>82</sup> .....	23
Figure 3-1. Survey Raman spectra of cocoa butter (CB), epoxide (EPX), and the ring opening product (ROP) in the region of 400-3200 $\text{cm}^{-1}$ .....	53
Figure 3-2. Raman spectra of cocoa butter (CB), epoxide under batch and flow conditions and diol.....	54
Figure 3-3. Raman spectrum of 30 minutes of epoxidation of cocoa butter. The first step in the normalization spectrum – the determination of the baseline of spectrum.....	56
Figure 3-4. <sup>1</sup> H NMR spectrum of a raw cocoa butter material with proton area integration. The integration area of the signal at 5.36 ppm contains the protons of oleic, palmitoleic and linoleic acid. The concentrations of oleic, palmitoleic and linoleic double bond are 84.1 %, 0.8 % and 15.1 %, respectively, (Table 3-4).....	57

Figure 3-5. <sup>1</sup> H NMR spectrum of epoxide products with proton area integration. The signal of two protons relative to oleic acid is at 2.89 ppm. The signals at 2.96 ppm and 3.09 ppm correspond to CH protons attached to oxirane bond of linoleic epoxide. <sup>1</sup> H NMR spectra of Adogen 464 is shown in Appendix A. 4 and of a ring opening product in Appendix A. 5. ....	58
Figure 3-6. Schematic diagram of a CPA202 reaction calorimeter. Adapted from <sup>157</sup> . ....	60
Figure 3-7. HPLC chromatogram of a raw material used for the reduction of ART. The concentrations of artemisitene was 0.3 % and 9-epi artemisinin was 0.07%. ....	63
Figure 3-8. HPLC chromatogram of standard dihydroartemisinin. ....	64
Figure 3-9. Tandem mass spectrometry: a) separation in space b) separation in time. Adapted from <sup>153b</sup> .....	67
Figure 3-10. HPLC chromatograph of a sample 7 (17.04.13) from the conversion of DHA to ARM in the presence of 0.5 mol eq. of Amberlyst 15 in a batch reactor. The analysis was performed twice separated by an interval of <i>ca.</i> 3 h. Analysis was performed using an ELSD detector. ....	72
Figure 3-11. HPLC chromatograph of conversion of DHA to ARM with Amberlyst 15 in a batch reactor in a 180 min experiment.....	73
Figure 3-12. HPLC chromatograph of conversion of DHA to ARM with Quadrasil SA in a batch reactor in a 180 min of experiment. ....	74
Figure 3-13. HPLC chromatogram of conversion of DHA to ARM with Amberlyst 15 in a microreactor. ....	75
Figure 3-14. HPLC chromatogram of conversion of DHA to ARM with Quadrasil SA in a microreactor. ....	76
Figure 3-15. Schematic diagram of the rig for the membrane permeability experiments. ....	79
Figure 3-16. The schematic diagram of the rig for the metathesis of cocoa butter with ethylene. ....	81
Figure 3-17. <sup>1</sup> H NMR spectrum of the raw cocoa butter material. The spectrum was used to determinate the methodology for the calculation of the results of the reaction. ....	83
Figure 3-18. <sup>1</sup> H NMR spectrum of ethenolysis products with respective assignments of the signals of raw material and products <sup>113g</sup> . ....	85

Figure 4-1. A schematic diagram of reactor configuration for epoxidation of cocoa butter under flow conditions. ....	87
Figure 4-2. A Vapourtec Teflon coil 10 mL reactor. ....	88
Figure 4-3. Evolution of the constant rate of reaction under batch conditions at 80 °C for a reaction mixture diluted with toluene as a function of agitation rate. ....	89
Figure 4-4. Mass balance over a system volume. ....	90
Figure 4-5. Dependence of the space-time-yield to epoxide as a function of residence time (in the flow system) and reaction time (in the batch reactor at 250 rpm)...	93
Figure 4-6. The influence of the ratio of the flow rates of the reactant to the catalyst on the conversion of cocoa butter to epoxide and its selectivity. Residence time was considered from the point of mixing of the two phases to the collection point (total length of tubing was 1388 cm). ....	94
Figure 4-7. Monitoring of reaction progress by Raman spectroscopy: (a) the decrease in 1660 cm <sup>-1</sup> band with the progress of reaction, (b) Comparison of conversion values calculated from Raman and NMR data. ....	95
Figure 4-8. Dependence of conversion and selectivity on the temperature of epoxidation under batch conditions. The conversion and selectivity were calculated to the total concentration of double bond in the raw material. ....	96
Figure 4-9. Effect of catalyst composition on conversion at 80 °C. The reaction numbers correspond to catalyst compositions shown in Table 3-1. ....	97
Figure 4-10. First order kinetic plot for epoxidation of cocoa butter, where CCB0 is the initial concentration of cocoa butter and CCB is the concentration of the cocoa butter in a particular time. Reactions were performed at agitation rates of 600 rpm. ....	98
Figure 4-11. A plot of ln(k) against 1/T is straight line described by Arrhenius equation $\ln k = \ln A - E_a/RT$ , where the coefficient k (s <sup>-1</sup> ) is the rate constant of reaction, the parameter A is the pre-exponential factor and corresponds to the intercept of the line at 1/T = 0 and E <sub>a</sub> is the activation energy and is calculated from the slope of the line (-E <sub>a</sub> /R). ....	98
Figure 4-12. Comparison of reaction selectivity to oleic triglyceride derivative calculated to the total concentration of double bond in the presence and absence of toluene under batch and flow conditions. ....	100

Figure 4-13. Raman spectrum of the epoxide product obtained in a flow reactor at 2.08 h residence time. ....	101
Figure 4-14. NMR spectrum of epoxide product obtained in a flow reactor at 2.08 h residence time. ....	101
Figure 4-15. Checking the decomposition of hydrogen peroxide in a non-reactive system, in which an aqueous mixture of catalyst ( $W^{VI}/P^V/H_2O_2/H_2O$ ) was pumped at a flow rate of $0.063 \text{ mL min}^{-1}$ . ....	103
Figure 4-16. Viscosity of cocoa butter, mixture of cocoa butter with toluene, mixture of cocoa butter, toluene and Adogen 464 and a mixture of catalyst as a function of temperature. ....	106
Figure 4-17. Measurements of interfacial tension for different compositions of the mixtures in different environments at $80 \text{ }^\circ\text{C}$ . Legend: CB =cocoa butter, TL = toluene, SRF = Adogen 464, ‘Cat’ corresponds to the aqueous catalyst solution containing hydrogen peroxide and dissolved tungsten. Each experiment was repeated three times. ....	107
Figure 4-18. Scheme of Taylor flow in Teflon tubing. $k_{La1}$ and $k_{La2}$ show the direction of mass transfer from the aqueous phase to the organic phase where $k_{La1}$ corresponds to mass transfer at the ends of a catalyst slug and $k_{La2}$ corresponds to mass transfer along the aqueous catalyst bubble. ....	114
Figure 4-19. Unit cell of the spherical cap-shape at the end of aqueous bubble with thin film. ....	114
Figure 4-20. Volumetric mass-transfer coefficient as a function of the total linear velocity of two phases in Taylor flow for 1-mm diameter tubing in biphasic epoxidation of cocoa butter. ....	118
Figure 4-21. Starks extraction mechanism <sup>159b</sup> adopted for the phase-transfer-catalysed epoxidation of cocoa butter. The nomenclature was used on the basis of <sup>106b</sup> . ....	119
Figure 4-22. Proposed mechanism of epoxidation in the interfacial region. ....	121
Figure 4-23. Identified by-products in the reduction of ART to DHA. ....	126
Figure 4-24. A schematic diagram of the continuous flow rig for the stoichiometric reduction. ....	128
Figure 4-25. Structure of 9-epi artemisinin and artemisinin. ....	130

Figure 4-26. Chromatogram shows tandem mass spectrometry MS/MS analysis of the ARM- $\beta$ in the product of the reduction of 9-epi-artemisinin. The reaction lasted 20 min.....	131
Figure 4-27. Chromatograms show tandem mass spectrometry MS/MS analysis of 9-epi-artemisinin in: a) the product etherification without a base quenching step, the product was analysed the next day after the reaction was complete b) the standard 9-epi-artemisinin and c) the product of the reduction of 9-epi-artemisinin. The reaction lasted 5 min. The product was analysed on the same day after the reaction was complete.....	132
Figure 4-28. Chromatograms show tandem mass spectrometry MS/MS analysis of DHA. Analysis of: a) the product etherification without a base quenching step, the analysis of the product was performed the next day after the reaction was finished b) the standard DHA sample and c) the product of the reduction of 9-epi-artemisinin. The reaction lasted 5 min. The product was analysed on the same day after the reaction was complete. ....	133
Figure 4-29. Chromatograms show tandem mass spectrometry MS/MS analysis of ARM- $\beta$ in: a) the product etherification without a base quenching step. The analysis of the product was performed the next day after the reaction was complete, b) the standard DHA sample and c) the product of the reduction of 9-epi-artemisinin. The reaction lasted 5 min. The product was analysed on the same day after the reaction was complete. ....	134
Figure 4-30. HPLC chromatogram of the reduction product of 9-epi artemisinin. The mobile phase used for the analysis was acetonitrile/water/ acetic acid in the ratio of 65/35/0.1.....	135
Figure 4-31. Yield of artemether as a function of reaction time during batch etherification catalysed by Amberlyst-15. Amount of catalyst and temperatures are shown. ....	137
Figure 4-32. The dependence of artemether- $\beta$ yield on the concentration of QuadraSil catalyst as a function of reaction time in batch etherification at 40 °C. ....	138
Figure 4-33. First order kinetic plots for QuadraSil and Amberlyst-15 catalysts...	139
Figure 4-34. Blank flow tests of the catalyst beds packed with Amberlyst and QuadraSil, showing leaching of free acid from Amberlyst. ....	140

Figure 4-35. The product of etherification of DHA with Amberlyst 15 after removing solvent a) without a base quench step b) with a base quench step. (Also see, Figure 4-27 - Figure 4-29). .....	141
Figure 4-36. Schematic process flow scheme for conversion of DHA into artemether. ....	142
Figure 4-37. Residence Time Distribution curves obtained in pulse experiments for the different lengths of the packed bed reactor packed by (a) Amberlyst and (b) QuadraSil. ....	144
Figure 4-38. Comparison of simulated reactor performance ( $\beta$ -ARM yield) with experimental results using both, Amberlyst-15 catalyst (a) and QuadraSil catalyst (b) at different flow rates and reactor lengths. ....	147
Figure 4-39. Reactor performance ( $\beta$ -ARM yield) as a function of reactor length ( $L_{R,max} = 8$ cm) at $T = 313$ K. ....	148
Figure 4-40. HPLC analysis of DHA and transformation of DHA $\beta$ into DHA $\alpha$ . .	150
Figure 4-41. The product of conversion DHA to ARM with Amberlyst under batch conditions a) in the presence of THF b) in the presence of TMOF. The reaction times for both reactions are the same. The solvents were removed by a rotovap at 40 °C. Mobile phase: acetonitrile/ water 65/35 (% v/v). Flow rate: 0.8 mL min <sup>-1</sup> . Wavelength: 216 nm. ....	151
Figure 4-42. Blank experiment with DHA, Amberlyst 15 and THF in a batch reactor. The experiment was carried out for 1 hour under stirring conditions. The solvent was removed by a rotavapor at 40°C. The residue was dissolved in pure acetonitrile. Mobile phase: acetonitrile/ water 65/35 (% v/v). Flow rate: 0.8 mL min <sup>-1</sup> . Wavelength: 216 nm. ....	152
Figure 4-43. CML impact scores and CED for the reaction of artemisinin to DHA reduction (vertical axis). Comparison of flow and batch processes and flow process without THF for superhydride. Legend; AP is Acidification Potential, GWP is Climate Change, HTP is Human Toxicity Potential, FAETP is Freshwater Aquatic Ecotoxicity, MAETP is Marine Aquatic Ecotoxicity, TAETP is Terrestrial Ecotoxicity, POCP is Photochemical Oxidation (summer smog), EP is Eutrophication Potential, ADP is Depletion of Abiotic Resources and ODP is Stratospheric Ozone Depletion.....	153
Figure 4-44. Individual processes contributions to CED of artemisinin to DHA reaction in batch and flow conditions. ....	154

Figure 4-45. CML impact scores (vertical axis) and CED for DHA to ARM reaction. Comparison of flow and batch processes. Legend; AP is Acidification Potential, GWP is Climate Change, HTP is Human Toxicity Potential, FAETP is Freshwater Aquatic Ecotoxicity, MAETP is Marine Aquatic Ecotoxicity, TAETP is Terrestrial Ecotoxicity, POCP is Photochemical Oxidation (summer smog), EP is Eutrophication Potential, ADP is Depletion of Abiotic Resources and ODP is Stratospheric Ozone Depletion and CFD is Computer Fluid Dynamic..... 155

Figure 4-46. Individual processes contributions to CED of DHA to ARM reaction in batch and flow conditions. .... 156

Figure 4-47. Dependence of flow rate on pressure for measurements of ethylene permeability for a 112 cm membrane length (used membrane 3). ..... 160

Figure 4-48. The impact the pressure of ethylene in the Tube-in-Tube reactor on the formation of linear alkene products from oleic and linoleic acids in cocoa butter. .... 162

Figure 4-49. Progress of the scaled-up reaction using the parameters from entry 17 in Table 4-9 under flow conditions. .... 164

## List of Schemes

Scheme 2-1. Structure of Teflon AF 2400. ....	16
Scheme 2-2. A chemical structure of cocoa butter. ....	24
Scheme 2-3. The structures of artemisinin related molecules of interest to this study. .....	25
Scheme 2-4. Formation of epoxide from cocoa butter.....	28
Scheme 2-5. A mechanism of epoxidation using Ishii-Venturello system, adapted from <sup>106c</sup> .....	28
Scheme 2-6. A common route to conversion of artemisinin to artemisinin-based APIs. ....	30
Scheme 2-7. A reaction scheme of artemisinin reduction using conventional batch protocol.....	31
Scheme 2-8. A scheme of ARM synthesis and side reactions. Adapted from <sup>17</sup> .....	33
Scheme 2-9. Scheme of olefin metathesis.....	34
Scheme 2-10. Mechanism of metathesis introduced by Chauvin <sup>126</sup> .....	34
Scheme 2-11. A sample structure of a Schrock's molybdenum catalyst. i-Pr – iso propyl, Ph – phenyl.....	35
Scheme 2-12. Structures of the first and second-generation Grubbs and Hoveyda Grubbs catalysts.....	36
Scheme 2-13. Structures of Ru catalyst complexes used in our research. ....	37
Scheme 2-14. Self-metathesis of methyl oleate. <i>Cis-trans</i> isomers were obtained where <i>trans</i> was dominated. ....	38
Scheme 2-15. Dieckmann condensation of diethyl 9-octadene-1,18-dioate ( <b>14</b> ). ....	39
Scheme 2-16. Metathesis of methyl 10-undecenoate.....	39
Scheme 2-17. Cross-metathesis between methyl oleate ( <b>11</b> ) and 3-hexene ( <b>20</b> ).....	40
Scheme 2-18. Cross-metathesis between methyl 10-undecenoate ( <b>17</b> ) and 3-hexene ( <b>20</b> ).....	40
Scheme 2-19. Ethenolysis of methyl oleate ( <b>11</b> ). ....	41
Scheme 2-20. A simplified mechanism of ring-opening metathesis polymerisation.	42
Scheme 2-21. A schematic mechanism of acyclic diene metathesis (ADMET).....	42
Scheme 2-22. Schematic depiction of metathesis of trioleins.....	43
Scheme 2-23. Production of tricaprins from olive oil via ethenolysis and after hydrogenation of the product of ethenolysis.....	44

Scheme 2-24. A scheme of ethenolysis of cocoa butter. Cocoa butter is a mixture of a variety of fatty acids. There are three unsaturated fatty acids. The main constituents are oleic and linoleic acids (see Section 3.1.5. Analytical methods – GC analysis). The scheme also shows potential products formed during the metathesis of cocoa butter. ....	45
Scheme 3-1. Potential products formed during the ethenolysis of cocoa butter. The products obtained from oleic triglyceride were the oleic triglyceride derivative ( <b>34</b> ) and 1-decene ( <b>25</b> ). The potential products obtained from linoleic acids ( <b>33</b> ) might be the oleic triglyceride derivative ( <b>34</b> ) and 1,4-decadiene ( <b>35</b> ) or the linoleic triglyceride derivative ( <b>36</b> ) and 1-heptene ( <b>37</b> ). ....	84
Scheme 4-1. Degradation product of DHA <sup>17</sup> .....	149

## List of Tables

Table 3-1. Molar equivalents of the catalyst components used in the epoxidation of cocoa butter. The equivalents of reagents were recalculated on the average number of moles of double bonds in cocoa butter. The average number of moles in 1 mole of cocoa butter (866.67 g) is 1.15 mol. This value was determined on the basis of the FAME analysis (Table 3-4). .....	47
Table 3-2. Composition of reagents used in the epoxidation of cocoa butter under batch and flow conditions. ....	48
Table 3-3. Raman bands for cocoa butter, epoxide and diol. ....	54
Table 3-4. GC analysis of fatty acid methyl ester. ....	59
Table 3-5. TQD parameters for MS/MS experiments. ....	66
Table 3-6. Impact categories of CML method implemented in this study. ....	77
Table 3-7. Ethenolysis results calculated on the base of the data shown in Figure 3-17 and Figure 3-18. ....	86
Table 4-1. Contributions to Sugden's parachor for cocoa butter. ....	108
Table 4-2. Composition of catalyst used during the epoxidation of cocoa butter. ....	109
Table 4-3. Values of capillary number obtained from the Sugden equation, literature estimation and the experimental data of interfacial tension. ....	110
Table 4-4. A summary of results of reduction of artemisinin under batch reaction conditions. ....	126
Table 4-5. A summary of results of reduction of artemisinin under flow conditions. ....	129
Table 4-6. Hydrodynamic parameters calculated from the experimental RTD curves for the packed bed reactors of different lengths packed with Amberlyst and QuadrasSil catalysts. ....	144
Table 4-7. Optimization of ethenolysis in a batch reactor. ....	158
Table 4-8. Results of permeability (in cB) for nitrogen and ethylene for different lengths of new and used membranes. ....	161
Table 4-9. A summary of results on ethenolysis in a Tube-in-Tube reactor. ....	164

## **Acknowledgements**

I would like to express my very great appreciation to Prof. Alexei Lapkin, my research supervisor, for allowing me to work on this project, for his guidance and support throughout this research and for his patience in reading draft after draft of this thesis. I am also sincerely thankful to Prof. André van Veen, my second research supervisor, for his useful and constructive recommendations about the interpretation of some of the results of this thesis.

I am grateful to Dr Andrew Clark, Prof. Lasse Greiner and Prof. Steven Nolan for allowing me to perform some experiments in their laboratories and for their valuable support.

My thanks are also extended to Dr John Suberu for helping with my HPLC and MS/MS analysis, Drs. Victor Sans Sangorrin, Xiaolei Fan and Konstantin Lophonov for introducing me to continuous flow protocol, Dr Aneta Pashkova for assisting with reaction calorimetry, Dr Tom Skelhom for his help with measurements of interfacial tension using a Drop Shaper Analyser, Mr Simone Manzini for introducing me to the metathesis process and the Andrew Clark group for introducing me to the epoxidation process.

I am also grateful to the University of Warwick for sponsoring my PhD study. The research leading to these results has received funding from the European Community's Seventh Framework Programme for SYNFLOW under grant agreement n° FP7-NMP-LARGE-3-2009-246461.

Also, I am grateful to my wonderful Warwick friends, especially Drs. Helena Stec, Polina Yaseneva and Ms Claudia Houben, for providing an exciting and enjoyable research life.

Finally I would like to thank my parents and siblings for their unconditional support in my education and my partner Grzegorz for being with me unconditionally, despite the fact that 200 miles separated us from each other. To them I dedicate this thesis.

## Declaration

This thesis is submitted to the University of Warwick in support of my application for the degree of Doctor of Philosophy. It has been composed by myself and has not been submitted in any previous application for any degree.

List of data provided and/or analysis carried out by collaborators and other group members:

- The experimental part of the metathesis of cocoa butter under flow conditions was performed in the University of Cambridge by a master student Ms Christiane Schotten from RWTH Aachen University.
- The life cycle assessment of conversion of artemisinin to artemether was carried out by Dr Polina Yaseneva.
- Simplified design of packed-bed continuous flow reactor was done by Dr Xiaolei Fan.
- Residence time measurements and calculations were done by Dr Konstantin Loponov.
- The flow protocol for reduction artemisinin with  $\text{LiBHET}_3$  was elaborated from the original work by Dr Xiaolei Fan and Dr Victor Sans.

List of publications including submitted papers:

- X. Fan, V. Sans, P. Yaseneva, D. Plaza, J. Williams, A. Lapkin. Facile Stoichiometric Reductions in Flow: An Example of Artemisinin. *Organic Process Research & Development* 2012 16 (5), 1039-1042
- P. Yaseneva, D. Plaza, X Fan, K Loponov, A. Lapkin. Synthesis of the antimalarial API artemether in a flow reactor. *Catalyst Today*. (accepted)
- C. Schotten, D. Plaza, S. Nolan, S. Ley, D. Browne, A. Lapkin. Valorisation of food waste: continuous metathesis of cocoa butter triglyceride. (manuscript)

## Abstract

This thesis is dedicated to continuous flow processes for the catalytic transformation of biofeedstocks into fine and speciality chemicals. Four processes, namely epoxidation and ethenolysis of a bio-waste triglyceride, reduction of artemisinin and etherification of dihydroartemisinin were developed under batch and flow conditions.

First, an epoxidation reaction was studied using a modified  $W^{VI}/P^V/H_2O_2/PTC$  catalyst complex. The reaction proceeded with high selectivity to oleic epoxide (86 %) and high conversion (100 %) towards the epoxidation reaction in both, batch and flow systems. The enthalpy of epoxidation of cocoa butter was found to be mildly exothermic at  $-168 \text{ kJ mol}^{-1}$ . Space time yield, a key process parameter, in both the systems were similar. The epoxidation of cocoa butter was controlled under both batch and flow conditions by mass transfer and chemical reaction.

Second, the ethenolysis of cocoa butter under batch conditions was optimised in terms of catalyst, solvent, temperature and pressure. The M11 catalyst proved to be the most active at room temperature and 2 bar ethylene pressure in THF solvent. The optimized system was transferred to a continuous membrane contactor system. A high yield of decene and 1,4-decadiene were achieved, 44.5 % in total, for a residence time of 59 min at 40 °C and ethylene pressure of 6 bar.

Third, the stoichiometric reduction of artemisinin to dihydroartemisinin (DHA) was successfully transferred from batch to continuous flow conditions with a significant increase in productivity and an increase in selectivity. A DHA space-time-yield of up to  $1.6 \text{ kg h}^{-1} \text{ L}^{-1}$  was attained, which represented a 42-fold increase in throughput compared to the conventional batch process.

Finally, a highly active heterogeneous catalyst was found for the etherification of dihydroartemisinin to a pharmaceutical API artemether. Using the QuadraSil catalyst allowed us to eliminate one step in the reaction workup. A comparative Life Cycle Assessment of both reduction and etherification reactions showed advantages of the flow process over the optimized literature batch protocols. The results of the LCA highlight the significance of solvents in pharmaceutical manufacture and the advantage of flow technology, enabling small solvent inventories to be used.

## List of Symbols

### Notation

A	surface area, $\text{m}^2$ ; pre-exponential factor
a	interfacial area, $\text{m}^{-1}$
C	concentration, $\text{mol dm}^{-3}$
D	diffusivity, $\text{m}^2 \text{s}^{-1}$
$E_a$	activation energy, $\text{J mol}^{-1}$
F	volumetric flow-rate, $\text{m}^3 \text{h}^{-1}$
G	molar generation rate of a species, $\text{mol h}^{-1}$
g	gravitational constant, $\text{m s}^{-2}$
H	enthalpy of reaction, $\text{kJ mol}^{-1}$
L	length, m
k	rate constant, $\text{s}^{-1}$
$k_L$	mass transfer coefficient, $\text{m s}^{-1}$
p	pressure, bar
R	gas constant, $\text{J K}^{-1} \text{mol}^{-1}$
r	reaction rate, $\text{mol m}^{-3} \text{s}^{-1}$
STY	space time yield, $\text{mol h}^{-1} \text{m}^{-3}$ , $\text{kg L}^{-1} \text{h}^{-1}$ , $\text{mol L}^{-1} \text{min}^{-1}$
T	temperature, K, $^{\circ}\text{C}$
t	time, s
V	volume, $\text{m}^3$
u	linear velocity, $\text{m s}^{-1}$
X	conversion, %
Y	yield, %

### Greek letters

$\gamma$	interfacial tension, $\text{N m}^{-1}$
$\delta$	film thickness, m; chemical shift, ppm, deformation frequency
$\varepsilon$	holdup, dimensionless
$\mu$	viscosity, Pa s
$\eta$	viscosity, Pa s
$\rho$	density, $\text{kg m}^{-3}$
$\sigma$	surface tension, $\text{N m}^{-1}$

$\tau$	twisting frequency
$\tau$	residence time, min
$\nu$	stretching frequency
$\phi$	dimensionless association factor
$\phi$	internal residence time distribution
$\Phi$	internal cumulative residence time distribution
$\lambda$	heat conductivity, $\text{W m}^{-2} \text{K}^{-1}$

#### Dimensionless groups

Ca	Capillary number
Ha	Hatta number
Pe	Peclet number
Re	Reynolds number
Sh	Sherwood number

#### Subscription

<i>A. annua</i>	<i>Artemisia annua</i>
ACTs	artemisinin combination therapies
ADMET	acyclic diene metathesis
AF	amorphous fluoropolymer
API	active pharmaceutical ingredient
ARM	artemether
ART	artemisinin
as	antisymmetric
Cat.	catalyst
CB	cocoa butter
CED	cumulative energy demand
CFD	computer fluid dynamics
CML	Centre of Environment Science
CNG	compressed natural gas
DB	double bond
DIBAL-H	diisobutylaluminium hydride
DHA	dihydroartemisinin

DRIEM	deep reaction etching method
DSA	drop shaper analyser
EPX	epoxide
ES	epoxidizing species $\{\text{PO}_4[\text{WO}(\text{O}_2)_2]_4\}^{3-}$
FA	fatty acid
FAME	fatty acid methyl esters,
FT	Fisher Tropsch
GC	gel chromatography
HDTMAB	hexadecyltrimethylammonium bromide
HPLC	high-performance liquid chromatography
HVO	hydrotreated vegetable oil
ID	internal diameter
LCA	life cycle assessment
LCI	life cycle inventory
LIF	laser induced fluorescence
MRM	multiple reaction-monitoring
NHC	<i>N</i> -heterocyclic carbene
NMR	nuclear magnetic resonance spectroscopy
OD	optical densities
PDMS	polydimethylsiloxane
PMMA	poly(methyl methacrylate)
PTC	phase transfer catalyst
PTFE	polytetrafluoroethylene
PTSA	para-toluenesulfonic acid
QX	quatarnary ammonium salt
r	rock frequency
ROP	ring opening product
ROMP	ring-opening metathesis polymerisation
rpm	revolution per minute
RTD	residence time distribution
s	symmetric
SA	sulphonic acid
t	trans

THF	tetrahydrofuran
TLC	thin layer chromatography
TQD	tandem quadrupole detector
TP	two-phase
WHO	World Health Organization

### 1 Introduction

Biomass is an alternative source of feedstocks for the chemical industry to fossil petrochemicals. Replacing fossil petrochemical feedstocks is important due to their predicted limited future availability, increasingly fluctuating price, negative contribution to climate change, and complex political situation in many regions that hold major reserves of oil and gas <sup>1</sup>.

Using biomass in production of chemicals leads to a reduction in the release of technogenic CO<sub>2</sub>, thus leading to more sustainable products and processes <sup>2</sup> in comparison to fossil petrochemicals-based manufacture. Natural raw materials, comprising different chemical compounds, such as fatty acids, sterols, alkaloids, flavonoids, glycosides, *etc* <sup>3</sup> find applications in manufacture of fine and speciality chemicals. These two sectors have some common approaches and significant differences.

Fine chemicals are complex building blocks obtained in limited quantities at relatively high cost, typically in multipurpose plants by chemical and biotechnological processes. Fine chemicals are defined in terms of their molecular properties. Thus, their chemical composition is important as we can see in the case of pharmaceuticals, pigments, agrochemicals, flavours and fragrances, electronics, and photographic film. The well-defined purity of compounds is a top priority in their production. Therefore, the development of chemical processes at each step of manufacture is very important <sup>4</sup>.

Speciality chemicals are manufactured from basic raw materials. On the other hand, they are defined in terms of their effect or performance on other chemical sectors. They are used in order to improve the manufacturing process or as finishing touches to provide required properties for a product. Examples of speciality chemicals include adhesives, cleaning materials, surfactants, cosmetic additives, industrial gaseous lubricants, polymers, elastomers, construction chemicals, flavours and textile auxiliaries <sup>4</sup>.

The production of fine and speciality chemicals from biofeedstocks is considered to be part of biorefining, see Figure 1-1 and the chapter on biofeedstocks (Section 2.2. Biofeedstocks). Biorefinery is a relatively new concept, in contrast to traditional petrochemical refining that has been developed over many decades. The principle difference between a biorefinery and a refinery is the chemical composition of the raw materials. Fossil feedstocks are a mixture of hydrocarbons with a lack of functional groups and are easily separated by distillation, after which the larger molecules undergo catalytic cracking to convert them into smaller compounds that are then used in the production of fuels and chemicals. Biofeedstocks are complex mixtures of highly functionalised compounds, typically with high oxygen content. Hence, biorefinery processes are more complex in comparison to the standard refinery industry. To make those processes efficient requires a combination of biological and chemical processes.

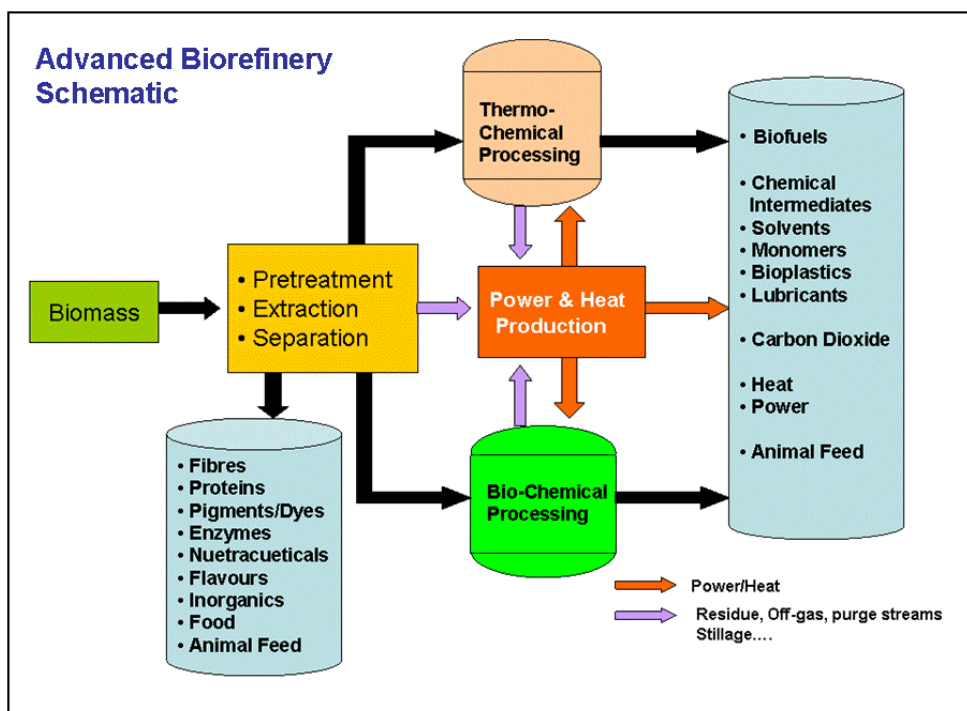


Figure 1-1. Schematic diagram of conversion of biomass into valuable products.

Adapted from <sup>5</sup>.

Thermo-chemical processes are the second route to obtain bio-chemicals in a biorefinery. There are three major thermo-processes such as gasification, pyrolysis

and combustion, which differ from each other by an amount of oxygen used during conversion of biofeedstock into primary products; heat and power. Gasification products; carbon monoxide and hydrogen are converted in Fisher Tropsh synthesis into a combination of linear hydrocarbons with a different number of carbons in chains;  $n\text{CO} + 2n\text{H}_2 \rightarrow n(\text{CH}_2) + n\text{H}_2\text{O}$ , which are used for the production of platform chemicals <sup>5</sup>.

Manufacturing processes involved in producing bio-based molecules from natural plants face a number of significant challenges. First, the price of biomass used in large scale production is not always cheaper than that of fossil petrochemical feedstocks due to the high cost of transporting biomass to the production plants <sup>6</sup>. The manufacture of bio-chemicals is also often in competition with food in terms of land use <sup>7</sup>.

Second, many biorefinery processes such as harvesting, extraction, purification and conversion are still in the early stages of development. They are not integrated in a continuous sequence as in the case of a conventional refinery.

Third, a significant challenge to chemical conversion of bio-based molecules is their variability in composition and content of oxygen and trace elements. There can be significant variability in the concentrations of target compounds due to local growth conditions, variations in climatic conditions and the age of the plant <sup>8</sup>. This variability makes it impossible to rely on standard protocols in the production process. Biofeedstocks require more effort in pre-treatment and purification processes, especially in the case of fine chemicals where purity is a major requirement.

Biofeedstocks also contain higher levels of oxygen (10–40%) than the petroleum hydrocarbons (0%) for which most conventional petrochemical processes were optimised. Biomass also contains alkali metals, which are known poisons for many heterogeneous catalytic processes in a refinery. Thus, commercially available refinery technologies are unsuitable for conversion of biofeedstocks into chemicals. Hence, bio-renewable feedstocks need to be pre-treated to remove oxygen

(reduction), water and alkali metals<sup>9</sup>. This variability in their composition makes biochemical processes difficult to scale up to industrial-level production.

The manufacture of fine and speciality chemicals is currently predominantly performed using batch technology, in which poor mixing and heat transfer are the main problems. Alternative technology may provide some solutions: intensive continuous chemical technologies allow flexibility in production scale and a significant gain in efficiency (space-time-yield) in comparison with batch technology, traditionally used in chemical processes within the speciality chemicals industry. Hence, new research on conversion of bio-based molecules using intensified flow technology is needed to make biorefineries competitive in the marketplace.

In this project four reactions of bio-based molecules are developed under continuous flow conditions: epoxidation of cocoa butter, metathesis of cocoa butter, reduction of dihydroartemisinin and etherification of dihydroartemisinin. Cocoa butter was sourced as a waste product of chocolate production. This kind of pure triglyceride including mainly one double bond may be of interest for the production of activated molecules such as epoxides, which in subsequent reactions are used to produce speciality chemicals such as polymers, emulsifiers and lubricants, and 1-decene, which is used as a co-monomer in certain copolymers<sup>10</sup> and as an intermediate in the production of epoxides, amines, oxo alcohols, synthetic fatty acids, synthetic lubricants, and alkylated aromatics<sup>11</sup>.

Artemisinin is a secondary metabolite and is extracted from *Artemisia annua* L. Currently, *A. annua* L. is the main commercially economical source of artemisinin<sup>12</sup>. Derivatives of artemisinin such as dihydroartemisinin and artemether are used in the treatment of malaria due to their high antiparasmodial effectiveness and low toxicity<sup>13</sup>.

The main goal of these four sub-projects was to demonstrate a step-change technology (flow technology) of the transformation of these bio-based molecules into fine and speciality chemicals in order to obtain a significant improvement in

productivity and selectivity, flexibility in production scale and safety, and also to demonstrate redundancy of work-up steps in the case of flow processes.

Batch syntheses of fatty epoxides are widely reported<sup>14</sup>. However, epoxidation of triglycerides rather than free fatty acids under flow conditions is sparsely reported in the literature<sup>15</sup>. The flow technology was used in the case of the epoxidation of cocoa butter with hydrogen peroxide catalysed by a modified Ishii-Venturello catalyst to reduce the mass transfer limitations and improve safety. Factors such as mass transfer, which occurs due to high viscosity of the cocoa butter mixture, and a significant safety hazard are the major drawbacks in scaling-up batch processes.

Unfortunately, the epoxidation in a flow reactor did not show any improvement in terms of productivity, due to the specific surface area being too small and due to coalescence of the slugs leading to further reduction in mass transfer area. However, the flow process improves safety. Around 100% selectivity to oleic and linoleic epoxides was obtained in both flow and batch processes. The attempt to determine the critical parameters controlling the epoxidation of cocoa butter in the Taylor flow system demonstrated the lack of literature regarding immiscible liquid-liquid phase transfer catalytic reactions in a microreactor, as opposed to gas-liquid-solid investigations.

The ethenolysis of triglycerides over M11 catalysts has not been reported in the literature. Our group was the first to perform this reaction. The biphasic ethenolysis of bio-waste triglyceride under flow condition was made possible using a continuous membrane contractor. This system enabled a 258-fold productivity to be achieved compared to the batch reactor. This system also improved the process safety. Ethylene is highly flammable and explosive and is often avoided in large-scale batch reactions.

In this study we developed the first sequential flow synthesis of an important medicinal small molecule of biological origin, in which a number of the problems had to be resolved. In the reduction of artemisinin,  $\text{NaBH}_4$  was replaced by  $\text{LiBHEt}_3$  which demonstrated good dissolution in 2-methyl-tetrahydrofuran. Thus, it enabled

the reaction to be performed under flow conditions. THF was also replaced by 2-MeTFH, which is a cleaner bio-derived solvent <sup>16</sup>.

In the case of the reduction of artemisinin under flow conditions, safety, productivity and selectivity were improved compared to the batch system. The DHA space-time-yield showed a 42-fold increase in throughput. The reduction under batch conditions was performed at low temperatures of around 0-4°C. The flow reactor enabled this reaction to be performed at room temperature, which leads to better energy efficiency.

In the literature, the catalytic etherification performed with inorganic acids, such as HCl <sup>17</sup>, or with acidic resins, such as Amberlyst-15 <sup>18</sup>, under batch conditions were reported. In this system, downstream neutralisation with a base was required, followed by separation of the product from the base solution.

In our research, a highly active heterogeneous catalyst was found for the etherification of dihydroartemisinin to a pharmaceutical API artemether. Using the QuadraSil catalyst allowed us to eliminate one step in the reaction workup. The flow system also allowed us to eliminate the separation catalyst from products. Moreover, the productivity was 46-fold higher in a 4 cm length packed-bed reactor.

## 2 Literature Review

### 2.1 Flow Chemistry

Flow chemistry is not a new concept in the chemical industry. Continuous chemical processes are widely used on a large scale in the petrochemical industry starting from crude oil heating, hydrotreating, cracking, refining and further reactions of bulk products. Continuous processes are used in the case of production of ammonia and sulphuric acid<sup>19</sup>. Flow chemistry is a smaller-scale technology in flow equipment that has become highly popular in synthetic chemistry applied in the synthesis of speciality and fine chemicals, pharmaceutical intermediates, active ingredients in agrochemicals and pharmaceuticals, surfactants *etc.* Continuous processes demonstrate significant benefits over traditional batch or fed-batch technologies in complex syntheses. The processes of interest to this project include multi-phase liquid-liquid and liquid-solid reactions. The review below thus concentrates on multiphase reactor technology for flow chemistry applications.

#### 2.1.1 Reaction Classification under Flow Conditions

Roberge<sup>20</sup> divided reactions in the fine chemicals and pharmaceutical industry into three groups, depending on their physicochemical properties in terms of kinetics and phases (solid, liquid and gas). In their next paper, Roberge *et al.*<sup>21</sup> performed analysis of these reactions in the context of continuous processes. They provided the following classification:

Type A are very fast reactions, with reaction half-lives less than 1 s. They are controlled by mixing. Microreactors allow improving yields of reactions by rapid mixing of reagents and better heat-exchange performance. The reactions of type A involve chlorine, bromine, acyl chlorides and organometallic species. Type B reactions are also fast, between 1 s and 20 min. However, mixing does not play major role in obtaining better yields. These reactions are predominantly kinetically controlled. Thus, the reaction is precisely controlled by residence time and temperature in order to obtain better yields.

Type C reactions are slow (>20 min), and would suit a batch process. However, continuous processes can be beneficial in terms of safety and quality advantages, especially for reactions in which heat is accumulated under batch

conditions. Process intensification in order to improve efficiency is required for these reactions<sup>21-22</sup>.

The second classification of reactions under a flow system can be made in the context of a number of phases in the flow microchannel such as single phase-flow and multiphase flow. Multi-phase processes – for example gas-liquid, liquid-liquid, solid-liquid and a combination of them – are performed under flow conditions in order to help overcome challenges in obtaining better contact between different phases<sup>23</sup>. Reactions with solid compounds are difficult to perform under flow conditions due to blocking of microchannels<sup>22</sup>. Packed-bed microreactors are designed to overcome this problem. Examples of reactions in a catalytic-bed reactor are described in<sup>19,24</sup>.

Different flow patterns are formed in the case of two immiscible phases in microchannels. These patterns depend on physical properties of the fluids used, and on operating parameters such as flow rate of the two immiscible phases, mixing elements geometry, microchannel geometry and its dimensions<sup>25</sup>. A larger number of studies had been performed to understand gas-liquid flow patterns<sup>26</sup> compared to the liquid-liquid flow regimes<sup>27</sup>.

Five main "representative patterns" are observed in the case of the gas–liquid flow in microchannels, as reported in Kreutzer *et al.* (Figure 2-1)<sup>26d,28</sup>.

- 1) Film flow is characterised by low fluid superficial velocities in the range of a few  $\text{mm s}^{-1}$ . It is possible that the fluid flows downwards on the walls of the channel and the gas flows through the core of the channel.
- 2) Bubble flow is described as non-wetting gas small bubbles drifting in a continuous wetting liquid.
- 3) Churn flow is characterised by the chaotic flow pattern, which appears at high velocity of liquid. Small bubbles attached to the rear of the slug are aerated<sup>29</sup>.
- 4) Annular flow appears at high velocities and low liquid fraction. The wavy liquid flows along the wall with dispersed gas and enters the liquid in the centre<sup>26d</sup>.

- 5) Taylor flow is also known as segmented flow, bubble train flow, slug flow, plug flow or intermitted flow. This pattern is characterised by reproducible long gas bubbles that occupy the cross-section of channel. The lengths of slugs are determined by inlet conditions. This pattern shows a high degree of control over the slugs' length distribution <sup>27b</sup>.

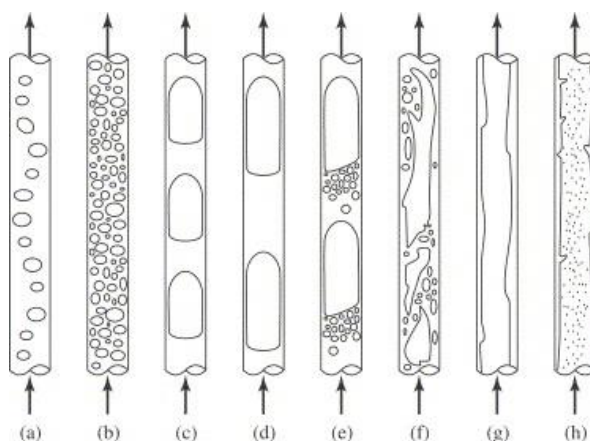


Figure 2-1. Flow patterns observed in capillary channels: (a,b) bubble flow, (c,d) Taylor flow, (e) transitional slug/churn flow, (f) churn flow, (g) film flow (down flow only), (h) annular flow. Adapted from <sup>28</sup>

A Taylor flow pattern of two immiscible phases is generated in microchannels by "T" or "Y" mixing elements (Figure 2-2). This pattern is characterised by stability, reproducibility and high interfacial area. Internal circulation occurs inside of slugs. Internal circulation inside each slug is due to a shearing motion in laminar flow in the microchannel combined with the liquid interface. This fluid motion improves mixing inside each slug as well as enhancing the rate of diffusion of reagents across an aqueous-organic interface by shearing perturbation of concentration gradient inside each slug <sup>30</sup>. Hydrodynamic studies of liquid-liquid slug flows in a microchannel by using the laser induced fluorescence (LIF) methodology and computer fluid dynamics (CFD) simulation was done by Ghaini *et al.* <sup>31</sup>.

This type of flow pattern provides the advantage that the mass transfer occurs as a result of two mechanisms: a) diffusion due to the concentration gradient between adjacent slugs, and b) convection due to internal circulation in each slug <sup>32</sup>.

Concentration of a reactant in the bulk of a segment is not constant due to the presence of recirculation and stagnant zones <sup>32a</sup>.

Nitration <sup>33</sup>, extraction <sup>34</sup> and the Wittig reaction <sup>27b</sup> are examples of liquid-liquid reactions in a microchannel reactor, described in the open literature. A reaction in a biphasic liquid-liquid system may be accelerated by a phase-transfer catalyst (PTC). A small amount of PTC agent transfers reagent from one phase across the interface between two immiscible aqueous-organic phases <sup>27b, 35</sup>.

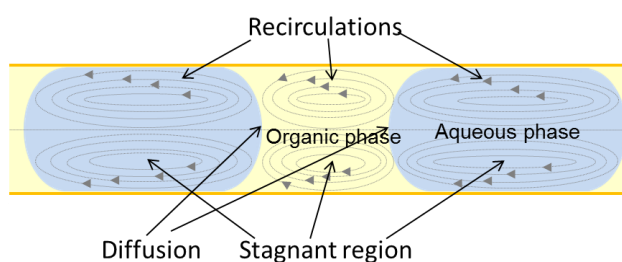


Figure 2-2. Hydrodynamics of a segmented flow pattern.

In this work, catalytic phase-transfer epoxidation of cocoa butter using a quaternary ammonium salt as the phase-transfer agent was performed in a biphasic system in a microreactor.

### 2.1.2 Advantages of Continuous Flow Processes

Flow chemistry reactions and processes occur in micro- and compact reactors. They typically consist of a series of small-diameter channels (50-5000  $\mu\text{m}$ ), where reagents are introduced by pumps. Reactors are produced from glass <sup>36</sup>, metal <sup>37</sup>, silicon <sup>38</sup>, polymers <sup>39</sup> or ceramics <sup>40</sup>. Each of these materials has benefits and drawbacks with respect to price, compatibility with reagents or heat conductivity. Metal reactors are resistant to high temperature and pressure, but are not compatible with strong acids, unless using expensive alloys <sup>41</sup>. Ceramic microreactors are able to withstand high temperatures and are chemically inert <sup>23</sup>. Polymer reactors from poly(dimethylsiloxane) are easy to fabricate but they dissolve and swell in common organic solvents <sup>39a, 39c</sup>. Fluoropolymer-integrated microstructures are chemically inert, but may have limitations to moderate pressures and temperatures <sup>39d, e</sup>. Glass reactors show better properties compared with fluoropolymer devices, and they are

applied to most organic syntheses<sup>36b</sup>. A typical fabrication of a glass device is described in<sup>36a</sup>. Silicon-based devices are manufactured using photolithography, wet etching, and deep reaction etching (DRIEM) methods. These reactors can be used at high temperature and pressure, but may also have limited chemical stability, especially in the presence of strong bases<sup>23</sup>.

Generally, using microreactors allows processes to be more efficient in terms of a higher throughput per unit volume and per unit of time. Substrates are introduced continually into miniaturised channels and products are also removed continuously<sup>19, 42</sup>. Specific surface areas in microstructured reactors are much higher, between  $10,000 \text{ m}^2 \text{ m}^{-3}$  and  $50,000 \text{ m}^2 \text{ m}^{-3}$ , than in batch reactors, where the specific surface area is around  $100 \text{ m}^2 \text{ m}^{-3}$ <sup>41</sup>. This leads to better control of mass and heat transfer<sup>43</sup>. To illustrate, Figure 2-3 shows results of a simulation of a neutralisation reaction between hydrogen chloride and sodium hydroxide. It can be observed that the cooling system works more efficiently under flow conditions as a result of a smaller diameter of the channel, resulting in higher heat transfer area. In the case of the  $5\text{-m}^3$  batch reactor under stirred conditions at 500 rpm (Figure 2-3), distribution of cooling temperature is much worse. Cooling occurs just around the surface of the reactor wall. There is a significant temperature gradient from the reactor wall to its centre<sup>44</sup>.

Feasibility of precise control of temperature is important in the case of exothermic reactions that have a risk of thermal runaway and explosion. The yield and the rate of slow reactions can also be enhanced by increasing temperature of the process. Similarly, high surface area to volume ratio under flow conditions enables better mixing of reagents, see Figure 2-3<sup>44</sup>.

The process of mixing in laminar flow microreactors occurs by the principle of diffusion, whereas, in a conventional batch reactor, mixing is by rigorous stirring<sup>41</sup>. It is also worth remembering the general conclusions from residence time distribution theory, that flow reactors necessarily give higher space time yields (for positive reaction orders) compared to stirred tank reactors due to the nature of the corresponding residence time distributions<sup>45</sup>.

The flow regime in microreactors is always laminar, unless specific mixing elements are introduced<sup>23</sup>. Their Reynolds numbers are in the range of 1 to 1000 and depend on velocity and channel dimensions<sup>41</sup>. Due to good control over flow regime, reactions are generally more stable under flow conditions and therefore reproducible. Once again, this gives a much higher product yield than in a batch reactor, see Figure 2-4.

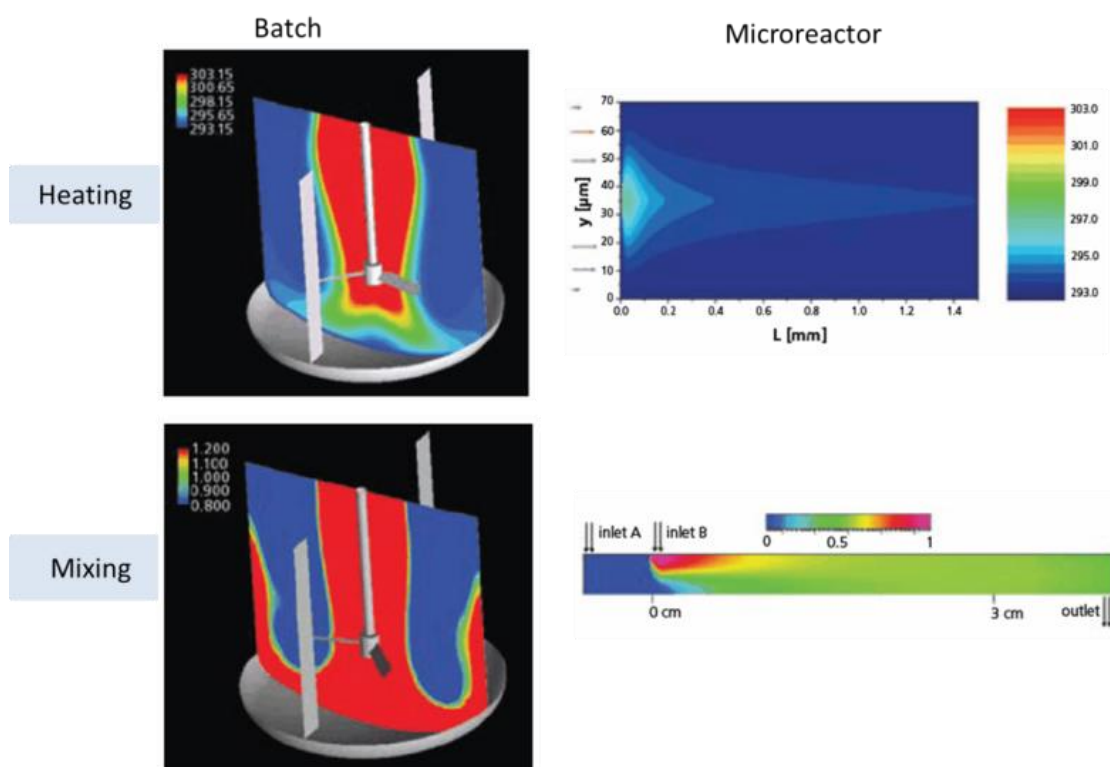


Figure 2-3. Heat and mass distribution recorded during a simulation of neutralisation exothermic reaction HCl and NaOH. Adapted from<sup>44</sup>.

Furthermore, in Figure 2-4 a comparison is shown of temperature distributions in a stirred tank reactor and a microreactor under kinetic control of reactions in the process of a by-product formation. The temperature distribution in the batch reactor is wider than in the case of the microreactor. This broad temperature distribution impacts on formation of side products. Temperature distribution in a microreactor is more convergent with ideal temperature distribution<sup>37, 46</sup>. An example of a reaction in which an improvement in temperature control has an impact on reaction yield is presented in<sup>37</sup> involving nitration of naphthalene.

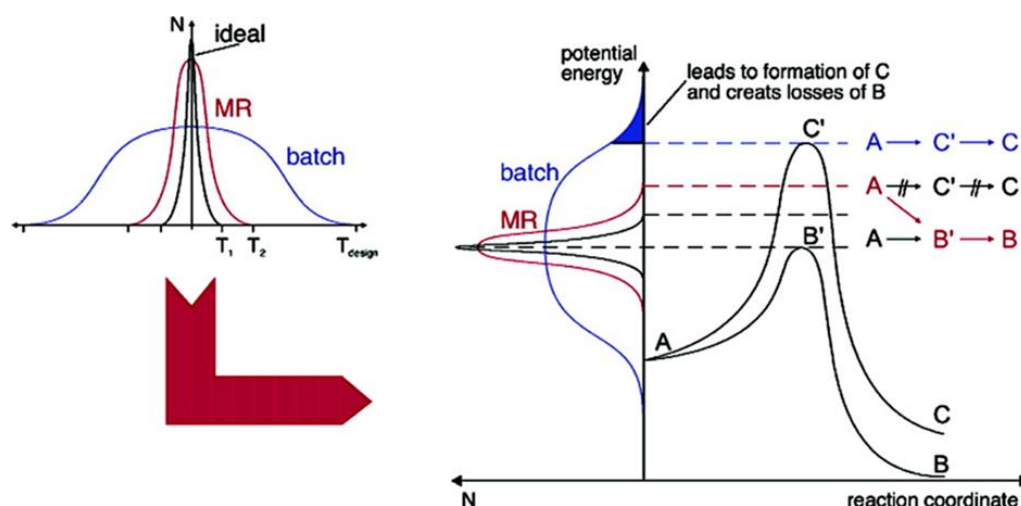


Figure 2-4. Comparison of temperature distribution of a batch reactor and a microreactor with ideal temperature distribution in the process of formation side products. Adapted from <sup>37</sup>.

An example of an application of a microreactor in which precise control of temperature and concentration is critical is in heterogeneous catalytic gas-phase reactions. A microreactor in such a system allows an improvement in selectivity and yield. Active sites of catalysts are more efficiently used and, as a result of this, the amount of catalyst required for the same application can be reduced. In addition, the catalysts' lifetime may be increased as a result of better optimisation of reaction conditions such as mixing and concentration of reagents. This can prevent catalyst poisoning. Inert gases can be used in lower amounts in the case of explosive gas mixtures. Small quantities of reactants are introduced into the microchannel and, therefore, small amount of heat is generated. The high surface area-to-volume ratio with the small dimension of a reactor enables better cooling than in the stirred tank reactor <sup>47</sup>.

Reactions involving highly toxic substances can be carried out in microreactors with an improved safety <sup>23</sup>. Microreactors allow synthetic intermediates to be produced and used up *in situ*, which eliminates the need to store toxic, reactive, and explosive materials, and therefore makes the continuous processes safer. An example of this is the reaction of 5-substituted 1H-tetrazoles to form nitriles and hydrazoic acid, where  $\text{NH}_3$  was generated in situ from  $\text{NaN}_3$  (extremely toxic) and acetic acid <sup>48</sup>.

The reactor volume in a microreactor is determined by the residence time and flow rates of reagents. Due to more intensive mass and heat transfer and, hence, the use of higher concentrations, productivity of flow reactors is generally higher than that of stirred tank reactors. Continuous flow chemical processing was also shown to be more environmentally friendly due to lower waste levels as compared with batch processes<sup>42, 46</sup>.

All in all, continuous processes play a crucial role in many industries especially in the biotechnology and pharmaceutical industry where low cost of process operation, high yields and high safety are demanded<sup>44</sup>. In addition, fine chemicals and pharmaceuticals are produced on a small scale in the amounts less than a few metric tonnes per year, which make such processes particularly suitable to continuous flow processing<sup>49</sup>. In this work, sequential conversion of APIs materials, namely artemisinin to artemether, is considered under flow conditions.

### 2.1.3 Process Intensification

Recently, a significant effort has been put into producing chemical products using Process Intensification technology. One of the first definitions of Process Intensification was provided by Cross and Ramshaw as "the strategy of reducing the size of chemical plant needed to achieve a given production objective". According to Ramshaw, chemical plant size should be reduced by about 100 or more. His definition is quite narrow, because he focused on reducing the size of apparatus to reach a given production objective. A more comprehensive definition of Process Intensification is given by Stankiewicz and Moulijn in their review<sup>50</sup>. According to them: "Process Intensification consists of the development of novel apparatuses and techniques that, compared to those commonly used today, are expected to bring *dramatic* improvement in manufacturing and processing, substantially decreasing equipment-size/production-capacity ratio, or waste production, and ultimately resulting in cheaper sustainable technologies". In a simpler way, Process Intensification is any chemical engineering development that is conducive to a significantly smaller, cleaner and more-energy efficient technology<sup>50</sup>. Figure 2-5

shows that the concept of Process Intensification can be divided into process-intensifying equipment and process-intensifying methods. For instance:

- a novel reactor can provide a high ratio of surface area to volume
- intense mixing equipment
- apparatus that combine several units operations
- an alternative way of delivering energy to process devices (e.g. via solar energy, microwaves, electric fields, etc.).

Using these chemical engineering developments can increase the rate of physical and chemical processes. Moreover, the strategies for process intensification are in good agreement with those for inherently safer process design<sup>51</sup>. Performing processes in smaller chemical plants, generally improves safety by reducing both the amount of hazardous reagent that can be released in case of loss of control of process and potential energy contained in a reactor<sup>51a</sup>.

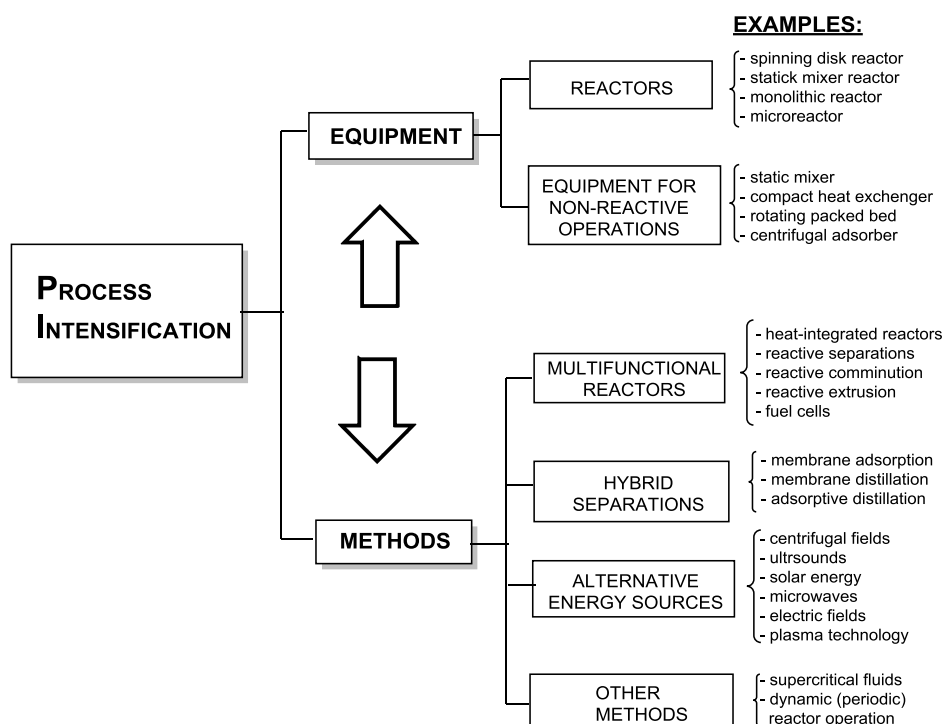
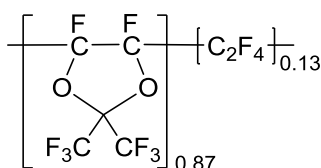


Figure 2-5. The concept of Process Intensification and its elements. Adapted from<sup>50</sup>.

### 2.1.4 Semi-Permeable Membranes

Membrane reactors are used to perform reactions and separations of reagents/products in a single unit operation to enhance product yield. Membrane reactors are used in biochemical, chemical, environmental and petrochemical industries<sup>52</sup>. There are a number of membrane separation processes, differentiated according to membrane pore sizes and transport mechanism (pore transport or solution-diffusion model), e.g., reverse osmosis<sup>53</sup>, nanofiltration, ultrafiltration, microfiltration, electrodialysis, gas separation, vapour permeation, *etc.* The membrane shape can be a flat film, hollow fibres, tubules or tubes. The structure can be microporous, both symmetric and asymmetric, nanoporous or composite. The membranes can be produced from a variety of polymers, ceramics, and zeolitic and metallic materials<sup>52</sup>.

In this work, we considered a semi-permeable polymeric membrane, which was the contactor between the gas and the liquid phases, owing to its macroporous structure, which allowed gas to pass from one side to the other. These membranes have high specific surface areas, thus enabling high rates of interfacial mass transport<sup>54</sup>. Namely, Teflon AF 2400 was considered. This is a highly permeable material to a variety of gases which also has broad chemical resistance. Teflon AF 2400 is an amorphous copolymer of perfluorodimethyldioxolane and tetrafluoroethylene (see Scheme 2-1)<sup>55</sup>.



Scheme 2-1. Structure of Teflon AF 2400.

The perfluorodimethyldioxolane part of the copolymer prevents the formation of the semi-crystalline microstructure, as can be seen in other perfluorinated polymers, for instance poly(tetrafluoroethylene) (PTFE). Conversely, Teflon AF 2400 has a highly macroporous and amorphous structure, which is characterised by a low dielectric constant, a low reflection index and permeability to a wide range of gases (compared

to PDMS membranes) <sup>39c, 56</sup>. These membranes are commercially available in the form of small diameter tubing which is characterised by a high surface to volume ratio.

In the group of Ley at University of Cambridge, a Teflon AF 2400 membrane was configured as the inner part of the Tube-in-Tube flow reactor, whereas the outer tubing was non-porous Teflon. This reactor was used to perform several reactions with gases such as ozone <sup>57</sup>, carbon dioxide <sup>58</sup>, carbon monoxide <sup>59</sup>, hydrogen <sup>54</sup>, ethylene <sup>60</sup>, oxygen <sup>61</sup> and syngas <sup>62</sup>. The important part of this reactor is a back pressure regulator which enables control of reaction process and a pressure drop to be maintained, which aids in dissolving gas in the liquid phase <sup>54</sup>.

In our research, a Tube-in-Tube flow reactor was used to perform ethenolysis of cocoa butter using a catalyst developed in the group of Nolan. This part of research was done by a student Christiane Schotten from Aachen University; the work was undertaken in the laboratories of Lapkin and Ley at University of Cambridge following initial catalyst screening and batch conditions optimisation performed by myself in the group of Nolan at the University of St Andrews.

## 2.2 Biofeedstocks

Traditional fossil petrochemical feedstocks have been the main source for production of energy in the form of heat, electricity, and transport fuels and have also met the demand for the manufacture of platform chemicals<sup>7, 63</sup>. The report of International Energy states that currently, world oil demand is roughly 86 million barrels a day. It is expected that this daily oil consumption will increase up to a value of about 116 million barrels a day by 2030, as a result of increasing use of vehicles. Transport constitutes 60% of this rise in demand<sup>64</sup>. The proportion of petrochemicals in the overall consumption of oil is only about 4%<sup>65</sup>.

However, such factors as predicted future limited availability of fossil petrochemical feedstocks, their increasingly fluctuating price, negative contribution to climate change<sup>1</sup>, and complex political situation in the producing countries force industry and scientists to search for alternative feedstocks for production of both chemicals and energy. Electricity and heat can be produced from a variety of alternative renewable resources such as sun, wind, water, and biomass. Currently, biomass is known as the only source of organic carbon. Thus, an alternative source for production of chemicals and fuels is limited to biomass<sup>7, 66</sup>.

### 2.2.1 Biorefinery

Biomass is generated as a result of the photosynthetic process from carbon dioxide and water in the presence of sun irradiation. Biomass is converted into platform chemicals using a variety of technologies in a biorefinery. A biorefinery, as opposed to a petrochemical refinery, is a relatively new concept. The route of production of biochemical and biofuels is different than from that of fossil hydrocarbons. Primary, biomass required preparatory processes such as pre-treatment, extraction and separation in order to obtain a complex mixture. Then thermochemical and biochemical processing can be used to produce biofuels and chemicals. The schematic diagram of conversion biomass into valuable products was shown in Figure 1-1.

The mixture of different molecules in biomass needs new catalysts to produce chemicals in a selective and efficient way. Thus, designing processing routes for

delivering platform chemicals from biomass in terms of the technology used, economy, and sustainability needs time for optimisation<sup>7, 63, 67</sup>. In this way, new valuable bioproducts characterised by natural carbon content and sustainability<sup>68</sup> can be delivered.

Platform chemicals are converted into chemical intermediates and polymers<sup>69</sup>. References<sup>66, 70</sup> provide the pathway of converting biomass into chemicals. The scheme of conversion of biomass is shown in Figure 2-6. First, biofeedstocks are converted into platform molecules by a depolymerisation and/or fermentation processes. In subsequent homo- or heterogeneous catalytic reactions, the platform molecules are transformed into intermediate and fine chemicals. In the second pathway, biofeedstocks are chemically synthesised in one or several steps to form a mixture of molecules of similar functionalities which, as a whole, are used to produce surfactants, lubricants, foams, cosmetics, binders, etc. Lastly, natural biopolymers occurring in biomass are chemically changed into new functional polymers, which may also be transformed into functional products.

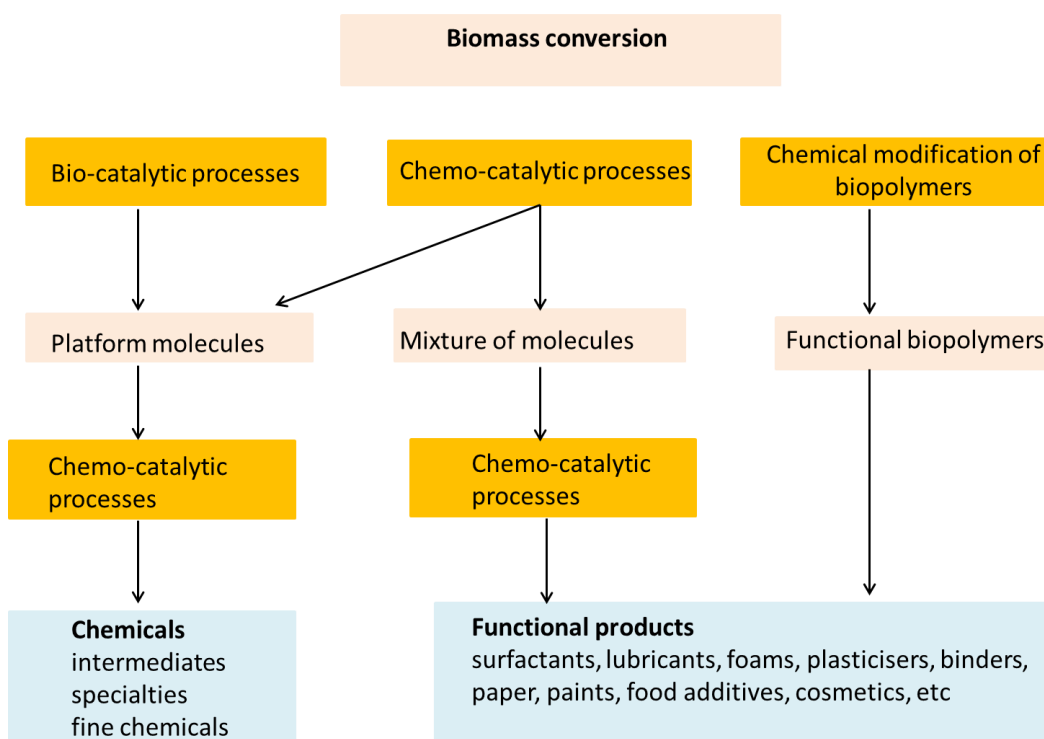


Figure 2-6. A scheme of biomass conversion processes, adapted from<sup>66</sup>.

The current level of optimisation of refinery production was achieved during more than a century of continuous development <sup>71</sup>. Therefore, it is important to gain knowledge about biofeedstock molecules and their transformation in speciality and platform chemicals and biofuels to improve biorefinery processes.

### 2.2.2 Biofuels

At present, biofuels are generated as first-generation, second-generation and also third generation biofuels. First generation biofuels are obtained from field grains, sugar crops, and also vegetable oils. Bioethanol, biodiesel, starch-derived biogas, and biomethanol and bioether from vegetable oils are included in first-generation biofuels. The scheme of derivation of biofuels is shown in Figure 2-7.

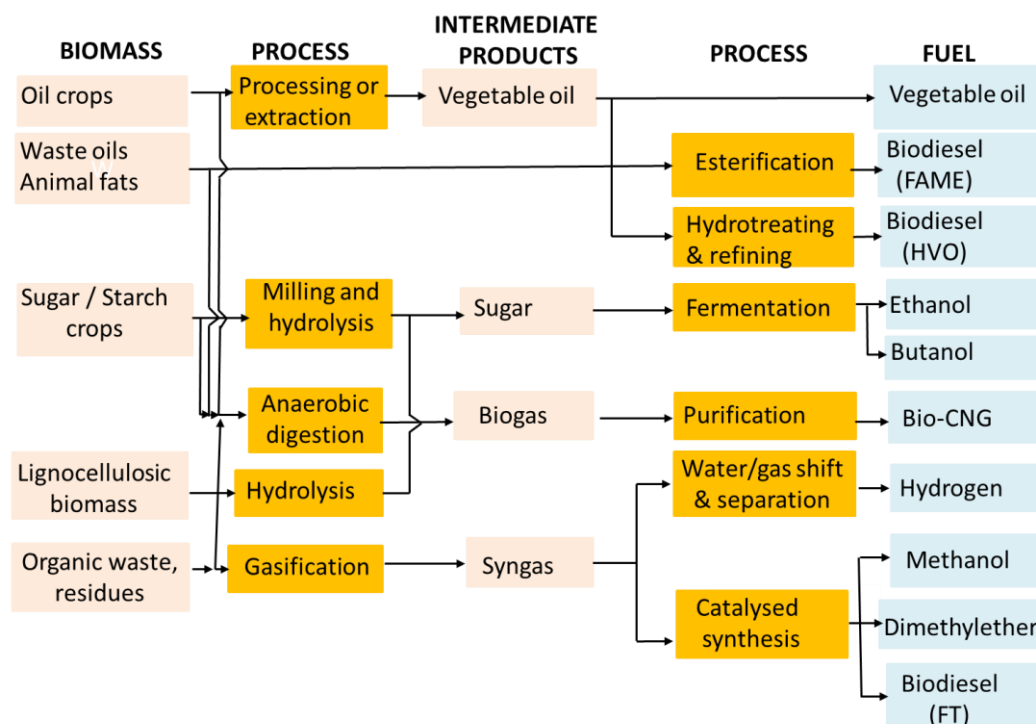


Figure 2-7. Scheme of production process of biofuels from biomass, adapted from <sup>72</sup>.

Legend: FAME – fatty acid methyl esters, HVO – hydrotreated vegetable oil, FT – Fisher Tropsch, CNG – compressed natural gas.

On one hand, field biomass can be easily transformed by hydrolysing and then fermenting sugars into ethanol as biomass is characterised by high content of starch

and sugars in crops. On the other hand, the biomass used to produce first-generation biofuels is in competition with food and feed due to the use of agricultural land. The high price of fossil fuels causes agricultural fields for growing corn to be used to produce biofuels instead of food. Subsequently, this factor has an impact on the increase in food prices. The potential availability of first-generation biofuels is limited by land impoverishment, which has an impact on crop yields per hectare of land <sup>7,72</sup>. Moreover, reduction of CO<sub>2</sub> emission and fossil fuel use is limited by high energy input for crop cultivation and conversion into biofuels <sup>7,73</sup>.

The second-generation biofuels are produced mainly from lignocellulosic materials. They consist of different concentrations of cellulose, hemicellulose and lignin, depending on the type of raw materials. They may be biomass of crops such as grasses, residues from forestry, agricultural waste such as straw or wood obtained from short rotation cultivation <sup>74</sup>. These biofuels do not compete with production of food and feed. Currently, 99% of the biofuels available on the market are still first-generation biofuels <sup>72</sup>.

The process of manufacture second-generation biofuels from lignocellulosic materials includes four primary steps: pre-treatment, hydrolysis to sugars, fermentation, and recovery of product and co-products. The production cost of the second-generation biofuels is 250–300% higher than that of the first-generation biofuels <sup>75</sup> due to difficulties in separation of lignin from polysaccharides. The most expensive part of ethanol production is pre-treatment of lignocellulosic materials so that in the next step, enzymes can more easily hydrolyse them to sugars <sup>76</sup>. In the case of a scaled up process, in the pre-treatment step a reactor resistant to high temperature and pressure and also a corrosive catalyst, which should be recovered after the process, is needed. To make the second-generation biofuels attractive in comparison with first the generation-biofuels, the capital and operating cost of the majority of units should be reduced significantly <sup>75</sup>. The economical balance sheet of production and the predicted market entry of second-generation of biofuels are presented in the following literature, refs <sup>77</sup>. Life cycle assessment of bioethanol and biodiesel has also been performed <sup>78</sup>.

In addition, algae are also under consideration for production of biofuels as they could be independent of land in the case of marine algae <sup>79</sup>. Currently, research is needed on the commercially viable scale of algal fuels, which could be possible by genetic modification of algal strains <sup>80</sup>.

### 2.2.3 Oleochemistry

The issue of production of chemicals from renewable sources such as biomass has recently grown in importance <sup>81</sup>. This production is developed by industrial companies as well as academic research supported by international and national organisations <sup>66</sup>. It is expected that in 2025, up to 30% of feedstocks for production of chemicals and materials will be provided by biomass. Bioproducts are mainly obtained from lignocellulosic materials, starch crops, vegetable oils, and also marine biomass. Here, triglycerides will be considered.

Vegetable oils and animal fats comprise triglycerides, which have a glycerol molecule and three fatty acid moieties. Main commercial sources of triglycerides are vegetable oils from tropical countries, such as coconut, palm, and palm kernel oils, and those from moderate climates such as soybean, rapeseed, and sunflower. Animal triglycerides are obtained from meat and fishing industries <sup>82</sup>. The path of synthesis of different chemicals based on oils is shown in Figure 2-8.

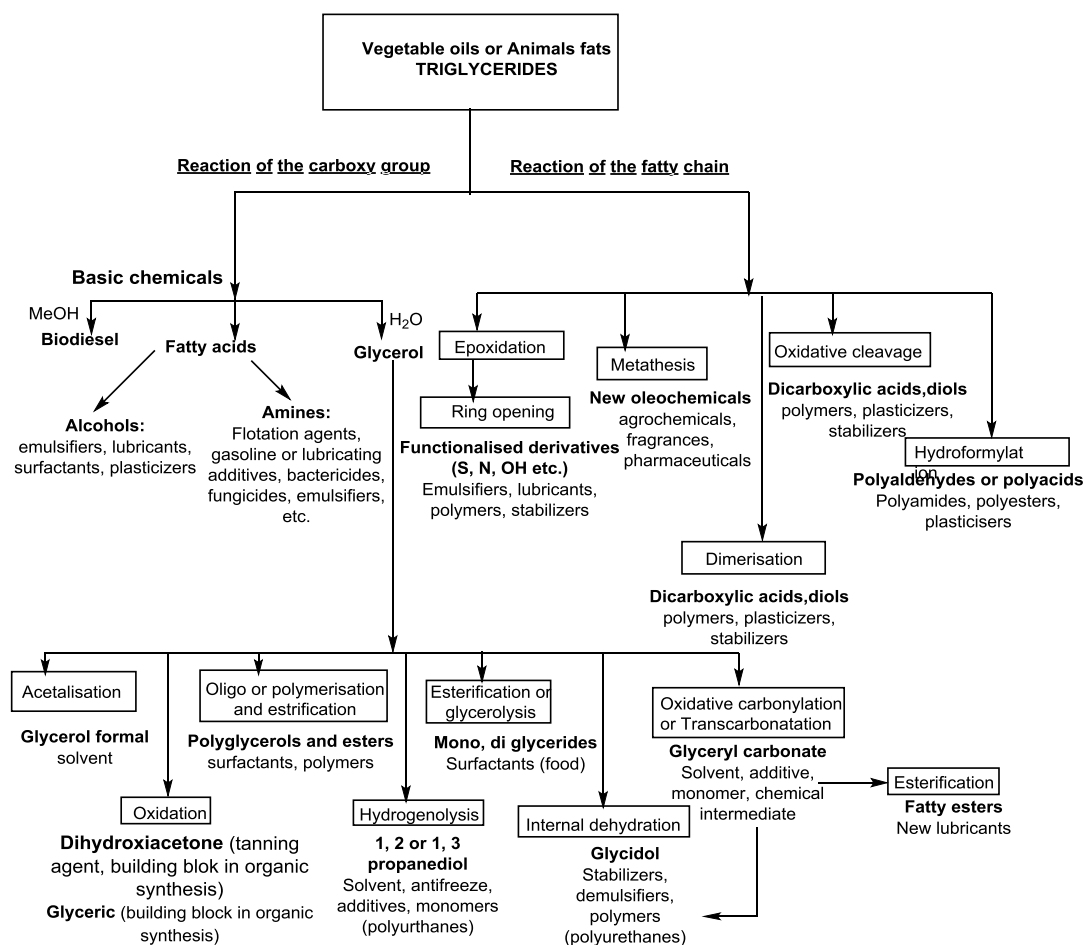
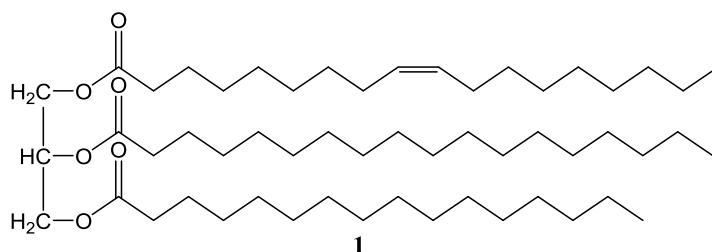


Figure 2-8. A scheme of production of valuable chemicals from vegetable oils and fatty acids, adapted from <sup>82</sup>.

In this work, as an example triglyceride, cocoa butter (**1**) is considered. Cocoa butter is a natural compound, extracted from *Theobroma cocoa* seeds, the main constituent of which is a mixture of fatty acid triglycerides, see Scheme 2-2 <sup>8a</sup>. The exact composition depends on the origin: cocoa butter sourced from Africa (Ghana and Ivory Coast) contains a slightly lower amount of oleic acid than cocoa butter sourced from South America (Ecuador and Brazil), with the concentration of oleic acid in cocoa butter from East Asia (Malaysia and Java) in between <sup>8b, 83</sup>. However, composition of fatty acids in the cocoa butter recorded in the literature consists of mainly palmitic, stearic, oleic, linoleic, and arachidic acids <sup>83-84</sup>. Cocoa butter is used in confectionary first of all to chocolate production. In addition, cocoa butter has application in cosmetics to produce moisturising creams and soaps and also in pharmaceutical industries <sup>85</sup>. In our work we used a cocoa butter waste from a

chocolate industry as an example of triglyceride. Triglycerides are worldwide available. The vegetable and fatty triglycerides are a promising source of biofeedstocks in the manufacturing of valuable chemicals, Figure 2-8. In this thesis cocoa butter was used to produce epoxide and 1-decene under flow conditions.



Scheme 2-2. A chemical structure of cocoa butter.

#### 2.2.4 Secondary Metabolites

In all plants occur compounds that are essential for their survival, which are called primary metabolites. Primary metabolites are crucial building blocks of sugar, nucleotides, amino acids, lipids and energy sources <sup>86</sup>. There are also compounds that do not directly take part in the life processes of plants and do not occur in all plants, such as secondary metabolites. They are responsible for unique character of plants such as colour, fragrance of flowers and fruits and taste of species, vegetables and fruits <sup>87</sup>. Mostly secondary metabolites play an important role in protection of plants against viral and microbial infections, snails, slugs, vertebrates, arthropods, UV radiation and *etc.* <sup>86, 88</sup>. Plants provide three types of secondary metabolites compounds, such as:

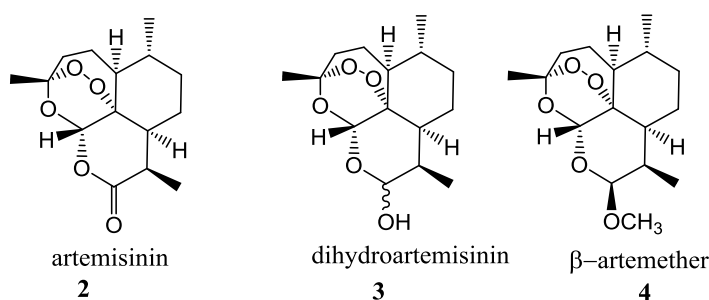
- 1) phenolic complexes,
- 2) terpenoids/isoprenoids compounds,
- 3) compounds containing sulphur and nitrogen such as the glucosinolates and alkaloids, respectively <sup>86</sup>.

Secondary metabolites have a wide range of applications such as in the manufacture of pharmaceuticals, food colours, flavours, fragrances, and agricultural chemicals. The impact of plant secondary metabolites on human health is presented in a review <sup>89</sup>. However, very often production of secondary metabolites from plants has very low yields. For instance, to produce 1 kg of paclitaxel, 10,000 kg of dry biomass of

*Taxus* sp. is needed<sup>90</sup>. Currently 200,000 structures of secondary metabolites are known<sup>91</sup>.

In this thesis, a sesquiterpene lactone with an endoperoxide bridge is being used as a precursor to antimalarial drugs APIs. This secondary metabolite is extracted from *Artemisia annua* L. Currently, *A. annua* L. is the only known commercially economical source of artemisinin (ATR)<sup>12</sup>. This plant is cultivated first of all in Asia and also in Africa, Australia, North and South Americas<sup>12</sup>. ART comprises from 0.01–1.4% of the dry residue of *A. annua*<sup>92</sup>. Simultaneously, ART can be obtained chemically roughly in eight steps, with an average yield of approximately 10%. This process is currently not cost-effective from a commercial point of view<sup>93</sup>. The isolation of artemisinin from *A. annua* L. is described in<sup>12,94</sup>.

At present, ART (**2**) and its derivatives are used in the treatment of *Plasmodium falciparum* malaria due to their high antiplasmodial effectiveness and low toxicity<sup>13</sup>. ART drugs overcome the symptoms of malaria in 32 hours while other antimalarial drugs need 2–3 days. With ART drugs, the parasites are completely removed in 5–7 days<sup>95</sup>. However, ART drugs are characterised by short plasma half-life. Thus, for faster treatment and to avoid renewal of parasites, ART drugs are combined with other antimalarial drugs with longer half-lives<sup>95b</sup>. Since 2005, World Health Organization (WHO) has recommended these ART combination therapies for the treatment of malaria. Currently, this method is used worldwide<sup>96</sup>. ART as a drug has a number of drawbacks such as the aforementioned short plasma half-life, high rate of renewal of parasites after treatment, poor solubility in water and oil, and low oral absorbency of this compound<sup>97</sup>. Dihydroartemisinin and artemether present better solubility in water and oil (Scheme 2-3). Thus, the synthesis of these molecules is considered in this work.



Scheme 2-3. The structures of artemisinin related molecules of interest to this study.

### 2.3 Epoxidation of Long-Chain Olefins

The epoxidation of long chain olefins and fatty acids is an important reaction in organic synthesis, leading to intermediates for production of polymers, emulsifiers and lubricants<sup>98</sup>. Batch syntheses of fatty epoxides are widely reported<sup>14</sup>. Due to high viscosity the reaction suffers from severe mass transfer limitations and represents a significant safety hazard if run as a large-scale batch process. Continuous flow processing may have considerable advantages in the production of epoxides compared to batch conditions if the benefits of enhanced mass and heat transfer, typically reported for flow processes<sup>99</sup> could be exploited in the case of a high-viscosity reaction medium.

There are few literature examples of epoxidations being carried out under flow conditions. Epoxidations of 1,5-cyclooctadiene, 1,2-dihydronaphthalene, ethyl *trans*-3-hexenoate, dodec-1-ene, duroquinone, *trans*-stilbene, *cis*-stilbene, ethyl *trans*-cinnamate, methyl *trans*-2-methyl-2-pentenoate using homogeneous stoichiometric reactant HOF·MeCN was performed with high yields under continuous flow<sup>100</sup>. The byproduct hydrogen fluoride can be recycled by electrolysis.

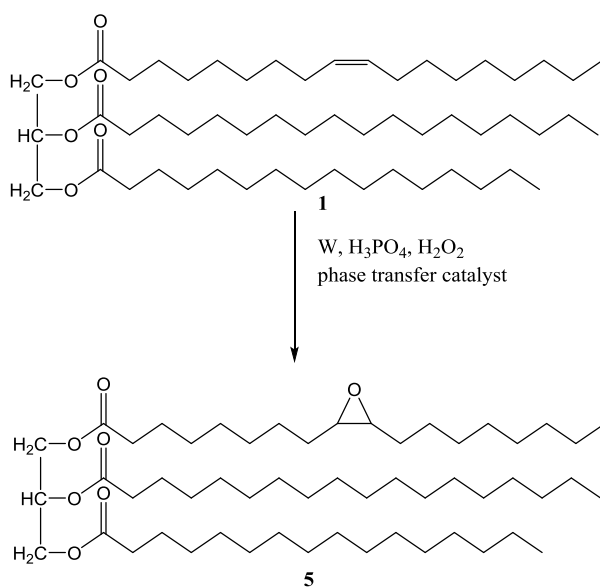
Enantioselective epoxidation of chalcone catalysed by polyethylene glycol-poly-L-leucine was investigated in a low-cost SU8/PEEK plate flow microreactor<sup>101</sup>. Maximum conversion of 87 % with 88 % ee were obtained with diluted reactants when heat effects and surface fouling of the reactor do not present a problem. However, even at these conditions formation of bubbles and decomposition of reactive species through side reactions reduce performance of the system.

Several examples of epoxidation in flow using heterogenised reagents or catalysts were reported. Thus, epoxidation of cyclohexene, *trans*-3-heptene, *cis*-3-heptene, 3-methyl-2-pentene, bicyclo[2.2.1]hept-2-ene, 1-hexene, methyl 2-cyclohexenylcarboxylate, *trans*-2-hexenyl acetate, 2-cyclohexenylacetate, *trans*-2-hexenyl acetate, 5-hexenyl acetate were performed using 2-percarboxyethyl-functionalized silica in supercritical carbon dioxide at a pressure of 250 bar and temperature 40 °C in flow, reporting products yields of > 99 %<sup>102</sup>. Side reactions to acid catalysed ring opening or other side products were suppressed due to using an

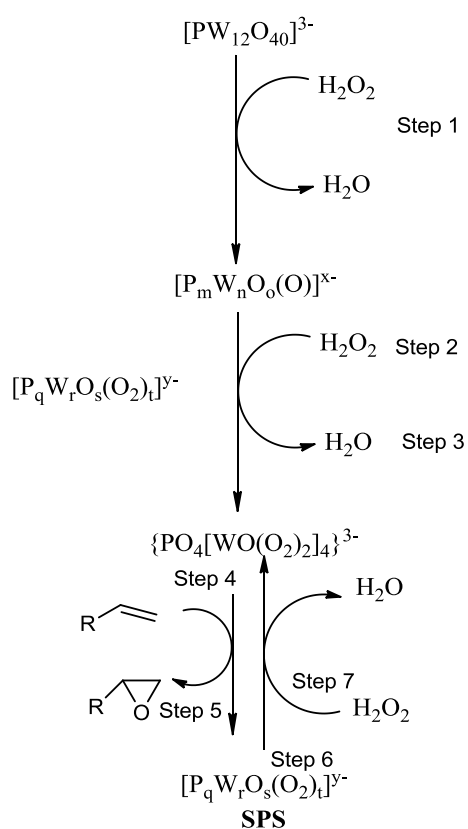
anhydrous supported peracid. Epoxidation of styrene with *meta*-chloroperoxybenzoic acid in the presence of excess methylmorpholine-*N*-oxide in a microfluidic reactor coated with a polymer-immobilized Mn (III)-salen catalyst<sup>103</sup> was reported with a 190-fold increase in space time yield compared to a batch recipe. The improvement was attributed to a better contact between reactants and the catalyst.

Epoxidation of triglycerides rather than free fatty acids is sparsely reported in the literature. Epoxidation of soybean oils was investigated in a series of papers<sup>15</sup>. Conventional batch epoxidation with hydrogen peroxide in the presence of acetic or formic acid and mineral acid was reported with a yield of up to 75 % at temperatures between 60 – 80 °C with a typical batch time of 300 min. A decrease in reaction time and a slight improvement in the overall energy efficiency were possible if reaction temperature was increased and reaction performed in a microreactor with efficient heat transfer. However, at temperatures above 150 °C decomposition of hydrogen peroxide dominates and reaction yield is significantly reduced compared to the batch, lower-temperature process. The epoxidation of soybean oil is a single example of triglyceride epoxidation studied in the flow system.

In this thesis we report epoxidation of cocoa butter with hydrogen peroxide catalysed by an Ishii-Venturello catalyst, Scheme 2-4 and Scheme 2-5<sup>104</sup>. The reaction is performed as a phase transfer catalytic reaction with quaternary ammonium or phosphonium salts as phase transfer reagents<sup>104a, 105</sup>. Earlier papers report similar epoxidations performed in chlorinated solvents<sup>104-106</sup>. However, the reaction can be performed solventless as long as the reaction is properly emulsified<sup>14b, 107</sup>. Significant drawbacks of these reactions are the decomposition of hydrogen peroxide and the acid-catalysed side reactions to ring opening of epoxides, reducing the product yield. A modified Ishii-Venturello catalyst was reported in<sup>108</sup> with tungsten powder being used for *in-situ* formation of the active form of the catalyst. The modified catalytic system is characterized by high selectivity and conversion towards epoxidation reactions. Epoxidation of cocoa-butter sourced as a waste of confectionary industry with a modified  $W^{VI}/P^V/H_2O_2/PTC$  complex<sup>108b</sup> was studied in detail both in batch and flow conditions in this thesis.



Scheme 2-4. Formation of epoxide from cocoa butter.

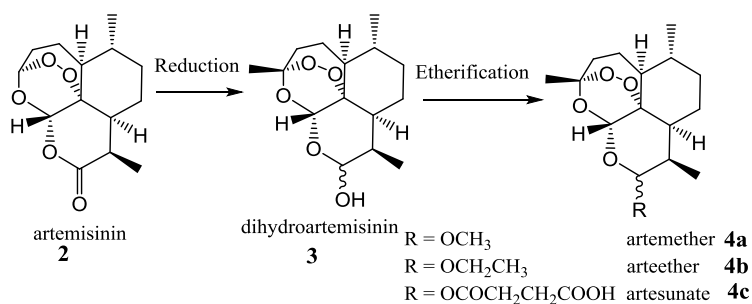
Scheme 2-5. A mechanism of epoxidation using Ishii-Venturello system, adapted from <sup>106c</sup>.

## 2.4 Sequential Reaction in the Synthesis of Artemisinin to Final API Products under Flow Conditions

Until now, batch processing has totally dominated the manufacturing of pharmaceuticals and speciality chemicals. However, the role of continuous processes, and especially of clean catalytic processes, in these important areas of chemical manufacturing is increasing rapidly <sup>109</sup>. Key challenges in translating conventional synthetic protocols into flow processes are typically related to issues of low solubility of reactants and products, the use of mutually incompatible solvents at different steps in multi-step syntheses, the need for intermediate work-up steps and, finally, the lack of standardised equipment for assembling of flow catalytic processes.

Here we report the first sequential flow synthesis of an important medicinal small molecule of biological origin, in which a number of the aforementioned problems had to be resolved. Natural products-derived small molecules represent a major source of new drugs <sup>110</sup>. A well-publicised example is artemisinin, the WHO-recommended drug for treating uncomplicated *Plasmodium falciparum* malaria, which is obtained by extraction from *Artemisia annua* <sup>94f</sup>. Malaria is a very significant problem in many tropical regions, with 300 – 500 million cases reported and 1.5 – 2.7 million deaths annually.

The active pharmaceutical ingredients of artemisinin-based drugs are ethers, such as artesunate or artemether, obtained *via* reduction of artemisinin (**2**) into dihydroartemisinin (**3**) (DHA) followed by etherification to the final APIs, see Scheme 2-6 <sup>111</sup>.



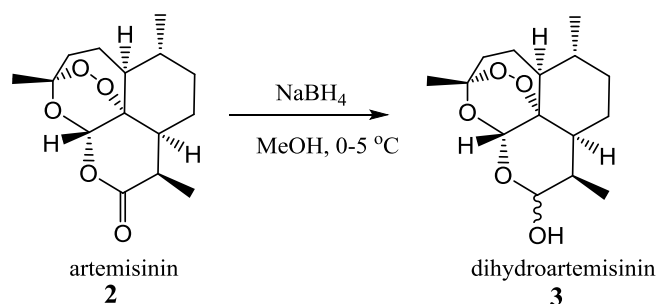
Scheme 2-6. A common route to conversion of artemisinin to artemisinin-based APIs.

### 2.4.1 Stoichiometric Reduction of Artemisinin

Stoichiometric reductions are ubiquitous in organic synthesis due to their synthetic utility and high selectivity. Many reductions are performed at low temperatures for reasons of safety and maintaining selectivity in the highly exothermic reactions. They also involve the handling of solids. Both factors complicate scale up of reductions. In this respect flow chemistry offers significant potential advantages for the generic class of stoichiometric reductions<sup>112</sup>. Here we present an example of a typical stoichiometric reduction of a current drug precursor transferred into a flow process with significant gains in productivity and selectivity.

The route to the active ingredient in artemisinin combination therapies (ACTs) for the treatment of *Plasmodium falciparum* malaria, e.g., artesunate is *via* reduction of artemisinin (ART) into dihydroartemisinin (DHA) using sodium borohydride in methanol or ethanol, see Scheme 2-7<sup>113</sup>. This synthetic protocol involves a batch reaction at low temperatures (0 – 5 °C) in a suspension of NaBH<sub>4</sub>, followed by a multi-step work-up procedure<sup>113</sup>. Diisobutylaluminium hydride (DIBAL-H)<sup>114</sup> is another reductant reported in the literature, requiring dry dichloromethane as solvent, lower reaction temperature (–78 °C) and with a smaller yield of DHA. Both protocols require long reaction times (0.75 – 3 h) at low temperatures due to the exothermic nature of the reaction. Scale-up of this reaction is problematic for four reasons: (i) artemisinin is pyrophoric due to the presence of a highly unstable endoperoxide function, (ii) batch protocol requires low temperatures to avoid thermal runaway, (iii) batch reaction with suspended solids is not easily scalable due to high sensitivity to variations in the feedstocks and the physical form of the

reactants (size of particles, crystal allotrope, *etc*), and (iv) the multi-step workup procedure required to obtain a stable formulation of DHA. These factors were assembled by the authors from heuristic data on end-user experiences with scaling up artemisinin reduction in the UK, India and China, an earlier project on artemisinin derivatisation sponsored by Medicines for Malara Ventures <sup>115</sup>, and the material safety data sheets information. Based on earlier studies of flow processes <sup>116</sup>, we undertook to develop a flow protocol for the synthesis of dihydroartemisinin, which is reported in this thesis. The flow protocol of the basic reduction of artemisinin with  $\text{LiBHET}_3$  was elaborated by Dr Xiaolei Fan and Dr Victor Sans. My task was to ensure reliability of the flow synthesis and to develop a methodology to link two flow reactions in a sequence.



Scheme 2-7. A reaction scheme of artemisinin reduction using conventional batch protocol.

#### 2.4.2 Etherification of Dihydroartemisinin

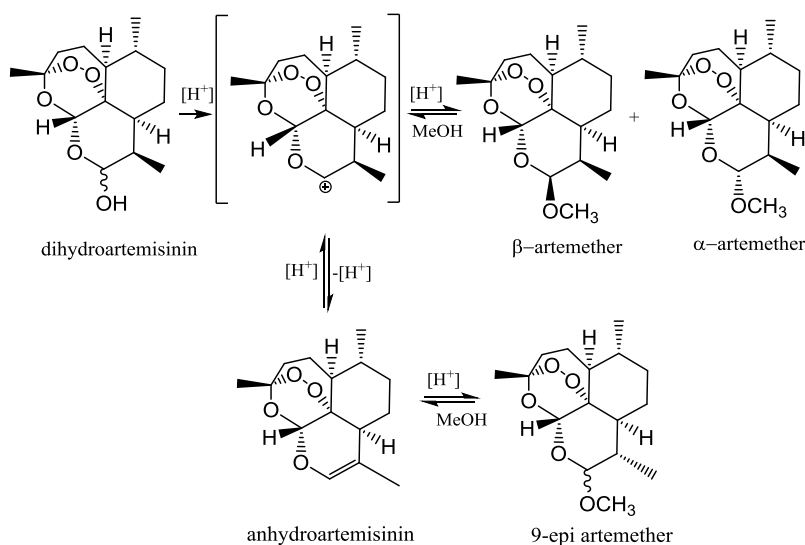
A considerable amount of literature has been published on the synthesis of ARM from DHA using acidic catalysts such as  $\text{BF}_3 \cdot \text{Et}_2\text{O}$  <sup>111b, 117</sup>,  $\text{Me}_3\text{SiCl}$  <sup>118</sup>, *para*-toluenesulfonic acid (PTSA) <sup>119</sup> and  $\text{HCl}$  <sup>17, 120</sup>, a heteropoly acid <sup>121</sup>, and Amberlyst 15 <sup>18</sup> under batch conditions. Lin *et al.* <sup>117, 122</sup> reported etherification of DHA in an appropriate alcohol such as methanol or ethanol using boron trifluoride etherate as the catalyst at room temperature for 24 hours, yielding 70 % to 90 % ethers. Bhakuni *et al.* <sup>118</sup> obtained ethers as a result of DHA synthesis in an appropriate alcohol (ethanol, isopropanol or butanol) and benzene in the presence of chlorotrimethylsilane (catalyst) for 2 – 4 hours, with the product purified by silica gel chromatography after removal of the solvent. El-Feraly *et al.* <sup>119</sup> carried out

etherification of DHA in absolute alcohol in the presence of *para*-toluene sulphonic acid for 22 hours, where the Lewis acid catalyst was far in excess of the DHA content. A one-pot batch protocol for ART to ARM reactions has been published<sup>123</sup>, where the reduction of ART was performed using  $\text{KBH}_4$  and HDTMAB (phase transfer catalyst) in the presence of ethyl alcohol at room temperature for 5 hours. The etherification was carried out using trifluoroacetic acid at 0 – 5 °C for 6.5 hours, yielding 84 % artemether.

When taken as a whole, the previous methods are quite expensive, have long reaction times and require aqueous workup. Additionally, solvents such as benzene and trifluoride etherate are toxic and these synthesis reactions should be avoided due to their potential biological impacts. Moreover,  $\text{Me}_3\text{SiCl}$  and  $\text{BF}_3 \cdot \text{Et}_2\text{O}$  are moisture sensitive, which also has a negative impact on the progress of reactions.

Another one-pot conversion method for the etherification of ART to ARM uses Amberlyst-15 as the catalyst for 72 hours, but has the disadvantage of using  $\text{CH}_2\text{Cl}_2$  during the extraction process<sup>18</sup>. This ecologically unfriendly dichloromethane was also used as a co-solvent in etherification with dodecatungstophosphoric acid hydrate in the presence of alcohol, as listed elsewhere<sup>121</sup>. Reaction in the presence of methanol lasted 3 h and in the case of ethanol 6 h<sup>121</sup>. In the research of Boehm *et al.*, dichloromethane was replaced by the more sustainable methyl acetate. The reaction was catalysed by HCl. The yield to ARM  $\beta$  for this solvent was 85 %<sup>120</sup>.

Stringham and Teager<sup>17</sup> used HCl (inorganic acid) during catalytic batch etherification (Scheme 2-8) with an immediate improvement in synthesis, where 1.35 kg of ART yielded 1 kg of ARM (compared to the average industry ART weight of 1.59 kg) and was attributed to the use of trimethyl orthoformate (TMOF) as the co-solvent. The description also details the neutralization with aqueous base, phase separation, concentration and crystallisation of ART. The catalytic etherification performed with inorganic acids, such as HCl<sup>17</sup>, or with acidic resins, such as Amberlyst-15<sup>18</sup>, required downstream neutralisation with a base, and was followed by separation of the product from the base solution. In order to develop a fully continuous process it is desirable to eliminate the intermediate work-up steps, as well as avoid the use of different solvents.

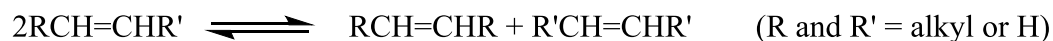


Scheme 2-8. A scheme of ARM synthesis and side reactions. Adapted from <sup>17</sup>.

Thus, the aim of the present study was two-fold: catalytic conversion of dihydroartemisinin to ARM, and to perform a cradle-to-gate life cycle assessment study to develop understanding of the sources of environmental impacts in the new process, and thus develop strategies for their reduction or elimination in further process optimisation. The life cycle assessment was carried out by Dr Polina Yaseneva. Simplified design of packed-bed continuous flow reactor was done by Dr Xiaolei Fan. Residence time measurements and calculations were done by Dr Konstantin Loponov.

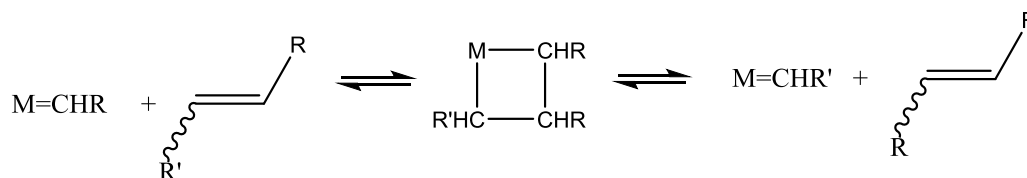
## 2.5 Olefin Metathesis

Olefin metathesis is an important organic catalytic synthetic methodology, which entails breaking of olefin double bond and formation of either a shorter or longer chain with reformation of the carbon-carbon double bonds, as shown in Scheme 2-9<sup>124</sup>. It was discovered by Bank and Bailey (Phillips Petroleum Company, Bartlesville) in 1964<sup>125</sup>.



Scheme 2-9. Scheme of olefin metathesis

The mechanism of metathesis can be described in the following way:



Scheme 2-10. Mechanism of metathesis introduced by Chauvin<sup>126</sup>.

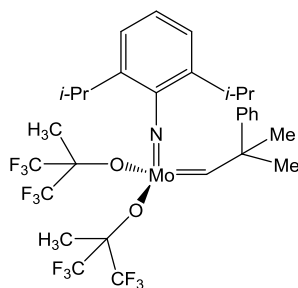
In the first step conversion between an olefin and a transition metal carbene system in a 2+2 mode occurs and a metallacyclobutane intermediate is formed. In the next step, the metallacyclobutane intermediate may be transformed into the initial substrate or ruptured to form a new metal alkylidene complex and a new olefin product<sup>124a</sup>.

### 2.5.1 Catalysts

The first well-defined metathesis catalysts were based on tantalum<sup>127</sup>, titanium<sup>128</sup> and tungsten<sup>129</sup>. However, these catalysts are not so suitable for metathesis reactions because they require harsh reaction conditions and have long initiation periods. The reactions are also difficult to control due to the diversity of catalyst species (quantity, shape).

The second well-defined catalyst complex used for metathesis reactions was based on molybdenum (Schrock's catalysts, Scheme 2-11). On the one hand, these

catalysts were characterised by high activity. They demonstrated much broader functional group tolerance in comparison with tungsten-based catalysts (esters, amides, ketal, ether, cyano, trifluoromethyl and primary halogens). Schrock's catalysts are more stable with regard to decomposition and also to the formation of by-products. They demonstrate high stereochemical control over chiral alkoxy ligands. On the other hand, the reaction should be performed under inert conditions due to oxygen and moisture sensitivity<sup>130</sup>.

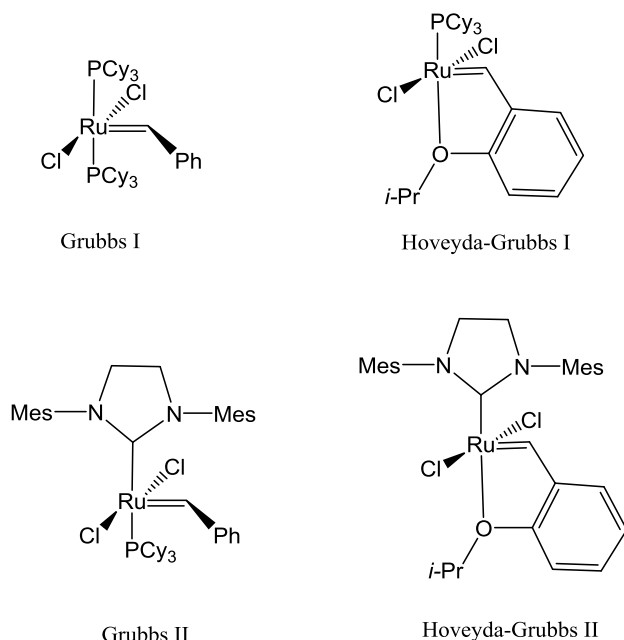


Scheme 2-11. A sample structure of a Schrock's molybdenum catalyst. i-Pr – iso propyl, Ph – phenyl.

The next group of catalysts introduced for metathesis reactions in the late 1980s are ruthenium catalyst systems. Ru demonstrates low oxophilicity, which makes ruthenium-based catalysts compatible with many organic functional groups. Grubbs' first-generation ruthenium catalyst complexes are characterised by high reactivity. However, molybdenum iminoalkylidenes show higher activity than Grubbs' first-generation catalysts. They are stable toward moisture, alcohols and acids. However, this complex has a limited lifetime in a reaction system. They are  $\sigma$  donating ligands. These catalysts are the precursors for other more reactive catalysts. They are selective toward alkyl-substituted double bonds. They are used in ring-opening metathesis polymerisation. They are definitely one of the cheapest forms of stable ruthenium catalysts<sup>130a, 131</sup>.

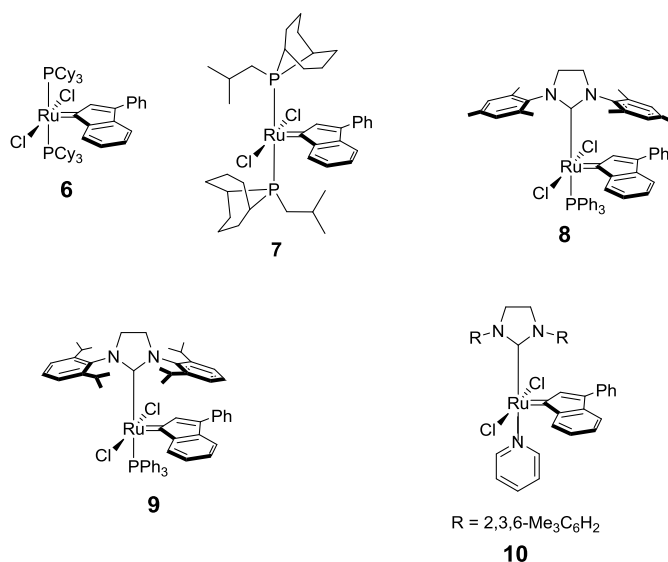
More expensive and more reactive are Grubbs' second-generation catalysts. They show an improved thermal stability. Nowadays they are widely used in metathesis processes. They are obtained by substituting one of the tricyclohexylphosphine ligands with the group of *N*-heterocyclic carbene (NHC) ligand  $H_2IMes$ <sup>132</sup>. This chelating ligand makes the second-generation, especially Hoveyda-Grubbs catalysts,

present high reactivity, stability and recovery profiles in comparison with the first-generation catalysts (Scheme 2-12)<sup>124a</sup>. The reactivity of these catalysts is better due to improvement  $\sigma$  donor ability of NHC which increases affinity for  $\pi$ -acidic olefins<sup>130a</sup>.



Scheme 2-12. Structures of the first and second-generation Grubbs and Hoveyda Grubbs catalysts.

In ethenolysis of cocoa butter under batch conditions catalysts developed by the group of Nolan were used; catalysts structures are shown in Scheme 2-13. It was concluded that the best performance was obtained in the presence of **(6)** (dichloro-(3-phenyl-1*H*-inden-1-ylidene)bis(isobutylphobane)ruthenium II). Thus, this catalyst was used for the ethenolysis of cocoa butter in the flow membrane reactor. (Ru)-indenylidene complex endures harsher conditions than other complexes and is tunable through their other ligands<sup>133</sup>. Also these catalysts seem to be less sensitive to ethylene than other Ru carbene complexes<sup>134</sup>. Synthesis and activity of these catalysts are already described in literature and a patent on this type of catalyst has been filed<sup>135</sup>. A comparable ethenolysis with methyl oleate under batch conditions was described by Forman *et al.*<sup>136</sup>.



Scheme 2-13. Structures of Ru catalyst complexes used in our research.

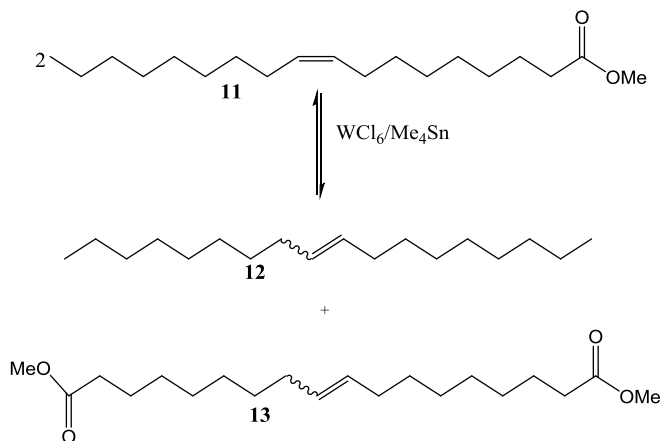
### 2.5.2 Applications of Metathesis

Olefin metathesis reactions are applied in petrochemical industry. Namely, in the Phillips triolefin process, in which polymerisation-grade propene is produced by cross-metathesis of ethene and 2-butene<sup>137</sup>. Next, in the production of neohexene, which is an intermediate in the process of manufacture of musk perfume<sup>137-138</sup>. A number of metathesis processes are applied in the Shell Higher Olefins Process (SHOP), in which ethene is transformed into detergent-range olefins<sup>137-138</sup>. In addition, ring-opening metathesis polymerisation of cycloalkenes is used to produce commercial linear polymers<sup>137</sup>. Apart from using olefin metathesis in the petrochemical industry, the process can also be applied in the case of unsaturated oils and fats and their derivatives to either produce new and valuable chemical products or existing chemicals using a new path of synthesis from renewable sources<sup>124a</sup>. Homogenous and heterogeneous catalysts are used in industrial metathesis processes.

### 2.5.3 Types of Olefin Metathesis

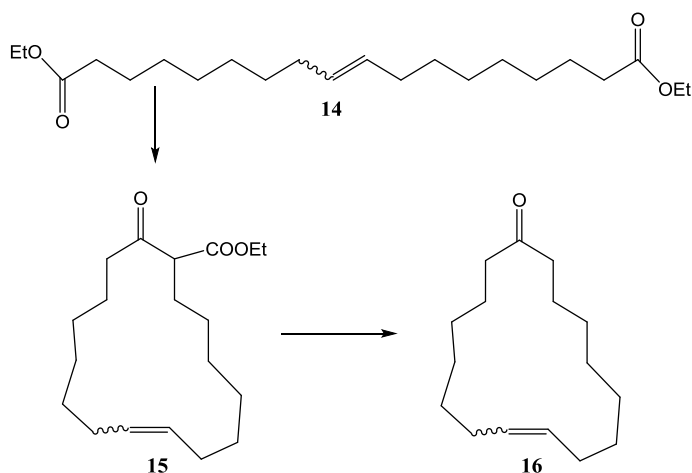
#### Self-metathesis

Self-metathesis occurs between two of the same alkene molecules. An example of this metathesis is the transformation of methyl oleate (**11**) into equimolar quantities of 9-octadene (**12**) and dimethyl 9-octadecene-1,18-dioate (**13**), as outlined in equation below <sup>124a</sup>.



Scheme 2-14. Self-metathesis of methyl oleate. *Cis-trans* isomers were obtained where *trans* was dominated.

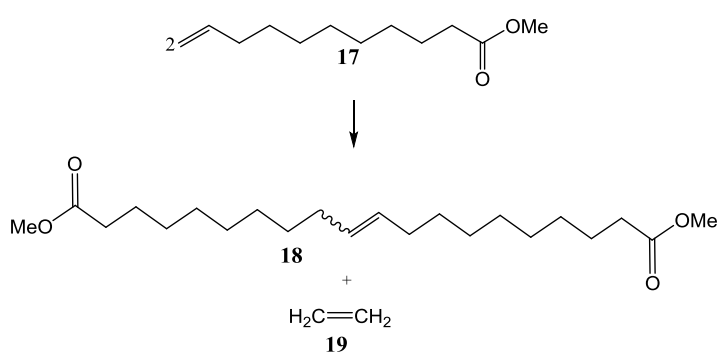
This reaction illustrates that in the presence of an appropriate catalyst it is possible to obtain an unsaturated diester and internal alkene without formation of by-products. The products of self-metathesis reaction are intermediates in further chemical syntheses of useful products. For instance, this diester can be applied in a Dieckmann condensation, through hydrolysis and decarboxylation, to obtain *cis* structure of unsaturated macrocyclic ketone 9-cycloheptadecane-1-one (**16**), *civetone*, which is a desired component in the production of musk perfumes, as shown in Scheme 2-15 <sup>124a</sup>.



Scheme 2-15. Dieckmann condensation of diethyl 9-octadene-1,18-dioate (**14**).

In addition, olefin dicarboxylic esters and acids are attractive raw materials for the synthesis of vulcanizable polyester and polyamides. However, 9-octadecene (**12**) can also be used to produce 10,11-dioctyleicosane, which is a lube-oil-range hydrocarbon intermediate<sup>133</sup>.

A similar example of self-metathesis is the reaction of  $\omega$ -unsaturated fatty acid esters to produce internally unsaturated long-chain dicarboxylic acid ester and ethene (**19**), for instance metathesis of methyl 10-undecenoate (**17**), as shown in Scheme 2-16<sup>124a</sup>.



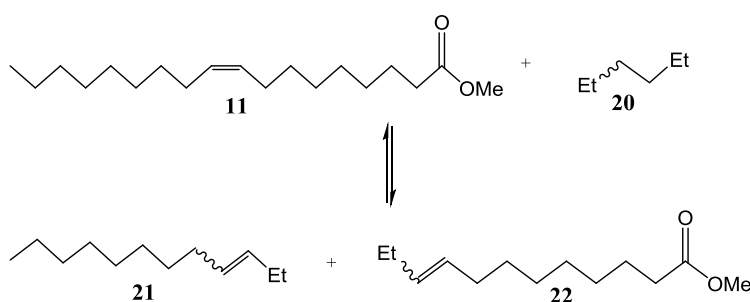
Scheme 2-16. Metathesis of methyl 10-undecenoate.

In the case of metathesis of polyunsaturated fatty acids, a variety of products can be obtained. An example of this is metathesis of methyl linoleate to produce polyenes, a monocarboxylic ester and a dicarboxylic ester<sup>124a</sup>. Holster and co-workers<sup>139</sup>

reported metathesis of methyl soyate with ruthenium catalysts. They concluded that a Grubbs' second generation catalyst was more suitable for this reaction under mild conditions.

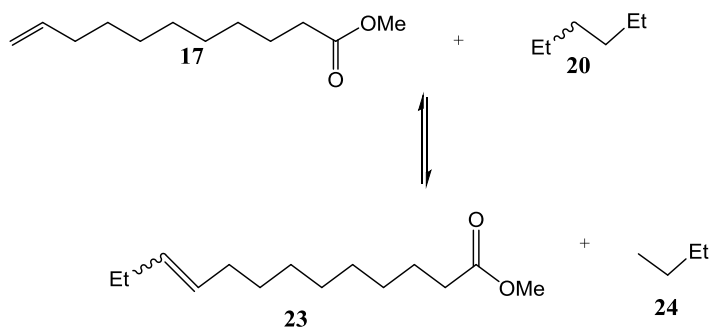
### Cross-metathesis

Cross-metathesis occurs between different alkene molecules. It can be applied to shortening a molecular chain. One example of this is metathesis of methyl oleate with 3-hexene leading to the formation of 3-dodecene (**21**) and methyl 9-dodecenoate (**22**), as shown in Scheme 2-17<sup>134</sup>.



Scheme 2-17. Cross-metathesis between methyl oleate (**11**) and 3-hexene (**20**).

The second application of cross-metathesis is to lengthen a carbon chain. One illustration is cross-metathesis between methyl 10-undecenoate (**17**) and 3-hexene (**20**), as shown in Scheme 2-18<sup>124a</sup>.

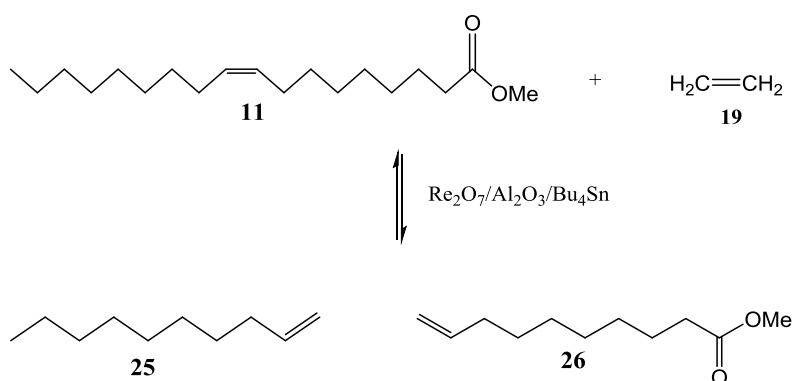


Scheme 2-18. Cross-metathesis between methyl 10-undecenoate (**17**) and 3-hexene (**20**).

Cross-metathesis is a useful tool in manufacturing fine chemicals that are difficult to obtain by other reactions.

### Ethenolysis

Ethenolysis is an example of cross-metathesis of alkenes with ethene. An example of this reaction is metathesis of methyl oleate (**11**) to produce methyl-9-decenoate (**26**), as shown in Scheme 2-19<sup>135b, c</sup>.

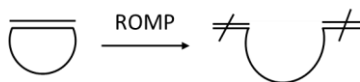


Scheme 2-19. Ethenolysis of methyl oleate (**11**).

Methyl-9-decenoate is an important intermediate in production of many chemicals such as lubricants, plasticizers, fragrances, pheromones and polymers. On the other hand, 1-decene is a useful intermediate in organic synthesis and is also used to produce polymers, surfactants and lubricants.

### Olefin metathesis to polymers

Metathesis of alkenes plays a crucial role in polymer chemistry. There are two types of metathesis reactions: ring-opening metathesis polymerisation (ROMP) and acyclic diene metathesis (ADMET). Ring-opening metathesis polymerisation involves transformation of a mixture of cyclic olefins to a polymeric product in the presence of a metathesis catalyst, as shown in Scheme 2-20<sup>130a, 140</sup>. The driving force for this reaction is the release of strain within the cyclic olefin reactant balanced by entropic penalties<sup>130a</sup>. A considerable amount of literature has been published on ring-opening metathesis polymerisation<sup>124b, 130a, 132, 141</sup>.



Scheme 2-20. A simplified mechanism of ring-opening metathesis polymerisation.

Acyclic diene metathesis (ADMET) is another example of metathesis synthesis that allows conversion of linear olefins into polymers with unsaturated polyethylene backbones, as shown in Scheme 2-21<sup>142</sup>.

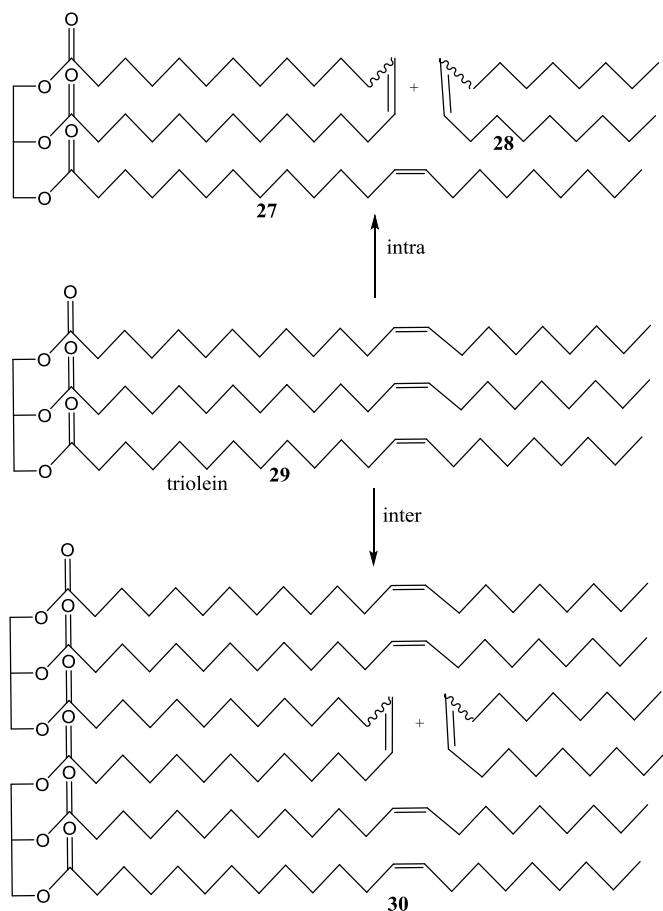


Scheme 2-21. A schematic mechanism of acyclic diene metathesis (ADMET).

ADMET can be applied to relatively small olefin molecules. The factor such as high-purity of monomers is necessary to obtain high molecular weight polymers. In addition, chain polymerization should be performed under vacuum condition in order to remove ethylene to avoid formation of side products with monomers<sup>142b</sup>. Examples of ADMET reactions can be found in the following literature<sup>143</sup>.

### Metathesis of natural oils and fats

Natural unsaturated fatty oils are raw materials for metathesis synthesis. They provide safer, less toxic fine chemicals<sup>9, 144</sup> and monomers for manufacturing of polymers<sup>2a, 144b</sup>. Drying (highly unsaturated triglycerides contain fatty acids with two or three double bonds such as linseed oil) or semidrying oils (contain one or two double bonds such as soybean oil) are able to polymerise to form a cross-linked film by air oxidation. Self-metathesis of them results in higher-molecular-weight oils (stand oils) in comparison to the raw material. Metathesis does not entail reducing the number of double bonds<sup>145</sup>. The improved drying properties of metathesis products are superior in production of printing ink, oil-based paint, synthetic resins, *etc*<sup>146</sup>. An example of self-metathesis of an unsaturated triglyceride is triolein (**29**), Scheme 2-22. This metathesis reaction, occurring in the presence of the catalyst complex  $WCl_6/Me_4Sn$ , illustrates this process<sup>147</sup>.

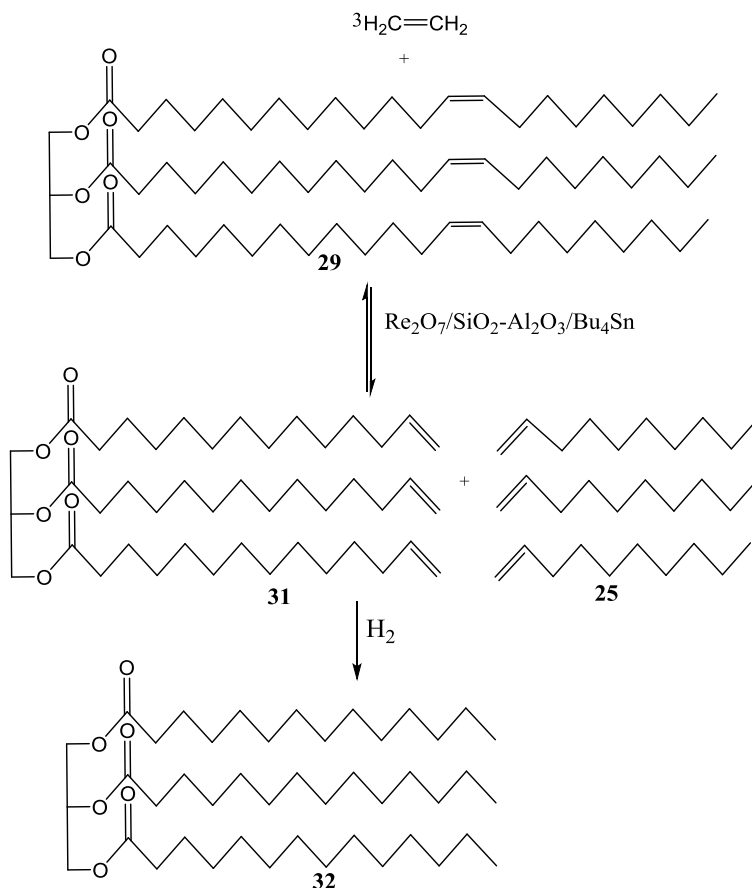


Scheme 2-22. Schematic depiction of metathesis of trioleins.

Metathesis of soybean oil was performed in the presence of the  $WCl_6/Me_4Sn$  catalyst complex<sup>148</sup>. This method has a number of disadvantages. Namely, an unsustainable chlorinated solvent was used, which induces a disposal problem. The reaction requires a large loading of this catalyst and then there is also the problem of disposing of the used catalyst. This catalyst is also sensitive to moisture and oxygen, which has an impact on reproducibility of the process<sup>149</sup>.

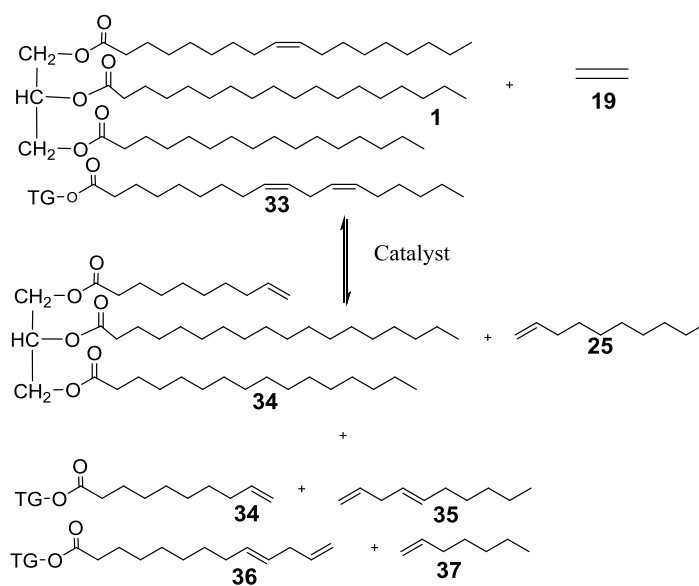
A considerable amount of metathesis of fatty oils has been carried out in the presence of the ruthenium catalyst  $Ru(=CHPh)Cl_2(PCy_3)_2$ ; an example of this work is noted in<sup>149</sup>. The reaction was carried out without the use of solvent. The reaction was carried out under moderate temperature and low pressure. An amount of the catalyst was 0.1 mol %.

Cross-metathesis of vegetable oils (soybean oil, olive, rapeseed oil) allows triglycerides to be transferred into lower triglyceride molecules and alkene products (for instance in the conversion of olive oil into tricaprin, Scheme 2-23)<sup>150</sup>.



Scheme 2-23. Production of tricaprin from olive oil via ethenolysis and after hydrogenation of the product of ethenolysis.

In our study, ethenolysis of cocoa butter over Ru catalyst complexes (**6**, **7**, **8**, **9**, **10**, Scheme 2-13)<sup>142a, 143b</sup> was performed in a batch reactor and over (**6**) and Grubbs catalyst was carried out in a flow reactor, Scheme 2-24. This work was performed by a master student Ms Christiane Schotten from RWTH Aachen University in the laboratories of the University of Cambridge.



Scheme 2-24. A scheme of ethenolysis of cocoa butter. Cocoa butter is a mixture of a variety of fatty acids. There are three unsaturated fatty acids. The main constituents are oleic and linoleic acids (see Section 3.1.5. Analytical methods – GC analysis). The scheme also shows potential products formed during the metathesis of cocoa butter.

### 3 Experimental

#### 3.1 Epoxidation of Cocoa Butter

##### 3.1.1 Materials and Chemicals

Cocoa butter raw material was obtained from Whitland Ltd and originally from Kraft Foods. It is a by-product of chocolate manufacturing process. Tungsten powder (12  $\mu\text{m}$ , 99.9%), Adogen 464 and deuterated chloroform were purchased from Aldrich. Orthophosphoric acid (85 wt. % in  $\text{H}_2\text{O}$ ), sodium chloride, chloroform, hydrogen peroxide (30 wt. % in  $\text{H}_2\text{O}$ ) were purchased from Fisher Chemicals. Anhydrous magnesium sulphate was received from Acros Organics. Reagents were used without further purification.

##### 3.1.2 Procedures of Epoxidation of Cocoa Butter in Batch and Flow Reactors

###### Batch Experiments

Tungsten powder (0.081 g, 0.44 mmol), hydrogen peroxide (1.2 mL) and deionised water (0.6 mL) were introduced into a 20 mL round-bottom flask with a stirrer bar. The mixture was heated to 50 °C and stirred until dissolving the tungsten powder for about 45 minutes. Cocoa butter (15 g, 17.3 mmol) and Adogen 464 (0.105 g, 0.26 mmol) were placed into a 250 mL round-bottom-flask, melted and stirred at a set reaction temperature: 50, 60 or 80 °C. The mixture containing the dissolved tungsten catalyst was cooled, then orthophosphoric acid (85 wt. %, 0.081 g, 0.703 mmol) in 2 mL of deionised water was added under continuous stirring. The solution of the catalyst, hydrogen peroxide (2.88 mL) and deionised water (22.9 mL) were added to the molten cocoa butter. The mixture was stirred and maintained at the desired reaction temperature. Four different catalyst compositions were used, these are listed in Table 3-1.

Table 3-1. Molar equivalents of the catalyst components used in the epoxidation of cocoa butter. The equivalents of reagents were recalculated on the average number of moles of double bonds in cocoa butter. The average number of moles in 1 mole of cocoa butter (866.67 g) is 1.15 mol. This value was determined on the basis of the FAME analysis (Table 3-4).

Catalyst composition number	W	H <sub>2</sub> O <sub>2</sub>	H <sub>3</sub> PO <sub>4</sub>	H <sub>2</sub> O	DB of CB
1	0.022	2.008	0.035	71.710	1.000
2	0.022	1.389	0.035	71.710	1.000
3	0.022	0.900	0.035	71.710	1.000
4	0.017	1.471	0.033	71.710	1.000

Legend: DB is double bond, CB is cocoa butter.

Reaction progress was monitored by disappearance of double bond in <sup>1</sup>H NMR and Raman spectra. Once the reaction was completed, the resulting emulsion was cooled and saturated sodium chloride (25 mL) and chloroform (25 mL) were added. The organic phase was separated and washed with saturated sodium chloride again (25 mL). The organic layer was dried over anhydrous magnesium sulphate and after filtration the solvent was removed using rotary evaporator.

### **Experiments under Flow Conditions**

Epoxidation of cocoa butter was performed using a Vapourtec R Series reaction system. The Vapourtec module was configured as shown in Figure 4-1. In the flow experiments viscosity of cocoa butter was reduced by adding 10 mL of toluene to the feed flask containing cocoa butter (15 g, 17.3 mmol) and Adogen 464 surfactant (0.105 g, 0.26 mmol). This mixture was maintained at 80 °C. Reaction was performed in a 10 mL volume tubular reaction module (Teflon tube of 1.00 mm ID and 12.74 m length). Reaction was performed at 80 °C.

Table 3-2. Composition of reagents used in the epoxidation of cocoa butter under batch and flow conditions.

Component	M <sub>w</sub> (g mol <sup>-1</sup> )	Batch reactor		Flow reactor	
		N (mmol)	Molar equivalent to CB (-)	N (mmol)	Molar equivalent to CB (-)
W powder	183.84	0.44	0.025	0.44	0.025
*Pure H <sub>2</sub> O <sub>2</sub>	34.01	39.99	2.31	39.95	2.31
H <sub>2</sub> O	18.01	1417	81.91	1417	81.91
H <sub>3</sub> PO <sub>4</sub>	98.00	0.70	0.040	0.70	0.040
Cocoa butter	866.67	17.3	1	17.3	1
Adogen 464	404	0.26	0.015	0.26	0.015
Toluene	92.14	-	-	0.0941	0.0054
Total		1458.39	Total	1458.48	

Legend; N is a number of mol, mmol, M<sub>w</sub> is molecular weight, g mol<sup>-1</sup>.

\*The example of the re-calculation of the amount of hydrogen peroxide (30 % wt. in water) used in the epoxidation on the pure hydrogen peroxide:

The total volume of hydrogen peroxide (30 % wt. in water) was 4.08 mL which was used in the epoxidation. The density of the hydrogen peroxide solution (30 % wt. in water) was 1.11 g cm<sup>-3</sup>.

Weight of hydrogen peroxide (30 % wt in water):

$$d = \frac{m}{V}$$

$$m = dV = 4.08 \text{ mL} \cdot 1.11 \frac{\text{g}}{\text{mL}} = 4.53 \text{ g}$$

The weight of pure hydrogen peroxide in 30 % wt. of the hydrogen peroxide solution:

$$30 \text{ g (pure hydrogen peroxide)} - 100 \text{ g (solution)}$$

$$x - 4.53 \text{ g (solution)}$$

$$x = \frac{30 \text{ g} \cdot 4.53 \text{ g}}{100 \text{ g}} = 1.36 \text{ g}$$

A number of moles of the pure hydrogen peroxide used in the epoxidation:

$$n = \frac{1.36 \text{ g}}{34.01 \frac{\text{g}}{\text{mol}}} = 0.03999 \text{ mol} = 39.99 \text{ mmol}$$

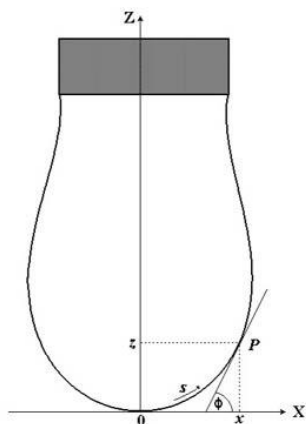
### 3.1.3 Viscosity

Rheological profiling was performed using a Kinexus Rheometer Ultra with rSpace software package (Malvern Instruments, UK). For measurements of viscosity as a function of shear rate over a range of temperatures were taken for three samples: pure cocoa butter, a mixture of cocoa butter and toluene (ratios of each), and a mixture of cocoa butter, toluene and Adogen 464 (ratios of each). These measurements were conducted at 50, 60, 70 and 80 °C over a range of shear rates 2 – 20 s<sup>-1</sup>. Additionally, viscosity as a function of temperature over the same range of shear rates was measured for a catalyst solution (concentration range) between 20 – 80 °C. In all measurements, approximately 17.1 mL of solution was introduced into a cup of geometry (PC25; C0022AL) and thermally equilibrated for 5 minutes.

### 3.1.4 Interfacial Tension

Measurements of interfacial tension between the organic and aqueous reaction phases were performed using a DSA-100 Drop Shape Analyser (Krüss GmbH Germany). This instrument provides a simple experimental setup to measure the contact angle and /or interfacial tension between two or more phases by optically measuring the profile of droplets and bubbles. For the experiments outlined in this thesis, the DSA was used in the pendant droplet mode whereby a liquid droplet of known volume is suspended in an immiscible liquid phase.

A 10 µL droplet of aqueous catalyst solution was suspended in various organic environment phases comprising of cocoa butter, toluene and the surfactant (Adogen 464) under isothermal conditions of 80 °C controlled by a Peltier temperature chamber. The droplet profile was imaged as a function of time, using the known syringe tip diameter of 1.830 mm as a scale reference. T<sub>0</sub> was taken as the formation of the droplet in the organic phase. Software analysis of the droplet profile images determines input values for the Young-Laplace Equation (3-1).



$$\Delta p = \gamma \left( \frac{1}{R_1} + \frac{1}{R_2} \right) \quad 3-1$$

where  $\Delta p$  is interfacial pressure difference (Pa),  $\gamma$  is interfacial tension ( $\text{mJ m}^{-2}$ ) and  $R_1, R_2$  are the principle radii of curvature (m).

$$\Delta p = \Delta \rho g h \quad 3-2$$

where  $\Delta \rho$  is difference in density between the drop and surrounding ( $\text{kg m}^{-3}$ ),  $g$  is acceleration of gravity ( $\text{m s}^{-2}$ )<sup>151</sup>.

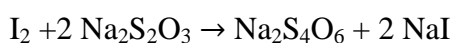
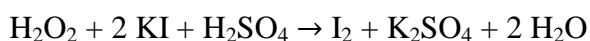
In the pendant drop method, the main assumptions are that the drop shape is symmetrical along the vertical axis and the drop is not in motion, therefore only interfacial tension and gravity influence on the shape of the droplet.

The density of cocoa butter was measured as weight of 1 mL of liquid and it is equal  $834 \text{ kg m}^{-3}$ .

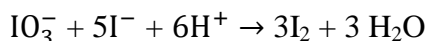
### 3.1.5 Analytical Methods

#### a) Determination of the Amount of Hydrogen Peroxide Using Iodometric Titration

The determination of the concentration of hydrogen peroxide consists in oxidation iodide to iodine by hydrogen peroxide in the presence of acid and molybdate catalyst. The iodine produced in the reaction is quantitatively titrated by thiosulfate in the presence of a starch indicator.



### Standardization of 0.1 N Thiosulfate Solution Against Potassium Iodate



Pure potassium iodate (0.14-0.15 g) was weighed, and dissolved in 25 mL of distillate water in a 250 mL of an Erlenmeyer flask. Next, 2 g of potassium iodate, 10 mL of 1 N sulphuric acid were added into the Erlenmeyer flask. Then, this solution was titrated by standard thiosulfate solution under constant stirring. A few drops of starch were added when the colour of solution became a pale yellow. The titration continued till the colour changed from blue to colourless. The analysis was repeated three times.

#### Reagents:

- Potassium iodide: potassium iodide (2 moles) was taken for hydrogen peroxide (1 mole).
- Ammonium molybdate solution: ammonium molybdate (9 g) was dissolved in 10 mL of  $\text{NH}_4\text{OH}$  (6 N).  $\text{NH}_4\text{NO}_3$  (24 g) was added to solution. Then, the whole content in the flask was diluted to 100 mL.
- Sulphuric acid solution (4 N).
- Starch indicator: starch (1 g) was dissolved into 100 mL of distilled water. The solution was brought to the boil under stirring conditions and boiled for 1 min.
- 0.1 N thiosulfate solution:  $\text{Na}_2\text{S}_2\text{O}_3 \cdot 5\text{H}_2\text{O}$  (25 g) was dissolved in 1 L of fresh boiled distilled water. Then, sodium carbonate (0.1 g) was added to solution.

#### Procedure of Determination of the Amount of Hydrogen Peroxide

The analyte solution (0.5 mL) was dissolved in 50 mL of distillate water in a 250 mL Erlenmeyer flask. Next, sulphuric acid (10 mL of 4N), potassium iodide (1 g) and three drops of ammonium molybdate solution were added into the flask. The sample was titrated by the standard thiosulfate solution using starch as an indicator.

#### b) Raman Spectroscopy

Raman spectrometer Jobin Yvon Horbia LabRam HR 800, equipped with an Olympus PX-41 microscope, 533 and 632 nm lasers and two gratings (600, 1200) was used.

Raman spectroscopy is a spectroscopic technique based on measuring inelastic scattering of monochromatic light, usually from a laser in the visible, near infrared or near ultraviolet range. Laser light interacts with the molecules of a sample, as a result the sample absorbs photons and then reemits them. The frequency of reemitted photons is shifted up and down with respect to incident light.

Many functional groups have characteristic vibration frequencies with a well-defined range. Therefore, in this investigation, Raman spectroscopy was used for qualitative and quantitative analysis of cocoa butter, epoxide and diol.

### Qualitative Analysis

Figure 3-1 shows the spectra of cocoa butter, epoxide and ring opening product in the region of 400-3200  $\text{cm}^{-1}$ . Generally, we can distinguish in all the spectra strong intense band at high frequencies of the  $\nu$  (C-H) stretching region (3000-2700  $\text{cm}^{-1}$ ) belonging to methyl ( $\text{CH}_3$ ) and methylene ( $\text{CH}_2$ ) groups of an aliphatic molecule. Next, less intense bands at lower frequencies are the ester carbonyl stretching region (1800-1700  $\text{cm}^{-1}$ ), the  $\delta$  ( $\text{CH}_2$ ) deformation region (1500-1400  $\text{cm}^{-1}$ ), the  $\tau$  ( $\text{CH}_2$ ) twisting region (1300-1250  $\text{cm}^{-1}$ ), the  $\nu$  (C-C) skeletal bands (1200-400  $\text{cm}^{-1}$ )<sup>152</sup>.

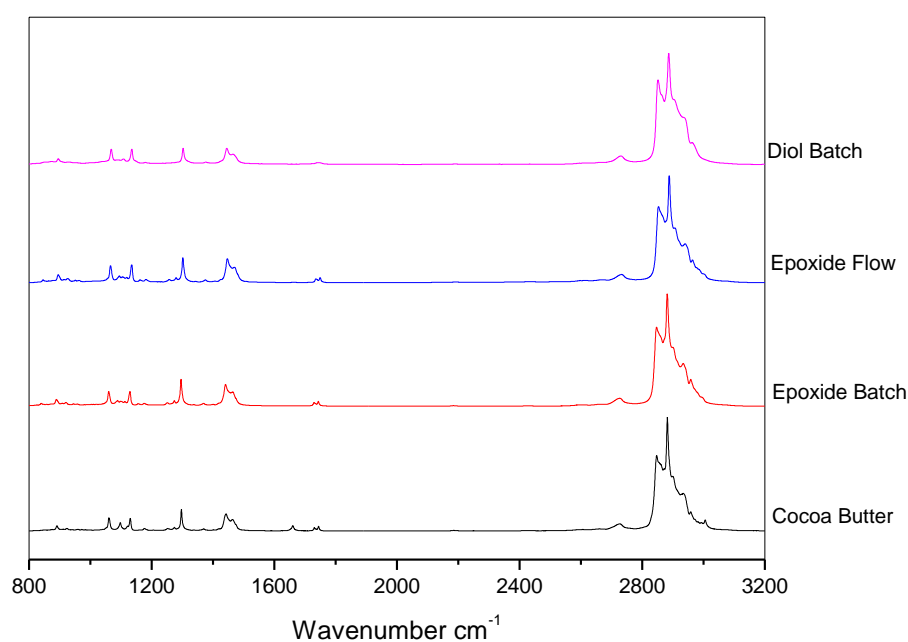


Figure 3-1. Survey Raman spectra of cocoa butter (CB), epoxide (EPX), and the ring opening product (ROP) in the region of 400-3200  $\text{cm}^{-1}$ .

The main differences in Raman spectra of these compounds are shown in more detailed spectra between 800-1700  $\text{cm}^{-1}$  in Figure 3-2. The band in the spectrum of cocoa butter at 1660  $\text{cm}^{-1}$  corresponds to stretching vibration of the double bond, the same type of vibration of the double bond is at 3005  $\text{cm}^{-1}$ . The band at 1156  $\text{cm}^{-1}$  represents the oxirane bond in the epoxide spectrum. The band at 1032  $\text{cm}^{-1}$  corresponds to stretching vibration between C-O in C-O-H group and is observed in the diol spectrum. In addition, Raman intensity of the band at 1096  $\text{cm}^{-1}$  is reduced if compared to the epoxide spectrum (Figure 3-2 and Appendix A. 2). The qualitative

analysis of spectrum was performed using the table of bonds in <sup>153</sup>. We did not observe differences between spectra of epoxides which were produced in a batch and flow reactors. Raman spectra from qualitative analysis of cocoa butter, epoxide and diol are attached in Appendices A. 1, A. 2 and A. 3 A. 3. Raman bands of compounds are given in Table 3-3.

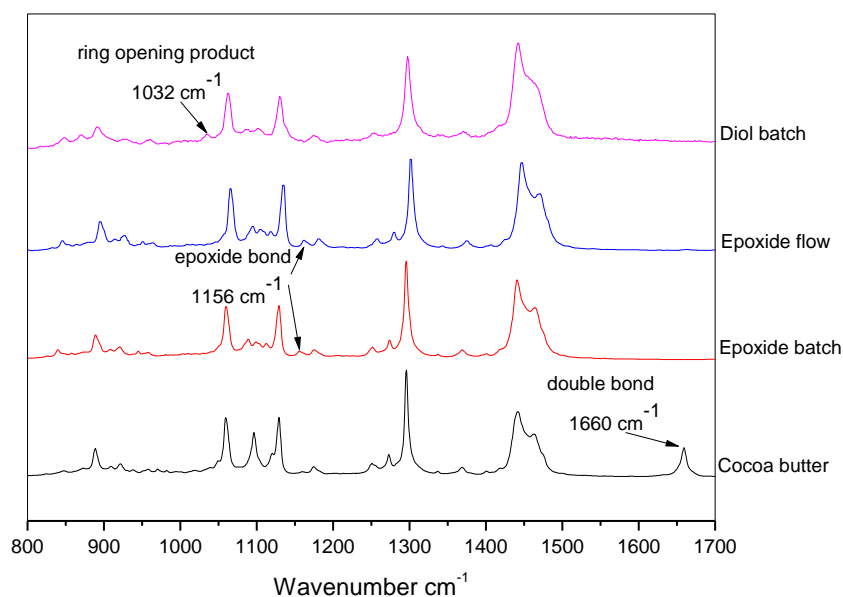


Figure 3-2. Raman spectra of cocoa butter (CB), epoxide under batch and flow conditions and diol.

Table 3-3. Raman bands for cocoa butter, epoxide and diol.

Assignments	Cocoa butter	Epoxide	Diol
	478	-	-
	-	503	-
	-	-	534
	-	578	-
	-	667	-
	-	-	708
	-	717	-
	-	-	760
	-	767	-

**Experimental**

$\nu$ (C-O) in C-O-H	-	-	1032
group			
$\nu_{\text{as}}$ (C-C)T	1060	1060	1060
$\nu$ (C-C)	-	-	1084
$\nu$ (C-C)	-	1088	-
$\nu$ (C-C)	1096	-	-
$\nu$ (C-C)	-	-	1106
$\nu$ (C-C)	-	1113	-
$\nu_{\text{s}}$ (C-C)T	1130	1130	1130
$\nu$ (C-O) oxirane	-	1156	-
bond			
r (CH <sub>2</sub> )	1174	1173	1176
$\tau$ (CH <sub>2</sub> )	1250	1250	1253
$\tau$ (CH <sub>2</sub> )	1273	1273	-
$\tau$ (CH <sub>2</sub> )	1296	1296	1296
$\tau$ (CH <sub>2</sub> )	1339	1339	1339
$\tau$ (CH <sub>2</sub> )	1372	1369	1371
$\tau$ (CH <sub>2</sub> )	1418	1399	1416
$\delta_{\text{as}}$ (CH <sub>2</sub> )	1444	1442	1442
$\delta_{\text{as}}$ (CH <sub>2</sub> )	1467	1463	1463
$\nu_{\text{s}}$ (C=C)	1660	-	-
$\nu$ (C=O)	1730	1730	1730
$\nu$ (C=O)	1743	1743	1743
$\nu$ (CH <sub>3</sub> -CH <sub>2</sub> )	2726	2727	2728
$\nu_{\text{s}}$ (CH <sub>2</sub> )	2847	2847	2847
$\nu_{\text{as}}$ (CH <sub>2</sub> )	2881	2881	2881
$\nu_{\text{s}}$ (CH <sub>3</sub> )	2933	2934	2933
$\nu_{\text{as}}$ (CH <sub>3</sub> )	2958	2961	2960
$\nu$ (C=C)	3005	-	-

Legend:  $\nu$  = stretch, as = antisymmetric, s = symmetric, T = trans,  $\delta$  = deformation,  $\tau$  = twist, r = rock.

### Quantitative Analysis of Cocoa Butter using Raman Spectroscopy

Raman spectra were used to monitor the progress of the epoxidation of cocoa butter. In this case the intensity of the band at  $1660\text{ cm}^{-1}$  relative to the double bond of cocoa butter and also the band at  $1372\text{ cm}^{-1}$  relative to the twisting bond of  $\text{CH}_2$  an internal standard were considered. The range of  $1220\text{-}1700\text{ cm}^{-1}$  in spectra was normalized. In the first step the baseline of the spectrum was determined see Figure 3-3.

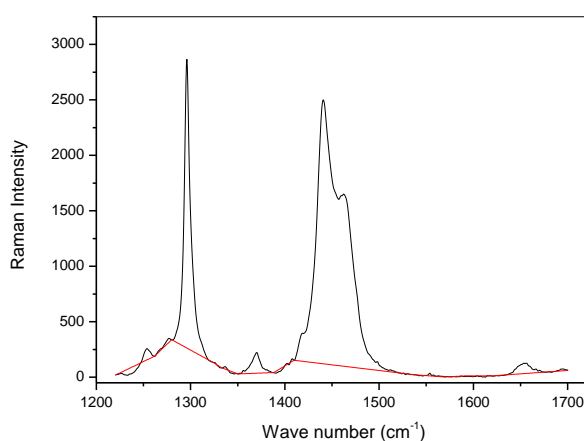


Figure 3-3. Raman spectrum of 30 minutes of epoxidation of cocoa butter. The first step in the normalization spectrum – the determination of the baseline of spectrum.

In the next step the spreadsheet data column of the baseline intensity ( $I^b$ ) was subtracted from the column of the initial intensity ( $I^0$ ) to determine the flat baseline of the spectrum.

$$I^0 - I^b = I^f \quad 3-3$$

In the next step, the area of the range was determined. The spreadsheet data column including flat intensity data was divided by the area of the spectrum in the range of  $1220\text{-}1700\text{ cm}^{-1}$  to determine the normalised intensity ( $I^n$ ).

$$\frac{I^f}{A} = I^n \quad 3-4$$

In this way the modified spectrum was used to determined heights of the bands of interest. The amount of double bond (C) which was left after the reaction at the considered time was calculated in the following way:

$$C = \frac{H^{1660}}{H^{1372}}$$

3-5

where  $H^{1660}$  and  $H^{1372}$  are heights of the double bond and the internal standard at  $1372\text{ cm}^{-1}$ , respectively.

### c) NMR Analysis

$^1\text{H}$  NMR measurements were obtained on a Bruker DPX-400 spectrometer at room temperature and using deuterated chloroform as solvent. The progress of epoxidation of cocoa butter was monitored by disappearance of double bond ( $\delta = 5.30 - 5.39$  ppm) and appearance of oxirane bond ( $\delta = 2.85 - 2.96$  ppm) relative to oleic epoxide. The glycerol bond signal at  $4.25 - 4.34$  ppm was used as an internal standard, according to methodology described in <sup>154</sup>. In this work the method of determination of the fatty acid composition was developed in edible oils using  $^1\text{H}$  NMR spectra. A good efficiency and accuracy was confirmed by comparing the findings with the AOCS (American Oil Chemists' Society) Official method by GC <sup>155</sup>. In our research accuracy of this method was confirmed by comparing with Raman analysis of the disappearance of double bond (Figure 4-7).

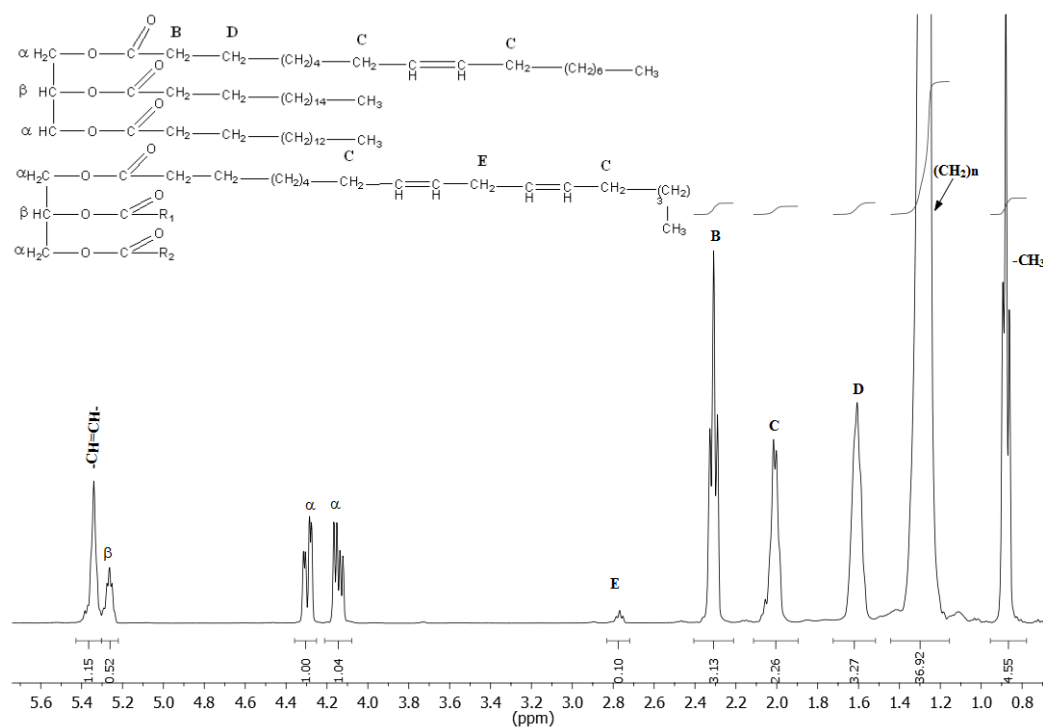


Figure 3-4.  $^1\text{H}$  NMR spectrum of a raw cocoa butter material with proton area integration. The integration area of the signal at 5.36 ppm contains the protons of

oleic, palmitoleic and linoleic acid. The concentrations of oleic, palmitoleic and linoleic double bond are 84.1 %, 0.8 % and 15.1 %, respectively, (Table 3-4).

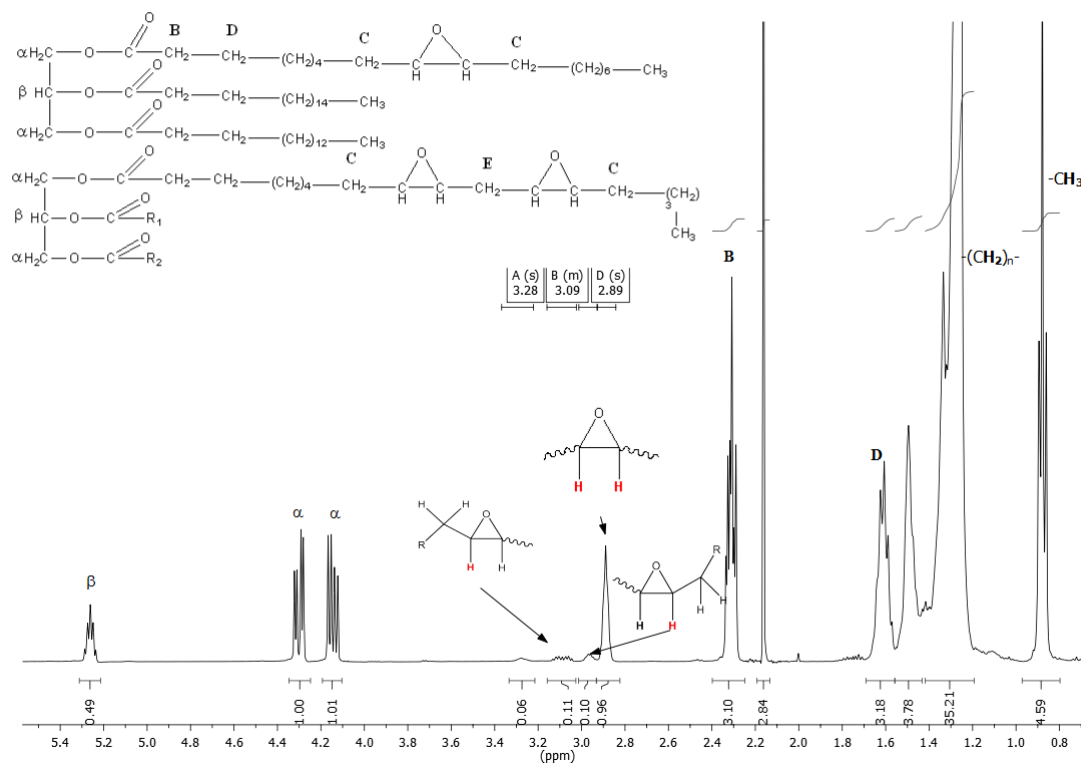


Figure 3-5. <sup>1</sup>H NMR spectrum of epoxide products with proton area integration. The signal of two protons relative to oleic acid is at 2.89 ppm. The signals at 2.96 ppm and 3.09 ppm correspond to CH protons attached to oxirane bond of linoleic epoxide. <sup>1</sup>H NMR spectra of Adogen 464 is shown in Appendix A. 4 and of a ring opening product in Appendix A. 5.

#### d) GC Analysis

A fatty acid methyl ester (FAME) analysis was carried out by the Clark group in Warwick Analytical Service.

Based on GC analysis, six fatty acids were identified in the sample of cocoa butter used in this study. The three main constituents were found to be: stearic, oleic and palmitic acids. Minor components found are: palmitoleic, linoleic and arachidic

acids. Results of the GC analysis are summarised in Table 3-4. This Table 3-4 shows that the cocoa butter composition of fatty acids is similar to the cocoa butter originated from Ghana. According to GC analysis the average weight of one fatty acid chain in the triglyceride is  $276.2 \text{ g mol}^{-1}$  therefore the average weight of cocoa butter is  $866.6 \text{ g mol}^{-1}$ .

Table 3-4. GC analysis of fatty acid methyl ester.

Fatty acids	Molecular weight of FA / $\text{g mol}^{-1}$	Fraction of FA / %	Molecular weight of FA in CB / $\text{g mol}^{-1}$	Fraction of FA Ghanaian CB / % <sup>156</sup>	Fraction of DB in CB / %
Palmitic					
C16:00	256	25.8	66	25.3	0
Palmitoleic					
C16:1n7	254	0.3	0.7		0.8
Stearic					
C18:00	284	37.9	107.6	37.6	0
Oleic					
C18:1n9c	282	32.2	90.8	32.7	84.1
Linoleic					
C18:2n6c	280	2.9	8.2	2.8	15.1
Arachidic					
C20:00	312	0.9	2.9	1.2	0
	$\Sigma =$	100	276.2		100

CB - cocoa butter; FA - fatty acid; DB - double bond.

#### e) Reaction Calorimetry

The heat of reaction was measured using the CPA202 reaction calorimeter from ChemiSens. This reactor is pre-calibrated. It means that the heat production rate is directly shown on line. In the CPA202 reaction calorimeter the temperature at two places inside the reactor wall is determined,  $T_1$  and  $T_2$ . The element which controls temperature in the reaction calorimeter is a Peltier element. It is located beneath the reactor bottom. The Peltier element does not take place in the measurement of heat

flow. It controls the temperature in the reactor by heating or cooling. The main heat flow sensor, recording the temperature  $T_1$  and  $T_2$ , is placed between the reactor bottom and the Peltier element, see Figure 3-6.

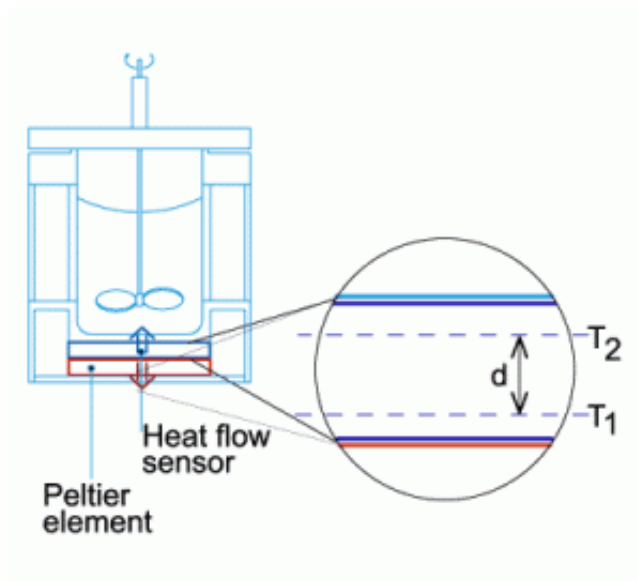


Figure 3-6. Schematic diagram of a CPA202 reaction calorimeter. Adapted from <sup>157</sup>.

The true heat flow  $\dot{q}_{\text{true flow}}$  (W) is calculated in the following way:

$$\dot{q}_{\text{true flow}} = \frac{\lambda}{d} \cdot A \cdot (T_2 - T_1) \quad 3-6$$

where  $\lambda$  transducer heat conductivity ( $\text{W m}^{-2} \text{K}^{-1}$ ) of assembly materials.  $A$  is the heat transfer area ( $\text{m}^2$ ) and  $d$  is the length between two points where the temperature difference is measured. The heat of reaction is determined from the following equation:

$$\Delta_r H = \frac{\int_0^\infty \dot{q}_{\text{true flow}} dt}{n_{i,0}} \quad 3-7$$

where  $n_{i,0}$  is the initial amount of reagent.

The measurements were carried out in DECHEMA Research Institute in Frankfurt, Germany, in Dr. Lasse Greiner' laboratory.

## 3.2 Reduction of Artemisinin

### 3.2.1 Materials and Chemicals

Artemisinin samples were kindly donated by Ipca Laboratories Ltd, India and Botanical Extracts EPZ Ltd., Kenya. Super Hydride<sup>®</sup> Solution (1.0 M lithium triethylborohydride in THF), 2-methyltetrahydrofuran (2Me-THF) (anhydrous  $\geq 99.0\%$ ), methanol (anhydrous  $\geq 99.8\%$ ), sodium borohydride, acetic acid (ReagentPlus<sup>®</sup>  $\geq 99\%$ ) were obtained from Sigma-Aldrich. Nitrogen was obtained from BOC Ltd. Sodium sulphate, ethyl acetate were purchased from Fisher Scientific.

### 3.2.2 Reduction of Artemisinin with NaBH<sub>4</sub>

Artemisinin (200 mg, 0.71 mmol) was suspended in methanol (10 mL) under moderate stirring speed and cooled in an ice-water bath to *ca.* 4 °C. Sodium borohydride (67 mg, 1.77 mmol, 2.5 equivalent) was added in portions to the suspension over a period of 5 minutes. The reaction mixture was stirred vigorously under N<sub>2</sub> until thin liquid chromatography (TLC) showed no artemisinin left in the reaction mixture (*ca.* 90 min). Then the reaction mixture was neutralised (pH 5-6) with 50 % v/v of a mixture of acetic acid/methanol (added by portion, 50  $\mu$ L each time). The reaction mixture was evaporated to dryness under vacuum (at 40 °C). This standard procedure was developed by Buzzi *et al*<sup>158</sup>.

Work up Procedure:

Dry residue was extracted using ethyl acetate 2-3 times (10 mL each time) for transferring the product completely (monitored by TLC) into ethyl acetate. The combined ethyl acetate extracts were dried with Na<sub>2</sub>SO<sub>4</sub> (for 6 hours), filtered and evaporated to dryness to give a white flake-like product.

### 3.2.3 Reduction of Artemisinin with LiBHET<sub>3</sub>

LiBHET<sub>3</sub> solution (1 M in THF) was added (with a syringe) dropwise to the solution of artemisinin in dry THF (200 mg, 0.71 mmol; 20 mL) stirred under N<sub>2</sub> (reactions were performed at *ca.* 2 °C and *ca.* 19 °C). The stirring was continued until TLC showed no artemisinin left in the reaction mixture (5 – 10 min). Temperature of the

reaction mixture was maintained constant by either using a water bath or ice-water bath. An acetic acid solution in THF (20 % v/v) was added by portions (100  $\mu$ L or 50  $\mu$ L each time) to quench the reaction mixture to pH 5-6. The reaction mixture was vacuum evaporated to dryness. Ethyl acetate and distilled water were used to extract the product from the dry residue. The two phases were separated and the aqueous layer was extracted with ethyl acetate twice. The combined ethyl acetate extracts were dried with  $\text{Na}_2\text{SO}_4$  for 6 hours, filtered, and evaporated to dryness under reduced pressure to give a white flake-like product.

HPLC was used to quantify substrate and products over the standards. Results of reduction of ART were identified in terms of the conversion ART

$$\text{Conversion}_{\text{ART}} = \frac{\text{Moles of ART reacted}}{\text{Initial moles of ART}} \quad 3-8$$

and in terms of the yield to the sum of DHA  $\alpha$  and DHA  $\beta$  as;

$$\text{Yield}_{\text{DHA}\alpha/\beta} = \frac{\text{Moles of sum DHA } \alpha \text{ and } \beta \text{ obtained}}{\text{Initial moles of ART}} \quad 3-9$$

### 3.2.4 Flow Synthesis Procedure

The reactor was an XXL-ST-03 by The Little Things Factory GmbH, with reactor internal volume of 3 mL and incorporating an internal cross-flow heat exchanger. Solution of artemisinin was pumped with a Kontron 42 HPLC pump. The  $\text{LiBHET}_3$  solution was prepared under inert atmosphere and pumped employing a Knauer 100 HPLC pump. After the reaction a Y-shaped micromixer was used to quench the reaction with an acetic acid solution. The pH of the solution was controlled in the collected aliquots.

### 3.2.5 Reduction of 9-epi Artemisinin

Approximately 0.2 mL of  $\text{LiBHET}_3$  solution (1 M in THF) was added (with a syringe) dropwise to a solution of 9-epi-artemisinin in dry THF (9.6 mg, 0.034 mmol; 1 mL) stirred under  $\text{N}_2$  at *ca.* 2  $^\circ\text{C}$ . Stirring continued for 10 min. Temperature of the reaction mixture was kept constant by an ice-water bath. Acetic acid solution in THF (20 % v/v) was added in stages (10  $\mu$ L each time) to quench the reaction mixture to pH 5-6. The reaction mixture was evaporated to dryness under  $\text{N}_2$ . Ethyl acetate and distilled water were used to extract the product from the dry

residue. The two phases were separated and the aqueous layer was extracted with ethyl acetate twice. The combined ethyl acetate extracts were dried with  $\text{Na}_2\text{SO}_4$  for six hours, filtered, and evaporated to dryness under  $\text{N}_2$ .

### 3.2.6 Analytical Protocols

(a) TLC, eluents:  $\text{CH}_2\text{Cl}_2$  + MeOH (v/v = 20/0.5). Developing agent: phosphomolybdic acid.

(b)  $^1\text{H-NMR}$ , Bruker ICONNMR.  $^1\text{H}$  NMR (300 MHz,  $\text{CDCl}_3$ ,  $25^\circ\text{C}$ , TMS):  $\delta$ = 0.94 (d,  $J$ = 6.8 Hz, 6H,  $\text{CH}_3$ ), 1.24 (s, 3H,  $\text{CH}_3$ ), 1.65 (dd,  $J_1$ = 3.4 Hz,  $J_2$ = 13.2 Hz, 2H) 1.8-1.9 (m, 4H), 2.0-2.1 (m, 1H), 2.33 (m, 1H), 4.73 (d,  $J$ =9.2 Hz, 1H), 5.26 (t,  $J$ =3.2 Hz, 1H), 5.37 (s, 1H), 5.58 (s 1H).

(c) HPLC, Shimadzu Prominence instrument equipped with ELSD-ET (low temperature-evaporative light scattering detector), cell temperature  $40^\circ\text{C}$ , polarity +, response time 1.5 s; column:

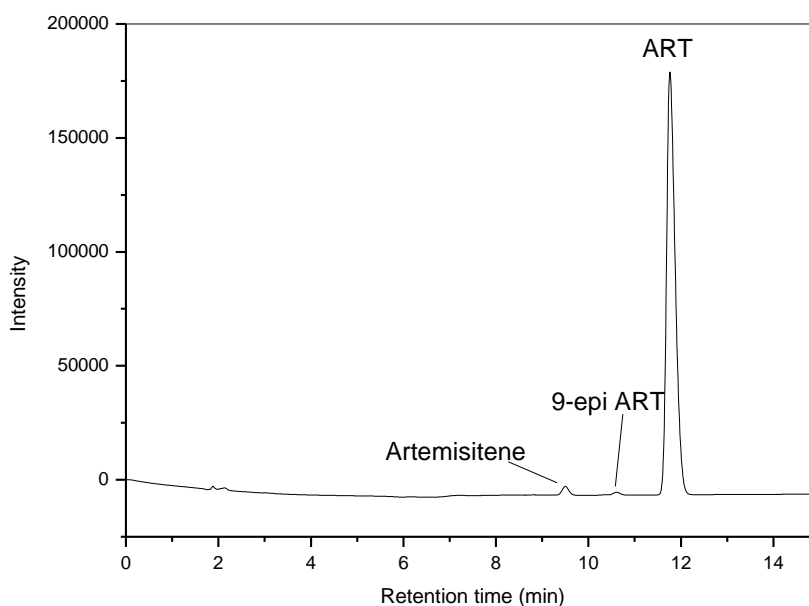


Figure 3-7. HPLC chromatogram of a raw material used for the reduction of ART.

The concentrations of artemisitene was 0.3 % and 9-epi artemisinin was 0.07%.

Column: Thermo, 250 x 4.6 mm, 5  $\mu$ m, Betasil C18, column oven temperature 45  $^{\circ}$ C

Mobile phase: acetonitrile/ water/ (65/35/ v/v)

Flow rate: 0.8 mL min<sup>-1</sup>

Run time: 15 min

Detection: UV detector

Sample: *ca.* 2 mg in 1 mL acetonitrile each time

Injection: 20  $\mu$ L

Retention time for: ART is 11.8 min, 9-epi artemisinin is 10.6 min, artemisitene is 9.5 min.

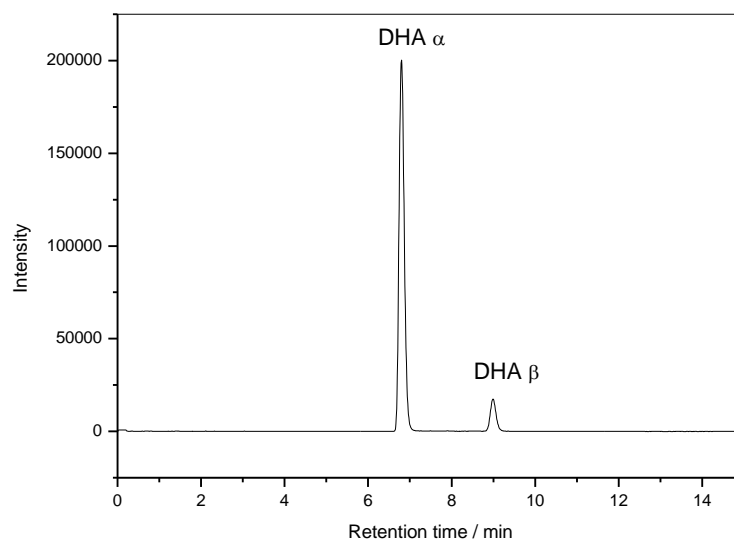


Figure 3-8. HPLC chromatogram of standard dihydroartemisinin.

Column: Thermo, 250 x 4.6 mm, 5  $\mu$ m, Betasil C18, column oven temperature 45  $^{\circ}$ C

Mobile phase: acetonitrile/ water/ (65/35/ v/v)

Flow rate: 0.8 mL min<sup>-1</sup>

Run time: 15 min

Detection: scattering detector

Sample: *ca.* 2 mg in 1 mL acetonitrile each time

Injection: 20  $\mu$ L

Retention time fo: DHA  $\alpha$  is 6.8 min, DHA  $\beta$  is 9.0 min

(d) LC-MS, Dionex 3000RS UHPLC coupled with Bruker MaXis Q-TOF mass spectrometer, A Sigma Ascentis Express column (C18, 150 × 2.1 mm, 2.7 μm) was used. Mobile phases were consisted of A (water with 0.1% formic acid) and B (as acetonitrile with 0.1% formic acid). A gradient of 30% B to 100% B in 15 minutes was employed with flow rate at 0.2 mL min<sup>-1</sup>, UV was set at 220 nm. A mass spectrometer was operated in electrospray positive mode with a scan range 50 – 2,000 m/z. Source conditions are: end plate offset at –500 V; capillary at –4500 V; nebulizer gas (N<sub>2</sub>) at 1.6 bar; dry gas (N<sub>2</sub>) at 8 L min<sup>-1</sup>; dry temperature at 180 °C. Ion transfer conditions as, ion funnel RF at 200 Vpp; multiple RF at 200 Vpp; quadruple low mass set at 55 m/z; collision energy at 5.0 eV; collision RF at 600 Vpp; ion cooler RF at 50 – 350 Vpp; transfer time set at 121 μs; pre-pulse storage time set at 1 μs. Calibration was done with sodium formate (10 mM) through a loop injection of 20 μL of standard solution at the beginning of each run.

### (e) Mass Spectrometry Analysis

#### Sample Preparation

A weighed amount of sample (reaction mixture) was dissolved in 0.5 mL of methanol and 50 μL of the solution was further diluted with 950 μL of mobile phase. The resulting dilution was used for MS analysis.

### Acquity Liquid Chromatography Method

The liquid chromatography analyses were performed with an Acquity TQD (Waters Corp., Milford, MA, USA) coupled to an Acquity tandem quadrupole detector. The high-pressure liquid chromatography (HPLC) system consisted of a binary pump and a cooling auto-sampler set at 10 °C with an injection loop of 10 μL. The column heater was set at 30 °C and a Genesis® Lightn C18 column (100 mm × 2.1 mm; 4 μm) (Grace, IL, USA) protected by an Acquity UPLC column in-line filter unit (0.2 μm in-line frit) was used for the separation of the metabolites. The mobile phase consisted of A: 0.1 % formic acid in water and B: 0.1 % formic acid in acetonitrile. Chromatographic separation was achieved with a linear gradient: 0–7.0 min, 25-98 % B; 7-9.5 min, 98 % B; 9.5-10 min, 98-25% B; 10-15 min, 25 % B; at a flow rate of 0.4 mL min<sup>-1</sup>. Weak wash solvent was 10 % acetonitrile. The strong and needle

wash solvents were a mixture of acetonitrile, propan-2-ol, methanol and water (30:30:30:10 v/v/v/v).

### **Tandem Mass Spectrometry (MS/MS) Method**

The MS/MS system was operated with an ESI interface in positive ionization mode (ESI+) and acquisition was performed in MRM mode. The cone and de-solvation gas flow rates were set at 45 L h<sup>-1</sup> and 800 L h<sup>-1</sup>, respectively and the capillary voltage, the source and the de-solvation temperatures were similar for all analytes at 28 kV, 150 °C and 350 °C, respectively. MS parameters were automatically defined by Waters IntelliStart® software for the tuning and calibration of the TQD and subsequently manually optimized as shown in Table 3-5. Quantification was determined by multiple reaction-monitoring (MRM) modes for the above transitions. The dwell time was automatically set at 0.161 seconds. Data were acquired by MassLynx V4.1 software and processed for quantification with QuanLynx V4.1 (Waters Corp., Milford, MA, USA).

Table 3-5. TQD parameters for MS/MS experiments.

Metabolites	Cone Voltage (V)	Collision Voltage (V)	MRM transitions
Artemisinin	24	7	283→219+229+247+265
9-Epi-artemisinin	30	12	283→209+219+247+265
DHA	32	10	285→222+250+268
β-artemether (IS)	20	5	299→221+249+267

#### **3.2.1 Mass Spectrometry**

Mass spectrometry is an analytical method which allows production and weighting of ions from a molecule in order to obtain its molecular weight and structural information. It is the most sensitive of all analytical techniques. Mass spectroscopy unlike other spectroscopy techniques does not rely on electromagnetic radiation. It relies on chemical manipulations such as ionization and fragmentation. The intensity of each peak corresponds to the quantity of relative ions <sup>153b</sup>.

The mass spectrometer used in this work comprises two components: it has a liquid chromatography part (which in our case is Acquity Liquid Chromatography – LC) and a tandem quadrupole detector (TQD) or, simply, a tandem mass spectrometer. This instrument enables the separation and detection of components of organic mixture.

### Tandem Mass Spectrometry (MS/MS) Method

Tandem mass spectrometry is applied to describe individual molecules in a complex mixture or to determine a molecule's structure. These aims are achieved by separating the ionization process from the fragmentation step and controlling the process of fragmentation. Mass analysis must be carried out twice in a tandem device in order to determine both the parent and the product ion. This can be done by splitting the mass analysis in space or by splitting them in time (see Figure 3-9)<sup>153b</sup>.

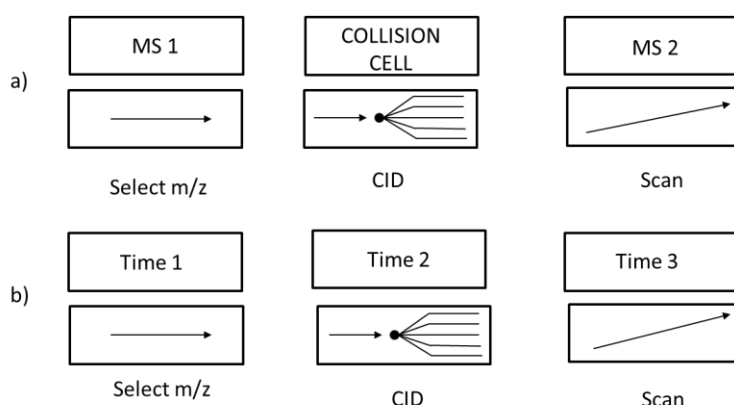


Figure 3-9. Tandem mass spectrometry: a) separation in space b) separation in time.

Adapted from<sup>153b</sup>.

A tandem mass spectrometer comprises two mass spectrometers separated by a special chamber. The abbreviation MS/MS derives from MS - chamber - MS = MS/MS. A prepared sample for analysis is injected into the first mass spectrometer. Ionization takes place in order to produce molecular ions. The molecules are characterised depending on their mass-to-charge ( $m/z$ ) ratio. The ionized ions are ordered and weighed. Then the ionized molecules are sent into the collision cell chamber. Inside the chamber, the ionized molecules are divided into fragmented pieces called *analytes*. After this process, the sample is transferred into the second

mass spectrometer. Inside that spectrometer, amounts of the second analytes are ordered and weighed according to their  $m/z$  ratio. The results of analysis are compared with the internal standard in terms of quality and quantity<sup>159</sup>.

### 3.3 Etherification of Dihydroartemisinin to Artemether

#### 3.3.1 Materials and Chemicals

To obtain DHA for etherification reaction, artemisinin was reduced by superhydride solution (1.0 M lithium triethylborohydride in THF) in a batch reactor according to procedure described elsewhere<sup>160</sup>. Artemisinin samples were kindly donated by Ipca Laboratories Ltd, India (impurities: 0.35 % of artemisitene and 0.10% of 9-epi artemisinin detected by Shimadzu HPLC) and Botanical Extracts EPZ Ltd., Kenya (impurities: 0.32 % of artemisinin and 0.52 % of 9-epi artemisinin detected by Shimadzu HPLC). The obtained DHA was analysed by HPLC and dissolved in a mixture of Me-THF (Sigma Aldrich, 99.0%) and methanol (Analar Normapur, 99.8%, anhydrous) to the concentration of 23.8 mmol L<sup>-1</sup> (batch system) and 54.6 mmol L<sup>-1</sup> (flow system). Then DHA etherification to artemether was performed in batch and flow reactors with two different types of acidic catalysts, Amberlyst-15 (Sigma Aldrich, concentration of acid sites is ~4.7 mol kg<sup>-1</sup>, specific surface area 53 m<sup>2</sup> g<sup>-1</sup>), and QuadraSil-SA (kindly provided by Johnson Matthey, concentration of acid sites is ~ 1.4 mol kg<sup>-1</sup>, specific surface area 700 m<sup>2</sup> g<sup>-1</sup>). Different equivalents of acidic sites to DHA were used and specified along with reported results. Sodium bicarbonate (Fisher, 99.7%) was used in both batch and flow conditions to quench the reaction catalysed by Amberlyst-15.

#### 3.3.2 Batch Etherification of Dihydroartemisinin

The procedure for batch reduction of ART to DHA with superhydride is described in chapter 3.2.3 Reduction of Artemisinin with LiBHET<sub>3</sub>.

- a) Etherification of a solution of  $\alpha/\beta$ -DHA to artemether with Amberlyst-15 (0.25 and 1 molar equivalents of active sites/DHA) in a batch reactor was performed as follows: DHA (0.3138 g; 1.1035 mmol) was dissolved in 2-Me-THF (45.79 mL) under stirring at ambient temperature. Anhydrous methanol (MeOH/DHA=12.6 excess) was injected into the flask. Then the calculated amount of Amberlyst-15 was added to the mixture to start the reaction. Reaction was typically continued for four hours. Periodic aliquots were taken for HPLC analysis. The size of the aliquots was sufficiently small to ignore

the influence of the change of volume and on the reaction kinetics. The same experiment was run at 40 °C using an oil bath.

Work-up procedure was as follows: 15 mL of cold water was added to the reaction mixture. Amberlyst-15 was separated from the mixture by filtration and washed by 5 mL of anhydrous methanol. The organic mixture was quenched by 15 mL of 5% NaHCO<sub>3</sub> and stirred for 1 hour in an ice bath. 2-Me-THF and methanol solvents were evaporated under vacuum at room temperature. The product was separated from water, washed several times with water and dried in a Buchner flask.

- b) Etherification of DHA to artemether with QuadraSil-SA (0.25 and 0.41 molar equivalents of active sites/DHA) in a batch reactor was performed as follows: DHA (0.1452 g; 0.511 mmol) was dissolved in 2-Me-THF (21.18 mL) under stirring at ambient temperature. Anhydrous methanol (MeOH/DHA=12.6 excess) was injected into the flask. Then the calculated amount of QuadraSil catalyst was added to the prior prepared mixture and stirred for four hours. The progress of reaction was monitored by HPLC. The same experiment was run at 40 °C using an oil bath.

Work-up procedure was as follows: 15 mL of cold water was added to the reaction mixture. QuadraSil was separated from the mixture by filtration and washed by 5 mL of anhydrous methanol. The filtrate was stirred for 1 hour in an ice bath. 2-Me-THF and methanol solvents were evaporated under vacuum at room temperature. The product was separated from water, washed several times with water and dried in a Buchner flask.

Results of etherification were quantified in terms of the yield of  $\beta$ -artemether with respect of the initial concentration of DHA. In the absence of a standard for  $\alpha$ -artemether it was not routinely analysed.

### 3.3.3 Flow Etherification of Dihydroartemisinin

Flow etherification of  $\alpha/\beta$ -DHA solutions to artemether was performed using an Omnifit column with an ID of 10 mm and an adjustable catalyst bed length of 4 – 12 cm. The column was thermostated in an oil bath at 40 °C. The feed mixtures of DHA in 2-Me-THF and MeOH were pumped using Kontron 42 and Knauer 100 HPLC pumps. In the case of the Amberlyst-15 catalyst the product mixture was quenched by 5 % aqueous sodium bicarbonate to neutralise leached acid. In the case of the QuadraSil catalyst was diluted with broken quartz prior to packing.

The work-up procedure was the same as in the batch experiments. Approximately 10 mL of ARM solution product was collected for analysis each time. Thus, 3 mL of cold water was added to the reaction mixture. Amberlyst-15 was separated from the mixture by filtration and washed with 1 mL of anhydrous methanol. The organic mixture was quenched with 3 mL of 5% NaHCO<sub>3</sub> and stirred for 1 hour in an ice bath. 2-Me-THF and methanol solvents were evaporated under vacuum at room temperature. The product was separated from water, washed several times with water and dried in a Buchner flask. In the case of the QuadraSil procedure, the quenching step was omitted.

### 3.3.4 Analytical Protocols

#### **pH Analysis**

A Jenway 3505 pH meter was used. It was calibrated using pH 4, 7 and 10 buffer solutions. The pH meter was used to measure the pH of the methanol at the exit of the catalyst column in the blank experiments. Pure methanol was pumped through the Amberlyst and QuadraSil-packed reactors.

#### **HPLC Analysis**

A 100  $\mu$ L aliquot of liquid from the reaction flask or from the product collected at the end of the flow reactor was taken and quenched with 100  $\mu$ L of 0.5 % NaHCO<sub>3</sub>. The solution was diluted with 1 mL of acetonitrile directly before filtering through a nylon syringe filter and placing the sample into a HPLC sample vial rack to reduce the possibility of DHA decomposing of in the acetonitrile. Decomposition of DHA was observed during reanalysis of the samples. For instance, reanalysis of a sample

after an interval of 3 h showed 7.4 % higher conversion of DHA than the prior analysis. The sample was stored at ambient temperature (Figure 3-10).

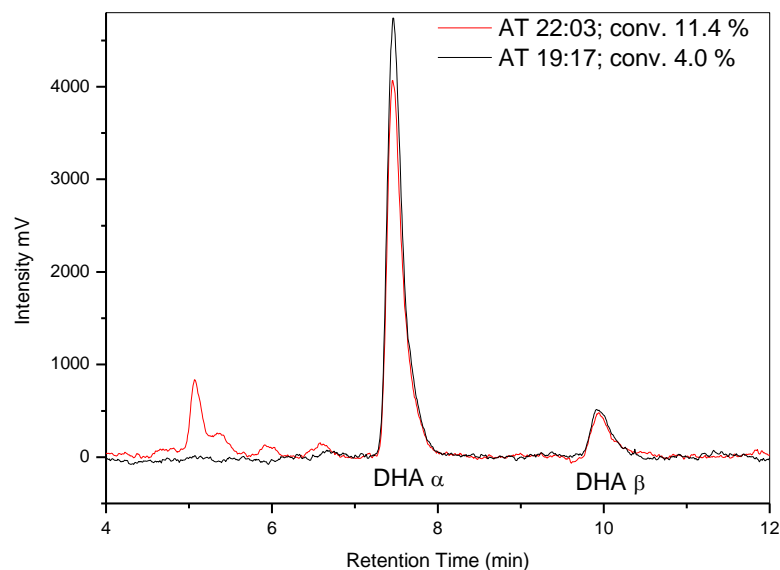


Figure 3-10. HPLC chromatograph of a sample 7 (17.04.13) from the conversion of DHA to ARM in the presence of 0.5 mol eq. of Amberlyst 15 in a batch reactor. The analysis was performed twice separated by an interval of *ca.* 3 h. Analysis was performed using an ELSD detector.

A Shimadzu Prominence HPLC equipped with an ELSD and UV/VIS photodiode array detector was used.

DHA  $\alpha$  and  $\beta$  were detected on ELSD–ET detector and ARM  $\beta$  was detected on a UV detector using its absorbance at 216 nm. DHA and  $\beta$ -artemether were quantified against standards. Due to the unavailability of  $\alpha$ -artemether standard, it was not routinely quantified. Assuming that  $\alpha$ -artemether has a similar response factor as the calibrated  $\beta$ -artemether, in several experiments the yield of  $\alpha$ -artemether was estimated to be *ca.* 16 – 24 % when the yield of  $\beta$ -artemether was between 53 – 74%, with  $\beta/\alpha$  ratio of *ca.* 3. Although a different length HPLC column was used from that reported in [8], a similar order of peaks was observed, which allow us to suggest that the earlier reported impurity, 9-*epi*-artemether, was also produced. Its quantification

was not performed; a very crude estimate based on the same response factor as  $\beta$ -artemether suggested < 9 % yield of the impurity.

Figure 3-11 and Figure 3-12 show the HPLC chromatograms results of the conversion DHA to ARM in batch reactors with Amberlyst and QuadraSil.

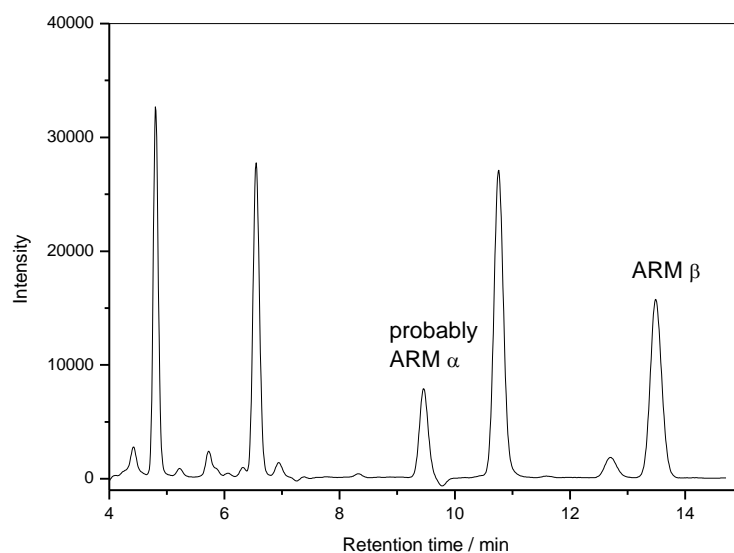


Figure 3-11. HPLC chromatograph of conversion of DHA to ARM with Amberlyst 15 in a batch reactor in a 180 min experiment.

Column: Thermo, 250 x 4.6 mm, 5  $\mu$ m, Betasil C18, column oven temperature 45  $^{\circ}$ C

Mobile phase: acetonitrile/ water/ acetic acid ( $\geq 99$  %) (70/30/0.1 % v/v/v)

Flow rate: 1.0 mL min $^{-1}$

Run time: 14.7 min

Detection: UV absorbance at 216 nm

Injection: 20  $\mu$ L

Retention time for ARM  $\beta$  is 13.5 mm

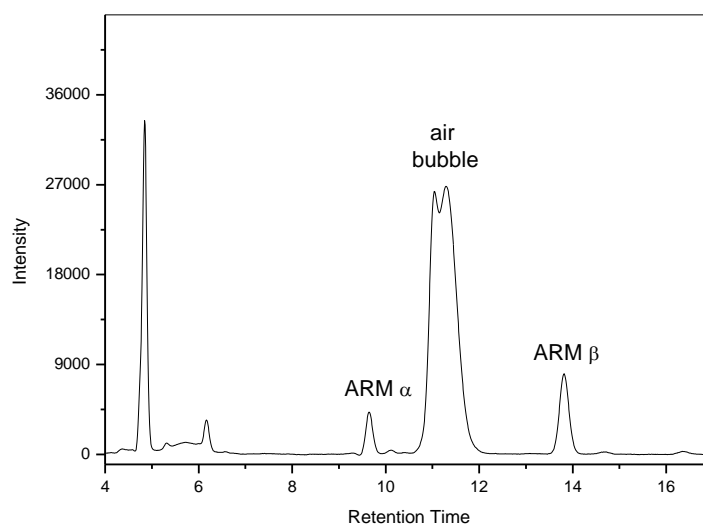


Figure 3-12. HPLC chromatograph of conversion of DHA to ARM with Quadrasil SA in a batch reactor in a 180 min of experiment.

Column: Thermo, 250 x 4.6 mm, 5  $\mu\text{m}$ , Betasil C18, column oven temperature 45  $^{\circ}\text{C}$

Mobile phase: acetonitrile/ water/ acetic acid ( $\geq 99\%$ ) (70/30/0.1 % v/v/v)

Flow rate: 1.0  $\text{mL min}^{-1}$

Run time: 17.0 min

Detection: UV absorbance at 216 nm

Injection: 20  $\mu\text{L}$

Retention time for ARM is  $\beta$  13.8 min

Acetic acid was used to avoid a tailing effect in the DHA peaks.

In the case of a flow system, the concentration of acetonitrile was raised 10 % in the mobile phase in order to reduce the retention time of the ARM  $\beta$  peak from 13.5 min to 8.8 min (Figure 3-13 and Figure 3-14).

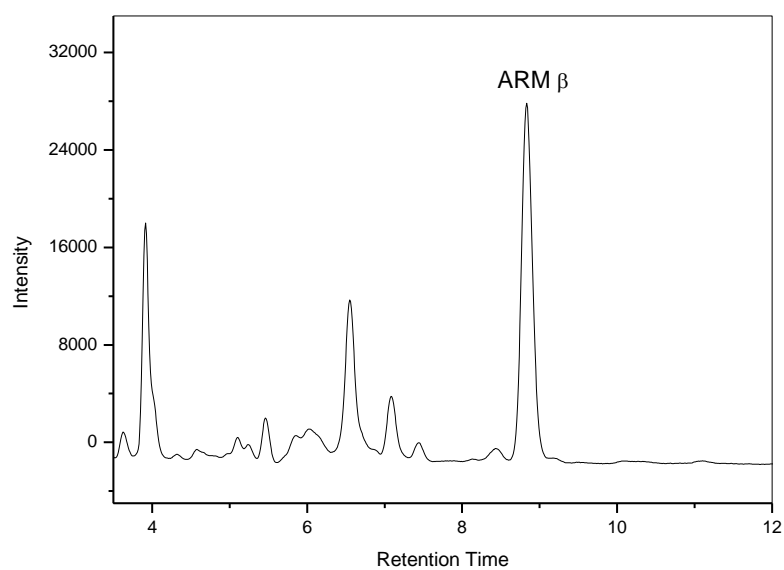


Figure 3-13. HPLC chromatogram of conversion of DHA to ARM with Amberlyst 15 in a microreactor.

Column: Thermo, 250 x 4.6 mm, 5  $\mu\text{m}$ , Betasil C18, column oven temperature 45  $^{\circ}\text{C}$

Mobile phase: acetonitrile/ water/ acetic acid ( $\geq 99\%$ ) (80/20/0.1 % v/v/v)

Flow rate: 1.0  $\text{mL min}^{-1}$

Run time: 12.0 min

Detection: UV absorbance at 216 nm

Injection: 20  $\mu\text{L}$

Retention time for ARM  $\beta$  is 8.8 min

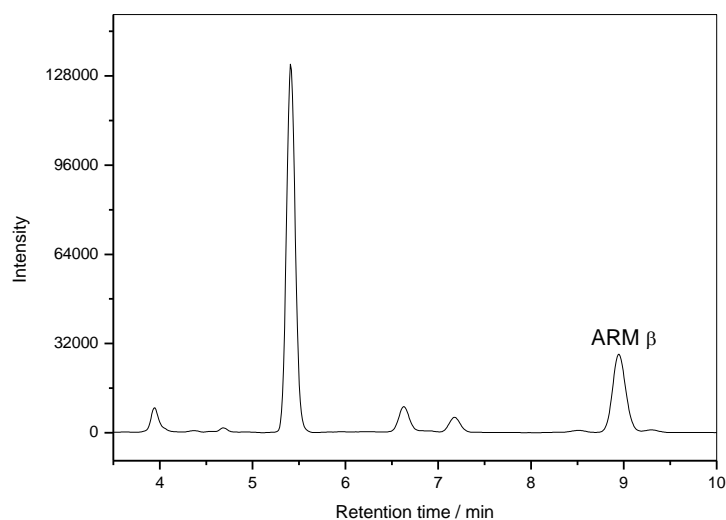


Figure 3-14. HPLC chromatogram of conversion of DHA to ARM with Quadrasil SA in a microreactor.

Column: Thermo, 250 x 4.6 mm, 5  $\mu\text{m}$ , Betasil C18, column oven temperature 45  $^{\circ}\text{C}$

Mobile phase: acetonitrile/ water/ acetic acid ( $\geq 99\%$ ) (80/20/0.1 % v/v/v)

Flow rate: 1.0  $\text{mL min}^{-1}$

Run time: 10.0 min

Detection: UV absorbance at 216 nm

Injection: 20  $\mu\text{L}$

Retention time for ARM  $\beta$  is 8.8 min

### Life Cycle Assessment Methodology

To build-up the cradle-to-gate life cycle inventory (LCI) of both batch and flow production of DHA from artemisinin and artemether from DHA, and to perform life cycle assessment, Umberto for LCA 5.6 software was used<sup>161</sup>. The environmental impact scores were calculated for CML 2001 impact categories, see Table 3-6<sup>162</sup>, and energy consumption was evaluated by Cumulative Energy Demand (CED) method<sup>163</sup>.

Table 3-6. Impact categories of CML method implemented in this study.

Category	Name	Unit
AP	Acidification Potential	kg SO <sub>2</sub> - Eq
GWP	Climate Change	kg CO <sub>2</sub> - Eq
HTP	Human Toxicity Potential	kg 1,4 DCB - Eq
FAETP	Freshwater Aquatic Ecotoxicity	kg 1,4 DCB - Eq
MAETP	Marine Aquatic Ecotoxicity	kg 1,4 DCB - Eq
TAETP	Terrestrial Ecotoxicity	kg 1,4 DCB - Eq
POCP	Photochemical Oxidation (summer smog)	kg ethylene - Eq
EP	Eutrophication Potential	kg PO <sub>4</sub> - Eq
ADP	Depletion of Abiotic Resources	kg antimony - Eq
ODP	Stratospheric Ozone Depletion	kg CFC-11 - Eq

Datasets of the production of all the materials involved in the processes, generated electrical consumptions and transportation were either extracted from Ecoinvent 2.2 library or model in our group. Pre-chains for NaBH<sub>4</sub>, superhydride and 2-Me-THF were supplied by Environmental Clarity, USA. Electricity production mixture in the UK and standard transport distances were used to model energy consumption and transportation respectively <sup>164</sup>. The life cycle inventory was built for a process scenario of a continuous plant for converting 20 tonnes per annum of artemisinin to artemether.

### 3.4 Ethenolysis of Cocoa Butter

#### 3.4.1 Reagents

All reagents used were commercially available and were used without further purification. The catalyst M11 was provided by the group of Professor Steven P. Nolan from the University of St. Andrews. The membrane AF 2400 was supplied by Biogeneral, Inc. The membrane in this work was previously used by the group of Professor Steven Ley for different reactions. The cocoa butter was provided by Cadbury's (now Kraft). Ethylene was purchased from BOC Ltd. THF, ethyl vinyl and  $\text{CDCl}_3$  were obtained from Sigma Aldrich.

#### 3.4.2 Batch Reactions

##### Screening Procedure

The catalyst **6** (see Scheme 2-13) (1.895 mg; 1 mol %; 0.0025 mmol) and a small stirrer bar were introduced into a 5 mL vial in an argon glove box. The vial was closed using a plastic septa cap and removed from the glove box. Then cocoa butter (216.7 mg; 0.25 mmol) was added into a second 5 mL vial and closed using the septa cap outside of the glove box. The cocoa butter vial was purged with argon from Schlenk line through a needle inserted into the cocoa butter septa cap. Next, 1 mL of dry and oxygen-free THF was introduced via a syringe into the cocoa butter vial; THF was dispensed from an SPS-800m. The cocoa butter was dissolved and introduced via syringe into the catalyst-containing vial. This reaction vial was loaded into an autoclave. The autoclave was connected to an ethylene cylinder. The reaction was carried out for 2 hours under 2 barg ethylene pressure at 23 °C. The reaction was completed by quenching with ethyl vinyl ether.

##### *Preparation of Samples for NMR Analysis*

The sample was filtered through pipettes containing silica. The solvent was removed from the vials using a rotavapor.  $\text{CDCl}_3$  was used to dissolve samples for NMR analysis. The reaction was monitored for the appearance of double bonds of 1-decene and a new triglyceride at 4.96 ppm (dd, 2 H). The internal standard was the glycerol bond signal at 4.21 ppm (ddd, 4 H).

### 3.4.3 Flow Experiments

#### Permeability Experiments in a Tube-in-Tube Membrane Contactor

Permeability of the membrane was measured *via* dead-end flow experiments using nitrogen and ethylene. The rig used is shown in Figure 3-15.

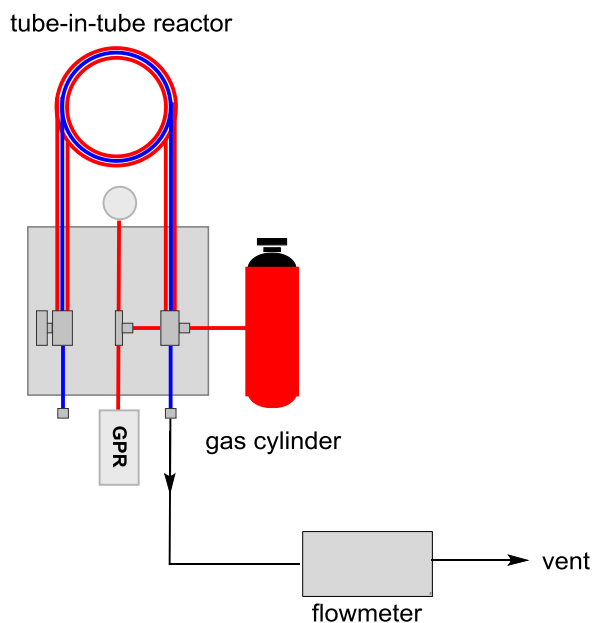


Figure 3-15. Schematic diagram of the rig for the membrane permeability experiments.

The rig consisted of a gas cylinder closed by a normal regulator valve and a gas pressure regulator to adjust the pressure in the membrane module, the membrane module itself, a flowmeter with a vent and a manometer with a shut-off valve. The flowmeter is a custom-built bubble column for measuring the time that a bubble needs to move on a scale for a certain volume; this is used to calculate the flow. In Figure 3-15, the red lines representing the gas phase in the tube-in-tube reactor are shown. Pressure can be adjusted and released as necessary. The blue lines represent the inner space of the tube-in-tube reactor which normally holds the liquid phase. For the flow experiments, a dry membrane was used. The inner space was closed at one end and the other one led to the flowmeter to measure the flow going through the Teflon AF 2400 membrane.

For each experiment, flows through the membrane were measured at different pressures and permeability was calculated using Equations 4-95 to 4-98 from the slope of the corresponding flow vs pressure graph.

### **Reaction in Tube-in-Tube Reactor**

In this work, a Tube-in-Tube gas-liquid membrane contactor was used. The reaction rig was developed in the group of Professor Steven Ley at the University of Cambridge.

The schematic diagram of the setup is shown in Figure 3-16. This reactor was constructed from an inner Teflon AF 2400 membrane tube (OD is 1.0 mm and ID 0.8 mm) and an outer PTFE tube (OD is 3.18 and ID is 1.59 mm). Ethylene was fed from a cylinder *via* a T-piece to the outer PTFE tube. This T-piece connected the gas line to the second T-piece, which was connected on one side to the gas pressure regulator (GPR); on the other side, the gas line was closed. The mixture of cocoa butter, catalyst and THF solvent was injected into the sample loop and pumped by the Uniqsis FlowSyn, K120i syringe pump to the lumen side of the Teflon AF 2400 membrane in the opposite direction to ethylene flow in the shell side. The concentration of cocoa butter in THF was 0.5 M and concentration of the catalyst was 1 mol %. Then, the mixture flowed into a 20 mL or 10 mL residence time coil to ensure a certain residence time for the reaction mixture. A back-pressure-regulator (BPR) enabled a pressurised liquid phase, so that no gas-liquid separation occurred. The BPR was rated to 6.9 bar (100 psi). The collected sample was flushed with argon to remove dissolved ethylene and to stop the reaction before determining conversion by NMR.

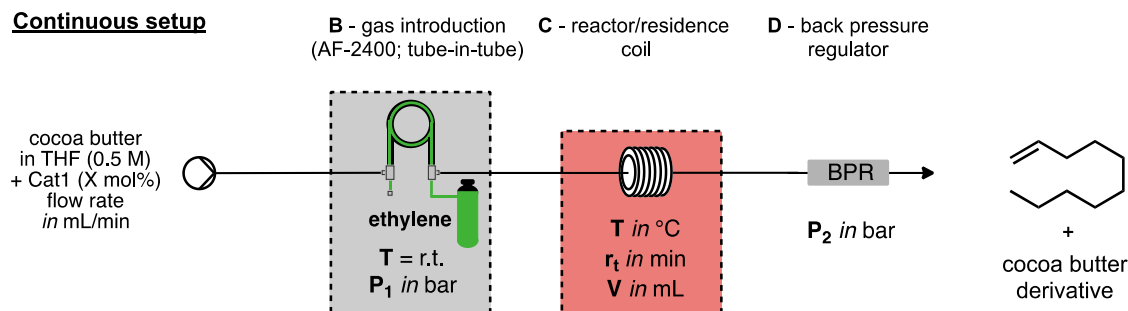


Figure 3-16. The schematic diagram of the rig for the metathesis of cocoa butter with ethylene.

The following parameters were changed during the reaction optimisation: flow rate, concentration of cocoa butter, concentration of catalyst, ethylene pressure, temperature of the reactor coil, and volume of reactor. In addition, Schlenk conditions were also applied using distilled THF and mixing cocoa butter and catalyst in a dried flask under an argon atmosphere.

Finally, the longest run was performed using 25 mL of the feed solution. In this case, the sample loop was bypassed and the solution was directly pumped into the Tube-in-Tube from a flask. Samples were taken every half hour for NMR analysis.

### 3.4.4 Analytical Methods

#### NMR-Spectroscopy

##### *Methodology for NMR Analysis of Ethenolysis Products*

##### *Internal Standard*

$^1\text{H}$  NMR spectra were collected using a Bruker Advance DRX 400. Chemical shifts  $\delta$  were reported in ppm and were compared to the signal of the glycerol bond at 4.21 ppm (ddd, 4H) of deuterated chloroform  $\text{CDCl}_3$  ( $\delta = 7.26$  ppm). The reliability of this standard was confirmed by the use of naphthalene during the ethenolysis of cocoa butter. Hydrogen concentration, recalculated from the area under glycerol bond at 4.21 ppm, was constant during the reaction. The accuracy of this method was also confirmed as in <sup>154</sup>, and by GC (AOCS) <sup>155</sup> and Raman spectroscopy, see Figure 4-7.

*Cocoa Butter Composition*

The composition of raw cocoa butter material used in the reaction is shown in Table 3-4. Based on GC analysis, six fatty acids were identified in the sample of cocoa and three unsaturated fatty acid acids (oleic, linoleic and palmitoleic) played a role in the ethenolysis. Concentration of double bonds in raw cocoa butter, corresponding to specific fatty acids was calculated from Equation 3-10 and reported in Table 3-4.

$$0.3x + 2.9 \cdot 2x + 32.2x = 100 \quad 3-10$$

where 0.3x, 2.9·2x and 32.2x are the fractions of the double bonds in specific fatty acids.

Both oleic and palmitoleic acids have one internal double bond which contain two chemically-equivalent protons (in *cis*), yielding a single signal at 5.36 ppm in the NMR spectrum. Linoleic acid has two internal double bonds with four equivalent protons, which yielded one signal at 5.36 ppm in the spectrum (Figure 3-17). The peak area (5.36 ppm) was used to calculate the initial concentration of double bonds (DB<sub>i</sub>) in cocoa butter, Equation 3-11.

$$[DB_i] = \frac{\frac{\text{Integral area of DB at 5.36ppm}}{\text{Number of nuclei}} \cdot [\text{Glycerol protons}]}{\frac{\text{Integral area of glycerol bond at 4.21 ppm}}{\text{Number of nuclei}}} \quad 3-11$$

Concentration of protons in glycerol backbone was constant during the reaction and assumed to be 1 (confirmed by separate experiments with naphthalene). The number of nuclei assigned to double bond at 5.36 ppm was 2, and 4 to the glycerol bond at 4.21 ppm. Using data from Figure 3-17, the initial concentration of double bonds in the starting material was calculated.

$$[DB_i] = \frac{\frac{0.53}{2} \cdot [1]}{\frac{1}{4}} = 0.53 \cdot 2 = 1.06 \quad 3-12$$

Calculations indicated the initial concentration of double bonds was higher than 1, because the concentration of double bonds was calculated for 2 protons. However, the signal at 5.36 ppm contain the two protons from oleic and palmitoleic, as well as the four equivalent protons from linoleic acid<sup>154</sup>.

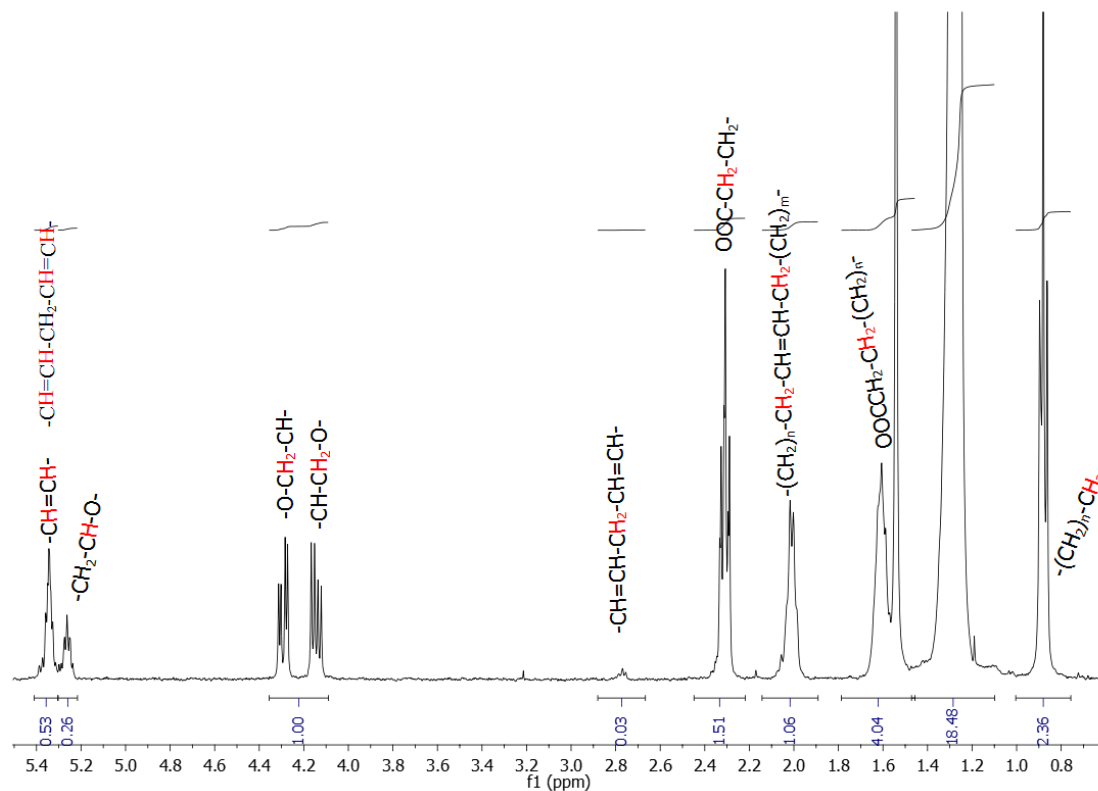
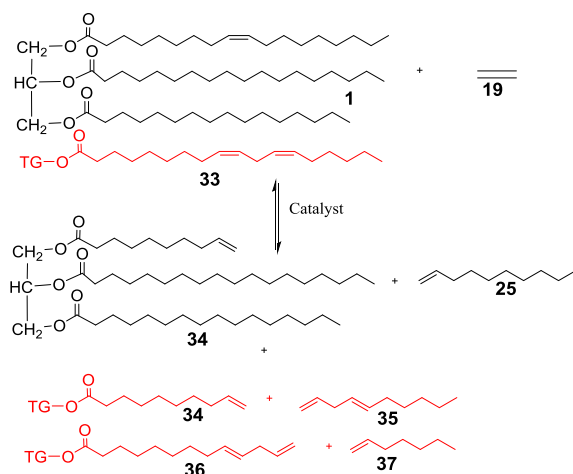


Figure 3-17.  $^1\text{H}$  NMR spectrum of the raw cocoa butter material. The spectrum was used to determinate the methodology for the calculation of the results of the reaction.

Scheme 3-1 shows the potential terminal alkene products formed during the ethenolysis of cocoa butter. The main terminal alkenes obtained from the oleic triglyceride (**1**) were the oleic triglyceride derivative (**34**) and 1-decene (**25**). Minor terminal alkenes obtained from the linoleic triglyceride (**33**) were the oleic triglyceride derivative (**34**) and 1,4-decadiene (**35**) or the linoleic triglyceride derivative (**36**) and 1-heptene (**37**). The assignment of products obtained from the linoleic triglyceride (**33**) was difficult to determine on the basis of the  $^1\text{H}$  NMR spectrum, Figure 3-18. All characteristic signals for these compounds in the high-field side of  $^1\text{H}$  NMR spectrum were overlapped by the signals from the raw cocoa butter material, oleic triglyceride products and the solvent. However, one of the products is the terminal alkene (with one double bond) and the second is alkene contained two carbon-carbon double bonds in the positions of C1 and C4 in the chain.

The chemical signals relative to terminal alkenes (oleic triglyceride derivative and 1-decene) are yielded at 4.85 ppm (2 protons) and at 5.68 ppm (1 proton) in  $^1\text{H}$  NMR spectrum, see Figure 3-18 (Appendix A. 12). However, the products with two double bonds in the position C1 and C4 in the chain contain five hydrogens yielded three signals in  $^1\text{H}$  NMR spectrum. The three protons relative to the terminal double bond show the same pattern of signals in  $^1\text{H}$  NMR spectrum as the terminal alkenes of the oleic triglyceride derivative and 1-decene, but they were more de-shielded. Two protons from the second double bond were slightly shifted in the low-field side of  $^1\text{H}$  NMR spectrum compared to the protons of internal double bonds of oleic (**1**) and the linoleic triglycerides (**33**). Generally, all proton signals corresponded to compounds which contain two double bonds in the position of C1 and C4 were shifted to higher frequency positions compared to compounds containing one terminal double bond (which was due to the increased electronegativity of the  $\text{sp}^2$  carbons and anisotropy of the carbon-carbon double bonds).



Scheme 3-1. Potential products formed during the ethenolysis of cocoa butter. The products obtained from oleic triglyceride were the oleic triglyceride derivative (**34**) and 1-decene (**25**). The potential products obtained from linoleic acids (**33**) might be the oleic triglyceride derivative (**34**) and 1,4-decadiene (**35**) or the linoleic triglyceride derivative (**36**) and 1-heptene (**37**).

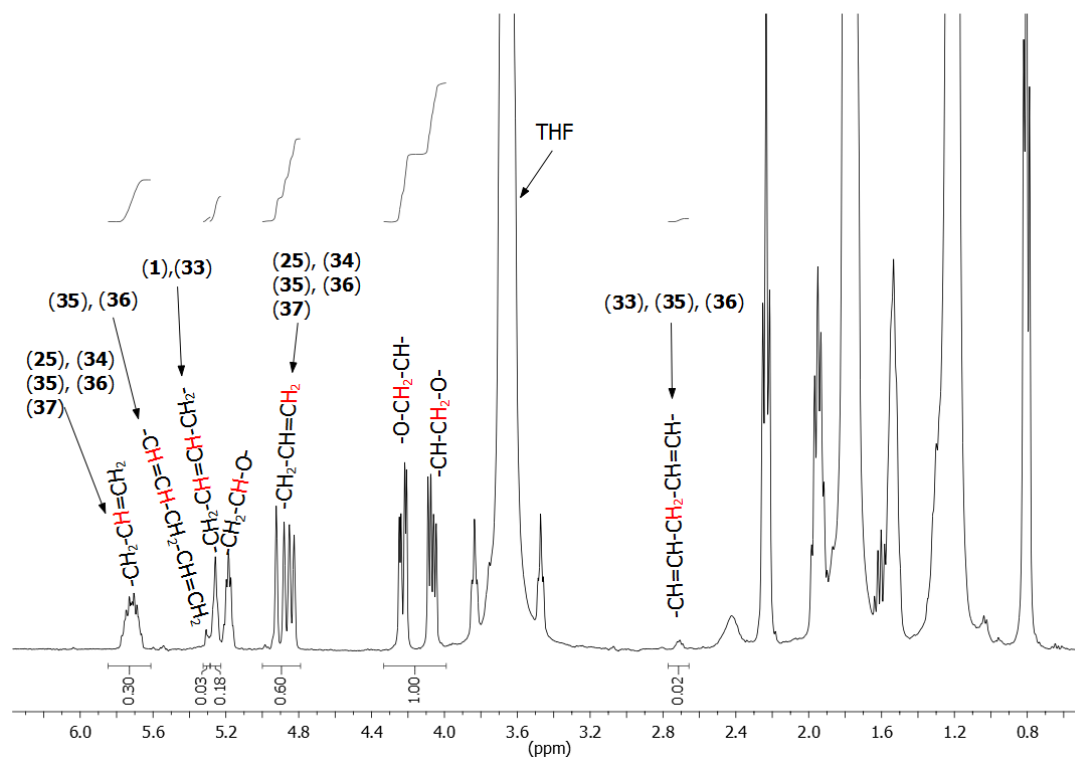


Figure 3-18.  $^1\text{H}$  NMR spectrum of ethenolysis products with respective assignments of the signals of raw material and products <sup>113g</sup>.

The reaction was monitored by the appearance of the signal at 4.85 ppm, which was related to concentration of all products formed during ethenolysis (oleic triglyceride derivative, linoleic triglyceride derivative, 1-decene, 1,4-decadiene and 1,4-heptadiene). However, the signal used for the calculations should include the entire signal of products contained two double bonds (which are shifted to higher frequency position). The total concentration of all ethenolysis products can be written as follows:

$$\begin{aligned}
 & [\text{DB}_{\text{alkenes+TG derivatives}}] && 3-13 \\
 & = \frac{\text{Integral Area of DB at 4.85 ppm}}{\text{Number of nuclei}} \cdot [\text{Glycerol}] \\
 & = \frac{\text{Integral area of glycerol bond at 4.21 ppm}}{\text{Number of nuclei}}
 \end{aligned}$$

$$\begin{aligned}
 [DB_{\text{alkenes+TG derivatives}}] & \qquad \qquad \qquad 3-14 \\
 & = \frac{\frac{\text{Integral Area of DB at 4.85ppm}}{2} \cdot [\text{Glycerol}]}{\frac{\text{Integral area of glycerol bond at 4.21 ppm}}{4}}
 \end{aligned}$$

And the concentrations of one and two double bonds are given by:

$$[DB_{\text{decene+1,4-decadiene}}] = \frac{[DB_{\text{alkenes+TG derivatives}}]}{2} \qquad \qquad \qquad 3-15$$

Hence, the yield is calculated as:

$$\text{Yield}_{\text{to sum of decene+1,4-decadiene}} \% = \frac{[DB_{\text{decene+1,4-decadiene}}]}{[DB_i]} \cdot 100 \% \qquad \qquad \qquad 3-16$$

The mass balance of the reaction shown in Figure 3-18 is given in Table 3-7.

Table 3-7. Ethenolysis results calculated on the base of the data shown in Figure 3-17 and Figure 3-18.

Reagents	CB <sub>raw material</sub> (estimated)	Decene +1,4-decadiene	TG derivatives
Fraction of double bond / (-)	0.36	0.6	0.6
Yield / (-)	-	0.56	0.56
Conversion / (-)	0.6	-	-

## 4 Results and Discussion

### 4.1 Epoxidation of Cocoa Butter

Epoxidation of cocoa butter was performed in a stirred tank reactor and in the highly automatable Vapourtec R Series reaction system. The Vapourtec module was configured as shown in Figure 4-1.

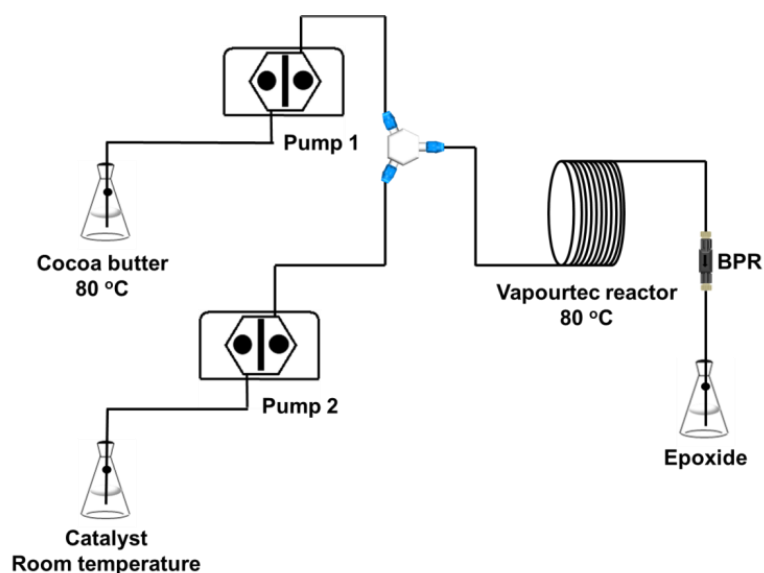


Figure 4-1. A schematic diagram of reactor configuration for epoxidation of cocoa butter under flow conditions.

The cocoa butter mixtures were diluted with toluene in both reactor systems, so that viscosities were similar in both cases. Emulsification in a batch reactor and segmentation of the immiscible fluids into liquid slugs in the continuous flow process were observed.

The slug pattern was observed in the 32 cm tubing of 1 mm ID connected with the T-mixer and a 10 mL coil reactor (Figure 4-1). However, coalescence of the slugs was observed in the coil reactor, which may lead to a disturbance in the control of liquid-liquid slugs resulting in reduced conversion and selectivity in the epoxidation process. This is probably caused by variations in the geometry of PTFE tubing due to wire obstacles on which the tubing is coiled (Figure 4-2). These obstacles can effect

liquid shearing on the walls, which can result in changes in fluid flow patterns. Kreutzer in his work <sup>165</sup> observed that if velocity of liquid was either too low or too high then gas bubbles started to coalesce before entering the microchannels. Second, toluene, used to decrease viscosity of the cocoa butter mixture, tends to saturate the aqueous phase, thus decreasing the interfacial surface area and hence the stability of the interface.

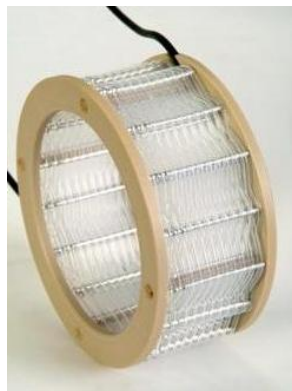


Figure 4-2. A Vapourtec Teflon coil 10 mL reactor.

In the case of phase transfer catalysis, a reaction is biphasic and dependent on interfacial area. Thus, we tried to compare the two systems with regards to the influence of the interfacial area. Under batch conditions the investigation in terms of stirring speed was performed with the diluted mixture of cocoa butter. The results of dependence of the rate constants of reactions in the batch reactor at 80 °C for the reaction mixture diluted in toluene as a function of stirring rate are shown in Figure 4-3. Precise measurements of droplet size were difficult to perform under our conditions. Hence only qualitative discussion is presented.

Formation of small droplets was observed in the emulsion in the batch reactor at the agitation rate of 250 rpm, which may represent the size of slugs under flow conditions. An increase in stirring rate leads to the decrease in the size of droplets, and consequently should increase the interfacial surface area and, hence, mass transfer. In fact, epoxidation of cocoa butter is controlled by mass transfer at stirring rates below 500 rpm, which is evident by linear dependence of reaction rate on the agitation rate. With this expectation, mass transfer and chemical reaction interact in

controlling this heterogeneous liquid-liquid reaction at agitation speeds higher than 500 rpm. No plateau was reached in this trend; at agitation rates above 1500 rpm stirring bar was not stable and mixing became inefficient.

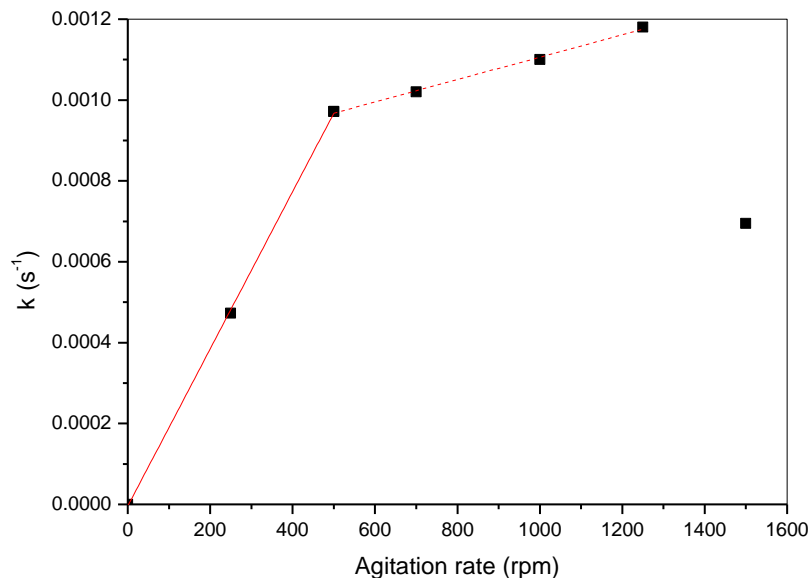


Figure 4-3. Evolution of the constant rate of reaction under batch conditions at 80 °C for a reaction mixture diluted with toluene as a function of agitation rate.

It should be noted that in batch reactors the size of droplets generated by stirring aqueous and organic phases varies from tens of micrometres to millimetres. Therefore, the liquid-liquid interfacial area differs significantly from one drop to another in the same reaction<sup>166</sup>. As a consequence of this broad distribution, heterogeneous liquid-liquid batch reactors can differ in terms of conversion and selectivity under the same conditions. In the flow reactor each pair of slugs may be considered a separate reactor. In the case of scale up of batch processes poor mixing is the main drawback, in contrast to reactions performed in Taylor flow in channels, where sizes of slugs are fixed by the flow rates, tube diameter and fluids properties. Stable segmented flow allows the slug size distribution and the liquid-liquid interfacial surface area to be controlled in a precise fashion. This interfacial surface area is in the range of 10,000 – 50,000 m<sup>2</sup> m<sup>-3</sup><sup>167</sup> in a microchannel with a diameter from tens to hundreds of μm; in comparison to the size of droplets under batch conditions, their interfacial surface area is 10 times smaller, *ca.* 2,000 m<sup>2</sup> m<sup>-3</sup><sup>168</sup>.

**Space-Time-Yield**

The overall rate of double bond conversion for the reaction in the batch reactor was calculated from equation 4-7. The equation was derived from the general mole balance equation 4-1<sup>169</sup>. The schematic diagram of mass balance is shown in Figure 4-4.

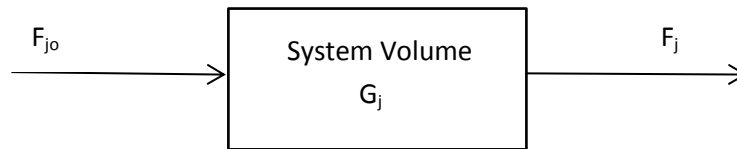


Figure 4-4. Mass balance over a system volume.

$$\left[ \begin{array}{c} \text{Rate of flow of } j \\ F_{j0} \\ \text{into the system} \\ \left( \frac{\text{moles}}{\text{time}} \right) \end{array} \right] - \left[ \begin{array}{c} \text{Rate of flow of } j \\ F_j \\ \text{out of the system} \\ \left( \frac{\text{moles}}{\text{time}} \right) \end{array} \right] + \left[ \begin{array}{c} \text{Rate of generation of } j \\ G_j \\ \text{by chemical reaction} \\ \text{within the system} \\ \left( \frac{\text{moles}}{\text{time}} \right) \end{array} \right] \\ = \left[ \begin{array}{c} \text{Rate of accumulation} \\ \text{of } j \frac{dN_j}{dt} \\ \text{within the system} \\ \left( \frac{\text{moles}}{\text{time}} \right) \end{array} \right]$$

$$F_{j0} - F_j + G_j = \frac{dN_j}{dt} \tag{4-1}$$

There is no inflow and outflow of reactants and product during the reaction.

$$F_{j0} = F_j = 0 \tag{4-2}$$

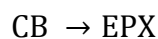
The rate of generation of species j,  $G_j$ , is considered as the product of the reaction volume,  $V$  ( $\text{m}^3$ ), and the rate of the formation of species j,  $r_j$  ( $\text{mole h}^{-1} \text{m}^{-3}$ ).

$$G_j = r_j V \tag{4-3}$$

Hence, the general mole balance in the case of the batch reactor is given as:

$$\frac{dN_j}{dt} = r_j V \tag{4-4}$$

In the case of the epoxidation of cocoa butter in a batch reactor



The number of unreacted moles of CB in the reactor after a time  $t$ ,  $N_{CB}$ , is given as

$$\begin{bmatrix} \text{Moles of A} \\ \text{in reactor} \\ \text{at time } t \\ N_{CB} \end{bmatrix} = \begin{bmatrix} \text{Moles of A} \\ \text{initially fed} \\ \text{into reactor} \\ \text{at } t = 0 \\ N_{CB0} \end{bmatrix} - \begin{bmatrix} \text{Moles of A that} \\ \text{have been consumed} \\ \text{by chemical reaction} \\ N_{CB0}X \end{bmatrix} \quad 4-5$$

where  $X$  is a conversion factor that can be defined as the quotient of the number of moles of CB that have reacted per moles of CB introduced into the reactor.

The differential form of Equation 4-5 with respect to time is given as

$$-N_{CB0} \frac{dX}{dt} = r_{CB} V_{CB0} \quad 4-6$$

Calculating the integration of Equation 4-6 for the initial conditions where  $t = 0$  and  $X=0$  gives the rate of disappearance of cocoa butter as:

$$-r_{CB} = \frac{XN_{CB0}}{tV_{CB0}} \quad 4-7$$

where  $V_{CB0}$  ( $m^3$ ) is the reaction volume. It is equal to the total volume of all the compounds located within the system as follows:

$$V_{CB0} = V_{CB,80^\circ C} + V_{\text{toluene}} + V_{H_2O_2} + V_{H_2O} \quad 4-8$$

In the case of reactions under continuous conditions, the rate of disappearance of double bonds can be calculated from Equation 4-14. This equation was also derived from the general mass balance Equation 4-1. However, reactants and products do not accumulate within the flow reactor. If the general mass balance for a flow reactor is given as:

$$F_{CB0} - F_{CB} + G_{CB} = 0 \quad 4-9$$

then:

$$F_{CB0} - F_{CB} = -r_{CB}V \quad 4-10$$

And we can express the molar flow rate that leaves the reactor:

$$\begin{bmatrix} \text{Molar flow rate} \\ \text{at which A is fed to} \\ \text{the reactor} \\ F_{CB0} \end{bmatrix} - \begin{bmatrix} \text{molar flow rate} \\ \text{at which A is consumed} \\ \text{within the reactor} \\ F_{CB0}X \end{bmatrix} = \begin{bmatrix} \text{Molar flow rate} \\ \text{at which A leaves} \\ \text{the reactor} \\ F_{CB} \end{bmatrix} \quad 4-11$$

Then, substituting Equation 4-11 into 4-10

$$F_{CB0} - (F_{CB0} - F_{CB0}X) = -r_{CB}V \quad 4-12$$

where  $V$  ( $m^3$ ) is the reactor volume. Hence, the rate of disappearance of double bonds under continuous conditions is given as:

$$-r_{CB} = \frac{F_{CB0} X}{V} \quad 4-13$$

The molar flow rate  $F_{CB0}$  is the product of the initial concentration of cocoa butter,  $C_{CB0}$  ( $mol\ m^{-3}$ ), and the entering flow rate of cocoa butter,  $v_0$  ( $m^3\ h^{-1}$ ). The reaction volume in this case is the volume of the reactor.

$$-r_{CB} = \frac{C_{CB0} v_0 X}{V} \quad 4-14$$

The space- time-yield to epoxide under batch conditions was calculated as

$$STY = \frac{YN_{CB0}}{tV_{EPX}} \quad 4-15$$

The space-time-yield to epoxide under flow conditions was obtained from Equation 4-16.

$$STY = \frac{C_{CB0} v_0 Y}{V} \quad 4-16$$

Figure 4-5 shows a comparison of space-time-yield (STY) as a function of reaction time (for a batch system at agitation rate of 250 rpm) and residence time (under continuous conditions for equal flow rates of cocoa butter and catalyst mixture). The cocoa butter mixtures in both systems were diluted with toluene, such that viscosities were similar in both cases. STY under batch conditions is higher than under flow conditions. It can be related to the observed coalescence of liquid droplets in microtubing, which significantly reduces the area of mass transfer and hence reduces the rate of the reaction.

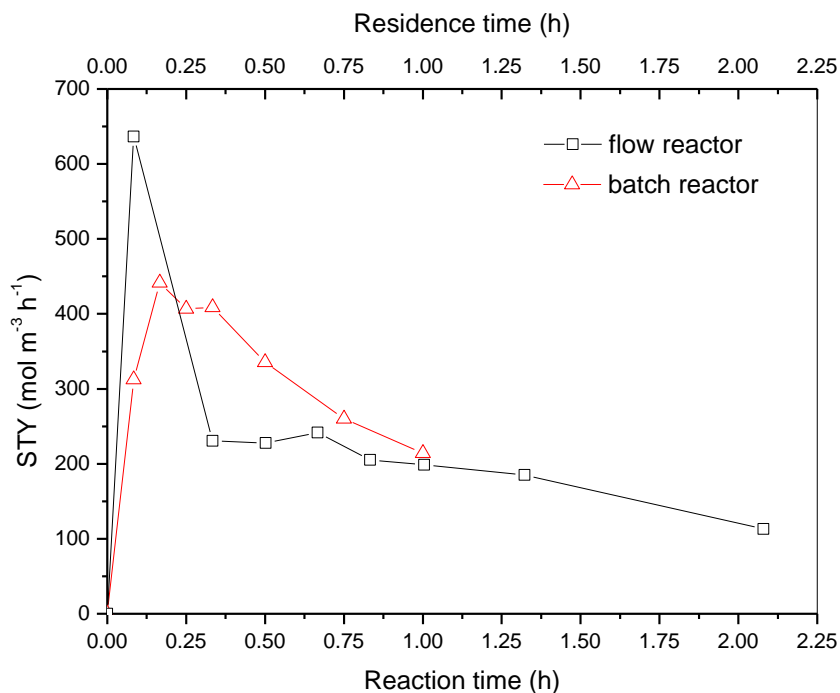


Figure 4-5. Dependence of the space-time-yield to epoxide as a function of residence time (in the flow system) and reaction time (in the batch reactor at 250 rpm).

### Effect of the Phase Ratio

The influence of the ratio of the flow rates of the reactant to the catalyst solutions was investigated. The ratio was varied from  $F_{cb} : F_{cat} = 1:1$  to 1:2 and 3:4. Variations in flow rates affect the relative sizes of the organic and the aqueous phase slugs under Taylor flow regime, see Figure 4-6, which should translate into variations in mass transfer coefficients, according to the literature correlations. Detailed analysis of mass transfer in Taylor flow is given in Section 4.2 (Determination of Critical Parameters Controlling Epoxidation of Cocoa Butter).

As expected an increase in residence time leads to the increase in conversion. The relationship between conversion and residence time is nearly linear, indicating a zero-order overall kinetics and, thus, external mass transfer limitation. There is a noticeable variation between the ratio of phases, residence time and conversion. Thus, at short residence times doubling the amount of catalyst phase per unit volume of the reactor leads to a higher conversion relative to the base case of 1:1 phase ratio. At long residence times opposite is true: the base case of 1:1 ratio of phases results in

a higher conversion. Since the main difference induced by the variation in the ratio of phases is in interface mass transfer coefficients, we speculate that this is the origin of the observed trends. However, this variation is not large and in the absence of detailed description of mass transfer in this complex reaction system further analysis is impractical.

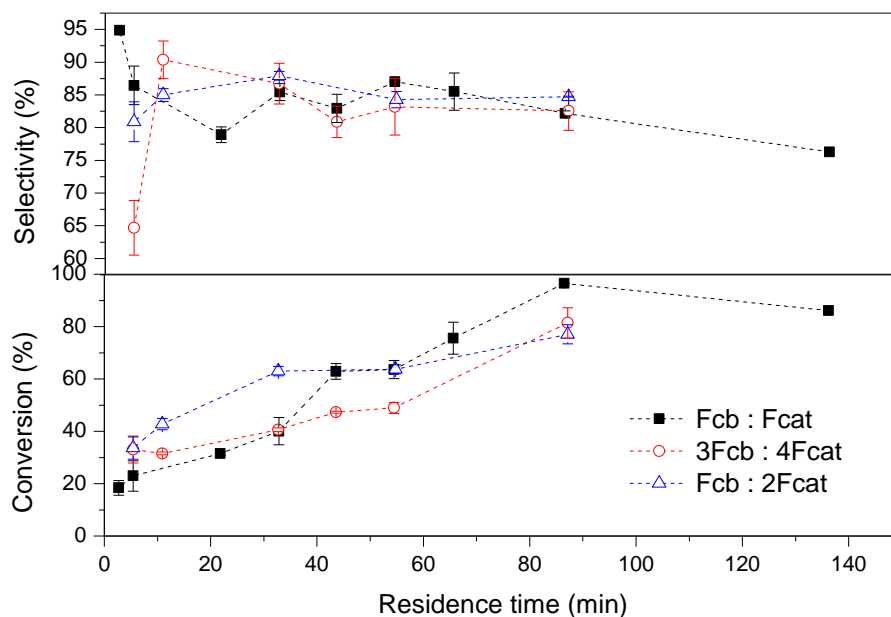


Figure 4-6. The influence of the ratio of the flow rates of the reactant to the catalyst on the conversion of cocoa butter to epoxide and its selectivity. Residence time was considered from the point of mixing of the two phases to the collection point (total length of tubing was 1388 cm).

Conversion was calculated as the ratio of moles of cocoa butter consumed during the reaction to the initial moles of cocoa butter introduced into the reaction system. Selectivity was determined as the ratio of the yields to oleic epoxide to the conversion of cocoa butter. Yield was calculated as the ratio of moles of oleic epoxide obtained as a result of the reaction. The amounts of cocoa butter and oleic epoxide after the reaction were calculated on the basis of  $^1\text{H}$  NMR analysis.

**Epoxidation of Cocoa Butter in the Stirred Tank Reactor without Using Solvent**

Epoxidation of cocoa butter without toluene was performed at different temperatures, catalyst concentrations and initial concentrations of the main reactant to determine basic reaction parameters. Batch experiments were also performed in a reaction calorimeter to determine the heat of reaction.

Reaction progress was performed by  $^1\text{H}$  NMR analysis. Disappearance of double bond ( $\delta = 5.30 - 5.39$  ppm) and appearance of oxirane bond ( $\delta = 2.85 - 2.96$  ppm) was considered in monitor reaction progress. The internal standard was the glycerol bond at  $4.25 - 4.34$  ppm. Good accuracy of NMR analysis was confirmed by Raman spectroscopy, which gives a strong band at  $1660\text{ cm}^{-1}$ , relative to double bond see Figure 4-7a. There is a good correlation between the reactant conversion values calculated from NMR and Raman data, as shown in Figure 4-7b. Raman confirmed that triglyceride is not decomposed to glycerol and fatty acids during the reaction and that the glycerol bond can be used as the internal standard. NMR analysis is much faster than Raman spectroscopy, thus NMR was used in further analysis of the reaction progress.

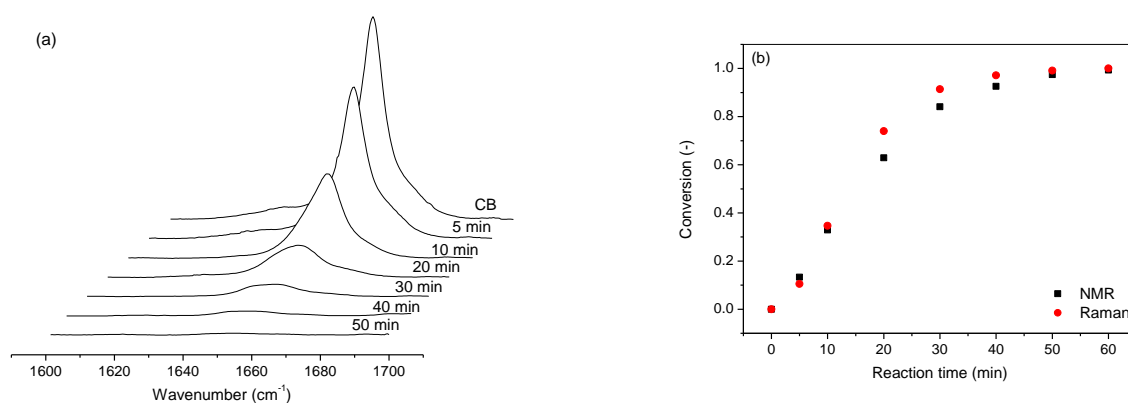


Figure 4-7. Monitoring of reaction progress by Raman spectroscopy: (a) the decrease in  $1660\text{ cm}^{-1}$  band with the progress of reaction, (b) Comparison of conversion values calculated from Raman and NMR data.

Figure 4-8 shows the progress of reaction conversion and selectivity to the epoxide as functions of time at different reaction temperatures. Recalculated to yield, the

yield at 40 min of reaction obtained in the reaction performed at 60 °C is slightly higher than at 50 °C, whereas the yield in the reaction performed at 80 °C is approximately twice higher than that at 50 °C. The selectivity of the reactions is above 80 %. The fastest reaction was at 80 °C and therefore this temperature was taken as the standard for the investigation of the effect of the catalyst composition.

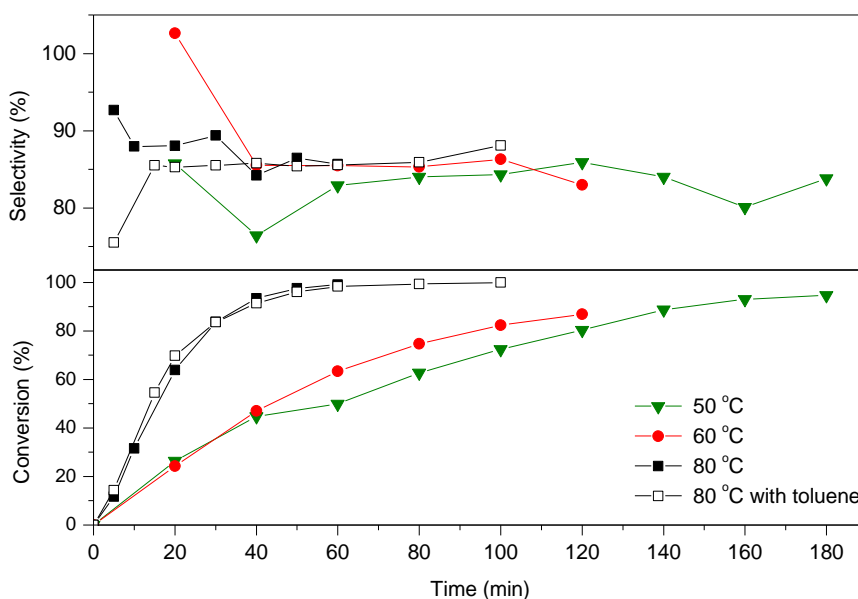


Figure 4-8. Dependence of conversion and selectivity on the temperature of epoxidation under batch conditions. The conversion and selectivity were calculated to the total concentration of double bond in the raw material.

In the second and third reactions performed to investigate the impact of catalyst, the amount of hydrogen peroxide was reduced. In the fourth reaction both hydrogen peroxide and the amount of ortho-phosphoric acid were reduced. The results are shown in Figure 4-9. The initial catalyst composition gives the fastest reaction and the reaction rate is limited by the amount of hydrogen peroxide. The best molar equivalent is 1.809 with respect to the cocoa butter concentration.

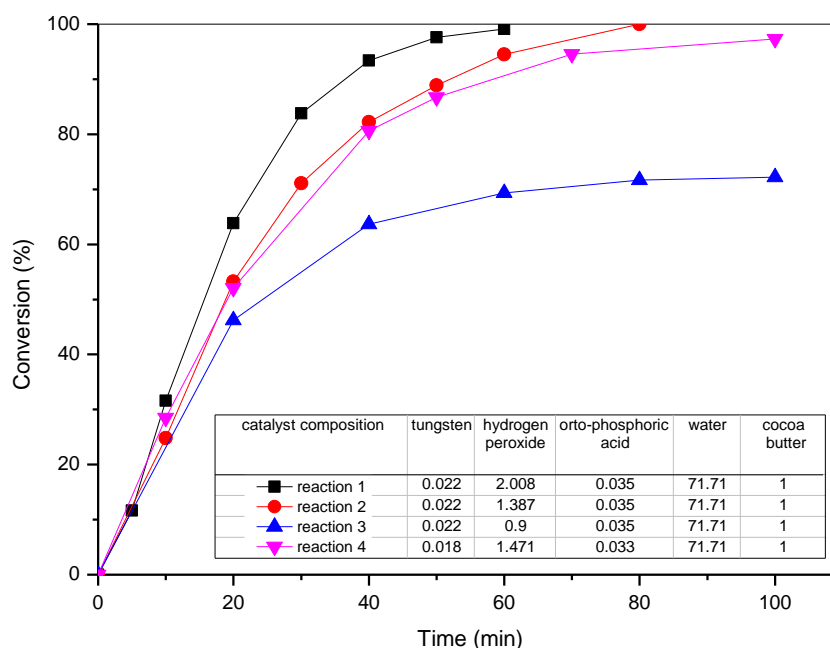


Figure 4-9. Effect of catalyst composition on conversion at 80 °C. The reaction numbers correspond to catalyst compositions shown in Table 3-1.

Figure 4-10 shows that all reactions are following first order kinetics with respect to cocoa butter. Based on Arrhenius rate expression the observed activation energy is in the order of 34 kJ mol<sup>-1</sup>. It is calculated from the slope given in Figure 4-11. However, this is not a true activation energy, since the increase in temperature results in a decrease in viscosity, as well as the increase in the reaction rate.

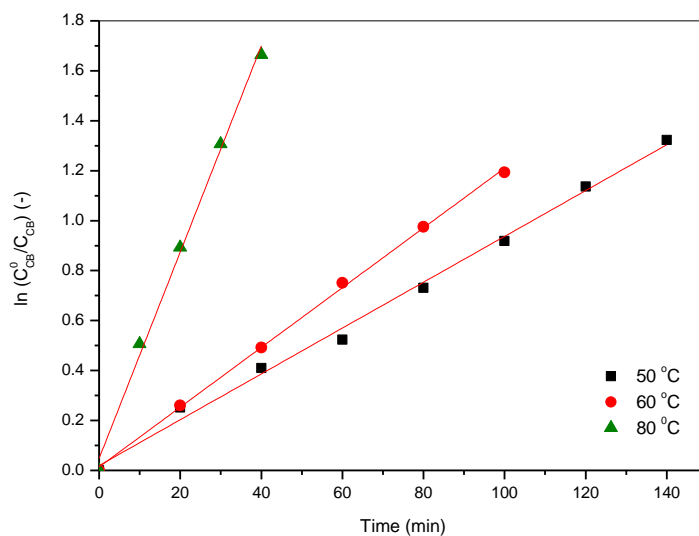


Figure 4-10. First order kinetic plot for epoxidation of cocoa butter, where  $C_{CB}^0$  is the initial concentration of cocoa butter and  $C_{CB}$  is the concentration of the cocoa butter in a particular time. Reactions were performed at agitation rates of 600 rpm.

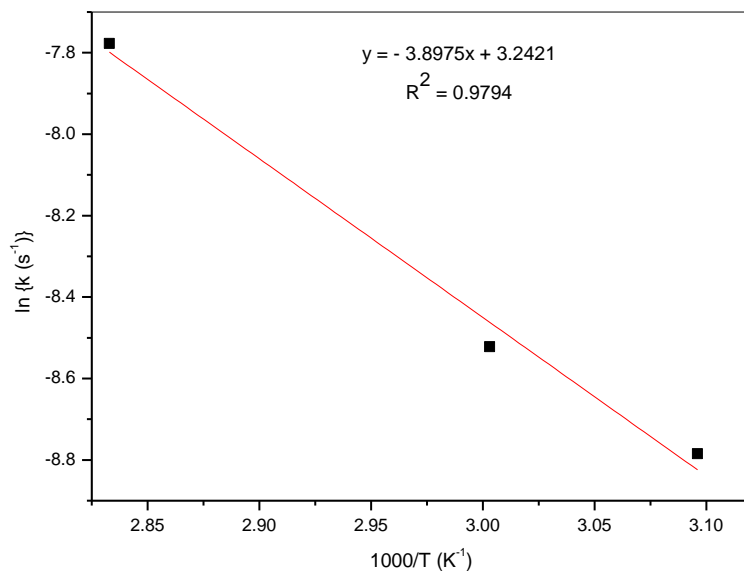


Figure 4-11. A plot of  $\ln(k)$  against  $1/T$  is straight line described by Arrhenius

equation  $\ln k = \ln A - \frac{E_a}{RT}$ , where the coefficient  $k$  ( $s^{-1}$ ) is the rate constant of reaction, the parameter  $A$  is the pre-exponential factor and corresponds to the

intercept of the line at  $1/T = 0$  and  $E_a$  is the activation energy and is calculated from the slope of the line ( $-E_a/R$ ).

#### 4.1.1 Reaction Calorimetry under Batch Conditions

The area of the true heat flow for the reaction was 3,997 J and the area for non-reactive system was 1,092 J. The enthalpy of reaction can be obtained then from equation:

$$\Delta_r H^\circ (80\text{ }^\circ\text{C}) = \frac{\text{Area of true heat flow in a reactive system} - \text{Area of true heat flow in the non reactive system}}{\text{number of moles of CB in the reaction}}$$

The enthalpy of epoxidation of cocoa butter was found to be mildly exothermic at  $-168\text{ kJ} \cdot \text{mol}^{-1}$ . From  $^1\text{H}$  NMR analysis of the reaction product obtained in the calorimeter, the starting cocoa butter reacted completely and the selectivity of reaction was 77 %. This is below the typical selectivities obtained in the batch reactions (85 %). The decrease was attributed to product decomposition in the case of the calorimeter experiment, when product composition was analysed after 18 hours following the reaction. Thus, we assume that composition at the end of the reaction was similar in the experiments performed in the calorimeter and in a flask.

#### Selectivity in Flow Experiments

The selectivity of oleic epoxide is roughly 86 %. It was calculated to the total concentration of double bond in the raw material (84.1 % of oleic, 15.1 % of linoleic and 0.8 % palmitoleic double bond, see Table 3-4). Thus, the selectivity of oleic epoxide converted to double bond of oleic acid is approximately 100 %. The selectivity towards oleic epoxide decreases significantly at residence times above 0.8 h (Figure 4-6 and Figure 4-12). This is attributed to degradation of hydrogen peroxide in the flow reactor system, which results in a higher water concentration and an increase in the concentration of ortho-phosphoric acid, which is a catalyst for diol formation<sup>15b</sup>. Figure 4-13 shows the Raman spectrum of the epoxide product at 2.08 h of residence time. There is the peak at  $1019\text{ cm}^{-1}$  which corresponds to the C-O stretching vibration in the C-O-H group<sup>170</sup>. Also NMR spectrum of this product

(Figure 4-14) shows the diol signal at 3.38 ppm. The conversion of cocoa butter was 87 % and the selectivity to oleic triglyceride derivative was 76 % calculated to the total initial concentration of double bond.

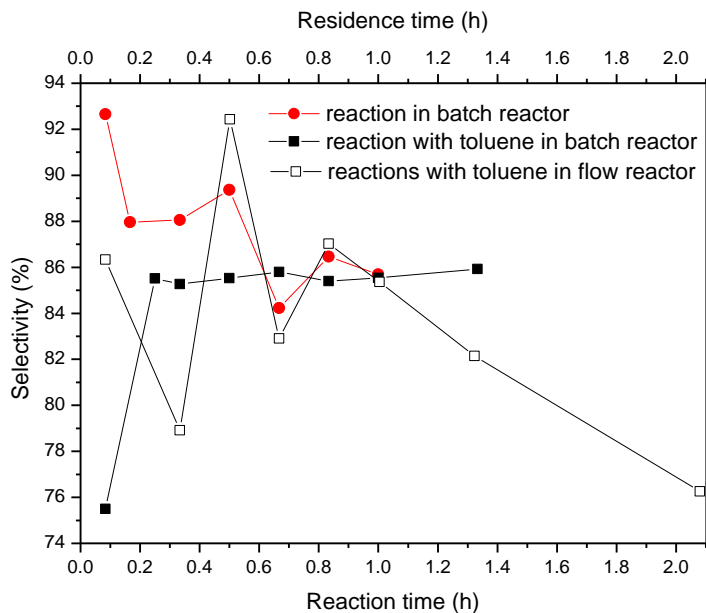


Figure 4-12. Comparison of reaction selectivity to oleic triglyceride derivative calculated to the total concentration of double bond in the presence and absence of toluene under batch and flow conditions.

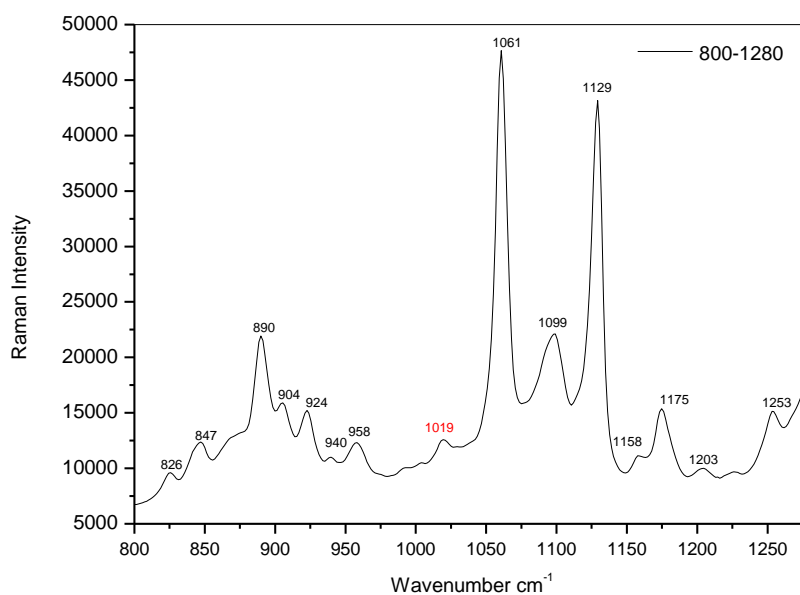


Figure 4-13. Raman spectrum of the epoxide product obtained in a flow reactor at 2.08 h residence time.

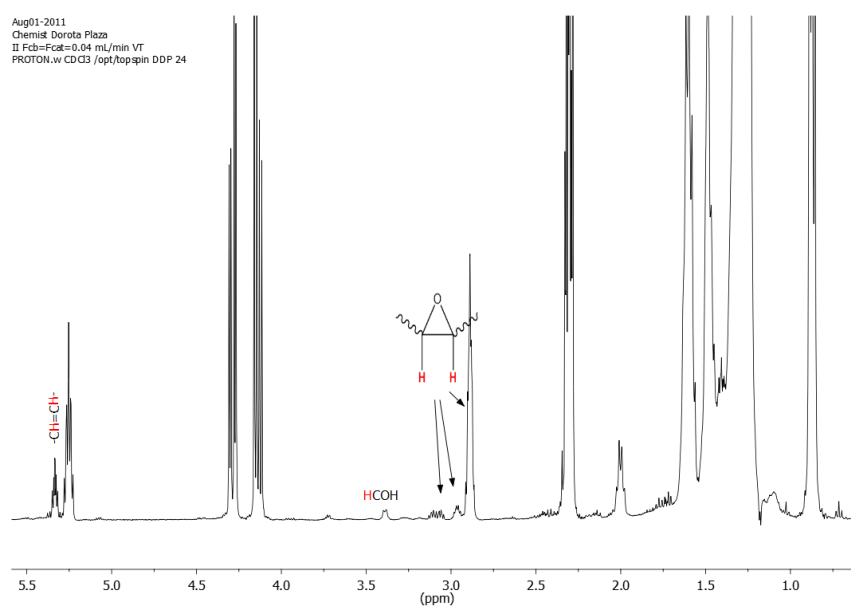


Figure 4-14. NMR spectrum of epoxide product obtained in a flow reactor at 2.08 h residence time.

### Decomposition of Hydrogen Peroxide under Flow Conditions

Decomposition of hydrogen peroxide was characterised by performing a blank reaction in the Vapourtec reactor (see Figure 4-15). In the first experiment, decomposition of hydrogen peroxide in the storage flask was considered at room temperature under continuous stirring conditions. The aqueous mixture of the catalyst ( $W^{VI}/P^V/H_2O_2/H_2O$ ) with an initial concentration of hydrogen peroxide of  $1.38 \text{ mol dm}^{-3}$  was fed into the reactor at a flow rate of  $0.063 \text{ mL min}^{-1}$  (residence time 158 min). Samples were then collected for analysis at the point of mixing of the two phases (see Figure 4-15).

The second experiment was performed in the same way as the first; however, the catalyst mixture was not stirred in the storage flask. In the final blank test without using the mixture of cocoa butter, samples were taken for iodometric titration analysis at the collection point of the epoxide product (see Figure 4-15).

The results of the two first experiments show that the time of storage of the catalyst mixture in the flask at room temperature under flow conditions has no impact on the decomposition of hydrogen peroxide. However it was observed that the feed pump works more stably when the catalyst mixture is stirred in the feed flask. Since pump stability depends strongly on the presence of bubbles in the liquid phase, this indicates that some decomposition of hydrogen peroxide does take place in the feed tank and bubbles can be removed by stirring the feed catalyst solution. From the final result it can be observed that decomposition of hydrogen peroxide was 97 % when measured at the collection point after the reactor.

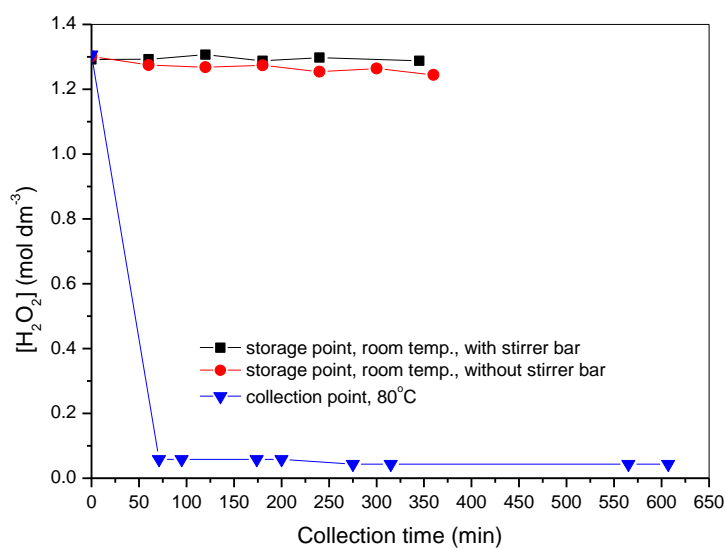


Figure 4-15 Checking the decomposition of hydrogen peroxide in a non-reactive system, in which an aqueous mixture of catalyst ( $\text{W}^{\text{VI}}/\text{P}^{\text{V}}/\text{H}_2\text{O}_2/\text{H}_2\text{O}$ ) was pumped at a flow rate of  $0.063 \text{ mL min}^{-1}$ .

## 4.2 Determination of Critical Parameters Controlling Epoxidation of Cocoa

### Butter

The reaction in a two-phase immiscible liquid-liquid system, performed in a capillary reactor can be characterised by a reproducible, stable slug-flow regime. It can be assumed that oxidation of the double bond occurs at this interface or in a bulk organic phase where the contact between the oxidizing reagent and double bond occurs. The oxidizing complex is transferred to the aqueous-organic interface or the organic bulk by a phase transfer agent. Next, the epoxide is either extracted into the organic phase (if the reaction occurs at the interface) or remains in the organic phase, whereas the catalyst complex  $W^{VI}/P^V/H_2O_2/PTC$  is transferred to the aqueous phase where it is regenerated. Mass transfer mechanisms include molecular diffusion and convection. Molecular diffusion takes place through the interface between the neighbouring slugs and within the slugs. Convection occurs within each slug, induced by internal circulation inside the slugs. In this investigation we aim to determine which mechanism controls this reaction and confirm where the reaction takes place.

### Viscosity

Viscosity is the resistance of a material to flow under an applied force (stress) (see Equation 4-17) and is a non-equilibrium property. It is, like pressure, temperature and volume, a function of the state of fluid, which may provide information about the compound or a mixture of compounds. Viscosity is introduced as a shearing stress per unit area divided by a velocity gradient.

$$\text{Viscosity } (\eta) = \frac{\text{Shear Stress}}{\text{Shear Rate}} = \frac{\tau}{\dot{\gamma}} \quad 4-17$$

The SI unit of viscosity is Poise, which may be given as:

$$1\text{P} = 1.00 \cdot 10^2 \text{cP} = 1.00 \cdot 10^6 \mu\text{P} = 0.1 \text{ N s m}^{-2} = 0.1 \text{ Pa s}$$

Under the conditions of epoxidation of cocoa butter the flow is laminar ( $Re \approx 0.5$ ). Based on this we can estimate the relevant range of shear rate, as a gradient of velocity in a flowing fluid in a pipe<sup>171</sup>.

$$\dot{\gamma} = \frac{8v}{d} \quad 4-18$$

In our conditions  $d = 0.1 \text{ cm}$  and the total flow rate  $= 0.126 \text{ mL min}^{-1} = 2.1 \cdot 10^{-3} \text{ mL s}^{-1}$ .

$$v = \frac{\text{Total flow rate}}{A} = \frac{\text{Total flow rate}}{\pi r^2} = \frac{2.1 \cdot 10^{-3}}{3.14 \cdot \left(\frac{0.1}{2}\right)^2} = 0.26 \frac{\text{cm}}{\text{s}} \quad 4-19$$

$$\dot{\gamma} = \frac{8 \cdot 0.26}{0.1} = 20.8 \frac{1}{\text{s}}$$

Measurements of viscosity were conducted at over a shear rate range of  $2 - 18 \text{ s}^{-1}$  (the results of measurements are shown in Appendixes from A. 6 to A. 9).

Experimental viscosities are shown in Figure 4-16 (a list of raw data of viscosity is given in Appendix A. 10).

Figure 4-16 shows that the measured viscosities of cocoa butter, of the mixture of cocoa butter and toluene and the mixture of cocoa butter, toluene and Adogen 464 decrease with increasing temperature. The addition of toluene to cocoa butter considerably decreases viscosity of the mixture. The addition of the surfactant to the mixture of cocoa butter and toluene slightly increases the viscosity of the mixture. In the case of the aqueous phase catalyst, which is a mixture of water, hydrogen peroxide, ortho-phosphoric acid and dissolved tungsten, the viscosity of the mixture predictably decreases slightly with temperature in the range of  $20$  to  $45 \text{ }^\circ\text{C}$ . However, in the range of  $45$  to  $70 \text{ }^\circ\text{C}$  the viscosity of the aqueous catalyst phase increases considerably. This may be connected with the process of transformation one molecule of the catalyst into another.

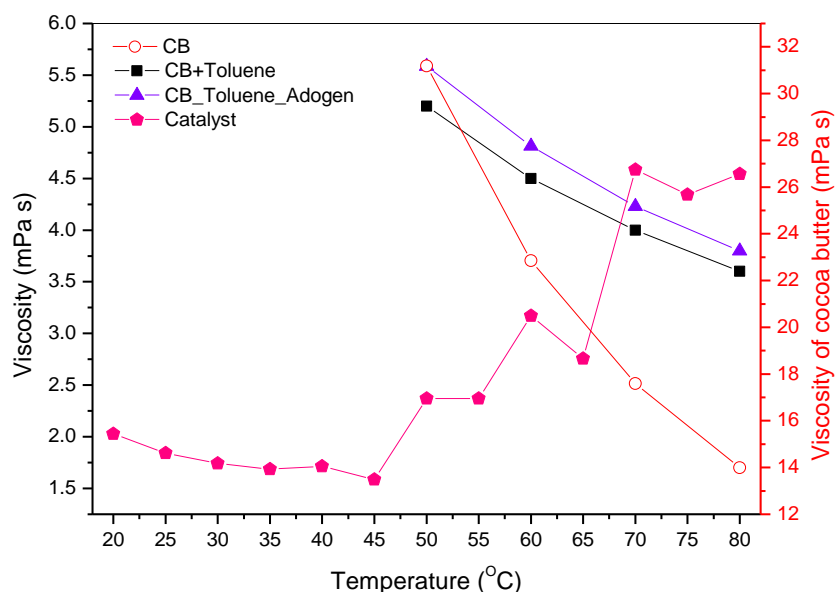


Figure 4-16. Viscosity of cocoa butter, mixture of cocoa butter with toluene, mixture of cocoa butter, toluene and Adogen 464 and a mixture of catalyst as a function of temperature.

### Interfacial Tension

The values of interfacial tension as a function of time as determined by droplet shape analysis are plotted in Figure 4-17. It may be observed that interfacial tension between water and cocoa butter melt (80 °C), and water and a mixture of cocoa butter with toluene are almost identical. This is due to the negligible differences in density and surface tension of toluene and cocoa butter.

Adding surfactant into the mixture of cocoa butter and toluene causes the decrease of the interfacial tension between the organic mixture and water due to high adsorption strength of Adogen 464 on a fluid interface. Initially, upon droplet formation, the interfacial tension drops quickly due to immediate adsorption of Adogen 464 at the interface. However, the rate of decrease slows over time until a quasi-equilibrium is reached as a result of complete droplet coverage by surfactant. Bon *et al.*<sup>172</sup> noted the same effect. They studied the impact of geometry and shape of amphiphilic Janus nanoparticles on a toluene-water interface using the same technique.

Possessing both hydrophilic and hydrophobic domains, the Janus particles served the same purpose as the surfactant Adogen 464.

When the catalyst ( $W^{VI}/P^V/H_2O_2/H_2O$ ) was included in the aqueous phase droplet against the organic environment phase of cocoa butter, toluene and surfactant, an increase of interfacial tension was observed. From  $t_0$  until  $t = 50$  s, an increase in interfacial tension from  $9 - 10 \text{ mN m}^{-1}$  is typical to newly formed droplets. We can attribute this behaviour to the catalysis of reaction occurring at the interface giving rise to products which slightly increase the interfacial tension. After  $t = 50$  s, the interfacial tension has reached an equilibrium either due to the cessation of reaction due to the exhaustion of reagents in the vicinity of the interface, or the establishment of steady-state conditions arising from the diffusion of reagents and products. The average interfacial tension of the complete reactive mixture is  $9.5 \text{ mN m}^{-1}$  and the standard deviation is  $0.1 \text{ mN m}^{-1}$ . The coefficient of variation is 1.0 %.

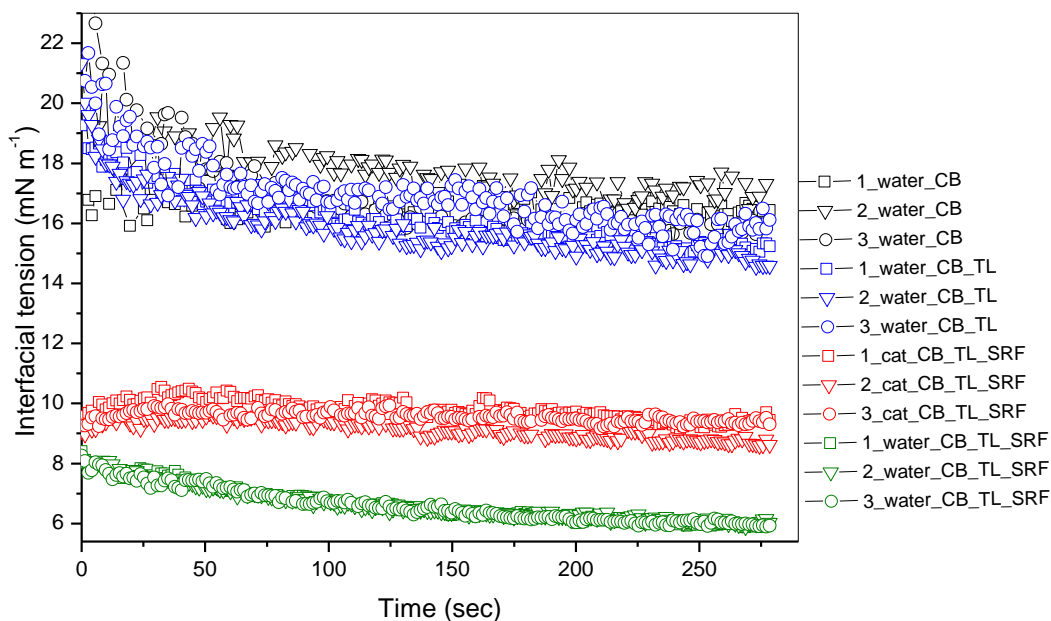


Figure 4-17. Measurements of interfacial tension for different compositions of the mixtures in different environments at  $80 \text{ }^\circ\text{C}$ . Legend: CB =cocoa butter, TL = toluene, SRF = Adogen 464, ‘Cat’ corresponds to the aqueous catalyst solution containing hydrogen peroxide and dissolved tungsten. Each experiment was repeated three times.

### Analytical Determination of Surface Tension

Surface tension of cocoa butter was estimated using the Sugden parachor equation based on a group contribution method<sup>173</sup>, Equation 4-20.

$$\sigma = \left[ \frac{P_{ch} (\rho_L - \rho_v)}{M} \right]^4 \cdot 10^{-12} \quad 4-20$$

where  $\sigma$  is surface tension, ( $\text{mN m}^{-1}$ ),  $P_{ch}$  is Sugden's parachor,  $\rho_L$  is liquid density ( $\text{kg m}^{-3}$ ),  $\rho_v$  is density of the saturated vapour ( $\text{kg m}^{-3}$ ),  $M$  is molecular mass ( $\text{g mol}^{-1}$ ). It was assumed that vapour density of cocoa butter is much smaller than its liquid density and was neglected. Contributions to Sugden's parachor for cocoa butter are given in Table 4-1.

Table 4-1. Contributions to Sugden's parachor for cocoa butter.

Group	Contribution	No.	$P_{ch}$
O	20	6	120
C	4.8	55	264
double bond	23.2	1	23.2
C-H	17.1	74	1265.4
		Total	1672.6

The density of cocoa butter at 80 °C is 834.25  $\text{kg m}^{-3}$  and the molecular mass of cocoa butter is 866.67  $\text{g mol}^{-1}$ . Substituting the above data we may obtain surface tension of cocoa butter.

$$\sigma_{CB} = \left[ \frac{1672.6 \cdot 834.25}{866.67} \right]^4 \cdot 10^{-12} = 10.07 \text{ mN m}^{-1}$$

In reference<sup>174</sup> the effective surface tension of cocoa butter at 60 °C was given as 25.7  $\text{mN m}^{-1}$  against air.

Surface tension of an organic mixture can be calculated as follows<sup>175</sup>:

$$\sigma_m = \sigma_{\text{toluene}} X_{\text{toluene}} + \sigma_{CB} X_{CB} \quad 4-21$$

where  $\sigma_m$  is surface tension of a mixture,  $\sigma_{\text{toluene}}$ ,  $\sigma_{CB}$  are the surface tensions of toluene and cocoa butter respectively. The surface tension of toluene was found as

28.40 mN m<sup>-1</sup> at 20 °C<sup>176</sup>, X<sub>toluene</sub>, X<sub>CB</sub> are mole fractions of toluene and cocoa butter, 0.8451 and 0.1549 for toluene and cocoa butter, respectively.

The surface tension of the mixture of cocoa butter and toluene, calculated using Equation 4-21 from the literature values of individual surface tensions is 27.98 mN m<sup>-1</sup>. The surface tension of the mixture, calculated from the same Equation 4-21 for surface tension of cocoa butter estimated from the Sugden equation is 25.04 mN m<sup>-1</sup>.

Table 4-2. Composition of catalyst used during the epoxidation of cocoa butter.

Component	Molecular number/ mole	Mole fraction	Surface tension at 20 °C / mN m <sup>-1</sup>
Tungsten powder	0.0004	0.0003	
H <sub>2</sub> O <sub>2</sub>	0.040	0.0274	73 <sup>177</sup>
H <sub>2</sub> O	1.417	0.9718	72.75 <sup>178</sup>
H <sub>3</sub> PO <sub>4</sub>	0.0007	0.0005	
Total	1.4581		

From Table 4-2, the fractions of tungsten powder and orthophosphoric acid are much smaller than those of water and hydrogen peroxide employed in the catalyst used for the epoxidation of cocoa butter. Secondly, surface tensions of water and hydrogen peroxide are roughly equivalent. Therefore, surface tension of water was taken for calculation of interfacial surface tension  $\gamma$  between the catalyst and the organic phases.

$$\gamma = \sigma_{water} - \sigma_m \tag{4-22}$$

Hence, the interfacial tension from literature data is 44.8 mN m<sup>-1</sup> and 47.7 mN m<sup>-1</sup> calculated from the Sugden Equation 4-20. These results are very similar. However, the calculation was conducted for the mixture without a surfactant. Surfactants, in this case Adogen 464, reduce interfacial tension. This was observed in the measurement of interfacial tension between water and the mixture of cocoa butter, toluene and surfactant (see Figure 4-17). The average interfacial tension was 16.2 mN m<sup>-1</sup> and the standard deviation was 0.3 mN m<sup>-1</sup>. This measurement is quite

accurate, with coefficient of variation 1.7 %. The average difference between the literature and Sugden's parachor data is 2.8 times higher than the experimental data with the surfactant.

### Determination of Capillary Number

Capillary number is the ratio of viscous force to interfacial tension and is calculated from the following equation:

$$Ca = \frac{\mu_{\text{org}} u_{\text{TP}}}{\gamma} \quad 4-23$$

where  $\mu_{\text{org}}$  is the viscosity of organic phase of cocoa butter at 80 °C, which is equal  $3.80 \cdot 10^{-3}$  Pa s,  $u_{\text{TP}}$  is the linear velocity of the two phases in Taylor flow through a capillary. Calculation was performed for the ratio 1:1 of the flow rates of cocoa butter and the catalyst mixture. Both flow rates were equal  $0.063 \text{ mL min}^{-1}$ . It was assumed that coalescence of slugs does not occur in Taylor flow in the microreactor.

$$u_{\text{TP}} = \frac{F_{\text{TP}}}{A} = \frac{2.10 \cdot 10^{-3} \frac{\text{cm}^3}{\text{s}}}{7.85 \cdot 10^{-3} \text{cm}^2} = 2.7 \cdot 10^{-3} \text{ m s}^{-1} \quad 4-24$$

where  $F_{\text{TP}}$  is the sum of flow rates of cocoa butter and the catalyst, A is the area of tubing of internal diameter 1mm.

Table 4-3. Values of capillary number obtained from the Sugden equation, literature estimation and the experimental data of interfacial tension.

Interfacial tension in units ( $\text{mN m}^{-1}$ ) obtained from	Capillary number
1. Sugden's parachor data between water and the mixture of cocoa butter and toluene	$2.151 \cdot 10^{-4} \mp 0.025 \cdot 10^{-4}$
2. Literature data between water and the mixture of cocoa butter and toluene	$2.290 \cdot 10^{-4} \mp 0.065 \cdot 10^{-4}$
3. Experimental data between water and the mixture of cocoa butter, toluene and Adogen 464	$1.584 \cdot 10^{-3} \mp 0.0165 \cdot 10^{-3}$
4. Experimental data for interfacial tension	$1.08 \cdot 10^{-3} \mp 0.01 \cdot 10^{-3}$

of reaction mixture

Table 4-3 shows that the literature and experimental data differ by one order of magnitude. Experimental data was obtained with good accuracy and hence is preferred over the estimated values. The variation between the results for pure water and the mixture of homogenous complex of catalyst ( $W^{VI}/P^V/H_2O_2/H_2O$ ) is small. However, a more accurate result is obtained for the reaction mixture, which takes into account the contributions as a result of the reaction at the interface.

### Determination of Diffusion Coefficient

Diffusion coefficient of the oxidizing complex in the multicomponent liquid mixture is considered. The oxidizing complex is diffusing from an aqueous phase into the organic phase. The method of Perkins and Geankoplis was adopted<sup>179</sup>:

$$D_{Am}^o \eta_m^{0.8} = \sum_{\substack{j=1 \\ j \neq A}}^n x_j D_{Aj}^o \eta_j^{0.8} \quad 4-25$$

where  $D_{Am}^o$  is an effective diffusion coefficient for a dilute substance A in a mixture ( $cm^2 s^{-1}$ ),  $D_{Aj}^o$  is an infinite dilution binary diffusion coefficient of solute A in the solvent j, ( $cm^2 s^{-1}$ ),  $x_j$  is the mole fraction of j,  $\eta_m$  is a mixture viscosity,  $cP = 0.1 Ns m^{-2} = 0.1 Pa s$ ,  $\eta_j$  is the pure component viscosity (cP).

The equation can be modified to the form including the mixing solvent<sup>179</sup>:

$$D_{Am}^o = 7.4 \cdot 10^{-8} \frac{(\phi M)^{1/2} T}{\eta_m V_A^{0.6}} \quad 4-26$$

The product  $\phi M$  is calculated as follows:

$$\phi M = \sum_{\substack{j=1 \\ j \neq A}}^n x_j \phi_j M_j \quad 4-27$$

where  $M_j$  is the molecular weight of solvent j, ( $g mol^{-1}$ ),  $\phi$  is the dimensionless association factor,  $V_A$  is the molar volume of solute A at its normal boiling temperature, ( $cm^3 mol^{-1}$ ), T is temperature, (K), x is mole fraction. The association

factor  $\phi$  is equal 2.6 for water, 1.9 for methanol, 1.5 for ethanol and 1.0 for unassociated solvents.

$$\text{Thus, } \phi M = x_{\text{toluene}} \phi_{\text{toluene}} M_{\text{toluene}} + x_{\text{CB}} \phi_{\text{CB}} M_{\text{CB}} \quad 4-28$$

$$\phi M = 1 \cdot 0.06 \cdot 92.14 + 1 \cdot 0.01 \cdot 866.67 = 14.20 \text{ g mol}^{-1}$$

The molar volume of a solute, in this case hydrogen peroxide, is calculated by addition of atoms using Schroeder's method<sup>180</sup> for H = 7 for O = 0. It is equal  $14 \text{ cm}^3 \text{ mol}^{-1}$ .

$$\eta_m = 3.80 \text{ mPa s} = 3.8 \text{ cP}$$

Calculation of diffusion coefficient of active species of the catalyst is given below:

$$D_{Am}^0 = 7.4 \cdot 10^{-8} \cdot \frac{14.20^{1/2} \cdot 353.15}{3.8 \cdot 14^{0.6}} = 5.32 \cdot 10^{-6} \text{ cm}^2 \text{ s}^{-1} = 5.32 \cdot 10^{-10} \text{ m}^2 \text{ s}^{-1}$$

The value of diffusion coefficient calculated from Equation 4-26 is different from diffusion coefficients calculated from the film theory, see below Equation 4-48. This estimation diffusion coefficient does not include the impact of the phase transfer agent.

### Mass Transfer

In order to determine the rate determining step of the epoxidation of cocoa butter at 80 °C under flow conditions, the volumetric mass transfer coefficient ( $k_L a$ ), ( $\text{s}^{-1}$ ), was estimated using Equation 4-29<sup>26d</sup>. This equation was originally developed for a two-phase flow of gaseous methane and liquid water flowing through a single glass capillary<sup>181</sup>.

$$k_L a = \frac{0.111 u_{TP}^{1.19}}{[(1 - \epsilon_{\text{Cat}})(L_{\text{CB}} + L_{\text{Cat}})]^{0.57}} \quad 4-29$$

In reference<sup>182</sup> a correction to Equation 4-29 was added as shown in Equation 4-30.

$$k_L a = \left( \frac{D_i}{D_{\text{CH}_4}} \right)^{0.5} (k_L a)_{\text{CH}_4} \quad 4-30$$

Diffusion coefficient of the oxidizing complex in the multicomponent liquid mixture was calculated using the modified Wilke-Chang Equation 4-26,<sup>179</sup>. Diffusion coefficient for methane diffusing into water was taken from Table 11-5 from the book<sup>179</sup>.

$$\begin{aligned}
 k_L a &= \left( \frac{D_{Am}^o}{D_{CH_4}} \right)^{0.5} \frac{0.111 u_{TP}^{1.19}}{[(1 - \varepsilon_{cat.})(L_{CB} + L_{cat.})]^{0.57}} \\
 &= \left( \frac{5.32 \cdot 10^{-6}}{8.5 \cdot 10^{-6}} \right)^{0.5} \frac{0.111 \cdot (2.675 \cdot 10^{-3} \frac{m}{s})^{1.19}}{[0.5 \cdot 2.0 \cdot 10^{-3} m]^{0.57}} \\
 &= 3.91 \cdot 10^{-3} s^{-1}
 \end{aligned} \tag{4-31}$$

where  $\varepsilon_{cat.}$  is the holdup fraction of the catalyst phase, which in this case is equal to the holdup fraction of the organic phase;  $L_{CB}$  and  $L_{cat.}$  are the lengths of slugs of cocoa butter and catalyst phase respectively (m),  $a$  is the specific surface area which is the interfacial area per unit volume of the system ( $m^{-1}$ ). The length of cocoa butter slug is  $1.2 \cdot 10^{-3}$  m and length of catalyst slug is  $8.0 \cdot 10^{-4}$  m.

A. Cybulski<sup>183</sup> in his work studied the impact of various parameters for different solvents and process conditions in a monolithic reactor. He estimated the specific surface area at the spherical ends between gas and liquid. In this case this equation can be given as:

$$a_1 \approx \frac{\pi}{(L_{CB} + L_{cat.})} \tag{4-32}$$

However, a convection phenomenon occurs at both sides of an aqueous slug. Thus, within the whole volume of two phases there are three specific areas where mass transfer takes place. Hence, the equation on the interfacial area per unit volume of a system takes the form of Equation 4-33:

$$a_1 \approx \frac{2A}{V} \approx \frac{2}{L_{CB}} \approx \frac{2}{1.2 \cdot 10^{-3} m} \approx 1666.7 m^{-1} \tag{4-33}$$

The same assumption was reported by Burn<sup>184</sup> for square channels in a microreactor. He observed that liquid layer surrounding the slugs did not occur.

However, Zhao in his work about liquid-liquid two-phase patterns in a rectangular microreactor<sup>25</sup> confirmed the occurrence of wetting between the wall and fluids. He used a CCD camera to observe flow patterns in the mixture of water and kerosene. In this case, we have, apart from mass transfer at the ends of caps of an aqueous slug also mass transfer along the aqueous slugs. Mass transfer between an aqueous and cocoa butter phase is shown in Figure 4-18.

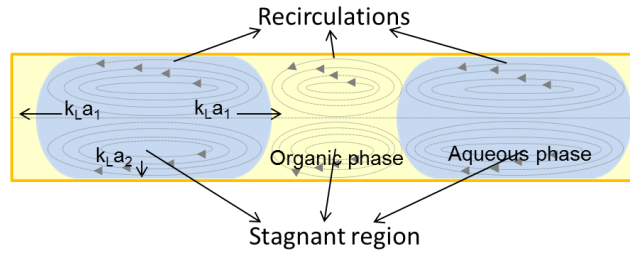


Figure 4-18. Scheme of Taylor flow in Teflon tubing.  $k_{L}a_1$  and  $k_{L}a_2$  show the direction of mass transfer from the aqueous phase to the organic phase where  $k_{L}a_1$  corresponds to mass transfer at the ends of a catalyst slug and  $k_{L}a_2$  corresponds to mass transfer along the aqueous catalyst bubble.

Therefore, the total specific surface area where mass transfer takes place is:

$$a = 2a_1 + a_2 \tag{4-34}$$

The specific surface area  $a_1$  should not be considered as a flat circle but as a spherical cap-shape, Figure 4-19.

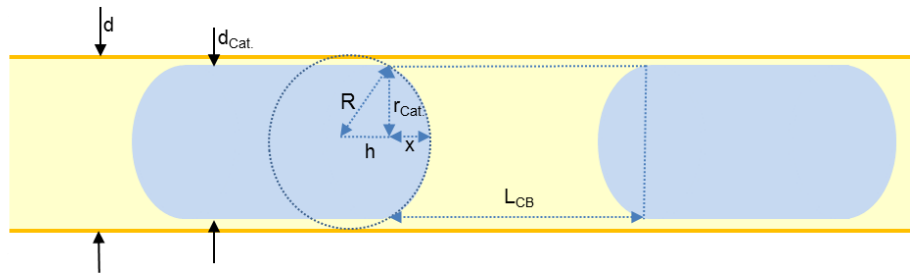


Figure 4-19. Unit cell of the spherical cap-shape at the end of aqueous bubble with thin film.

The volume of the organic phase is calculated by subtracting the volume of spherical caps  $V_{cap}$  ( $m^3$ ) from the volume of a cylinder  $V_{cyl}$  ( $m^3$ ), Figure 4-19.

$$V_{CB} = V_{cyl} - 2V_{cap} \tag{4-35}$$

$$V_{CB} = \pi r_{cat}^2 L_{CB} - \frac{2\pi x^2 (3R - x)}{3} \tag{4-36}$$

The radius of the catalyst bubble  $r_{cat}$  (m) was determined from the diameter of this bubble. This diameter was calculated using correlation <sup>26e</sup>.

$$\frac{d_{cat}}{d} = 0.64 + 0.36\exp(-3.08Ca^{0.52}) \quad 4-37$$

The diameter of the catalyst slug is a function of Capillary number. In this case, it is  $9.79 \cdot 10^{-4}$  m.  $x$  (m) is then calculated by subtraction:

$$x = R - h \quad 4-38$$

The radius of the catalyst slug  $R$  (m) is difficult to distinguish from the radius of the tubing using photographs of slugs in the tubing (Figure 4-19). Thus, the assumption was made that  $R$  is equal the radius of tubing. For this residence time  $R$  is equal  $7.0 \cdot 10^{-4}$  m.  $h = 5.0 \cdot 10^{-4}$  m was calculated from Pythagorean theorem of a right triangle ( $R, h, r_{Cat.}$ ), Figure 4-19. Hence,  $V_{CB}$  amounts to  $7.44 \cdot 10^{-10}$  m<sup>3</sup>. Both surface areas of spherical-caps at ends of a catalyst bubble are given by:

$$A_{caps} = 2(2\pi Rx) = 1.75 \cdot 10^{-6} \text{ m}^2 \quad 4-39$$

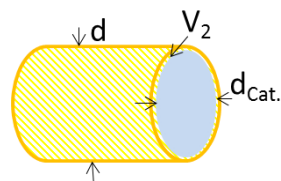
Hence,

$$2a_1 = \frac{A_{caps}}{V_{CB}} = 2357.24 \text{ m}^{-1} \quad 4-40$$

The surface area surrounding the catalyst phase was calculated as the surface area of the side of a cylinder:

$$A_{cyl} = 2\pi L_{Cat.} r_{cat.} = 2.46 \cdot 10^{-6} \text{ m}^2 \quad 4-41$$

The volume of organic phase  $V_2$  (m<sup>3</sup>) surrounding the catalyst phase was calculated from the following subtraction:



$$V_2 = V_d - V_{dCat.} = \pi L_{Cat.} \left( \left( \frac{d}{2} \right)^2 - \left( \frac{d_{Cat.}}{2} \right)^2 \right) \quad 4-42$$

$$= 2.64 \cdot 10^{-11} \text{ m}^3$$

The specific surface area  $a_2$  was:

$$a_2 = \frac{A_{cyl}}{V_2} = 93218.06 \text{ m}^{-1} \quad 4-43$$

Hence, the total specific surface area was

$$a = 2a_1 + a_2 = 95575 \text{ m}^{-1} \quad 4-44$$

The above analysis of the way of carrying out the calculation of the specific surface area shows that the simplified Burn method<sup>184</sup> of this calculation provides the

significantly lower result of this value. This method did not consider an organic liquid film on the Teflon capillary wall. Interfacial area of organic phase surrounding the catalyst phase ( $a_2$ ) is 40 times higher the interfacial area of spherical caps ( $2a_1$ ).

Hence, mass transfer coefficient  $k_L$  ( $\text{m s}^{-1}$ ) is defined as:

$$k_L = \frac{k_L a}{a} = \frac{0.0039 \text{ s}^{-1}}{95575 \text{ m}^{-1}} = 1.02 \cdot 10^{-8} \text{ m s}^{-1} \quad 4-45$$

Thickness of a laminar layer  $\delta$  (m) was calculated from Kreutzer equation <sup>26d</sup>.

$$\frac{\delta}{d} = \frac{0.66 \text{Ca}^{\frac{2}{3}}}{1 + 3.33 \text{Ca}^{\frac{2}{3}}} \quad 4-46$$

$$\delta = d \frac{0.66 \text{Ca}^{\frac{2}{3}}}{1 + 3.33 \text{Ca}^{\frac{2}{3}}} = 6.67 \cdot 10^{-6} \text{ m} \quad 4-47$$

Diffusion coefficient in the organic phase ( $\text{m}^2 \text{s}^{-1}$ ) was calculated:

$$k_L = \frac{D}{\delta} \quad 4-48$$

$$D = k_L \delta = 6.83 \cdot 10^{-14} \text{ m}^2 \text{ s}^{-1} \quad 4-49$$

### Hatta Number

The crucial parameter that determines how mass transfer is affected by chemical reaction is a dimensionless Hatta number.

$$\text{Ha} = \delta \sqrt{\frac{k_R}{D}} = \frac{\sqrt{D k_R}}{k_L} = 0.56 \quad 4-50$$

where  $k_R$  is the reaction rate constant; for epoxidation at 80 °C and the agitation rate at 250 rpm it is equal  $4.73 \cdot 10^{-3} \text{ s}^{-1}$ .

Hatta number is a criterion which describes whether reaction occurs completely in the liquid bulk or in the liquid film. When reaction is slow  $\text{Ha} < 0.3$ , reaction is taking place in the bulk phase. For the situation, where  $0.3 < \text{Ha} < 3$  the mass transfer is dependent on the chemical reaction as well as the diffusion process. A

reaction occurs in a film layer and also in a bulk phase. Fast reactions occur completely in a film layer when  $Ha > 3$ .

Based on the obtained values, epoxidation of cocoa butter at 80 °C is dependent on the chemical reaction as well as the diffusion process. The reaction occurs in a film layer and also in a bulk phase. However, calculation of Hatta number according to the above procedure uses two values, namely diffusion coefficient and thickness of laminar layer, derived from the same equation. Therefore, an independent estimate of diffusion coefficient was calculated Equation 4-25.

### **Effect of Flow Rates**

The volumetric mass-transfer coefficient with reference to Equation 4-29 is directly proportional to the total linear velocity of the two phases in Taylor flow through a capillary and inversely proportional to the lengths of slugs. Figure 4-20 shows that, with the increased total velocity of the two phases in Taylor flow, the volumetric mass-transfer coefficient also increases. This is due to the increased internal circulation inside the slugs with increased flow rate (Figure 4-18) <sup>32b, 168, 184-185</sup>.

Moreover, in the case of an increasing amount of the catalyst inside the slug in comparison to the 1:1 ratio of flow rates of the organic phase to the aqueous catalyst phase, the volumetric mass-transfer coefficient should be slightly higher according to Equation 4-29.

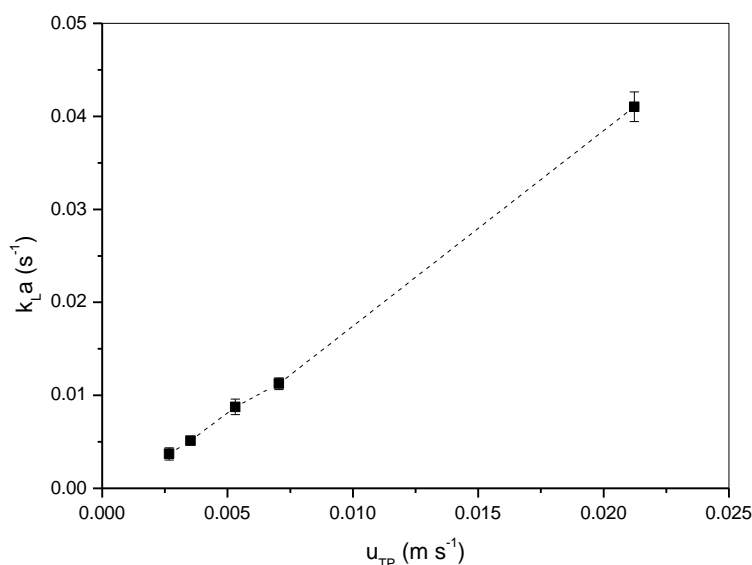


Figure 4-20. Volumetric mass-transfer coefficient as a function of the total linear velocity of two phases in Taylor flow for 1-mm diameter tubing in biphasic epoxidation of cocoa butter.

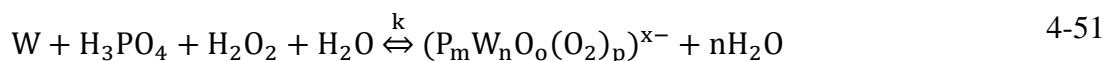
### Reaction Mechanism and Formulation of a Kinetic Equation

The reaction mechanism of phase-transfer-catalysed epoxidation with  $H_2O_2$  and heteropolyacid was elaborated by Yadav and Satoskar<sup>106b</sup>. They considered that epoxidation occurred in the organic phase. The chemical reaction was the limiting step in their mechanism. In our case, we concluded from Hatta number analysis that the epoxidation of cocoa butter is limited by both mass transfer and chemical reaction.

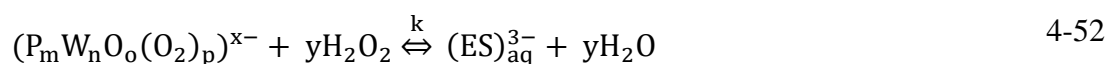
Several processes take part in the formation of epoxide, as shown in Figure 4-21.

The mechanism of epoxidation can be written in the following way:

1. Preparation of the catalyst complex  $W^{VI}/P^V/H_2O_2/$  was performed in a flask in water (Figure 4-21). This step was performed prior to flow epoxidation.



2. In the next step the epoxidizing species  $\{PO_4(WO(O_2)_2)_4\}^{3-}$ , (ES), was formed:



3. This epoxidizing species was reacted with quaternary ammonium salt, QX, in our case Adogen 464. This reaction occurs in the aqueous phase.



4.  $[\text{Q}_3\text{ES}]_{\text{aq}}$  was transferred to the aqueous-organic interface.



5. The reaction was performed at the interface and also in the organic bulk.



6.  $[\text{Q}_3\text{SPS}]_{\text{org}}$  species was transferred to the aqueous phase.



7. In the aqueous phase  $[\text{Q}_3\text{SPS}]_{\text{aq}}$  was reactivated to epoxidizing species.



8. We have also two side reactions. The first one is the decomposition of hydrogen peroxide in the aqueous phase.



9. The second side reaction is ring opening in the presence of ortho-phosphoric acid.

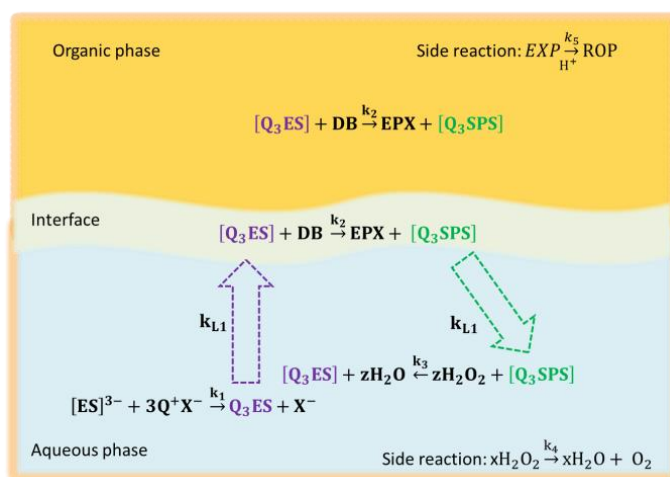


Figure 4-21. Starks extraction mechanism <sup>159b</sup> adopted for the phase-transfer-catalysed epoxidation of cocoa butter. The nomenclature was used on the basis of

106b

Reactions from 4-52 to 4-59 occur in the aqueous and organic slugs under flow conditions. All these above reactions except reactions 4-54, 4-55 and 4-56 are at equilibrium. The rate equations, which control this process, can be written as:

$$r_r = k_2[DB][Q_3ES]_{org} \quad 4-60$$

$$r_{m.t.1} = k_{L_1} a [Q_3ES]_{aq} \quad 4-61$$

$$r_{m.t.2} = k_{L_1} a [Q_3SPS]_{org} \quad 4-62$$

The rates of mass transfer  $r_{m.t.1}$  and  $r_{m.t.2}$  are assumed to be the same.

Rate of formation  $Q_3ES_{aq}$  can be written as:

$$r_{Q_3ES_{aq}} = k_1 [ES_{aq}^{3-}] [Q^+X^-]^3 - k'_1 [Q_3ES]_{aq} [X^-]^3 + k_3 [Q_3SPS]_{aq} [H_2O_2]^z - k'_3 [Q_3ES]_{aq} [H_2O]^z = 0 \quad 4-63$$

The concentrations of  $Q_3ES_{aq}$  and  $Q_3SPS$  are the same.

$$r_{Q_3ES_{aq}} = k_1 [ES_{aq}^{3-}] [Q^+X^-]^3 - k'_1 [Q_3ES]_{aq} [X^-]^3 + k_3 [Q_3ES]_{aq} [H_2O_2]^z - k'_3 [Q_3ES]_{aq} [H_2O]^z = 0 \quad 4-64$$

$$[Q_3ES]_{aq} = \frac{k_1 [ES^{3-}] [Q^+X^-]}{k'_1 [X^-]^3 + k'_3 [H_2O]^z - k_3 [H_2O_2]^z} \quad 4-65$$

$[Q_3ES]_{aq}$  in the rate of mass transfer,  $r_{m.t.}$  in Equation 4-61 is substituted by Equation 4-65.

$$r_{m.t.1} = k_{L_1} a \frac{k_1 [ES^{3-}] [Q^+X^-]}{k'_1 [X^-]^3 + k'_3 [H_2O]^z - k_3 [H_2O_2]^z} \quad 4-66$$

The chemical rate is proportional to the concentration of cocoa butter and to the amount of transferred oxidizing species into the organic phase, Equation 4-60. The amount of oxidizing species depends on mass transfer. Mass transfer depends on the volumetric mass transfer coefficient, which is enhanced with increasing flow rate and the decreasing length of slugs. Mass transfer is also enhanced by the rate of formation of epoxidizing species, Equation 4-66.

### Modelling of a Reactor for the Epoxidation of Cocoa Butter under Flow Conditions

Firstly, if we want to improve the process of epoxidation, the mass transfer of oxidizing species should be slower than the organic phase reaction, such that the reaction would occur in the interfacial region. The mechanism of this process is shown schematically in Figure 4-22.

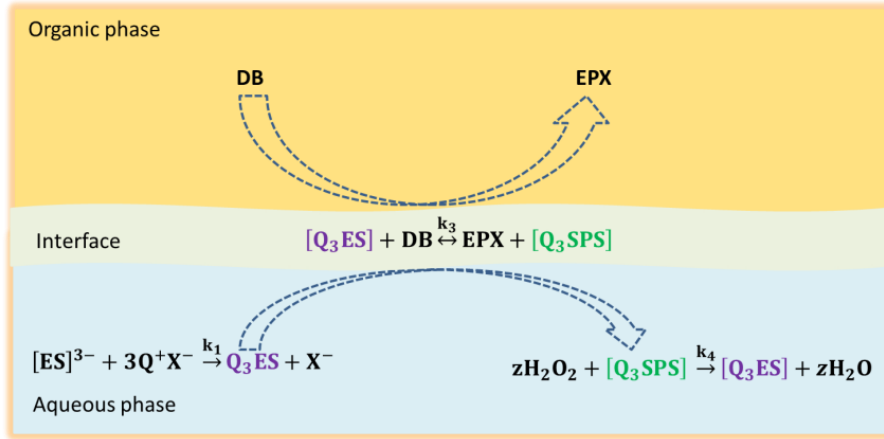
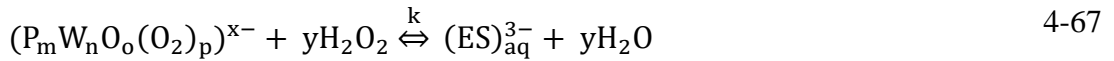


Figure 4-22. Proposed mechanism of epoxidation in the interfacial region.

The reaction's path in the aqueous and organic slugs for the above mechanism can be written in the following way:





The rates of steps 4-67, 4-68, 4-70 and 4-72 are faster than the distribution of epoxidizing species to the interface and again to the aqueous phase (Equations 4-69 and 4-71). The mass-transfer steps are rate-limited steps if we wish to perform the reaction in the interfacial region. Thus, the rate equations of mass transfer can be written as:

$$r_{m.t.1} = k_{L1} a [Q_3ES]_{aq} \quad 4-73$$

$$r_{m.t.2} = k_{L1} a [Q_3SPS]_{if} \quad 4-74$$

The concentration of  $Q_3ES_{aq}$  obtained from its rate of formation can be written as:

$$[Q_3ES]_{aq} = \frac{k_1[ES^{3-}][Q^+X^-] + k_3[Q_3SPS]_{aq}[H_2O_2]^z}{k'_1[X^-]^3 + k'_3[H_2O]^z} \quad 4-75$$

The concentration of species  $Q_3SPS_{if}$  can be written as:

$$[Q_3SPS]_{if} = \frac{k_2[DB]_{if}[Q_3ES]_{if}}{k'_2[EXP]_{if}} \quad 4-76$$

The rate of mass transfer of epoxidizing species to the interface can be written as:

$$r_{m.t.1} = k_{L1} a \frac{k_1[ES^{3-}][Q^+X^-] + k_3[Q_3SPS]_{aq}[H_2O_2]^z}{k'_1[X^-]^3 + k'_3[H_2O]^z} \quad 4-77$$

The rate of mass transfer of epoxidizing species to the interfacial region is dependent on the volumetric mass transfer and the rate of formation and reformation of epoxidizing species in the aqueous phase. The concentrations of chloride ions and water are assumed to be constant in the aqueous phase and so do not have an impact on the rate of mass transfer ( $r_{m.t.1}$ ).

The rate of mass transfer of peroxy species to the aqueous species can be written as:

$$r_{m.t.2} = k_{L1} a \frac{k_2 [DB]_{if} [Q_3 ES]_{if}}{k'_2 [EXP]_{if}} \quad 4-78$$

This rate is also directly proportional to the volumetric mass transfer and the rate of the formation of epoxide species and inversely proportional to the formation of raw material.

Secondly, the determination of critical parameters controlling epoxidation in the Vapourtec reactor of 1 mm diameter of the tubing shows that the process is limited by the reaction rate and also by the mass transfer. If we assume that the reaction will be fast and will occur in the interface, then the reaction will be controlled by mass transfer. The Hatta number will be higher than 3.

$$\frac{\sqrt{Dk_R}}{k_L} > 3 \quad 4-79$$

Thirdly, according to Equation 4-29, the volumetric mass transfer is inversely proportional to the lengths of aqueous and organic slugs, which can be made smaller by applying smaller diameter tubing. The Sherwood number for a fully laminar flow rate in a microchannel has the constant value:

$$Sh = \frac{k_L d}{D} = 3.66 \quad 4-80$$

This equation provides the possibility of experimentally checking the mass-transfer limitation by changing the diameter of the microchannel <sup>186</sup>.

In the case of a 1-mm diameter microchannel, the Sherwood number is ~ 149. To obtain a new diameter of microchannel, our experimental Sherwood number should be divided by the theoretical value:

$$\frac{Sh_{\text{experimental}}}{Sh_{\text{theoretical}}} = \frac{149}{3.66} = 40.7 \quad 4-81$$

The diameter of the microchannel should be 40.7 times smaller and hence the estimated diameter of the new channel is:

$$d_{\text{new}} = \frac{10^{-3}}{40.7} = 2.46 \cdot 10^{-5} \text{ m} = 24.6 \text{ } \mu\text{m} \quad 4-82$$

Once again, for  $Ha \geq 3$ ,  $k_R$  is assumed constant in Equation 4-50.  $D$  and  $k_L$  are dependent on each other, and therefore:

$$\frac{D}{k_L^2} \geq 8182 \tag{4-83}$$

The mass-transfer coefficient and the diffusion coefficient can be determined by the system of equations of the Hatta number (Equation 4-50) and the Sherwood number:

$$\begin{cases} \frac{D}{k_L^2} = 8182 \\ \frac{k_L d}{D} = 3.66 \end{cases} \tag{4-84}$$

$$\begin{cases} \frac{D}{k_L^2} = 8182 \\ k_L = D \cdot 148780 \end{cases} \tag{4-85}$$

$$\begin{cases} \frac{D}{D^2 \cdot 2.21 \cdot 10^{10}} = 8182 \\ k_L = D \cdot 148780 \end{cases} \tag{4-86}$$

$$\begin{cases} D = 5.52 \cdot 10^{-15} \text{ m}^2 \text{ s}^{-1} \\ k_L = 8.21 \cdot 10^{-10} \text{ m s}^{-1} \end{cases} \tag{4-87}$$

The estimated mass-transfer coefficient for the diameter of a channel of 24.6  $\mu\text{m}$  is lower by two orders of magnitude and the diffusion coefficient is smaller by one order of magnitude in comparison to a microchannel of 1 mm.

### 4.3 Reduction of Artemisinin

Batch experiments were carried out first to determine the best reducing agents for the continuous-flow processes. Due to the labile nature of the peroxy bond in ART and the requirement of the continuous-flow experiments, *i.e.* high solubility of a reducing agent, only three candidates were selected based on the literature<sup>187</sup> namely, lithium tri-*tert*-butoxyaluminum hydride ( $\text{LiAlH}(\text{O}^t\text{Bu})_3$ ), sodium bis(2-methoxyethoxy)aluminum hydride ( $\text{NaAlH}_2(\text{OCH}_2\text{CH}_2\text{OMe})_2$ , Red-Al) and lithium triethylborohydride ( $\text{LiBHEt}_3$ ).

We first examined the published protocol of  $\text{NaBH}_4$  reduction of ART<sup>115</sup>. The highest yield (90 %) of DHA was obtained at 4 °C after 100 min, Table 4-4, entry 2.  $\text{LiAlH}(\text{O}^t\text{Bu})_3$  was reported to be able to reduce a peroxy ester into the corresponding alcohol without breaking the peroxy bond<sup>187</sup>. 1 M solution of  $\text{LiAlH}(\text{O}^t\text{Bu})_3$  in THF was used in this study. The best result obtained for  $\text{LiAlH}(\text{O}^t\text{Bu})_3$  reduction was 67 % yield of DHA within 60 min (entry 5, 40 °C, 81 % conversion of ART). Reaction of ART with Red-Al was found to be fast at 3 °C: disappearance of ART was confirmed by TLC after 10 min. The yield of DHA was only 46 % by HPLC (93 % conversion of ART by HPLC, entry 6). The mass imbalance was most likely caused by the formation of by-products. These by-products, Figure 4-23, were identified by <sup>1</sup>H-NMR and LC-MS analysis.

The two by-products (**38** and **39**) have been well-documented for the process of reducing ART to DHA. The glycal (**38**) (anhydro dihydroartemisinin, MS: m/z (% intensity) 267.1588 [ $\text{MH}^+$ ] (calcd 267.1591); 284.1855 [ $\text{MNH}_4^+$ ] (calcd 284.1856))<sup>188</sup> is the dehydration product of DHA. By-product (**39**) (MS: m/z (% intensity) 297.2046 [ $\text{MH}^+$ ] (calcd 297.2036) is a product of fragmentation of DHA under reductive conditions<sup>113d, 188b</sup>. The two side-reductions may be attributed to poor mixing, *i.e.* uneven distribution of reactants and distribution of residence time, and poor temperature control in the batch reactor. Another by-product (trace amount) with a molecular mass of 143.1073 (MS calculated formulae:  $\text{C}_8\text{H}_{15}\text{O}_2$ ) was also detected by LC-MS. This by-product has previously been identified by us during the accelerated stressing of ART and is yet to be structurally characterised.

LiBHET<sub>3</sub> was found to be more effective in terms of reaction time and yield. The substrate was found to be fully consumed after 10 min of reaction at 2 °C. The yield of DHA was found to depend on the molar equivalent of LiBHET<sub>3</sub> (entries 7 – 10). The product DHA could be produced in 94% yield by using 3 molar equivalent of LiBHET<sub>3</sub>. The tolerance of synthesis of DHA with LiBHET<sub>3</sub> to temperature was also examined. Lower yield of DHA at *ca.* 20 °C was obtained after 5 min reaction (entries 15). Apart from the work-up procedure, a direct water precipitation method was also tested for quenching the reaction (entry 16). However, only 46 % yield of DHA was recovered after the work-up. Among the reductants examined, LiBHET<sub>3</sub> demonstrated the advantages of excellent reducing power and high chemoselectivity. Further advantages of using LiBHET<sub>3</sub> for synthesis of DHA are short reaction time and tolerance to reaction temperature.

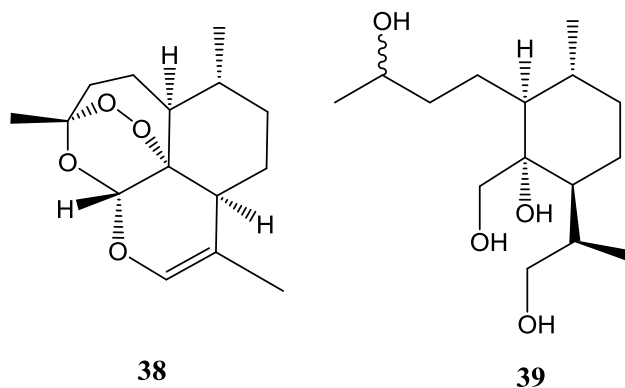


Figure 4-23. Identified by-products in the reduction of ART to DHA.

Table 4-4. A summary of results of reduction of artemisinin under batch reaction conditions.

Entry	Reductant	Mole eq (-)	T (°C)	t (min)	Solvent	Conversion of ART (%) <sup>[a]</sup>	Yield to DHA (%) <sup>[b]</sup>
1	NaBH <sub>4</sub>	2.5	4	90	MeOH	96	87
2		3	4	100		98	90
3 <sup>[c]</sup>		3	4	100		97	89
4	LiAlH(O <sup>t</sup> Bu) <sub>3</sub>	3	3	120	THF	65	42
5		3	40	60		81	67

## Results and Discussion

6	RedAl	3	3	10	Toluene	93	46
7	LiBHEt <sub>3</sub>	2	2	10	THF	100	75
8		2.5	2	10		100	87
9		3	2	10		100	94
10 <sup>[d]</sup>		3	2	10		100	92
11		2	18	5		100	80
12		2.5	18	5		100	81
13		3	19	5		100	83
14 <sup>[e]</sup>		3	20	15		100	75

[a] X - conversion determined by HPLC [b] isolated yield determined by HPLC (the total amount of  $\alpha$  and  $\beta$  dihydroartemisinin epimers), ratio of  $\alpha$ -DHA to  $\beta$ -DHA was *ca.* 40%/60% for fresh sample by H-NMR; [c] a synthesis with 1 g of substrate ART [d] 200 mg of ART in 5 mL THF [e] a synthesis with 1.412 g of substrate ART.

Experiments under flow conditions were performed in a rig shown schematically in Figure 4-24. Results are summarized in Table 4-5. Flow experiments showed very high conversion and selectivity under all experimental conditions tested. The residence times as low as 30 seconds were enough to produce DHA quantitatively when THF was employed as a solvent. This represents a reduction of at least one order of magnitude in reaction time compared to batch experiments. The reaction was performed at room temperature, thus reducing the overall energy intensity compared to the traditional reduction protocols, requiring cooling.

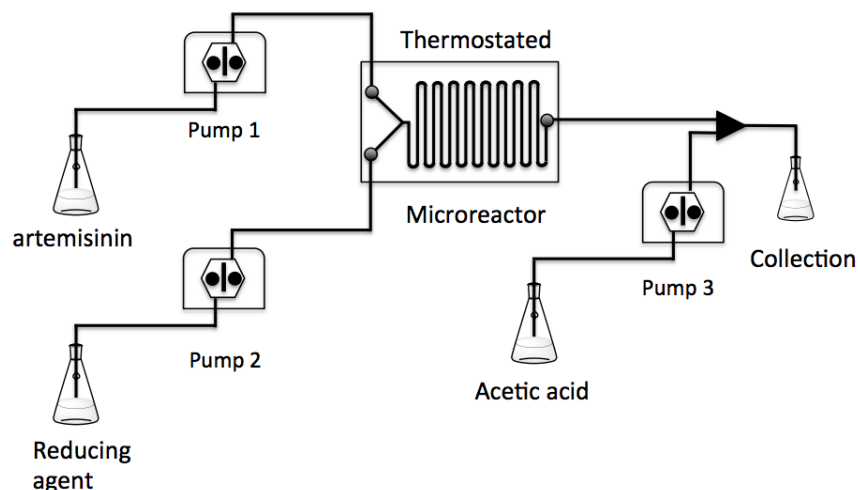


Figure 4-24. A schematic diagram of the continuous flow rig for the stoichiometric reduction.

The replacement of traditional solvents by less toxic and more environmentally benign is a key principle of green chemistry<sup>189</sup>. We studied the replacement of THF by a biomass-derived alternative solvent 2-methyl-tetrahydrofuran<sup>190</sup>. 2-Methyltetrahydrofuran is synthesized in two steps from 2-furaldehyde, a chemical obtained from agricultural waste<sup>16</sup>. It has Lewis base properties and polarity between that of THF and dimethyl ether. LiBHET<sub>3</sub> showed a good solubility in Me-THF and the reaction was conducted in flow, Table 2 entries 8-11. Conversion was found to be slightly lower than that with THF, compare entries 8 and 4. Traces of artemisinin were found under these conditions by HPLC and NMR, even though conversion was found to be very high (> 96%). An even lower residence time of 20 seconds (entries 10, 11) showed similar degrees of conversion and selectivity, indicating fast kinetics of the reaction. A small amount of side products from rearrangement or over-reduction (< 1%, **38** and **39**) was found by HPLC. Therefore, one can see that, in comparison with batch reactors, the well-controlled reaction conditions in the micro-flow reactors can significantly reduce the possibility of forming by-products.

Table 4-5. A summary of results of reduction of artemisinin under flow conditions.

Entry	Solvent	Residence time (min)	T (°C)	Conversion of ART (%) <sup>[a]</sup>	Yield of DHA (%) <sup>[b]</sup>
1	THF	2	5	99	98
2		1	5	99	98
3		2	25	99	98
4		0.5	25	99	98
5		1	25	99	98
6		1	15	99	97
7		1	0	98	95
8	2-MeTHF	0.5	25	97	93
9		0.5	5	96	95
10		0.33	25	97	94
11		0.33	5	97	94

[a] Calculated from NMR and HPLC data [b] yield means the total amount of  $\alpha$  and  $\beta$  dihydroartemisinin epimers, DHA was confirmed by MS and H-NMR, yields were determined by HPLC,  $\alpha$ -DHA/ $\beta$ -DHA  $\approx$  45%/55% by H-NMR. Reaction conditions: artemisinin 0.033 M, LiBHET<sub>3</sub> 0.1 M, acetic acid 20%.

Based on the reaction data we evaluated basic reaction mass metrics of the benchmark batch reaction and of the flow reaction using Me-THF solvent.

Atom economy is the concept developed by Barry Trost from Stanford University (US). This method shows how efficiently chemical process is in terms of all atoms

191.

$$\text{atom economy} = \frac{\text{molecular mass of desired product}}{\text{molecular mass of all reactants}} \cdot 100 \% \quad 4-88$$

Atom economy is better for the process using sodium borohydride due to its lower mass, *i.e.*, 0.89 against 0.73 for the flow process using LiBHET<sub>3</sub>. However, energy intensity and the life cycle data are required for more detailed comparison.

### Reaction Calorimetry under Batch Conditions

The area of the true heat flow for the reaction was equal 500 J. The enthalpy of reaction can be obtained then from equation:

$$\Delta_r H^\ominus(80\text{ }^\circ\text{C}) = \frac{\text{Area of true heat flow in a reactive system}}{\text{number of moles of ART in the reaction}} \quad 4-89$$

The enthalpy of reduction of artemisinin was found to be extremely exothermic at -704 kJ · mol<sup>-1</sup>.

### Reduction of 9-epi-Artemisinin

API raw materials used in the production of the highly important artemisinin-based combination therapies (ACTs) have well-defined chemical properties and structures. The WHO provides guidelines with regard to the concentration of artemisinin and impurities in a raw material, which can be found elsewhere<sup>192</sup>. One of the major impurities of artemisinin is 9-epi-artemisinin, which is an isomer of artemisinin (Figure 4-25). Suberu<sup>193</sup> conducted research into the role of 9-epi-artemisinin in the treatment of malaria. He concluded that, as seen in artemisinin, 9-epi-artemisinin shows antiplasmodial activity. However, this activity is three-fold lower compared to artemisinin. The difference in the activity can be related to a structural conformation which shows relatively more resistance to activation compared to artemisinin<sup>193</sup>.

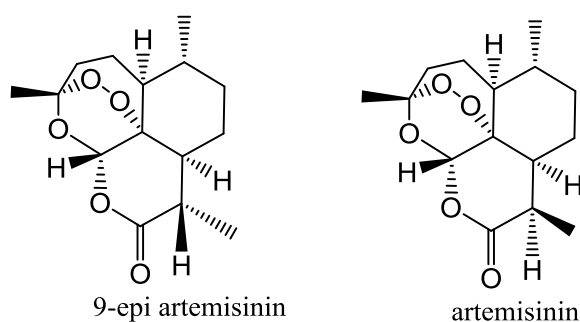


Figure 4-25. Structure of 9-epi artemisinin and artemisinin.

In our research, the reduction of 9-epi-artemisinin was performed. The analysis of products was achieved by using tandem mass spectrometry (MS/MS). The transitions used for the MS/MS analysis of the products are shown in (Table 3-5).

The reduction of 9-epi artemisinin was performed twice. The first experiment lasted for a total of 20 min. In MS/MS chromatograms related to DHA we did not observe any DHA product. However, the ARM- $\beta$  was detected, (see Figure 4-26).

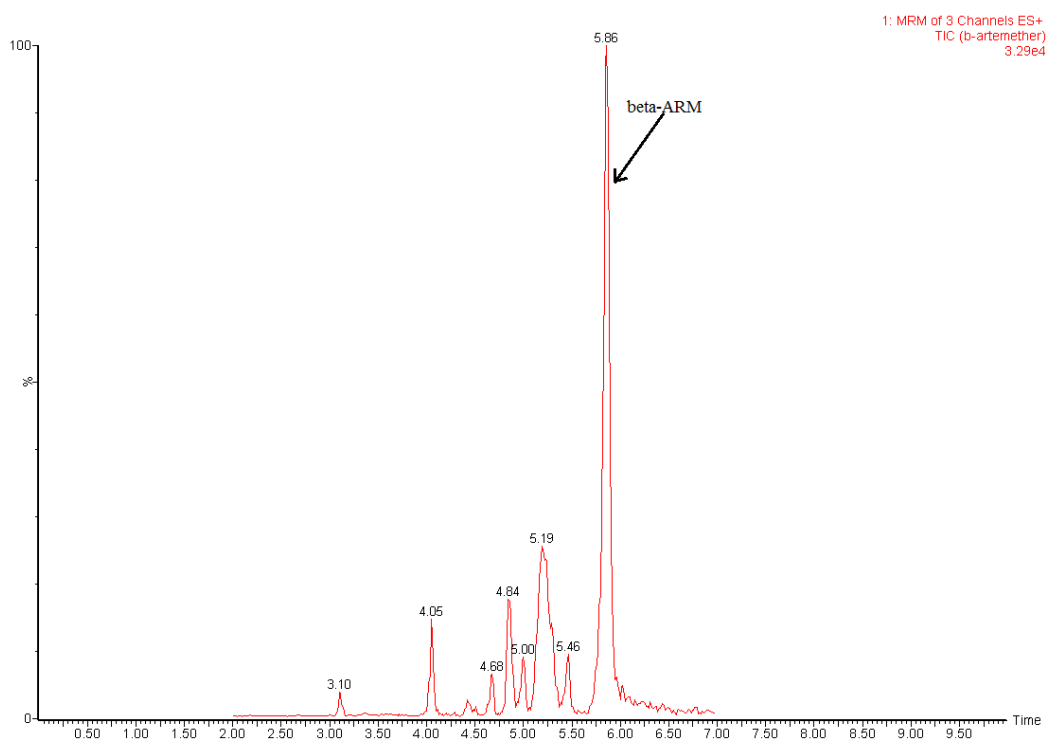


Figure 4-26. Chromatogram shows tandem mass spectrometry MS/MS analysis of the ARM- $\beta$  in the product of the reduction of 9-epi-artemisinin. The reaction lasted 20 min.

The second experiment was carried out for 5 min. The reaction was not completed. 9-epi-artemisinin was detected in MS/MS chromatogram, (Figure 4-27).

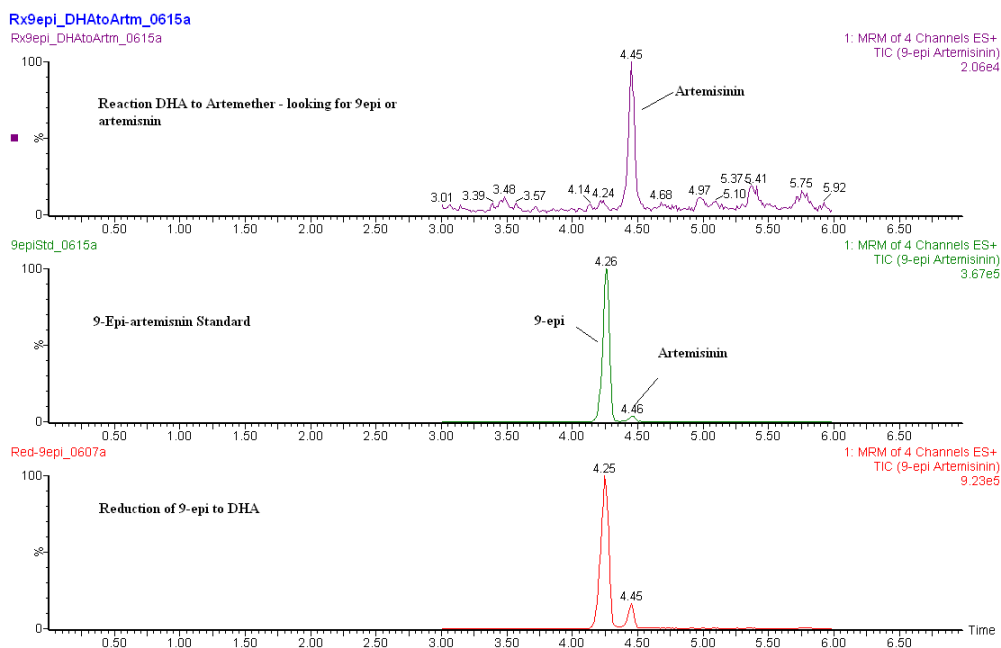


Figure 4-27. Chromatograms show tandem mass spectrometry MS/MS analysis of 9-epi-artemisinin in: a) the product etherification without a base quenching step, the product was analysed the next day after the reaction was complete b) the standard 9-epi-artemisinin and c) the product of the reduction of 9-epi-artemisinin. The reaction lasted 5 min. The product was analysed on the same day after the reaction was complete.

The products of the reduction of 9-epi-artemisinin are DHA (Figure 4-28) and artemether (Figure 4-29). In the ARM- $\beta$  and DHA chromatograms, we can see more peaks which may be relative to other isomers of ARM- $\beta$  or DHA; however, we cannot define those components without the standards used in MS/MS analysis. Artemether products can be the result of a trace of methanol in the reagents. In this case, acetic acid could have been the catalyst for artemether as is shown in Scheme 2-8.

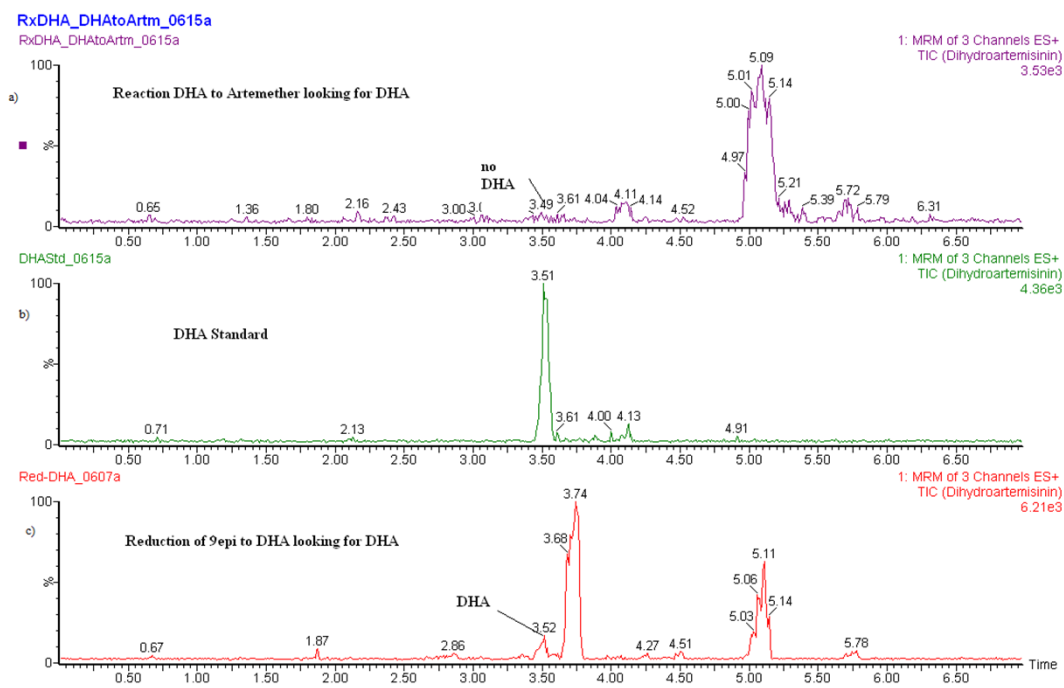


Figure 4-28. Chromatograms show tandem mass spectrometry MS/MS analysis of DHA. Analysis of: a) the product etherification without a base quenching step, the analysis of the product was performed the next day after the reaction was finished b) the standard DHA sample and c) the product of the reduction of 9-epi-artemisinin. The reaction lasted 5 min. The product was analysed on the same day after the reaction was complete.

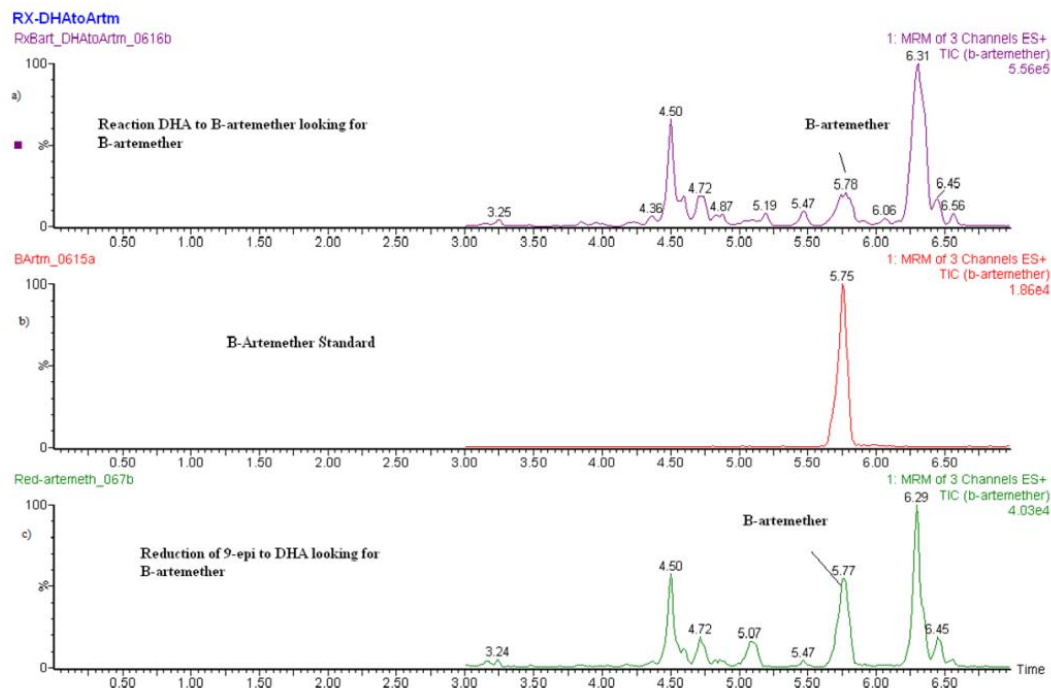


Figure 4-29. Chromatograms show tandem mass spectrometry MS/MS analysis of ARM- $\beta$  in: a) the product etherification without a base quenching step. The analysis of the product was performed the next day after the reaction was complete, b) the standard DHA sample and c) the product of the reduction of 9-epi-artemisinin. The reaction lasted 5 min. The product was analysed on the same day after the reaction was complete.

Also, the reaction product was analysed by HPLC. ARM  $\alpha$  and  $\beta$  and 9-epi-artemether were detected; however, DHA peaks can be overlapped by peaks of the solvents used in the analysis, (Figure 4-30).

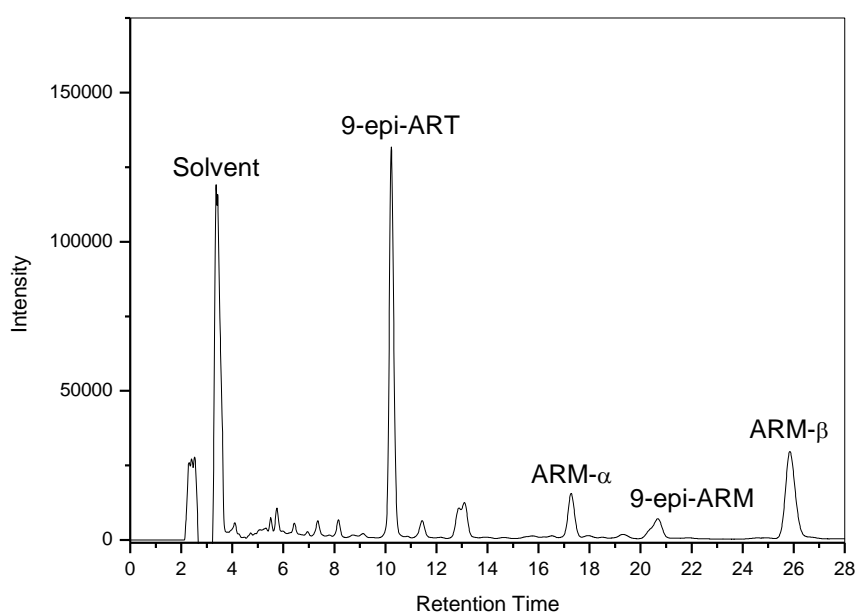


Figure 4-30. HPLC chromatogram of the reduction product of 9-epi artemisinin. The mobile phase used for the analysis was acetonitrile/water/ acetic acid in the ratio of 65/35/0.1.

#### 4.4 Etherification of Dihydroartemisinin

From our previous study (Section 4.3 Reduction of Artemisinin) we know that batch reduction of artemisinin to DHA in methanol with NaBH<sub>4</sub> can achieve a 90 % yield in 100 minutes at 4 °C, whereas reduction under flow conditions using 2-Me-THF solvent and superhydride reducing agent (1.0 M Li(C<sub>2</sub>H<sub>5</sub>)<sub>3</sub>BH in THF) result in a higher yield of 95 % and reaction could be run at ambient temperature with a residence time of ca. 20 s<sup>160</sup>. Yield is reported as combined yield to  $\alpha$ - and  $\beta$ -DHA isomers with the ratio of the two isomers in solution at the end of reaction 45/55% by NMR<sup>160</sup>. In the solid state only  $\beta$ -DHA isomer is present which, upon dissolution equilibrates with the  $\alpha$ -isomer. This interconversion is shown Figure 4-40.

##### 4.4.1 Batch Etherification of Dihydroartemisinin

Etherification of a mixture of  $\alpha/\beta$ -isomers of DHA to artemether over Amberlyst-15 catalyst was performed at different catalyst loadings and at different temperatures, see Figure 4-31. It was shown that increasing the molar equivalent of acid with respect to the reactant results in the increase of  $\beta$ -artemether yield: at 170 min of reaction time the samples with 0.25, 0.5 and 1 molar equivalents of active sites gave 13, 28 and 39 % yields respectively. Increasing reaction temperature from ambient to 40 °C for the reaction with 1 molar equivalent of acid sites resulted in the increase of reaction yield from 39 to 70 % at 170 min of reaction time.

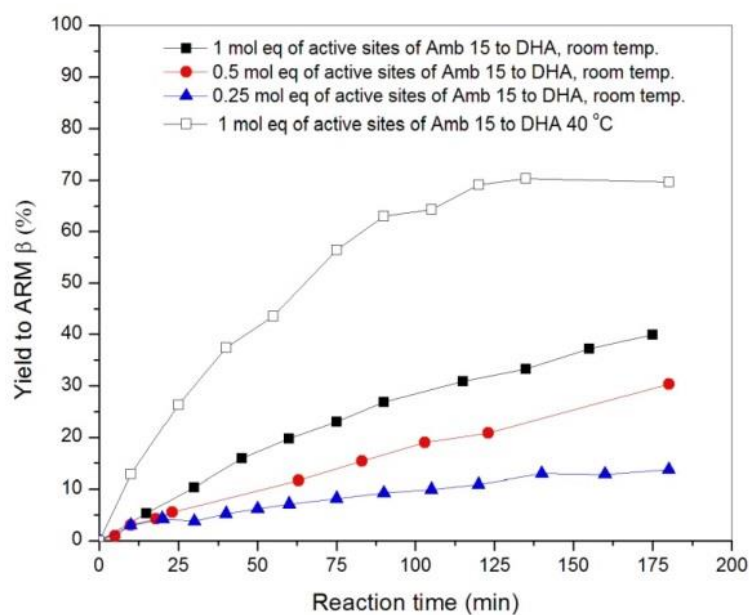


Figure 4-31. Yield of artemether as a function of reaction time during batch etherification catalysed by Amberlyst-15. Amount of catalyst and temperatures are shown.

The results of etherification of DHA to artemether over Quadrasil catalyst are shown in Figure 4-32. Using a higher ratio of active sites of QuadraSil to DHA, 0.41 vs 0.25, results in a higher yield of artemether. Thus, when 0.41 molar equivalents are taken instead of 0.25, the yield of artemether at 170 min increases from 41 to 57 %.

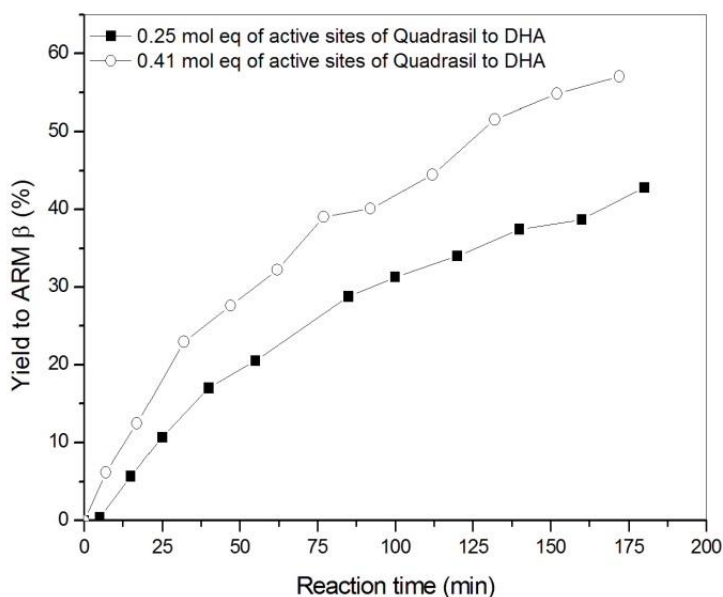


Figure 4-32. The dependence of artemether- $\beta$  yield on the concentration of Quadrasil catalyst as a function of reaction time in batch etherification at 40 °C.

Initial rates were estimated from the batch data at short reaction times and first order rate constants were calculated. MeOH was used in excess, therefore DHA can be considered as limiting species and the rate law for conversion of DHA to  $\beta$ -artemether can be written as Equation 4-90, assuming the first-order kinetics with respect to DHA. Applying the boundary conditions,  $t = 0$ ,  $C = C_{DHA}^0$ ;  $t = t$ ,  $C = C_{DHA}$ , the integral form of rate equation can be obtained as Equation 4-91.

$$r = -r_{DHA} = \frac{dC_{DHA}}{dt} = kC_{DHA} = kC_{DHA}^0 (1 - X_{DHA}) \quad 4-90$$

$$\ln\left(\frac{C_{DHA}^0}{C_{DHA}}\right) = \ln\left(\frac{1}{1 - X_{DHA}}\right) = kt \quad 4-91$$

where  $k$  is the first order rate constant ( $\text{min}^{-1}$ ) and  $X_{DHA}$  is the conversion.

Plotting the experimental data obtained from batch experiments against time (shown in Figure 4-33), one can see a linear relationship between  $\ln(C_{\text{DHA}}^0 / C_{\text{DHA}})$  and  $t$  can be established, which validates the use of the first-order kinetics (Equation 4-91).

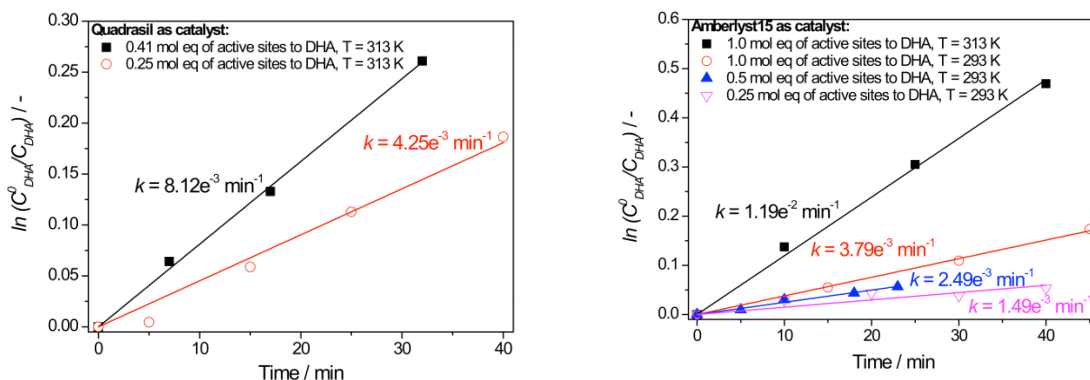


Figure 4-33. First order kinetic plots for QuadraSil and Amberlyst-15 catalysts.

The rate constants attained with QuadraSil catalyst are considerably higher than those in the case of the more conventional Amberlyst catalyst, compared for the similar amount of acid sites in the reaction system. We also highlight that the amount of Amberlyst required to attain high conversion of DHA is in excess of stoichiometry of the acid sites to the reactant. A significant leaching of acid was observed with the Amberlyst catalyst. Activity of the leached acid is not necessarily identical to that of the supported acid and this may cause the gradual reduction in the reaction rate, observed in the batch reaction profiles and, hence, the stoichiometric excess of solid acid that was required for the reaction.

Namely, a series of blank tests were performed in which methanol (without DHA) was pumped through Amberlyst- and QuadraSil-packed reactors and the pH of the mixture after the reactor was monitored. In the case of the QuadraSil catalyst, leaching of free acid was not observed, while in the case of Amberlyst-15, low pH indicated the leaching of free acid, see Figure 4-34.

Data indicated the removal of free acid from 4 cm Amberlyst beds by methanol, though after 40 minutes of MeOH washing, the pH was  $\sim 6.5$ . In the case of 8 cm and 12 cm Amberlyst 15 beds, the 10 mm diameter of the column may be too wide,

making the free acid residue difficult to wash and required a quenching of the reaction by  $\text{NaHCO}_3$  to neutralize  $\text{H}^+$  ions, avoiding the formation of peak between ARM –  $\alpha$  and ARM –  $\beta$ , see (Scheme 2-8). Moreover, in our experiments the reactions catalyzed by fresh Amberlyst required a base quench, without which no product was isolated at the end of the reactions, see Figure 4-36. This is also related to leaching of acid from the catalyst. Leaching of acid from Amberlyst was tested with pure methanol under flow conditions and hence is not related to any upstream impurities. A potential work-around is to pre-leach any poorly attached acid groups prior to experiments. This was not tested in this study as this will lead to the significant reduction in activity: we observe a clear drop of activity of Amberlyst catalyst over time. This reduction of activity would make flow process with this catalyst even less attractive. Thus, current industrial strategy of batch reaction with Amberlyst followed by a base quench and work up cannot be effectively directly translated into a flow process.

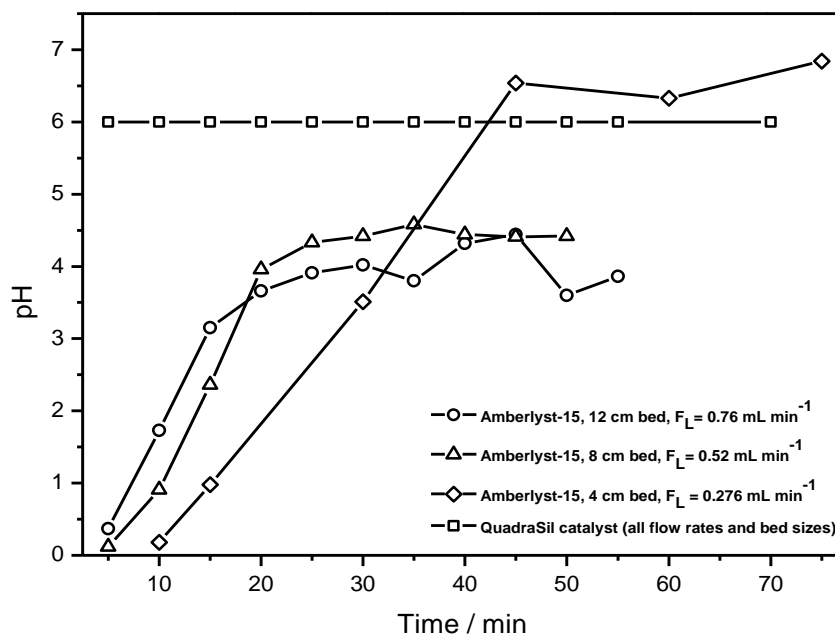


Figure 4-34. Blank flow tests of the catalyst beds packed with Amberlyst and QuadraSil, showing leaching of free acid from Amberlyst.

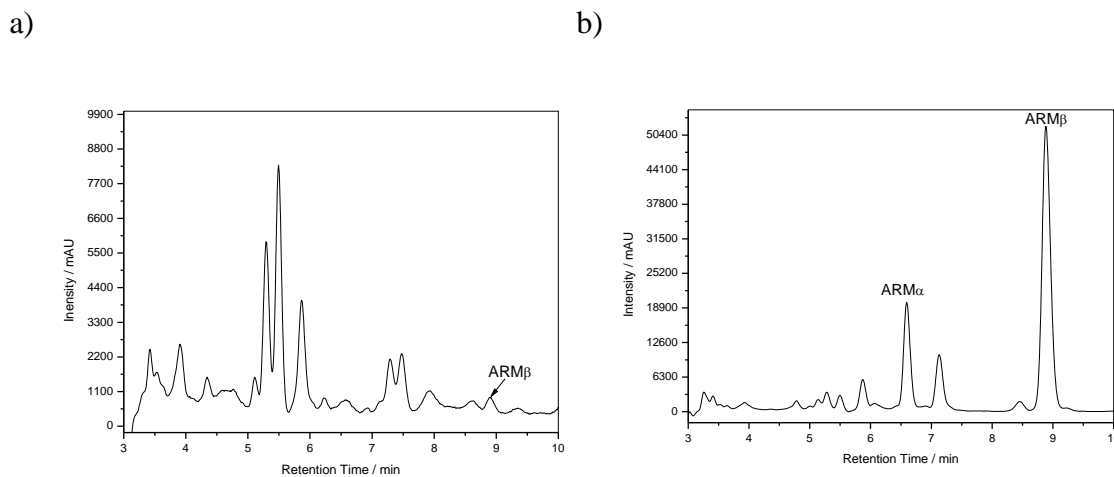


Figure 4-35. The product of etherification of DHA with Amberlyst 15 after removing solvent a) without a base quench step b) with a base quench step. (Also see, Figure 4-27 - Figure 4-29).

The reaction with QuadraSil proceeds much cleaner and no acid leaching was observed (See, Figure 4-34). Stability of acid sites and, most likely, good accessibility of sites in the mesoporous structure of QuadraSil could be responsible for this.

In our study fresh Amberlyst catalyst was used in each run and no attempt to recycle the catalyst was used, mainly due to apparent deactivation during the first run. However, QuadraSil catalyst was used repeatedly in more than five experiments with no apparent deactivation. A specific long-term flow run and large number of batch reactions would be required to properly characterize recyclability of this catalyst.

#### 4.4.2 Flow Etherification Reaction

The process flow scheme is shown schematically in Figure 4-36. However, in the present study DHA was obtained in the batch reactor as described in Experimental (Section 3.2.3 Reduction of Artemisinin with LiBHET<sub>3</sub>). The mixture of  $\alpha$ - and  $\beta$ -DHA and pure methanol were pumped into a packed-bed column which operates at ambient or slightly elevated temperature (40 °C). The reaction does not require base

quench in the case of QuadraSil. However, in the case of Amberlyst free acid is present in the reaction mixture (Figure 4-34) and a base quench step is required.

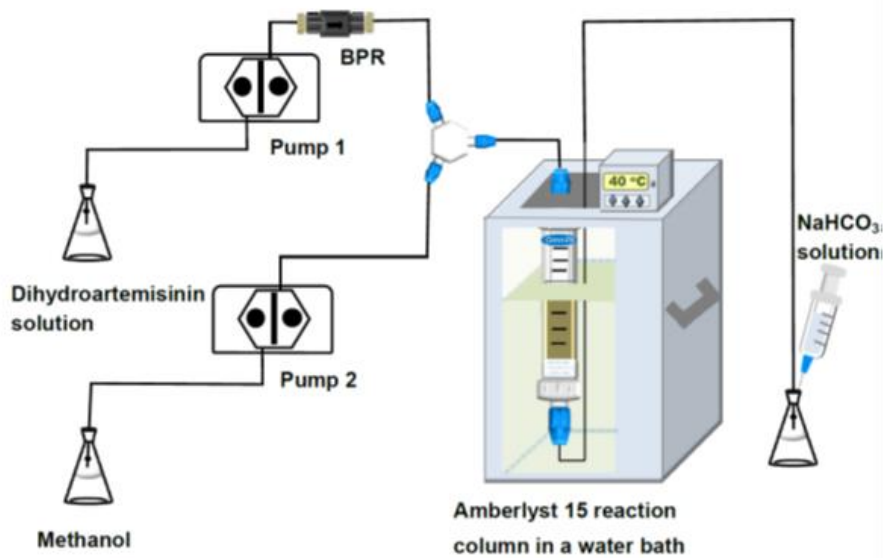


Figure 4-36. Schematic process flow scheme for conversion of DHA into artemether.

### Residence Time Distribution Measurements and Calculations

Residence Time Distributions (RTD) were measured at various flow rates for different lengths of bed packed in OmniFit column and using VapourTech R2 flow chemistry system. Briefly, the experiments started from a pulse injection of a concentrated solution of a tracer (saturated solution of diphenylisobenzofurane in methanol-Me-THF=1:1 vol) introduced by syringe to the main stream *via* a T-connection (PTFE, 0.5 mm through holes, Upchurch Scientific). The main flow was then connected to the inlet of the packed-bed column assembly (borosilicate glass HPLC column with PTFE end pieces, 10 mm ID, OmniFit). The column was packed with different volumes of the catalysts providing bed lengths of 1, 4, 8 and 12 cm or 1.2 and 4 cm for Amberlyst or QuadraSil correspondingly. The outlet of the column was connected to the custom-made spectroscopic quartz cell (1 mm optical pathlength) in turn connected by quartz optical fibres to the monochromator and a detector. The absorbance of dye in the response signal was continuously measured at 416 nm. The temperature of the packed bed reactor was maintained at 40 °C during the measurements.

The obtained response voltage curves were recalculated to optical densities (OD) and normalized in order to obtain RTD curves:

$$f(t) = \frac{OD(t)}{\int_0^{\infty} OD(t)dt}$$

4-92

Moments were used to characterize the RTD functions in terms of statistical parameters such as mean residence time  $\tau$  and standard deviation  $\sigma^2$ :

Peclet numbers,  $Pe = (Lu_L/D) = 2\tau^2/\sigma^2$  were estimated using simple axial dispersed plug flow model.

Figure 4-37 shows normalized RTD functions obtained in the experiments with a dye tracer. One can see from these data that Amberlyst demonstrates a higher degree of peaks asymmetry with long tailings compared to those for the QuadraSil packed column. Tailing indicates the presence of stagnant volume with a slow exchange of flow between the active and the stagnant volumes. Single modality of the RTD curves also indicates that no channeling of the tracer flow occurs directly from the input to the output of the packed bed column.

Mean experimental residence times (Table 4-6) were found generally to be about two times longer than these calculated for the plug flow which again indicates the presence of stagnant zones. In this case the residence time was calculated as  $\tau_{PF} = V_V/u_L$  where  $u_L$  is fluid velocity and  $V_V$  is the void volume in the reactor. Volume of void was estimated in the approximation of close random packing of ideal spheres (void fraction is 0.375).

Peclet numbers were found to be about one order of magnitude higher for the QuadraSil indicating much higher domination of the convective over diffusive mixing inside the reactor packed with this catalyst.

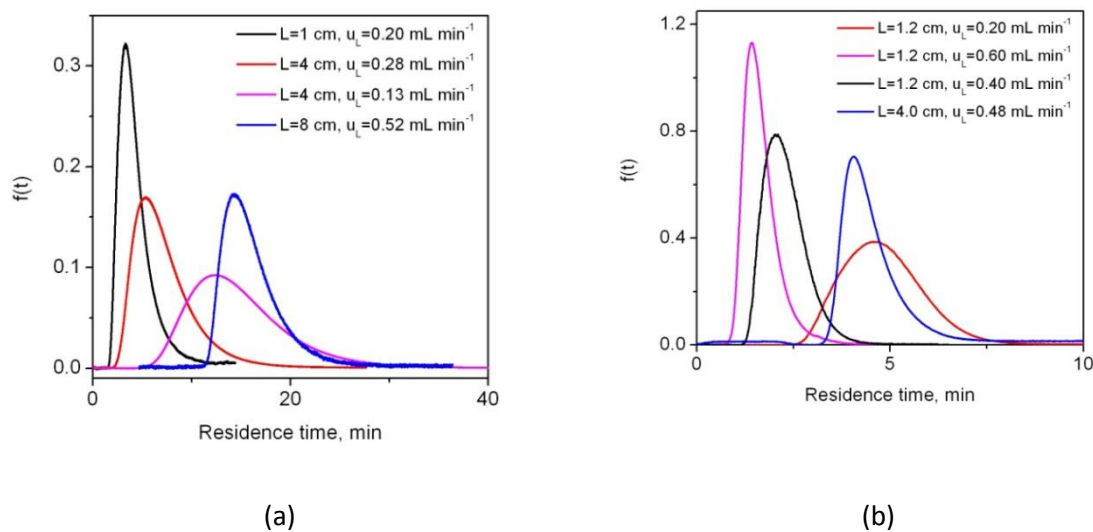


Figure 4-37. Residence Time Distribution curves obtained in pulse experiments for the different lengths of the packed bed reactor packed by (a) Amberlyst and (b) QuadraSil.

Table 4-6. Hydrodynamic parameters calculated from the experimental RTD curves for the packed bed reactors of different lengths packed with Amberlyst and Quadrasil catalysts.

L	$u_L$	$\tau$	$\tau_{PF}$	$\sigma$	Pe
(cm)	( $\text{mL min}^{-1}$ )	(min)	(min)	(min)	
Amberlyst 1	0.2	2.9	1.5	1.9	1.5
4	0.28	6.2	4.3	3.3	7.0
4	0.13	12	9.4	5.3	11.2
8	0.52	7.2	4.6	3.1	1.3
12	0.76	5.1	4.6	2.9	1.5
QuadraSil 1.2	0.2	4.9	1.7	1.1	39.7
1.2	0.4	2.3	0.9	0.6	29.4
1.2	0.6	1.7	0.6	0.4	36.1

---

4	0.48	4.6	2.5	1.3	26.5
---	------	-----	-----	-----	------

---

### Simplified design of a packed-bed continuous flow reactor based on the approximation of the first order kinetics and plug-flow behaviour

For designing plug-flow reactors, the differential forms of the mole balance can be written as Equation 4-93 in terms of initial substrate molar flow rate ( $\dot{n}_{DHA}^0 = F \times C_{DHA}$ , where  $F$  is volumetric flow-rate in  $\text{m}^3 \text{s}^{-1}$ ) and conversion ( $X_{DHA}$ ). Considering cylindrical reactor with constant cross sectional area ( $A_c$ ), the design equation can be rearranged as Equation 4-94, where  $F_{total}$  is the total volumetric flow-rate in  $\text{m}^3 \text{s}^{-1}$ ;  $A_c$  is the cross sectional area of the reactor in  $\text{m}^2$ ;  $L_R$  is the length of the reactor in m.

$$\frac{dX_{DHA}}{dV_R} = \frac{kA_C}{F_{total}}(1 - X_{DHA}) \quad 4-93$$

$$\frac{dY_{DHA}}{dL_R} = \frac{kA_C}{F_{total}}(1 - Y_{DHA}) \quad 4-94$$

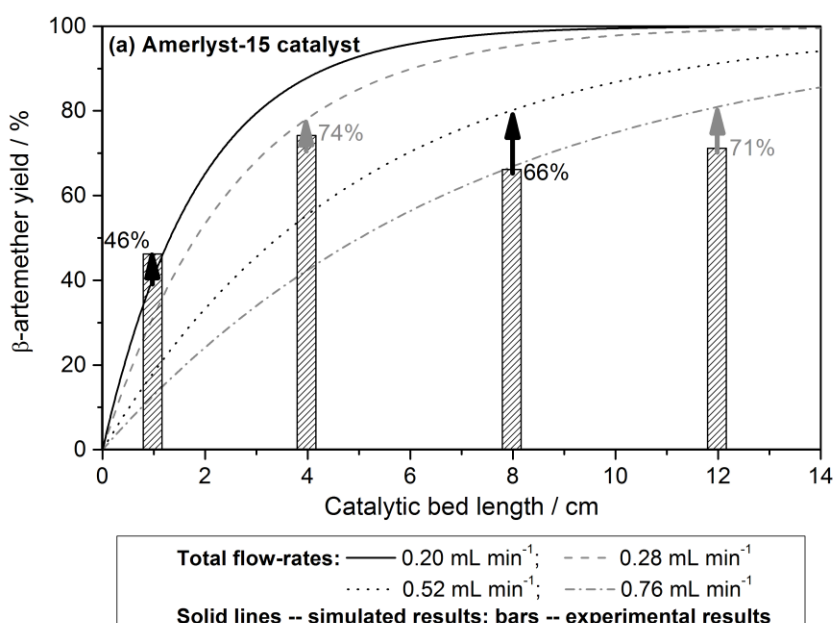
Here we assume perfect selectivity such that yield of artemether is identical to conversion of DHA.

In order to reflect the effect of active concentration on reactor performance, the obtained rate constants were normalised against surface concentration of active sites. For Amberlyst-15, active sites concentration is  $\leq 4.7 \text{ mmol g}^{-1}$  and specific surface area is  $53 \text{ m}^2 \text{ g}^{-1}$ , therefore the surface concentration of active sites can be calculated as *ca.*  $8.87 \times 10^{-2} \text{ mmol m}^{-2}$ . For QuadraSil, active sites concentration is *ca.*  $1.2 \text{ mmol g}^{-1}$  and specific surface area is  $700 \text{ m}^2 \text{ g}^{-1}$ , therefore the surface concentration of active sites can be calculated as *ca.*  $1.71 \times 10^{-3} \text{ mmol m}^{-2}$ .

The reactor design equations were coded in MatLab. The surface concentration-normalized rate constant was used for Amberlyst-15 only. The weight of catalysts can be calculated based on reactor volume ( $V_R, \text{m}^3$ ) and bulk density ( $\rho_b, \text{kg m}^{-3}$ ). For Amberlyst-15,  $\rho_b = 610 \text{ kg m}^{-3}$  (dry); for Quadrasil,  $\rho_b$  is not available from the technical data sheet.

Residence time distribution (RTD) analysis confirmed that for the case of the QuadraSil-packed column the reactor is behaving close to the ideal plug-flow RTD. In the case of the Amberlyst catalyst the deviation from the ideal plug flow behaviour is more pronounced. Therefore, we would expect a larger deviation of the experimental and simulated results. The latter are required for designing a large-scale process to enable a life cycle assessment study.

Performance of both catalysts is shown in Figure 4-38, along with the simulated results. First of all we note that a simple plug-flow model based on the first-order kinetics works a lot better in the case of QuadraSil than in the case of Amberlyst. The reason is due to a much closer to the plug-flow regime in the QuadraSil-packed column. Nevertheless, such a simple model describes behavior of the flow reactor packed with Amberlyst also reasonably well. We later use this model to estimate the amount of catalyst required for a scaled-up flow process, in order to calculate LCA impacts for a given rate of production of artemether.



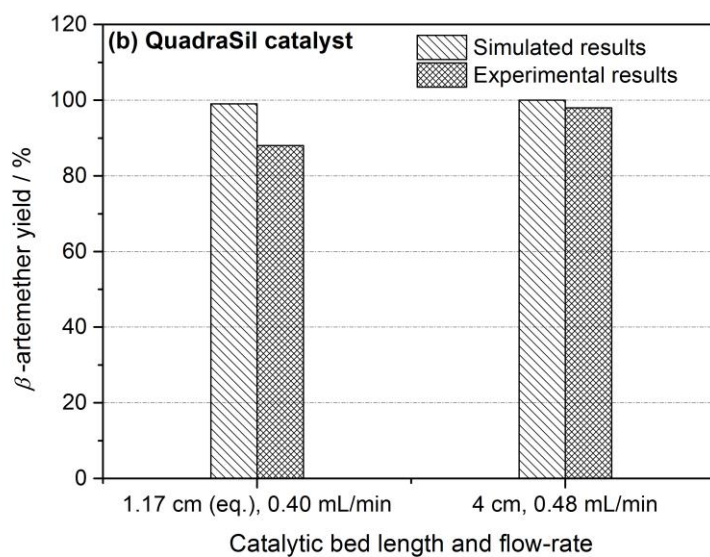


Figure 4-38. Comparison of simulated reactor performance ( $\beta$ -ARM yield) with experimental results using both, Amberlyst-15 catalyst (a) and QuadraSil catalyst (b) at different flow rates and reactor lengths.

The flow reactor packed with QuadraSil shows a significantly better performance, compared with Amberlyst catalyst. A higher yield is attained at a shorter residence time. This is also clearly seen by comparing results of the model simulation for both catalysts, see Figure 4-38.

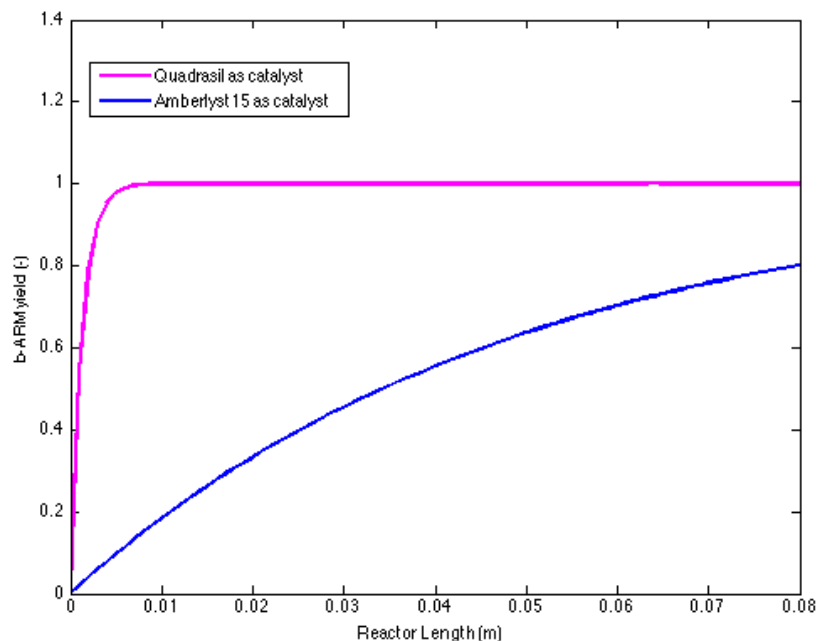


Figure 4-39. Reactor performance ( $\beta$ -ARM yield) as a function of reactor length ( $L_{R,max} = 8$  cm) at  $T = 313$  K.

One of the more significant advantages of the QuadraSil catalyst is its stability. Blank experiments with both catalyst showed that Amberlyst is continuously leaching acid, see Figure 4-34. This results in the necessity to quench the reaction with a weak base in order to obtain the product. In the case of QuadraSil catalyst the base quench is not necessary.

Generally, comparison of performance of batch and flow reactions can be done on the basis of space-time-yield (STY) which is calculated as kg of product produced within 1 hour in a reactor of 1 L volume. This could either involve the work-up stage or not. If the work-up stage is to be included, the results are likely to be highly inaccurate for the lab-scale experiments due to significant discrepancies in washing volumes and filtration/drying procedures (times and volumes).

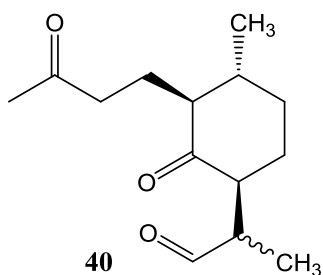
In the case of the reduction reaction, based on the experimental results published earlier<sup>160</sup>, and using only reaction time, solvent volume and product yield, and excluding work-up, batch and flow STYs are 0.011 and 1.60 kg h<sup>-1</sup> L<sup>-1</sup> respectively. The considerable reduction in STY in the flow experiment was attained due to a

massive reduction in reaction time, which was due to a significant increase in reaction temperature, as well as the change of the reducing agent.

In the case of the etherification reaction the reaction times are comparable between the batch and the flow experiments. Therefore, we do not expect a massive improvement in the flow process over a batch one. Based on the reactions performed at 40 °C with QuadraSil-SA catalyst at 0.41 molar ratio to the reactant, the batch STY is estimated to be  $1.4 \times 10^{-3} \text{ kg L}^{-1} \text{ h}^{-1}$  whereas in the case of a 4 cm length packed bead and liquid flow rate of  $0.48 \text{ mL min}^{-1}$  the estimated STY is  $65 \times 10^{-3} \text{ kg L}^{-1} \text{ h}^{-1}$ . This increase in STY of the flow catalytic process over the batch one is a manifestation of a well-known effect of flow chemistry: in the case of the flow process the relative amount of a catalyst to reactant is orders of magnitude higher than what is typically used in batch. This results in considerably higher volumetric production rates, which manifest as larger STY.

### By-products

During analysis of etherification samples in the batch experiments, decomposition of DHA was observed (see Figure 3-10). The acetonitrile/water mobile phase and high temperature enhanced this process. A similar DHA degradation to by-product (**40**) was observed in the work of Stringham and Teager<sup>17</sup>. In their work, the rate of degradation of DHA was higher 12 % /h in the sample diluted in the acetonitrile/water mixture. However, dissolving this sample in pure acetonitrile reduced this degradation process. In our case the rate of degradation of DHA was approximately 2.5 % /h in pure acetonitrile. The mechanism of DHA degradation is unknown. However, in both protocols  $\text{NaHCO}_3$  was used to quench the reaction.



Scheme 4-1. Degradation product of DHA<sup>17</sup>.

This hypothesis can be confirmed by the interconversion experiment. The standard DHA was dissolved in pure acetonitrile. The sample was analysed by HPLC at several-hour intervals for three days. DHA decomposition did not occur during that time; however, the transformation of DHA  $\beta$  into DHA  $\alpha$  was observed (Figure 4-40).

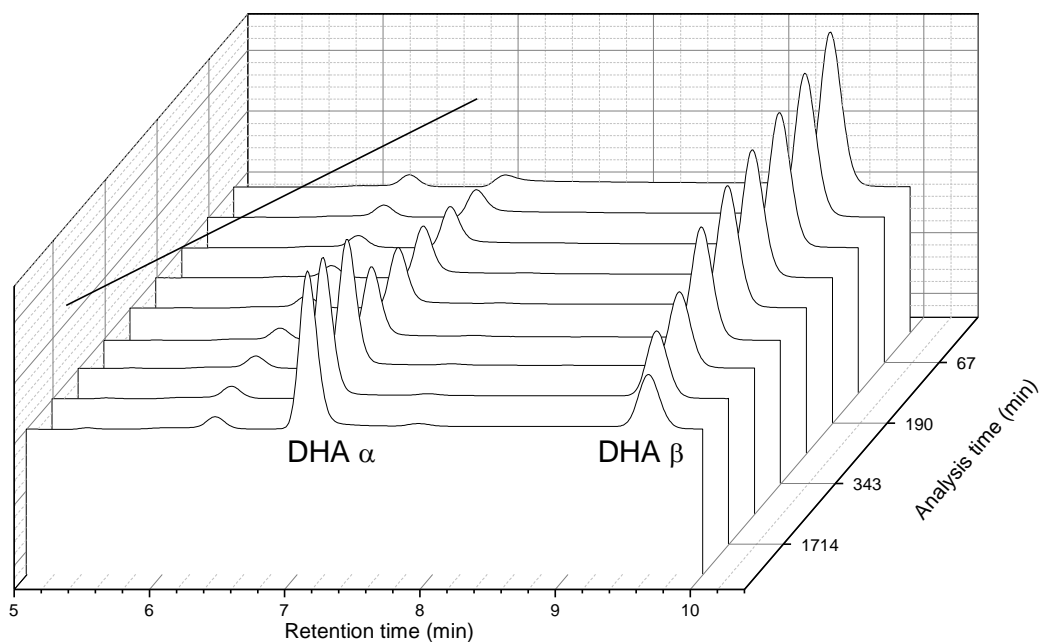


Figure 4-40. HPLC analysis of DHA and transformation of DHA  $\beta$  into DHA  $\alpha$ .

Another by-product positioned between ARM –  $\alpha$  and ARM –  $\beta$  was recorded in the HPLC chromatograms. The retention time of the by-product is similar/the same as for 9-epi-artemether. This by-product was formed by the high temperature during removal of the solvent on a rotovap at 40 °C. The level of this by-product was enhanced more in the presence of THF than in trimethyl orthoformate (TMOF) in the reaction with Amberlyst 15, see Figure 4-41.

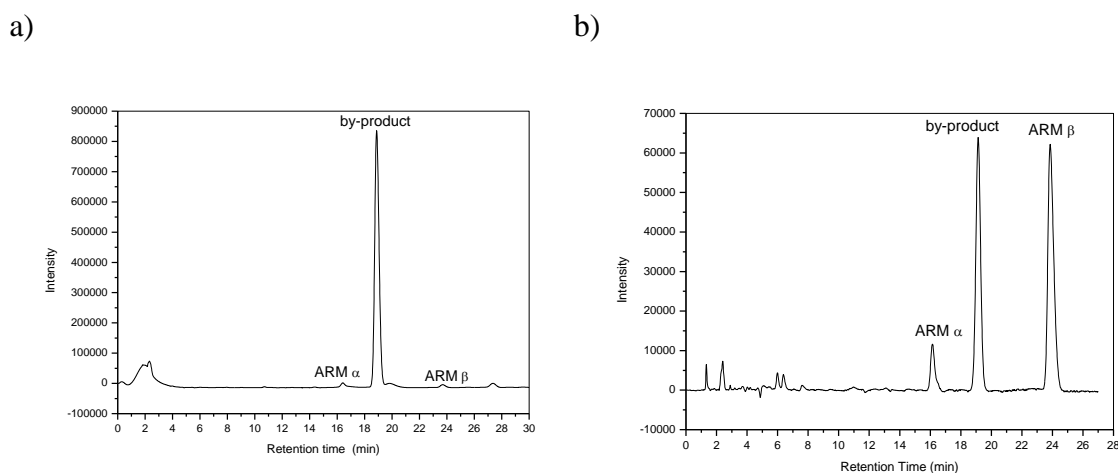


Figure 4-41. The product of conversion DHA to ARM with Amberlyst under batch conditions a) in the presence of THF b) in the presence of TMOF. The reaction times for both reactions are the same. The solvents were removed by a rotovap at 40 °C. Mobile phase: acetonitrile/ water 65/35 (% v/v). Flow rate: 0.8 mL min<sup>-1</sup>. Wavelength: 216 nm.

In the next step, a series of blank experiments was performed in order to find the source of by-product formation. We took into consideration possible systems in which this side product could be formed such as THF, THF + methanol, THF + DHA, methanol +DHA, THF + Amberlyst, methanol +Amberlyst and THF + DHA +Amberlyst. Samples of each experimental mixture and its residue after removing the solvent by the rotoevaporation at 40 °C were analysed by HPLC. The samples for HPLC analysis were dissolved in pure acetonitrile. A signal which might be related to the by-product formed in the etherification process was observed in the residue of THF + DHA + Amberlyst (Figure 4-42). According to the mechanism shown in Scheme 2-8 this signal of the by-product may be relative to anhydroartemisinin<sup>17</sup>.

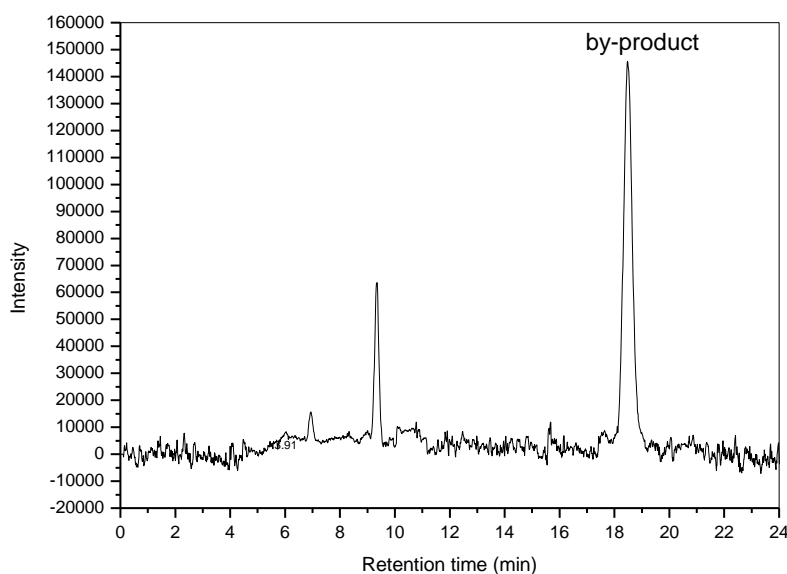


Figure 4-42. Blank experiment with DHA, Amberlyst 15 and THF in a batch reactor.

The experiment was carried out for 1 hour under stirring conditions. The solvent was removed by a rotavapor at 40°C. The residue was dissolved in pure acetonitrile.

Mobile phase: acetonitrile/ water 65/35 (% v/v). Flow rate: 0.8 mL min<sup>-1</sup>.

Wavelength: 216 nm.

In summary, in order to reduce the formation of anhydroartemisinin, in subsequent investigations the solvent was removed from a final product by the rotoevaporation at ambient temperature. An aliquot of the reaction solution was also quenched and taken for HPLC analysis.

### LCA of the Combined Process

Cradle-to-gate life cycle assessment is performed to reveal the impact of the significant changes in the materials upon the switch from the established batch protocols and the new flow synthesis. Due to the change of solvent and reducing agent in the first reaction, and the change of the catalyst in the second, the environmental impacts of the two alternative processes (all batch vs flow) are expected to be different. To obtain more detailed information about both flow

reactions we show separately comparative assessment of the reduction and of the catalytic etherification.

Reduction in flow is compared with reduction in batch using NaBH<sub>4</sub>, as the best literature recipe and, what we believe to be, the industrial recipe. Figure 4-43 shows CML impacts and cumulative energy demand (CED) for three alternatives: conventional batch reduction of artemisinin to DHA, reduction in flow using Me-THF solvent and superhydride reducing agent, and a hypothetical scenario in which THF solvent (reducing agent is supplied in THF) is removed from the impacts, thus simulating the scenario when reagent is supplied in Me-THF and recycled along with the reaction solvent.

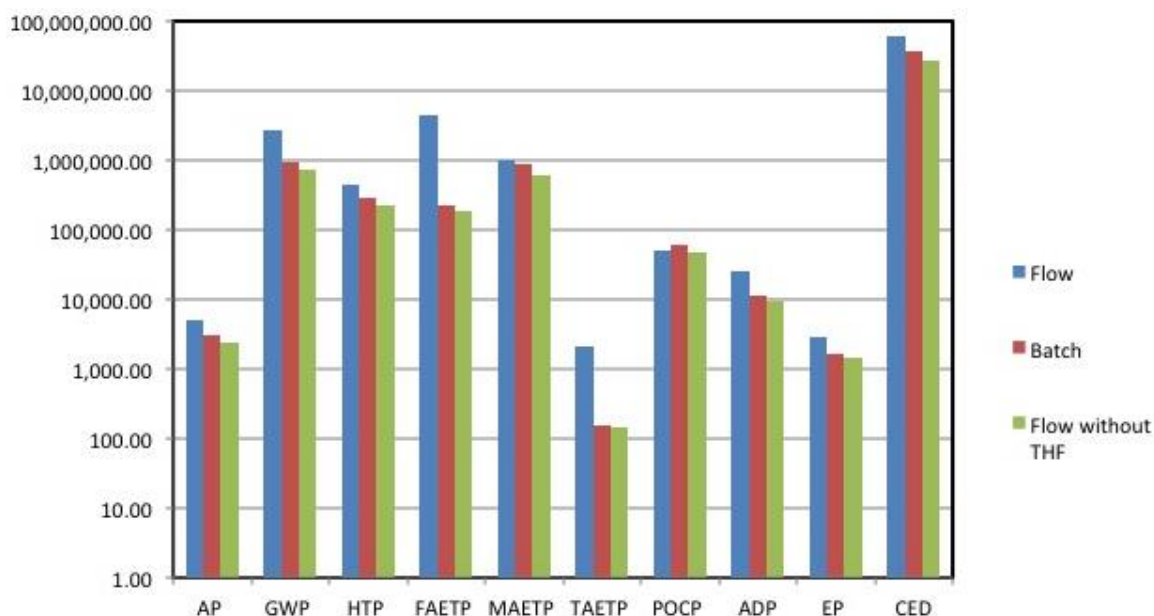


Figure 4-43. CML impact scores and CED for the reaction of artemisinin to DHA reduction (vertical axis). Comparison of flow and batch processes and flow process without THF for superhydride. Legend; AP is Acidification Potential, GWP is Climate Change, HTP is Human Toxicity Potential, FAETP is Freshwater Aquatic Ecotoxicity, MAETP is Marine Aquatic Ecotoxicity, TAETP is Terrestrial Ecotoxicity, POCP is Photochemical Oxidation (summer smog), EP is

Eutrophication Potential, ADP is Depletion of Abiotic Resources and ODP is Stratospheric Ozone Depletion.

It is clear that introduction of the more complex solvent and the reducing agent result in a slight increase in the environmental impacts and CED if we compare the best batch results with the reduction of artemisinin in flow. However, we cannot distinguish which is the most important factor without running different process scenarios with the LCA model. Figure 4-44 shows the relative contributions of different factors on CED, which allows one to elaborate the importance of solvent, *vs* energy input *vs* transport, *etc.*

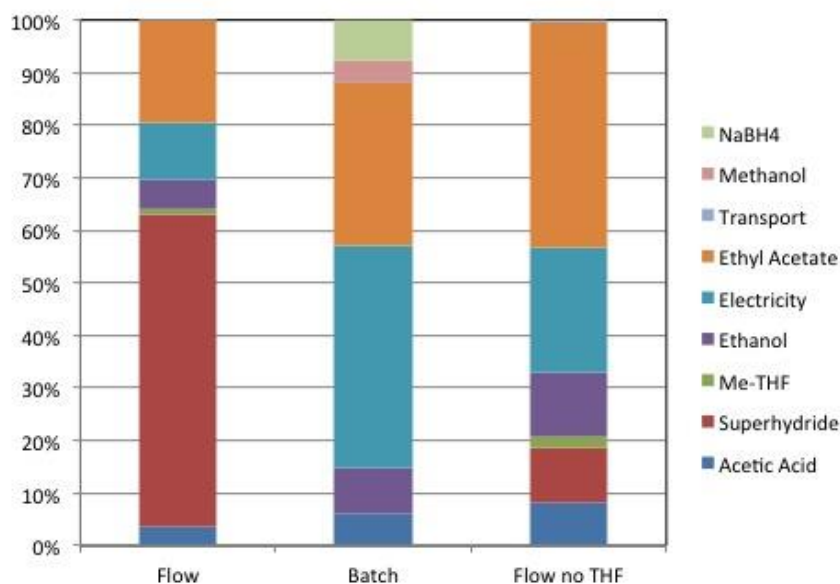


Figure 4-44. Individual processes contributions to CED of artemisinin to DHA reaction in batch and flow conditions.

From the data in Figure 4-44, it is evident that the unoptimised flow process is dominated by the impact of superhydride reducing agent. Looking into its impact in more detail we recognise that this is largely due to the fact that it is being supplied as THF solution. Simulation of an alternative scenario when the reducing agent is supplied in Me-THF results in a significant reduction of its impact on CED, see Figure 4-44, and also results in an overall lower LCA impacts of the flow process

compared to the batch, see Figure 4-43. The impact of the solvent Me-THF is relatively small, mainly due to small inventory and recycle of the solvent, which is one of the key features of the flow process.

In the case of etherification of dihydroartemisinin to artemether we show comparison of the recently published batch protocol using HCl as a catalyst Figure 4-44<sup>194</sup> with the flow process based on QuadraSil-SA catalyst. To illustrate the significance of the solvents we performed analysis of the scaled-up potential flow process *without* solvent recycle as well as *with* solvent recycle. Results are shown in Figure 4-45 for CML impacts and CED and in Figure 4-46 for the detailed contributions towards CED.

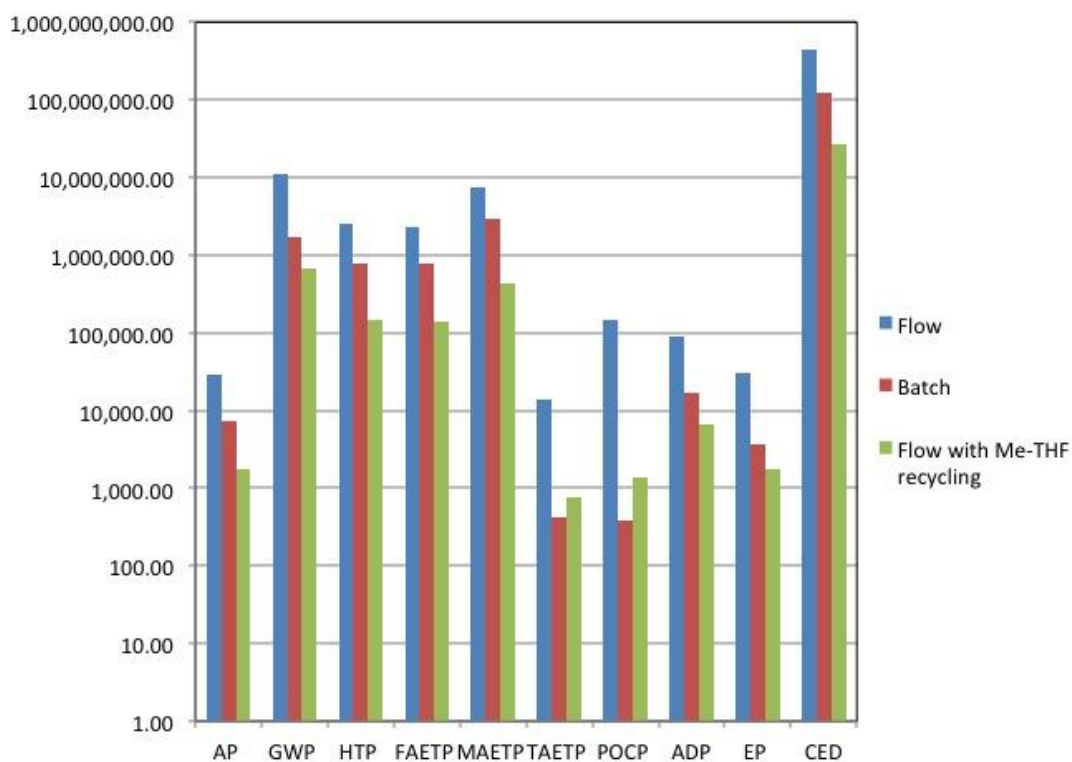


Figure 4-45. CML impact scores (vertical axis) and CED for DHA to ARM reaction. Comparison of flow and batch processes. Legend; AP is Acidification Potential, GWP is Climate Change, HTP is Human Toxicity Potential, FAETP is Freshwater Aquatic Ecotoxicity, MAETP is Marine Aquatic Ecotoxicity, TAETP is Terrestrial

Ecotoxicity, POCP is Photochemical Oxidation (summer smog), EP is Eutrophication Potential, ADP is Depletion of Abiotic Resources and ODP is Stratospheric Ozone Depletion and CFD is Computer Fluid Dynamic.

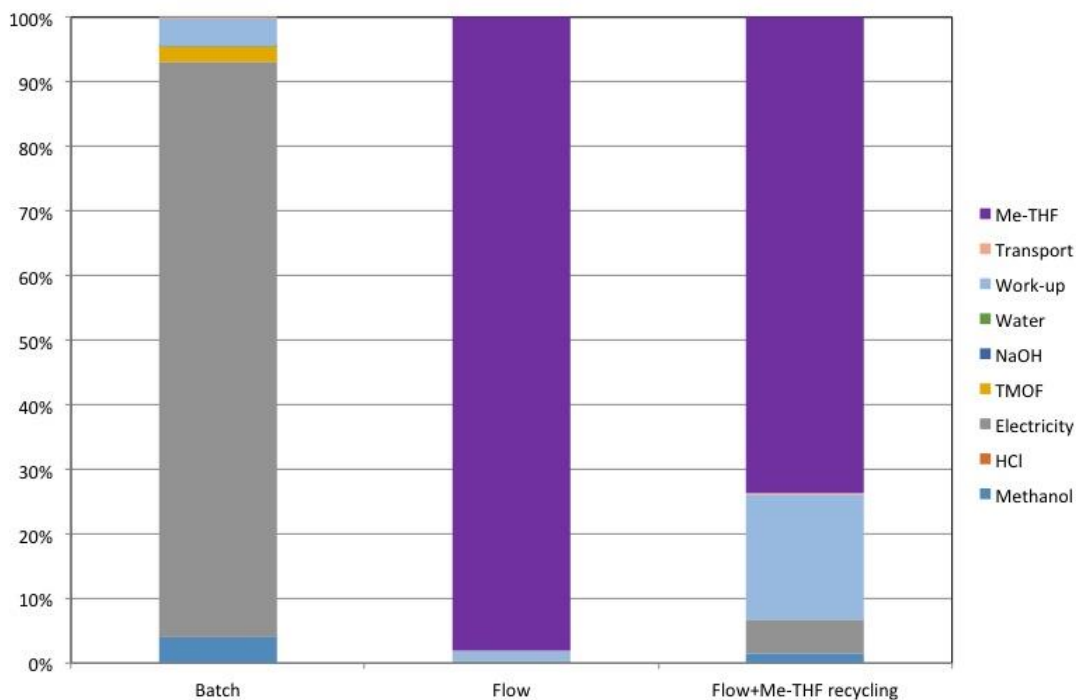


Figure 4-46. Individual processes contributions to CED of DHA to ARM reaction in batch and flow conditions.

## 4.5 Ethenolysis of Cocoa Butter

### 4.5.1 Batch Experiments

#### Screening of Catalysts

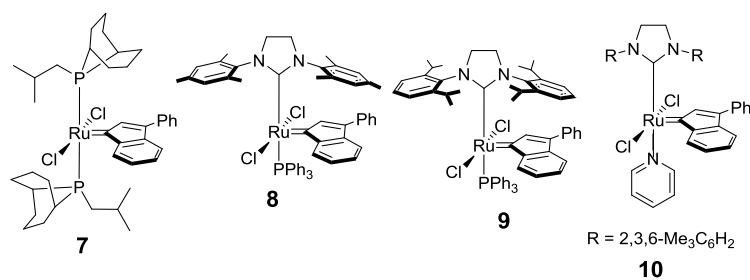
Results of the ethenolysis of cocoa butter are shown in Table 4-7. Ethenolysis was optimized for the type of catalyst and reactions were carried out in the presence of toluene at room temperature for 2 h. The amounts of catalysts in the reaction were 1 mol %, calculated on the basis of the number moles of cocoa butter. Ethylene was purged at *ca.* 1 barg into the reaction vessel from a balloon (entry 1-4). The catalyst (**7**) proved to be the most active catalyst at room temperature and in the presence of toluene.

The effect of solvent in the ethenolysis of cocoa butter was screened. Reactions were incubated overnight at 1 barg in the presence of toluene, THF and DCM (entry 5-7). The yields to the sum of decene and 1,4-decadiene in the presence of toluene, THF and DCM were 34 %, 44.5 % and 43 % respectively. THF was used for further work as it was less toxic (and in subsequent research may be replaced by 2-Me-THF). Also, the reaction with THF was performed overnight at 50 °C, however, the yield to double bond of alkenes was 33.5 % and was lower than at room temperature at 1 bar (entry 8), which could be attributed to deactivation of the catalyst at a higher temperature.

The reactivity of (**7**) and (**8**) catalysts were compared and the reactions performed in an autoclave (which allowed us to obtain higher concentration of ethylene in the reaction system) at 2 barg, where the yield in the presence of the catalyst (**7**) was better than that in the presence of (**8**) catalyst (entry 9-10).

Ethenolysis of cocoa butter was performed in the presence of various amounts of (**7**) catalyst under different conditions (entry 1, 7, 9 and 11-13). We can conclude that reacting in the autoclave at 2 barg reduced time of the process and catalyst (entry 9) due to the higher concentration of ethylene in the reaction Table 4-7.

Table 4-7. Optimization of ethenolysis in a batch reactor.



Entry	Catalyst	Solvent	A of catalyst (mol%)	p (barg)	Time (h)	Temp (°C)	Yield to decene and 1,4-decadiene (%)
1	7	toluene	1	1	2	rt	29
2	8	toluene	1	1	2	rt	21
3	9	toluene	1	1	2	rt	1
4	10	toluene	1	1	2	rt	1
5	7	toluene	1	1	16	rt	34
6	7	DCM	1	1	16	rt	45
7	7	THF	1	1	16	rt	43
8	7	THF	1	1	16	50	34
9	7	THF	1	2	2	rt	47
10	8	THF	1	2	2	rt	15
11	7	THF	0.25	2	2	rt	24
12	7	THF	0.5	2	2	rt	25
13	7	THF	2	1	16	rt	45

Legend; A is amount, p is pressure, Temp is temperature.

#### 4.5.2 Flow Experiments

##### Permeability Experiments

The flow of gas (dV/dt) through a membrane gives the flux and permeability according to Darcy equation, which is related to Fick's law<sup>195</sup>.

$$J = \frac{273.15 \text{ K}}{T} \cdot \frac{p_a}{76} \cdot \frac{1}{A} \cdot \frac{dV}{dt}$$

4-95

$$P = \frac{J \cdot l}{\Delta p} \quad 4-96$$

$$P = \frac{273.15 \text{ K}}{T} \cdot \frac{p_a}{76 \text{ cmHg}} \cdot \frac{l}{A} \cdot \frac{dV}{\Delta p dt} \quad 4-97$$

$$P = \frac{273.15 \text{ K}}{T} \cdot \frac{l}{A} \cdot \frac{dV}{\Delta p dt} = \frac{273.15 \text{ K}}{T} \cdot \frac{l}{A} \cdot m \quad 4-98$$

where  $J$  is the steady gas flux in  $\text{cm}^3$  (STP)  $\text{cm}^{-2} \text{min}^{-1}$ ,  $T$  is temperature (K),  $p_a$  is atmospheric pressure in (bar),  $A$  is surface area membrane ( $\text{cm}^2$ ),  $\frac{dV}{dt}$  is the flow rate ( $\text{mL min}^{-1}$ ),  $l$  is the thickness of membrane (cm) (in this study, the value was 0.01 cm),  $\Delta p$  is the pressure drop across the membrane (bar),  $m$  is the slope in ( $\text{mL min}^{-1} \text{bar}^{-1}$ ) and  $P$  is the permeability coefficient (cB: centiBarrer) <sup>179</sup>,

$$1 \text{ cB} = 10^{-12} \frac{\text{cm}^3 \cdot \text{cm}}{\text{cm}^2 \cdot \text{s} \cdot \text{cmHg}} = 4.5 \cdot 10^{-9} \frac{\text{mL} \cdot \text{cm}}{\text{cm}^2 \cdot \text{min} \cdot \text{bar}}$$

The fractions with temperature and pressure ( $\frac{dV}{\Delta p dt}$ ) are correction terms. The pressure difference was neglected, and when the experiment was performed at room temperature ( $\sim 20^\circ \text{C}$ ), the temperature correction coefficient was used. Flow divided by pressure drop was the slope of the line in the resolving graph (Figure 4-47). The surface area of the membrane tubing was calculated as the surface area of a cylinder for the length (cm) and outer diameter (OD = 0.1 cm). The membrane ('used 3') had 3 cm metal fittings on each side, and the final length of the membrane was 106 cm (original length of 112 cm).

$$A = \pi \cdot \text{OD} \cdot s = \pi \cdot 0.1 \text{ cm} \cdot 106 \text{ cm} = 33.3 \text{ cm}^2 \quad 4-99$$

An example calculation is made for the permeability of ethylene in 'used membrane 3', see Table 4-8. Permeability coefficient calculated on the basis of the first experiment was:

$$P_1 = \frac{273.15 \text{ K}}{T} \cdot \frac{l}{A} \cdot m = \frac{273.15 \text{ K}}{293.15 \text{ K}} \cdot \frac{0.01 \text{ cm}}{33.3 \text{ cm}^2} \cdot 0.8688 \frac{\text{mL}}{\text{min} \cdot \text{bar}} \quad 4-100$$

$$P_1 = 2.43 \cdot 10^{-4} \frac{\text{mL} \cdot \text{cm}}{\text{cm}^2 \cdot \text{min} \cdot \text{bar}} = 54050 \text{ cB}$$

4-101

Permeability coefficient calculated on the basis of the second experiment was:

$$P_2 = \frac{273.15 \text{ K}}{T} \cdot \frac{l}{A} \cdot m = \frac{273.15 \text{ K}}{293.15 \text{ K}} \cdot \frac{0.01 \text{ cm}}{33.3 \text{ cm}^2} \cdot 0.7395 \frac{\text{mL}}{\text{min} \cdot \text{bar}}$$

$$P_2 = 2.07 \cdot 10^{-4} \frac{\text{mL} \cdot \text{cm}}{\text{cm}^2 \cdot \text{min} \cdot \text{bar}} = 45982 \text{ cB}$$

The average permeability from two experiments was:

$$P_{\text{ave}} = \frac{P_1 + P_2}{2} = \frac{54050 \text{ cB} + 45982 \text{ cB}}{2} = 50016 \text{ cB}$$

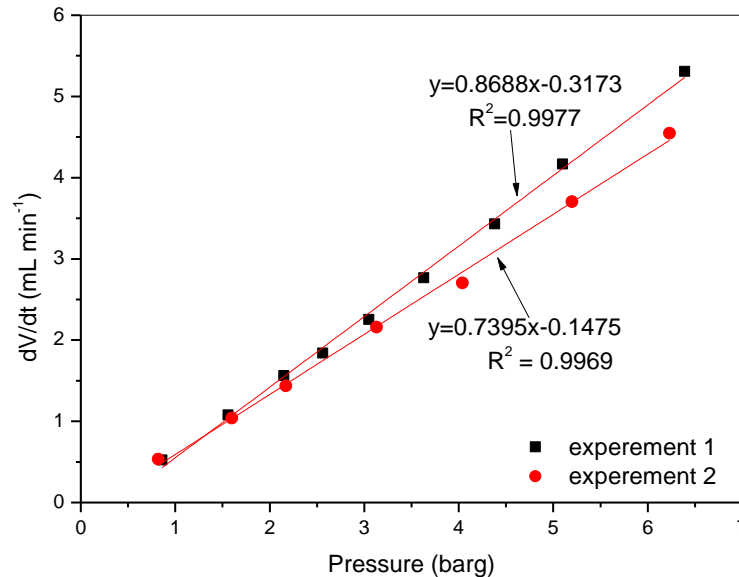


Figure 4-47. Dependence of flow rate on pressure for measurements of ethylene permeability for a 112 cm membrane length (used membrane 3).

A linear correlation between flux and pressure was observed up to 7 barg of ethylene pressure, and higher pressure was not applied to avoid crushing the membranes. The experimental permeabilities were calculated for nitrogen and ethylene according to Equation 4-98 (see Table 4-8) and compared to the literature (nitrogen is 49000 cB and ethylene is 35000 cB) <sup>196</sup>.

Table 4-8. Results of permeability (in cB) for nitrogen and ethylene for different lengths of new and used membranes.

Membrane	Length (cm)	gas	Experimental permeability (cB)
new 1	105	nitrogen	41527
new 1	105	ethylene	22137
new 1	99	ethylene	19634
new 2	111.5	ethylene	20960
used 3	112	ethylene	50016
used 4	106.5	ethylene	22285

The permeabilities of nitrogen and ethylene were lower than those reported in the literature (nitrogen at 15 % and ethylene at 40 % less). The third used membrane (Table 4-8) had a much higher permeability than the rest of the membranes tested. Both the third and fourth used membranes had been used with typical organic solvents prior to gas flux measurements. The only significant difference between them was that the third membrane was used with liquid pressures up to 30 barg. It is believed that physical stress changed the membrane properties, thus the observed permeability value was higher. Membrane number 3 was used for metathesis experiments.

**Metathesis of Cocoa Butter under Flow Conditions**

Results of performances of ethenolysis of cocoa butter in a Tube-in-Tube reactor are shown in Table 4-9 (the rig for this experiment is described in Experimental Figure 3-16).

A starting flow rate of  $0.33 \text{ mL min}^{-1}$  and a 20 mL residence coil were used. The ethenolysis of cocoa butter was optimised in terms of pressure, where the residence coil was not heated (entry 1-5) and heated up to  $40 \text{ }^\circ\text{C}$  (entry 6-10), where the yields to sum of decene and 1,4-decadiene were higher at  $40 \text{ }^\circ\text{C}$ . However, a similar pattern was observed in both experiments: yields increased up to 6 barg and then decreased with increasing pressure (Figure 4-48). These increases indicated the reaction was limited by the amount of ethylene, and pressures above 6 barg could deactivate the (7) catalyst.

Grubbs noted the decomposition of phosphine-based ruthenium catalysts contained methyldiene complexes  $^{166d}$  which form methylphosphonium salts in the presence of ethylene, and that the decomposition routes of these catalysts follow first-order kinetics. The decomposition mechanism implicated nucleophilic attack of a dissociated phosphine on the methyldiene carbon. However, the phosphine-based catalyst (7) does not possess the methyldiene complex and the mechanism of decomposition could be different from that presented by Grubbs.

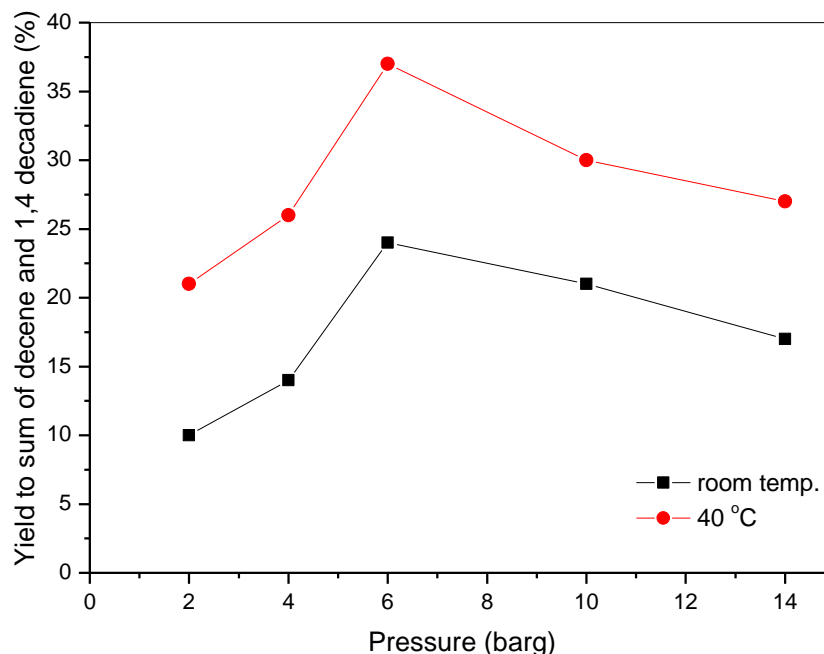


Figure 4-48. The impact the pressure of ethylene in the Tube-in-Tube reactor on the formation of linear alkene products from oleic and linoleic acids in cocoa butter.

Further heating of the residence coil to 60 °C at 6 barg decreased the yield to 31 % (entry 11). As expected, reducing the catalyst (7) by half at 40 °C and 60 °C reduced yields of the linear products 25 % and 19 %, respectively, while the feed pressure of ethylene was constant (entry 12-13). Increasing the concentration of (7) by half at 40 °C also reduced the yield (entry 14). These data suggest that catalyst activation is thermodynamically limited, while the reaction is kinetically limited (by the amount of ethylene in the reaction mixture).

Reducing the residence time by half did not reduce the yield (entry 15), while increasing the residence time twice caused the increased yield from 37 to 47.5 % (entry 16). This yield increase could be attributed to higher concentration of ethylene in the solvent at longer residence times<sup>60</sup>. Also, the yield to product was limited by the saturation concentration of ethylene in the mixture (dissolving hydrogen in DCM<sup>54, 60, 197</sup>).

The effect of residence coil length on yield was evaluated, where the 20 mL coil was replaced by a 10 mL coil while the flow rate remained the same (entry 17), and the yield of sum for 1-decene and 1,4-decadiene decreased from 47.5 % to 44.5 %. This indicated the reaction occurred completely in the Tube-in-Tube reactor, the length of the residence coil had a negligible impact on the reaction yield and the parameter with the greatest impact on yield was temperature. This was better seen when the reaction was scaled-up using the data from entry 17, where 25 mL of the mixture was pumped into the reaction from the feed flask and the reaction allowed to proceed for 2.5 h, which had an average yield of 52.5 %. The results are shown in Figure 4-49.

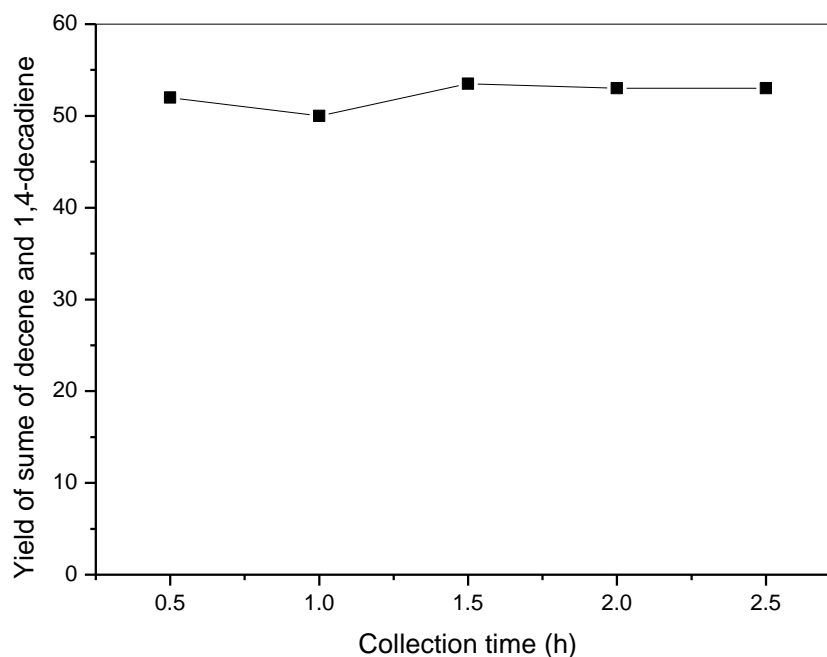


Figure 4-49. Progress of the scaled-up reaction using the parameters from entry 17 in Table 4-9 under flow conditions.

Table 4-9. A summary of results on ethenolysis in a Tube-in-Tube reactor.

Entry	Flow rate ( $\frac{\text{mL}}{\text{min}}$ )	C of CB in THF ( $\frac{\text{mol}}{\text{L}}$ )	A of catalyst (mol%)	p (barg)	Temp (°C)	$\tau$ (min)	V of reactor (mL)	Yield of sum for decene and 1,4- decadiene (%)
1	0.33	0.5	1	2	rt	61	20	10
2	0.33	0.5	1	4	rt	61	20	14
3	0.33	0.5	1	6	rt	61	20	24
4	0.33	0.5	1	10	rt	61	20	21
5	0.33	0.5	1	14	rt	61	20	17
6	0.33	0.5	1	2	40	61	20	21
7	0.33	0.5	1	4	40	61	20	26
8	0.33	0.5	1	6	40	61	20	37
9	0.33	0.5	1	10	40	61	20	30
10	0.33	0.5	1	14	40	61	20	27
11	0.33	0.5	1	6	60	61	20	31

12	0.33	0.5	0.5	6	40	61	20	25
13	0.33	0.5	0.5	6	60	61	20	19
14	0.33	0.25	1	6	40	61	20	30
15	0.67	0.5	1	6	40	30	20	35
16	0.17	0.5	1	6	40	118	20	47.5
17	0.17	0.5	1	6	40	59	10	44.5

Legend; C is concentration, A is amount, p is pressure, Temp is temperature,  $\tau$  is residence time, V is volume.

These data indicated the dynamic equilibrium for the ethenolysis of cocoa butter was obtained in a Tube-in-Tube reactor of 99 cm at 40 °C and at 6 barg.

The equilibrium constant could be written as:

$$K_a = \frac{[\text{decene}][1,4 - \text{decadiene}][\text{new TG}]_{\text{oleic}}[\text{new TG}]_{\text{linoleic}}}{[\text{TG}]_{\text{oleic}}[\text{TG}]_{\text{linoleic}}[\text{C}_2\text{H}_4]} \quad 4-102$$

The position of equilibrium could be changed towards the products by using a longer Tube-in-Tube reactor with the same permeability to the increased ethylene concentration at 6 barg.

The batch STY is estimated to be  $1.88 \cdot 10^{-4} \text{ mol L}^{-1} \text{ min}^{-1}$  and the flow STY calculated for the volume of Tube-in-Tube reactor is  $4.85 \cdot 10^{-2} \text{ mol L}^{-1} \text{ min}^{-1}$ . The efficiency of the flow process is 258-fold higher than under batch conditions.

## 5 Conclusions and Future Work

### 5.1 Epoxidation of Cocoa butter

#### 5.1.1 Conclusions

In this work epoxidation of cocoa butter was performed under batch and flow conditions. Cocoa butter was quantitatively and qualitatively analysed by GC,  $^1\text{H}$  NMR and Raman spectroscopy (Table 3-4, Table 3-3, Figure 3-4 and Figure 3-5). The enthalpy of epoxidation of cocoa butter was found to be mildly exothermic at  $-168 \text{ kJ mol}^{-1}$  using a reaction calorimeter. Epoxidation of cocoa butter under batch conditions was performed in terms of reaction temperature and catalyst composition (Figure 4-9). Here, 100 % conversion and 100 % selectivity for the oleic epoxide represent the typical batch result (Figure 4-8). Under flow conditions the reaction was run as a segmented flow in the presence of toluene to reduce viscosity. In this specific case reaction under flow conditions gives similar conversion and selectivity as batch reactions (Figure 4-12).

Generally, performing reactions in microreactors is advantageous if they are limited by mass transfer. Microreactors offer a better surface to volume ratio than in batch reactors. In this case, epoxidation of cocoa butter is controlled under batch and flow conditions by mass transfer and chemical reaction. The efficiency of this process can be improved by using tubing of a smaller diameter. Moreover, the coalescence of slugs was observed during the process in a flow reactor, which can also have an impact on STY. This coalescence could be a result of using toluene, which is partially miscible with water, or due to phase-transfer-catalyst, which can lead to the forming of emulsion, or due to the geometry of the cartridge on which the tubing was coiled. The changes in the geometry of cartridge can have an impact on tension of flowing fluid on the tubing wall. However, it was also observed that decomposition of hydrogen peroxide in the tubular reactor was quite significant. A reduction in tube diameter would lead to an increase in surface area and, most likely, a further increase in the rate of hydrogen peroxide decomposition. Therefore, there could be an optimal reactor configuration, maximising the rate of mass transfer and minimising the decomposition of the key reactant.

### 5.1.2 Future Work

In the literature there are not enough publications regarding immiscible liquid-liquid reactions under PTC in a microreactor as opposed to gas-liquid-solid investigations. The mixing of heterogeneous liquid-liquid in a phase-transfer-catalysis is an important issue in understanding the mechanism, which has an impact on a reaction in Taylor flow. The evidences presented above demonstrate that the catalytic phase transfer epoxidation in both batch and flow reactors are not an effective processes. It should be evident that we need to devote more time to performing analysis of the rheological aspect of the segmented flow regime. The flow pattern map for the mixture of cocoa butter and the mixture diluted by toluene, which shows the impact velocity on conversion and selectivity, should be determined, as well as explaining the phenomena of the coalescence of slugs. In addition, the impact of the geometry of the reactor on the formation of the coalescence of slugs should be studied. Furthermore, studding on the alternative phase transfer catalyst would also be valuable in enhancing this reaction.

In the next step, after gaining knowledge on the flow rate, the reaction should be performed in a reactor of a smaller diameter to improve the ratio of surface to volume.

If the Taylor flow system will not be effective enough for PTC epoxidation, then performing this reaction in an oscillatory baffled reactor should be considered, as was used in the papers <sup>198</sup>. The oscillatory baffled reactor is characterised superimposing fluid oscillation onto a cylindrical column inside which orifice baffles are located periodically. The mixing of mixture can be precisely controlled by this device which is important in the case of reaction in an emulsion system.

## 5.2 Reduction of Artemisinin

### 5.2.1 Conclusions

In this work was demonstrated a new flow protocol for stoichiometric reductions using an example reaction of reduction of artemisinin to dihydroartemisinin. DHA was obtained in high yields using LiBHEt<sub>3</sub> at room temperature. Short residence time and full conversion attained result in high overall productivity *ca.* 1.60 kg h<sup>-1</sup> L<sup>-1</sup>. A

biomass-derived solvent Me-THF was successfully employed to substitute THF in this protocol. The developed flow protocol for reduction using stoichiometric reducing agents is likely to have broader applicability in organic synthesis as well as synthesis of ligands.

### 5.2.2 Future Work

An appropriate pump should be found to scale up of the continuous flow process. This pump should be resistant to 2-Me-THF and LiBHEt<sub>3</sub> in THF solution.

In our research, a scale-up on trial the reduction of artemisinin was performed unsuccessfully due to problems with the pumps. According to the Knauer pump 100 manual, THF solvent is suitable 'only to a limited extent for use in the pump'. Moreover, bases are also unsuitable for the use in a pump, because they react with components of this device<sup>199</sup>. LiBHEt<sub>3</sub> has an alkaline reaction. A syringe pump with a Teflon tip on the syringe piston is also not suitable for this reaction because 2-Me-THF reacts with the piston tip.

## 5.3 Etherification of Dihydroartemisinin

### 5.3.1 Conclusions

Derivatization of an important bio-pharmaceutical molecule artemisinin into its final API artemether was performed under flow conditions for the first time. A highly effective catalyst for etherification of dihydroartemisinin, QuadraSil, was found. A close to quantitative yield of the product artemether was obtained. This catalyst shows excellent stability in the reaction and allows the complexity of the product work-up to be reduced significantly.

A detailed LCA study of the reduction and etherification steps showed the importance of solvents in pharmaceutical processes: replacement of THF by Me-THF, as well as introduction of solvent recycling, led to significant decreases in the LCA impacts of the flow processes, making them cleaner than the best literature batch reactions.

### 5.3.2 Future Work

The process of derivatizing ART to ARM could potentially be run as a tandem sequence without intermediate work-up of dihydroartemisinin. The mechanisms of formation of the side products should also be explained. The investigation into eliminating these side reactions should also take into consideration reducing impurities in the final API artemether. Future work should also focus on the possibility of scaling up the flow process.

Although some work was done to elaborate the role of epimerisation in the formation of epi-artemether, at the scale of reactions that were done in this study, it was impossible to detect all isomers. Since impurities profile is a hugely important issue of pharmaceutical active ingredients, a more detailed study of the formation of by-products under more intensive flow conditions should be done.

## 5.4 Ethenolysis of Cocoa Butter

The first-time ethenolysis of bio-waste molecule found in cocoa butter (triglyceride) was performed over the catalyst (7) using a continuous membrane contractor. A Tube-in-Tube reactor improved the process safety. Ethylene is highly flammable and explosive and is often avoided in large-scale batch reactions.

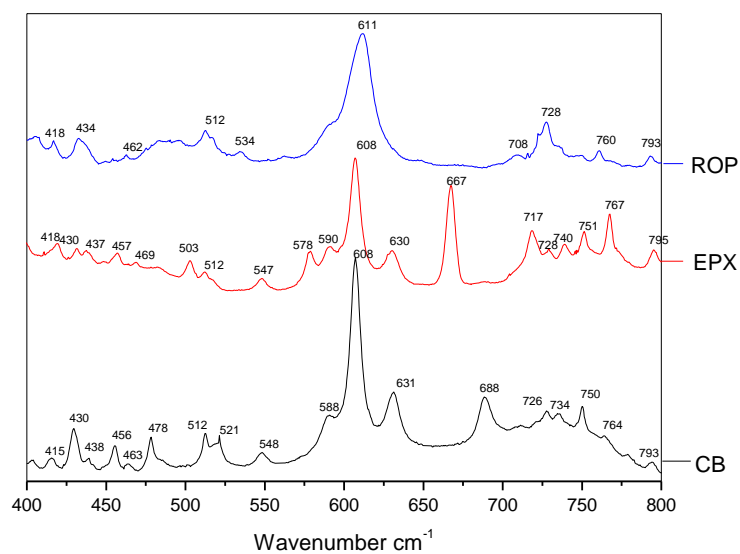
### 5.4.1 Future Work

The equilibrium constant could be written as:

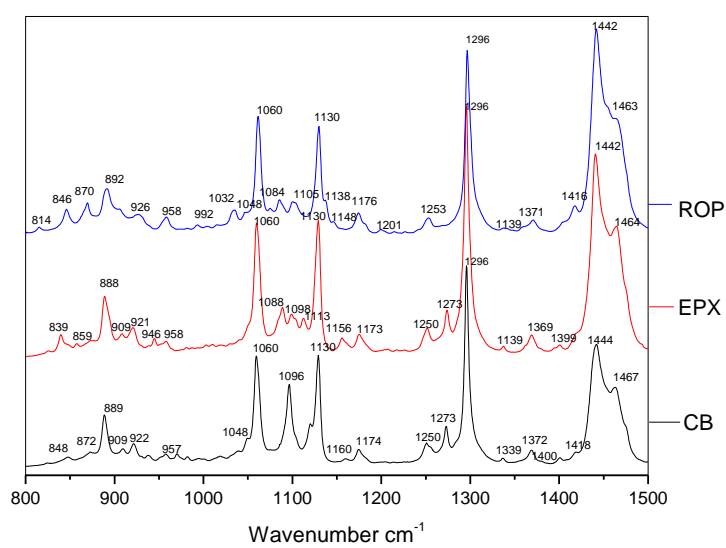
$$K_a = \frac{[\text{decene}][1,4 - \text{decadiene}][\text{new TG}]_{\text{oleic}}[\text{new TG}]_{\text{linoleic}}}{[\text{TG}]_{\text{oleic}}[\text{TG}]_{\text{linoleic}}[\text{C}_2\text{H}_4]}$$

The position of equilibrium could be driven towards the products by using a longer Tube-in-Tube reactor with the same permeability to the increased ethylene concentration at 6 barg. Second, the equilibrium position can be altered by removing one of the products by taking advantage of the differences in physical properties between 1-decene and triglyceride derivatives.

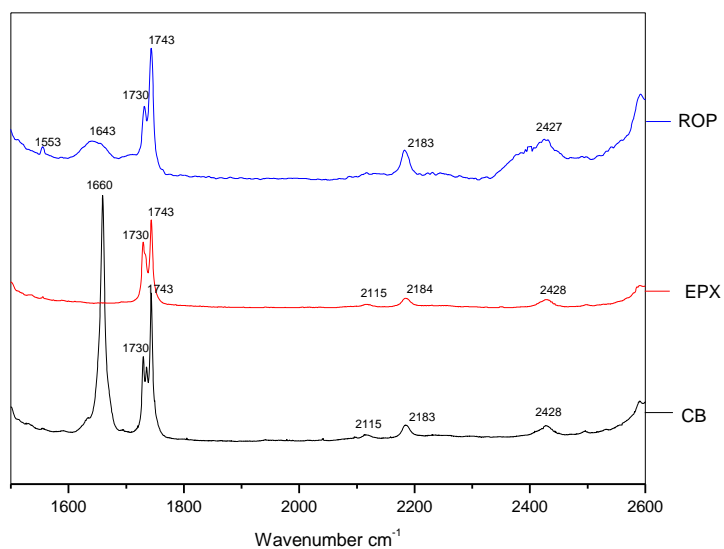
## Appendix



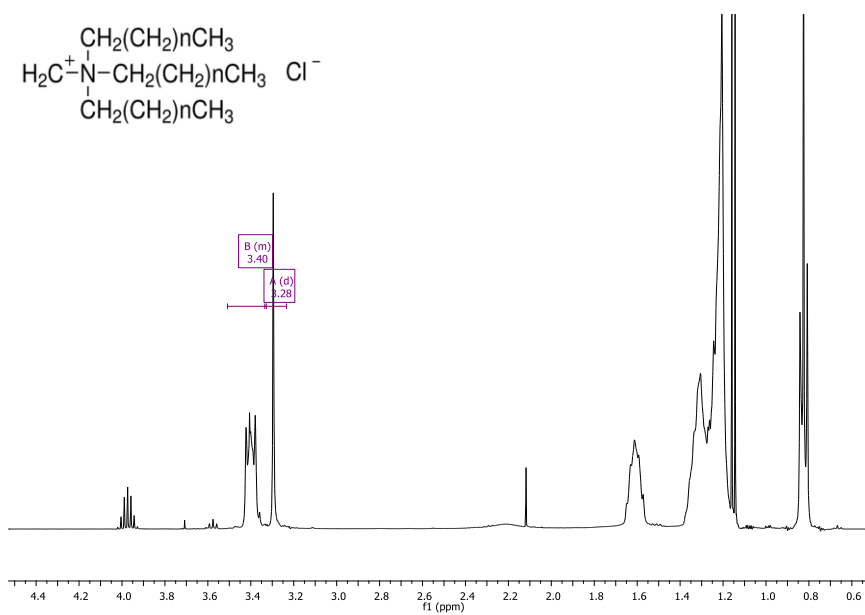
A. 1. Raman spectra of cocoa butter (CB), epoxide (EPX) and diol (ROP) in 400 – 800 cm<sup>-1</sup>.



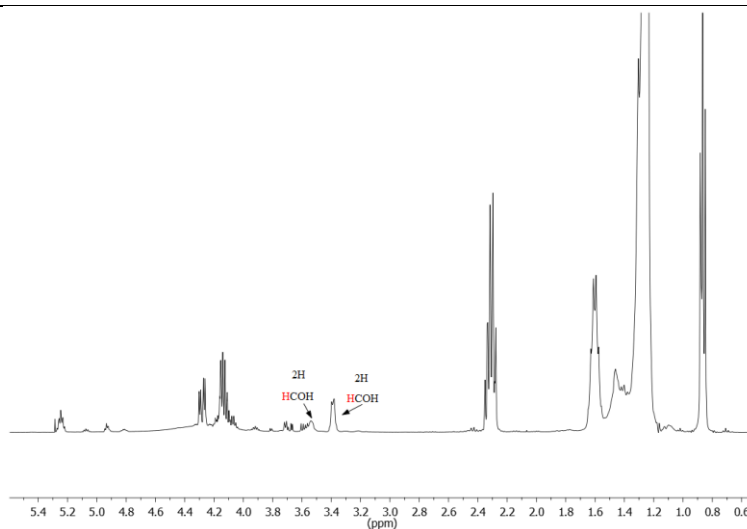
A. 2. Raman spectra of cocoa butter (CB), epoxide (EPX) and diol (ROP) in 800 – 1500 cm<sup>-1</sup>.



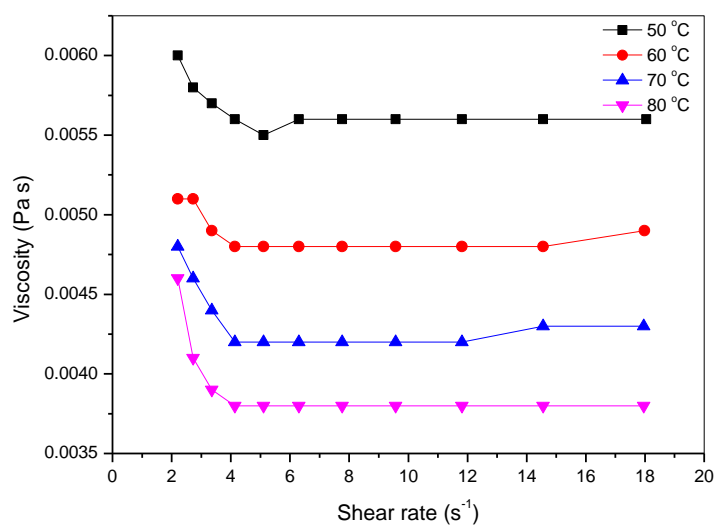
A. 3. Raman spectra of cocoa butter (CB), epoxide (EPX) and diol (ROP) in 1500 – 2600 cm<sup>-1</sup>.



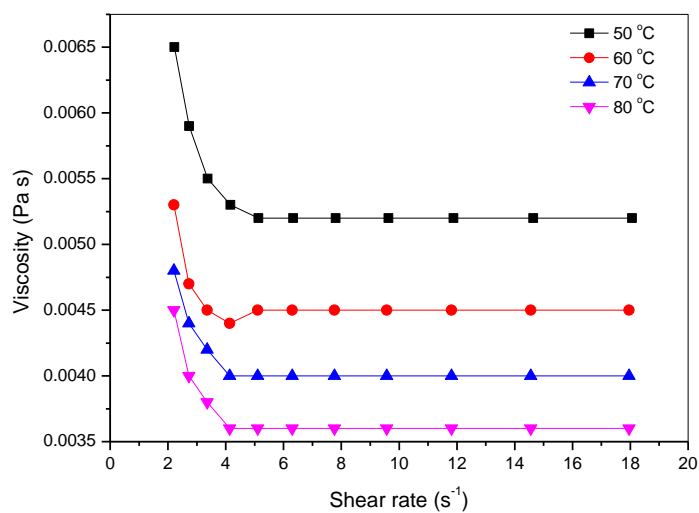
A. 4. <sup>1</sup>H NMR spectrum of Adogen 464.



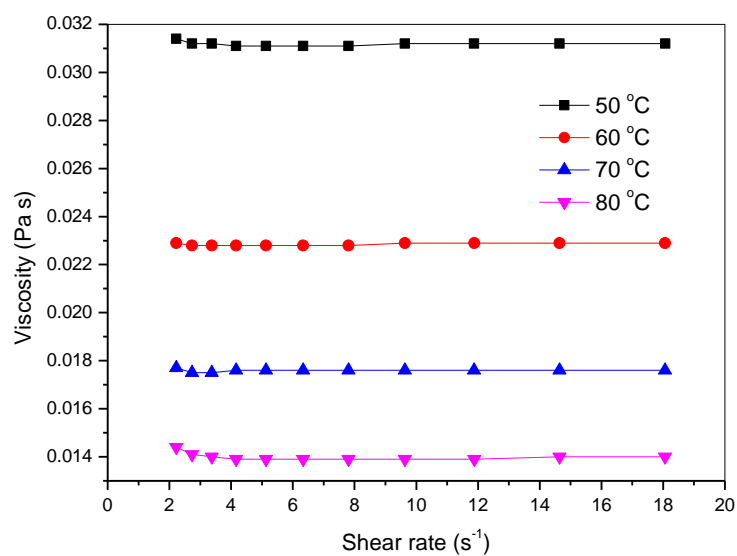
A. 5.  $^1\text{H}$  NMR spectrum of ring opening product.



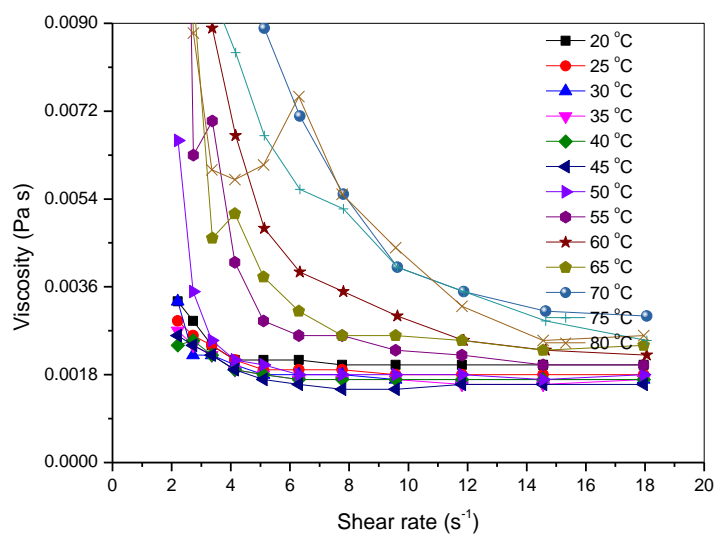
A. 6. Viscosities of the mixture cocoa butter, toluene and Adogen 464 at 50, 60, 70 and 80 °C using a Kinexus Rheometer Ultra with rSpace software package (Malvern Instruments, UK).



A. 7. Viscosities of the mixture cocoa butter, toluene and Adogen 464 at 50, 60, 70 and 80 °C using a Kinexus Rheometer Ultra with rSpace software package (Malvern Instruments, UK).



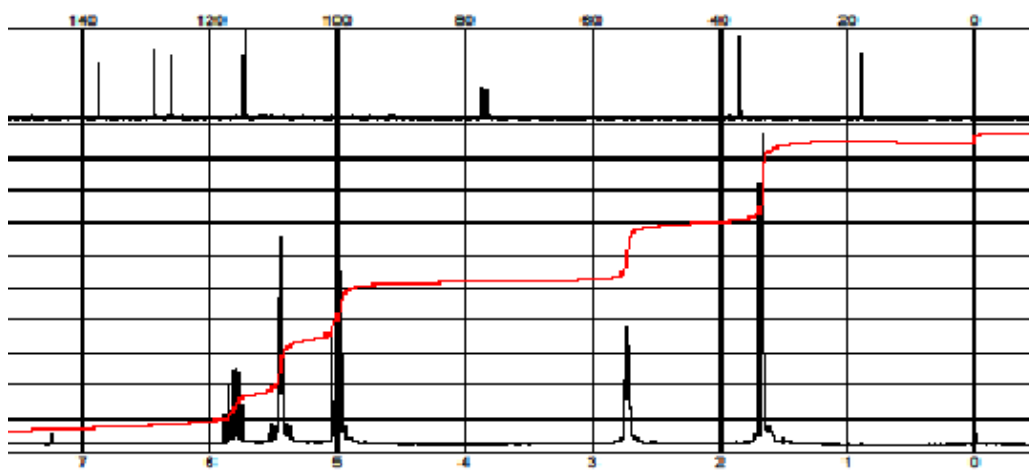
A. 8. Viscosities of cocoa butter at 50, 60, 70 and 80 °C using a Kinexus Rheometer Ultra with rSpace software package (Malvern Instruments, UK).



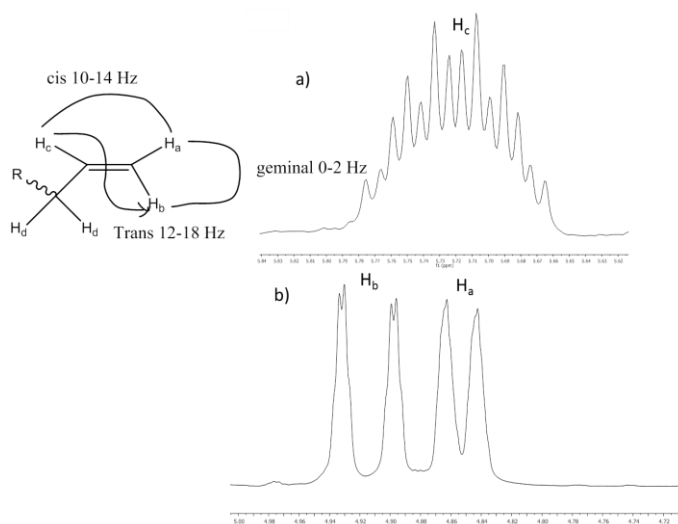
A. 9. Viscosities of aqueous at temperature range between 20 and 80 °C using a Kinexus Rheometer Ultra with rSpace software package (Malvern Instruments, UK).

Temperature / °C	Catalyst	Viscosity / mPa s		
		CB	CB + toluene	CB + toluene + Adogen 464
20	2.03			
25	1.84			
50	2.37	31.18	5.20	5.59
60	3.17	22.85	4.50	4.81
70	4.59	17.59	4.00	4.21
80	4.54	13.99	3.60	3.80

A. 10. Lists of the raw data for viscosities of fluids at different temperatures.



A. 11  $^1\text{H}+^{13}\text{C}$  NMR spectrum of 1,4-hexadiene adapted from <sup>200</sup>.



A. 12. Splitting pattern of double bond signals found in 1-decene and the oleic triglyceride derivative. Vicinal proton-proton coupling signal at 5.68 ppm (a) and vicinal- germinal proton-proton coupling signal at 4.85 ppm (b).

The mechanism of splitting of the signal is as follows: the  $\text{H}_c$  hydrogen of the terminal double bond was split by coupling to the *trans* hydrogen  $\text{H}_b$ , then was doubled by coupling to the *cis* hydrogen  $\text{H}_a$  and subsequently coupled to the two hydrogens  $\text{H}_d$ .

---

With respect to the signal at 4.85 ppm, the two H<sub>a</sub> and H<sub>b</sub> protons were also split by other protons. Hydrogen H<sub>a</sub> was doubled by coupling to the *cis* proton H<sub>c</sub> ( $J_{ac} = 10.2$  Hz) and split by proton H<sub>b</sub> into a doublet of doublets. The protons H<sub>b</sub> to H<sub>c</sub> are in geminal position to each other; thus the splitting are very small. The H<sub>b</sub> proton is split by the *trans* H<sub>c</sub> proton into a doublet ( $J_{bc} = 17.1$  Hz), and doubled by coupling to the geminal proton H<sub>a</sub> ( $J_{ab} = 1.6$  Hz).

---

**References**

1. Cubasch, U.; Wuebbles, D. *IPCC. Climate change 2013: The physical science basis. Working group I contribution to the IPCC fifth assessment report*; 2013.
2. (a) Bridgwater, A. V.; Peacocke, G. V. C., Fast pyrolysis processes for biomass. *Renew. Sust. Energ. Rev.* **2000**, *4* (1), 1-73; (b) Jin, F. M.; Enomoto, H., Hydrothermal conversion of biomass into value-added products: technology and mimics nature. *BioRes.* **2009**, *4* (2), 704-713.
3. Rotblatt, M.; Ziment, I., *Evidence-based herbal medicine*. Hanley and Belfus: Philadelphia, 2002.
4. NEPIC (North East Process Industry Cluster). Fine and speciality chemicals. [http://nepic.co.uk/about/sectors/fine\\_speciality.asp](http://nepic.co.uk/about/sectors/fine_speciality.asp).
5. Smith, W., Mapping the development of UK biorefinery complexes (NFC 07/008). A report prepared for the National Non Food Crops Centre. **2007**.
6. NEPIC (North East Process Industry Cluster). Alternative feedstocks [http://www.nepic.co.uk/low\\_carbon/alternatives.asp?qry=0,1993,1995](http://www.nepic.co.uk/low_carbon/alternatives.asp?qry=0,1993,1995). **2014**.
7. Cherubini, F., The biorefinery concept: Using biomass instead of oil for producing energy and chemicals. *Energ. Convers. Manage.* **2010**, *51* (7), 1412-1421.
8. (a) Kaphueakngam, P.; Flood, A.; Sonwai, S., Production of cocoa butter equivalent from mango seed almond fat and palm oil mid-fraction. *As. J. Food Ag-Ind.* **2009**, *2* (04), 441-447; (b) Lipp, M.; Anklam, E., Review of cocoa butter and alternative fats for use in chocolate - Part B. Analytical approaches for identification and determination. *Food Chem.* **1998**, *62* (1), 99-108; (c) Abdin, M. Z.; Israr, M.; Rehman, R. U.; Jain, S. K., Artemisinin, a novel antimalarial drug: biochemical and molecular approaches for enhanced production. *Planta Med.* **2003**, *69*, 289-299; (d) Delabays, N.; Simonnet, X.; Gaudin, M., The genetics of artemisinin content in *Artemisia annua* L. and the breeding of high yielding cultivars. *Curr. Med. Chem.* **2001**, *8* (15), 1795-1801; (e) Mueller, M. S.; Karhagomba, I. B.; Hirt, H. M.; Wemakor, E., The potential of *Artemisia annua* L. as a locally produced remedy for malaria in the tropics: agricultural, chemical and clinical aspects. *J. Ethnopharmacol.* **2000**, *73*, 487-493; (f) Khudsar, T.; Iqbal, M.; Sairam, R. K., Zinc-induced changes in morpho-physiological and biochemical parameters in *Artemisia annua*. *Biol. Plantarum* **2004**, *2*, 255-260; (g) Yekuan, W.; Longyun, L.; Ma, P.; Xiaoli, W.; Fangyi, L.; Zhixue, W., Effects of zinc, manganese and boron on artemisinin and yields of *Artemisia annua*. *J. Chin. Mater. Med.* **2010**, *35* (3), 275-278.
9. Holmgren, J.; Gosling, C.; Couch, K.; Kalnes, T.; Marker, T.; McCall, M.; Marinangeli, R., Refining biofeedstock innovations. [www.eptq.com](http://www.eptq.com). **2007**, 119-125.
10. Blecke, R.; Hill, R., Process for copolymerization of maleic anhydride with 1-olefins. Google Patents: 1973.
11. <http://www.ineos.com/businesses/ineos-oligomers/products/>.
12. Covello, P. S., Making artemisinin. *Phytochemistry* **2008**, *69* (17), 2881-2885.
13. Mohamed, S. S.; Khalid, S. A.; Ward, S. A.; Wan, T. S. M.; Tang, H. P. O.; Zheng, M.; Haynes, R. K.; Edwards, G., Simultaneous determination of artemether and its major metabolite dihydroartemisinin in plasma by gas chromatography-mass spectrometry-selected ion monitoring. *J. Chromatogr. B* **1999**, *731* (2), 251-260.
14. (a) Cai, C.; Dai, H.; Chen, R.; Su, C.; Xu, X.; Zhang, S.; Yang, L., Studies on the kinetics of in situ epoxidation of vegetable oils. *Eur. J. Lipid Sci. Technol.* **2008**, *110* (4), 341-346; (b) Poli, E.; Clacens, J. M.; Barrault, J.; Pouilloux, Y., Solvent-

- free selective epoxidation of fatty esters over a tungsten-based catalyst. *Catal. Today* **2009**, *140* (1-2), 19-22; (c) De Torres, M.; Arends, I.; Mayoral, J. A.; Pires, E.; Jimenez-Oses, G., A highly efficient, green and recoverable catalytic system for the epoxidation of fatty esters and biodiesel with H<sub>2</sub>O<sub>2</sub>. *Appl. Catal. A-Gen.* **2012**, *425*, 91-96; (d) Sun, S. D.; Yang, G. L.; Bi, Y. L.; Liang, H., Enzymatic epoxidation of corn oil by perstearic acid. *J. Am. Oil Chem. Soc.* **2011**, *88* (10), 1567-1571; (e) Dinda, S.; Goud, V. V.; Patwardhan, A. V.; Pradhan, N. C., Selective epoxidation of natural triglycerides using acidic ion exchange resin as catalyst. *Asia-Pac. J. Chem. Eng.* **2011**, *6* (6), 870-878.
15. (a) Kralisch, D.; Streckmann, I.; Ott, D.; Krtschil, U.; Santacesaria, E.; Di Serio, M.; Russo, V.; De Carlo, L.; Linhart, W.; Christian, E.; Cortese, B.; de Croon, M.; Hessel, V., Transfer of the epoxidation of soybean oil from batch to flow chemistry guided by cost and environmental issues. *ChemSusChem* **2012**, *5* (2), 300-311; (b) Cortese, B.; de Croon, M.; Hessel, V., High-temperature epoxidation of soybean oil in flow-speeding up elemental reactions wanted and unwanted. *Ind. Eng. Chem. Res.* **2012**, *51* (4), 1680-1689.
16. Kottke, R. H., Furan Derivatives. In *Kirk-Othmer encyclopedia of chemical technology*, 4th ed.; Kroschwitz, J. I.; Howe-Grant, M., Eds. Wiley: New York, 1998; Vol. Supplement.
17. Stringham, R. W.; Teager, D. S., Streamlined process for the conversion of artemisinin to artemether. *Org. Process Res. Dev.* **2012**, *16* (5), 764-768.
18. Singh, C.; Tiwari, P., A one-pot conversion of artemisinin to its ether derivatives. *Tetrahedron Lett.* **2002**, *43* (40), 7235-7237.
19. Luis, S. V.; Garcia-Verdugo, E., *Chemical reactions and processes under flow conditions*. The Royal Society of Chemistry: Cambridge, 2009; p 213.
20. Roberge, D. M., An integrated approach combining reaction engineering and design of experiments for optimizing reactions. *Org. Process Res. Dev.* **2004**, *8* (6), 1049-1053.
21. Roberge, D. M.; Ducry, L.; Bieler, N.; Cretton, P.; Zimmermann, B., Microreactor technology: A revolution for the fine chemical and pharmaceutical industries? *Chem. Eng. Technol.* **2005**, *28* (3), 318-323.
22. Roberge, D. M.; Gottsoner, M.; Eyholzer, M.; Kockmann, N., Industrial design, scale-up, and use of microreactors. *Chim. Oggi-Chem. Today* **2009**, *27* (4), 8-11.
23. Hartman, R. L.; Jensen, K. F., Microchemical systems for continuous-flow synthesis. *Lab. Chip.* **2009**, *9* (17), 2495-2507.
24. (a) Tsubogo, T.; Ishiwata, T.; Kobayashi, S., Asymmetric carbon-carbon bond formation under continuous-flow conditions with chiral heterogeneous catalysts. *Angew. Chem. Int.* **2013**, *52* (26), 6590-6604; (b) Liu, X. Y.; Unal, B.; Jensen, K. F., Heterogeneous catalysis with continuous flow microreactors. *Catal. Sci. Tech.* **2012**, *2* (10), 2134-2138.
25. Zhao, Y. C.; Chen, G. W.; Yuan, Q., Liquid-liquid two-phase flow patterns in a rectangular microchannel. *Aiche J.* **2006**, *52* (12), 4052-4060.
26. (a) Triplett, K. A.; Ghiaasiaan, S. M.; Abdel-Khalik, S. I.; Sadowski, D. L., Gas-liquid two-phase flow in microchannels - Part I: two-phase flow patterns. *Int. J. Multiph. Flow* **1999**, *25* (3), 377-394; (b) Mishima, K.; Hibiki, T., Some characteristics of air-water two-phase flow in small diameter vertical tubes. *Int. J. Multiph. Flow* **1996**, *22* (4), 703-712; (c) Coleman, J. W.; Garimella, S., Characterization of two-phase flow patterns in small diameter round and rectangular tubes. *Int. J. Heat Mass Transf.* **1999**, *42* (15), 2869-2881; (d) Kreutzer, M. T.;

- Kapteijn, F.; Moulijn, J. A.; Heiszwolf, J. J., Multiphase monolith reactors: Chemical reaction engineering of segmented flow in microchannels. *Chem. Eng. Sci.* **2005**, *60* (22), 5895-5916; (e) Thulasidas, T. C.; Abraham, M. A.; Cerro, R. L., Bubble-train flow in capillaries of circular and square cross-section. *Chem. Eng. Sci.* **1995**, *50* (2), 183-199.
27. (a) Liu, L.; Matar, O. K.; Lawrence, C. J.; Hewitt, G. F., Laser-induced fluorescence (LIF) studies of liquid-liquid flows. Part I: Flow structures and phase inversion. *Chem. Eng. Sci.* **2006**, *61* (12), 4007-4021; (b) Sinkovec, E.; Krajnc, M., Phase transfer catalyzed Wittig reaction in the microtube reactor under liquid-liquid slug-flow pattern. *Org. Process Res. Dev.* **2011**, *15* (4), 817-823.
28. Dowe, D. C.; Rezkallah, K. S., Flow regime identification in microgravity two-phase flows using void fraction signals. *Int. J. Multiph. Flow* **1999**, *25* (3), 433-457.
29. Reinecke, N.; Mews, D., Oscillatory transient two-phase flows in single channels with reference to monolithic catalyst supports. *Int. J. Multiph. Flow* **1999**, *25* (6-7), 1373-1393.
30. Harries, N.; Burns, J. R.; Barrow, D. A.; Ramshaw, C., A numerical model for segmented flow in a microreactor. *Int. J. Heat Mass Transf.* **2003**, *46* (17), 3313-3322.
31. Ghaini, A.; Mescher, A.; Agar, D. W., Hydrodynamic studies of liquid-liquid slug flows in circular microchannels. *Chem. Eng. Sci.* **2011**, *66* (6), 1168-1178.
32. (a) Dessimoz, A. L.; Cavin, L.; Renken, A.; Kiwi-Minsker, L., Liquid-liquid two-phase flow patterns and mass transfer characteristics in rectangular glass microreactors. *Chem. Eng. Sci.* **2008**, *63* (16), 4035-4044; (b) Jovanovic, J.; Rebrov, E. V.; Nijhuis, T. A.; Hessel, V.; Schouten, J. C., Phase-transfer catalysis in segmented flow in a microchannel: fluidic control of selectivity and productivity. *Ind. Eng. Chem. Res.* **2010**, *49* (6), 2681-2687; (c) Kashid, M. N.; Renken, A.; Kiwi-Minsker, L., Influence of flow regime on mass transfer in different types of microchannels. *Ind. Eng. Chem. Res.* **2011**, *50* (11), 6906-6914.
33. Burns, J. R.; Ramshaw, C., A microreactor for the nitration of benzene and toluene. *Chem. Eng. Commun.* **2002**, *189* (12), 1611-1628.
34. Tokeshi, M.; Minagawa, T.; Uchiyama, K.; Hibara, A.; Sato, K.; Hisamoto, H.; Kitamori, T., Continuous-flow chemical processing on a microchip by combining microunit operations and a multiphase flow network. *Anal. Chem.* **2002**, *74* (7), 1565-1571.
35. Dehmlow, E. V., Phase-transfer catalyzed 2-phase reactions in preparative organic-chemistry. *Angew. Chem. Int.* **1974**, *13* (3), 170-179.
36. (a) Fletcher, P. D. I.; Haswell, S. J.; Pombo-Villar, E.; Warrington, B. H.; Watts, P.; Wong, S. Y. F.; Zhang, X., Micro reactors: principles and applications in organic synthesis. *Tetrahedron* **2002**, *58* (24), 4735-4757; (b) Kikutani, Y.; Horiuchi, T.; Uchiyama, K.; Hisamoto, H.; Tokeshi, M.; Kitamori, T., Glass microchip with three-dimensional microchannel network for 2 X 2 parallel synthesis *Lab. Chip.* **2003**, *3* (1), 51-51.
37. Schwalbe, T.; Autze, V.; Hohmann, M.; Stirner, W., Novel innovation systems for a cellular approach to continuous process chemistry from discovery to market. *Org. Process Res. Dev.* **2004**, *8* (3), 440-454.
38. Rournanie, M.; Delattre, C.; Mittler, F.; Marchand, G.; Meille, V.; de Bellefon, C.; Pijolat, C.; Tournier, G.; Pouteau, P., Enhancing surface activity in silicon microreactors: Use of black silicon and alumina as catalyst supports for chemical and biological applications. *Chem. Eng. J.* **2008**, *135*, S317-S326.

39. (a) Xia, Y. N.; Whitesides, G. M., Soft lithography. *Annu. Rev. Mater. Sci.* **1998**, *28*, 153-184; (b) Anzenbacher, P.; Palacios, M. A., Polymer nanofibre junctions of attolitre volume serve as zeptomole-scale chemical reactors *Nat. Chem.* **2009**, *1* (2), 165-165; (c) Lee, J. N.; Park, C.; Whitesides, G. M., Solvent compatibility of poly(dimethylsiloxane)-based microfluidic devices. *Anal. Chem.* **2003**, *75* (23), 6544-6554; (d) Willis, P. A.; Hunt, B. D.; White, V. E.; Lee, M. C.; Ikeda, M.; Bae, S.; Pelletier, M. J.; Grunthaner, F. J., Monolithic Teflon (R) membrane valves and pumps for harsh chemical and low-temperature use. *Lab. Chip.* **2007**, *7* (11), 1469-1474; (e) Grover, W. H.; von Muhlen, M. G.; Manalis, S. R., Teflon films for chemically-inert microfluidic valves and pumps. *Lab Chip* **2008**, *8* (6), 913-918; (f) Yoon, T. H.; Park, S. H.; Min, K. I.; Zhang, X. L.; Haswell, S. J.; Kim, D. P., Novel inorganic polymer derived microreactors for organic microchemistry applications. *Lab. Chip.* **2008**, *8* (9), 1454-1459.
40. Knitter, R.; Gohring, D.; Risthaus, P.; Hausselt, J., Microfabrication of ceramic microreactors. *Microsyst. Technol.* **2001**, *7* (3), 85-90.
41. Jähnisch, K.; Hessel, V.; Löwe, H.; Baerns, M., Chemistry in microstructured reactors. *Angew. Chem. Int.* **2004**, *43* (4), 406-446.
42. Warmington, A.; Challener, C., Microreactors could play a vital role in transitioning fine chemicals from batch processes to continuous. *Spec. Chem. Magaz.* **2008**, *28* (3), 40-46.
43. Schubert, K.; Brandner, J.; Fichtner, M.; Linder, G.; Schygulla, U.; Wenka, A., Microstructure devices for applications in thermal and chemical process engineering. *Microscale Thermophys. Eng.* **2001**, *5* (1), 17-39.
44. Schwalbe, T.; Autze, V.; Wille, G., Chemical synthesis in microreactors. *Chimia* **2002**, *56* (11), 636-646.
45. Froment, G. F.; Bischoff, K. B.; Wilde, J. D., *Chemical reactor analysis and design*. third ed.; John Wiley & Sons, Inc.: Danvers, 2011; p 860.
46. Mason, B. P.; Price, K. E.; Steinbacher, J. L.; Bogdan, A. R.; McQuade, D. T., Greener approaches to organic synthesis using microreactor technology. *Chem. Rev.* **2007**, *107* (6), 2300-2318.
47. Markowz, G.; Schirrmeyer, S.; Albrecht, J.; Becker, F.; Schutte, R.; Caspary, K. J.; Klemm, E., Microstructured reactors for heterogeneously catalyzed gas-phase reactions on an industrial scale. *Chem. Eng. Technol.* **2005**, *28* (4), 459-464.
48. Gutmann, B.; Roduit, J.-P.; Roberge, D.; Kappe, C. O., Synthesis of 5-Substituted 1H-tetrazoles from nitriles and hydrazoic acid by using a safe and scalable high-temperature microreactor approach. *Angew. Chem. Int.* **2010**, *49* (39), 7101-7105.
49. Jensen, K. F., Microreaction engineering - is small better? *Chem. Eng. Sci.* **2001**, *56*, 293-303.
50. Stankiewicz, A. I.; Moulijn, J. A., Process intensification: Transforming chemical engineering. *Chem. Eng. Prog.* **2000**, *96* (1), 22-34.
51. (a) Hendershot, D. C., Process minimization: Making plants safer. *Chem. Eng. Prog.* **2000**, *96* (1), 35-40; (b) Benson, R. S.; Ponton, J. W., Process miniaturization - a route to total environmental acceptability. *Chem. Eng. Res. Des.* **1993**, *71* (A2), 160-168; (c) Hendershot, D. C., Inherently safer chemical process design. *J. Loss Prevent. in the Proc.* **1997**, *10* (3), 151-157.
52. Sirkar, K. K.; Shanbhag, P. V.; Kovvali, A. S., Membrane in a reactor: A functional perspective. *Ind. Eng. Chem. Res.* **1999**, *38* (10), 3715-3737.

- 
53. Jensen, K. H.; Lee, J.; Bohrc, T.; Bruus, H., Osmotically driven flows in microchannels separated by a semipermeable membrane. *Lab. Chip.* **2009**, *9*, 2093-2099.
54. O'Brien, M.; Taylor, N.; Polyzos, A.; Baxendale, I. R.; Ley, S. V., Hydrogenation in flow: Homogeneous and heterogeneous catalysis using Teflon AF-2400 to effect gas-liquid contact at elevated pressure. *Chem. Sci.* **2011**, *2* (7), 1250-1257.
55. Yampolskii, Y. P., Amorphous perfluorinated membrane materials: Structure, properties and application. *Russ. J. Gen. Chem.* **2009**, *79* (3), 657-665.
56. Maurya, R. A.; Park, C. P.; Kim, D. P., Triple-channel microreactor for biphasic gas-liquid reactions: Photosensitized oxygenations. *Beilstein J. Org. Chem.* **2011**, *7*, 1158-1163.
57. O'Brien, M.; Baxendale, I. R.; Ley, S. V., Flow Ozonolysis Using a Semipermeable Teflon AF-2400 Membrane To Effect Gas-Liquid Contact. *Org. Lett.* **2010**, *12* (7), 1596-1598.
58. Polyzos, A.; O'Brien, M.; Petersen, T. P.; Baxendale, I. R.; Ley, S. V., The continuous-flow synthesis of carboxylic acids using CO<sub>2</sub> in a Tube-In-Tube gas permeable membrane reactor. *Angew. Chem. Int.* **2011**, *50* (5), 1190-1193.
59. Koos, P.; Gross, U.; Polyzos, A.; O'Brien, M.; Baxendale, I.; Ley, S. V., Teflon AF-2400 mediated gas-liquid contact in continuous flow methoxycarbonylations and in-line FTIR measurement of CO concentration. *Org. Biomol. Chem.* **2011**, *9* (20), 6903-6908.
60. Bourne, S. L.; Koos, P.; O'Brien, M.; Martin, B.; Schenkel, B.; Baxendale, I. R.; Ley, S. V., The continuous-flow synthesis of styrenes using ethylene in a palladium-catalysed Heck cross-coupling reaction. *Synlett* **2011**, (18), 2643-2647.
61. Petersen, T. P.; Polyzos, A.; O'Brien, M.; Ulven, T.; Baxendale, I. R.; Ley, S. V., The oxygen-mediated synthesis of 1,3-butadiynes in continuous flow: Using Teflon AF-2400 to effect gas/liquid contact. *ChemSusChem* **2012**, *5* (2), 274-277.
62. Kasinathan, S.; Bourne, S. L.; Tolstoy, P.; Koos, P.; O'Brien, M.; Bates, R. W.; Baxendale, I. R.; Ley, S. V., Syngas-mediated C-C bond formation in flow: Selective rhodium-catalysed hydroformylation of styrenes. *Synlett* **2011**, (18), 2648-2651.
63. Fernando, S.; Adhikari, S.; Chandrapal, C.; Murali, N., Biorefineries: Current status, challenges, and future direction. *Energy Fuels* **2006**, *20* (4), 1727-1737.
64. IEA, World Energy Outlook International Energy Agency: Paris, 2007.
65. PMM In *White biotechnology: Replaying black gold?*, Fifth International Conference on Renewable Resources and Biorefineries, Ghent, Belgium, Ghent, Belgium, 10-12 June 2009.
66. Gallezot, P., Conversion of biomass to selected chemical products. *Chem. Soc. Rev.* **2012**, *41* (4), 1538-1558.
67. Kamm, B., Production of platform chemicals and synthesis gas from biomass. *Angew. Chem. Int.* **2007**, *46* (27), 5056-5058.
68. Hatti-Kaul, R.; Tornvall, U.; Gustafsson, L.; Borjesson, P., Industrial biotechnology for the production of bio-based chemicals - a cradle-to-grave perspective. *Trends Biotechnol.* **2007**, *25* (3), 119-124.
69. Jang, Y.-S.; Kim, B.; Shin, J. H.; Choi, Y. J.; Choi, S.; Song, C. W.; Lee, J.; Park, H. G.; Lee, S. Y., Bio-based production of C<sub>2</sub>-C<sub>6</sub> platform chemicals. *Biotechnol. Bioeng.* **2012**, *109* (10), 2437-2459.

70. (a) Gallezot, P., Direct routes from biomass to end-products. *Catal. Today* **2011**, *167* (1), 31-36; (b) Gallezot, P., Alternative value chains for biomass conversion to chemicals. *Top. Catal.* **2010**, *53* (15-18), 1209-1213.
71. Gallezot, P., Process options for converting renewable feedstocks to bioproducts. *Green Chem.* **2007**, *9* (4), 295-302.
72. *Biofuels - What role in the future energy mix? facts, trends and perspective.*; Hamburg, 2012.
73. Kendall, A.; Yuan, J. H., Comparing life cycle assessments of different biofuel options. *Curr. Opin. Chem. Biol.* **2013**, *17* (3), 439-443.
74. Kim, S.; Dale, B. E., Global potential bioethanol production from wasted crops and crop residues. *Biomass Bioenerg.* **2004**, *26* (4), 361-375.
75. Stephen, J. D.; Mabee, W. E.; Saddler, J. N., Will second-generation ethanol be able to compete with first-generation ethanol? Opportunities for cost reduction. *Biofuels Bioprod. Biorefining* **2012**, *6* (2), 159-176.
76. Sanderson, K., A field in ferment. *Nature* **2006**, *444* (7120), 673-676.
77. (a) Hayes, D. J. M., Second-generation biofuels: Why they are taking so long. *Energ. Environ.* **2013**, *2* (3), 304-334; (b) Clark, J. H., Green chemistry for the second generation biorefinery - sustainable chemical manufacturing based on biomass. *J. Chem. Technol. Biotechnol.* **2007**, *82* (7), 603-609; (c) Wright, M. M.; Brown, R. C., Comparative economics of biorefineries based on the biochemical and thermochemical platforms. *Biofuels Bioprod. Biorefining* **2007**, *1* (1), 49-56; (d) Froese, R. E.; Waterstraut, J. R.; Johnson, D. M.; Shonnard, D. R.; Whitmarsh, J. H.; Miller, C. A., Lignocellulosic ethanol: Is it economically and financially viable as a fuel source? *Environ. Qual. Manage.* **2008**, *18* (1), 23-45; (e) Klein-Marcuschamer, D.; Oleskowicz-Popiel, P.; Simmons, B. A.; Blanch, H. W., The challenge of enzyme cost in the production of lignocellulosic biofuels. *Biotechnol. Bioeng.* **2012**, *109* (4), 1083-1087; (f) Ajanovic, A., Renewable fuels - A comparative assessment from economic, energetic and ecological point-of-view up to 2050 in EU-countries. *Renew. Energy* **2013**, *60*, 733-738; (g) Glithero, N. J.; Wilson, P.; Ramsden, S. J., Straw use and availability for second generation biofuels in England. *Biomass Bioenerg.* **2013**, *55*, 311-321; (h) Bernardi, A.; Giarola, S.; Bezzo, F., Spatially explicit multiobjective optimization for the strategic design of first and second generation biorefineries including carbon and water footprints. *Ind. Eng. Chem. Res.* **2013**, *52* (22), 7170-7180; (i) Pourhashem, G.; Adler, P. R.; McAloon, A. J.; Spatari, S., Cost and greenhouse gas emission tradeoffs of alternative uses of lignin for second generation ethanol. *Environ. Res. Lett.* **2013**, *8* (2), 1-18.
78. Kim, S.; Dale, B. E., Life cycle assessment of various cropping systems utilized for producing biofuels: Bioethanol and biodiesel. *Biomass Bioenerg.* **2005**, *29* (6), 426-439.
79. (a) Fenton, O.; Uallachain, D. O., Agricultural nutrient surpluses as potential input sources to grow third generation biomass (microalgae): A review. *Algal Res.* **2012**, *1* (1), 49-56; (b) Chen, C. Y.; Zhao, X. Q.; Yen, H. W.; Ho, S. H.; Cheng, C. L.; Lee, D. J.; Bai, F. W.; Chang, J. S., Microalgae-based carbohydrates for biofuel production. *Biochem. Eng. J.* **2013**, *78*, 1-10.
80. (a) Singh, A.; Olsen, S. I.; Nigam, P. S., A viable technology to generate third-generation biofuel. *J. Chem. Technol. Biotechnol.* **2011**, *86* (11), 1349-1353; (b) Qin, S.; Lin, H. Z.; Jiang, P., Advances in genetic engineering of marine algae. *Biotechnol. Adv.* **2012**, *30* (6), 1602-1613.

81. Climent, M. J.; Corma, A.; Iborra, S., Converting carbohydrates to bulk chemicals and fine chemicals over heterogeneous catalysts. *Green Chem.* **2011**, *13* (3), 520-540.
82. Corma, A.; Iborra, S.; Velty, A., Chemical routes for the transformation of biomass into chemicals. *Chem. Rev.* **2007**, *107* (6), 2411-2502.
83. Lipp, M. S., C.; Ulberth, F.; Anklam, E.; Crews, C.; Brereton, P.; de Greyt, W.; Schwack, W.; Wiedmaier, C., Composition of genuine cocoa butter and cocoa butter equivalents. *J. Food Comp. Anal.* **2001**, *14* (4), 399-408.
84. (a) Calvignac, B.; Rodier, E.; Letourneau, J.-J.; Santos, P. M. A. d.; Fages, J., Cocoa Butter Saturated with Supercritical Carbon Dioxide: Measurements and Modelling of Solubility, Volumetric Expansion, Density and Viscosity. *Intern. J. Chem. React. Eng.* **2010**, *8* (1); (b) Abigor, R.; Marmer, W.; Foglia, T.; Jones, K.; DiCiccio, R.; Ashby, R.; Uadia, P., Production of Cocoa Butter-Like Fats by the Lipase-Catalyzed Interesterification of Palm oil and Hydrogenated Soybean Oil. *J. Am. Oil Chem. Soc.* **2003**, *80* (12), 1193-1196.
85. Lima, L. J. R.; Almeida, M. H.; Nout, M. J. R.; Zwietering, M. H., *Theobroma cacao* L., "the food of the gods": Quality determinants of commercial cocoa beans, with particular reference to the impact of fermentation. *Crit. Rev. Food Sci. Nutr.* **2011**, *51* (8), 731-761.
86. Aharoni, A.; Galili, G., Metabolic engineering of the plant primary-secondary metabolism interface. *Curr. Opin. Biotechnol.* **2011**, *22* (2), 239-244.
87. Hartmann, T., The lost origin of chemical ecology in the late 19th century. *Proc. Natl. Acad. Sci.* **2008**, *105* (12), 4541-4546.
88. Dixon, R. A., Plant natural products: the molecular genetic basis of biosynthetic diversity. *Curr. Opin. Biotechnol.* **1999**, *10* (2), 192-197.
89. Davies, K. M.; Espley, R. V., Opportunities and challenges for metabolic engineering of secondary metabolite pathways for improved human health characters in fruit and vegetable crops. *N. Z. J. Crop Hortic. Sci.* **2013**, *41* (3), 154-177.
90. Chandra, S.; Chandra, R., Engineering secondary metabolite production in hairy roots. *Phytochem. Rev.* **2011**, *10* (3), 371-395.
91. Schwab, W., Metabolome diversity: too few genes, too many metabolites? *Phytochemistry* **2003**, *62* (6), 837-849.
92. Liu, N. Q.; Schuehly, W.; von Freyhold, M.; van der Kooy, F., A novel purification method of artemisinin from *Artemisia annua*. *Ind. Crop. Prod.* **2011**, *34* (1), 1084-1088.
93. Yadav, J. S.; Thirupathiah, B.; Srihari, P., A concise stereoselective total synthesis of (+)-artemisinin. *Tetrahedron* **2010**, *66* (11), 2005-2009.
94. (a) Soktoeva, T. E.; Ryzhova, G. L.; Dychko, K. A.; Khasanov, V. V.; Zhigzhitzhapova, S. V.; Radnaeva, L. D., Artemisinin content in *Artemisia annua* L. extracts obtained by different methods. *Russ. J. Bioorg. Chem.* **2013**, *39* (7), 761-764; (b) Kopetzki, D.; Levesque, F.; Seeberger, P. H., A continuous-flow process for the synthesis of artemisinin. *Chem.-Eur. J.* **2013**, *19* (17), 5450-5456; (c) Briars, R.; Paniwnyk, L., Effect of ultrasound on the extraction of artemisinin from *Artemisia annua*. *Ind. Crop. Prod.* **2013**, *42*, 595-600; (d) Briars, R.; Paniwnyk, L., Examining the extraction of artemisinin from *artemisia annua* using ultrasound. In *International Congress on Ultrasonics*, Linde, B. B. J.; Paczkowski, J.; Ponikwicki, N., Eds. Amer Inst Physics: Melville, 2012; Vol. 1433, pp 581-585; (e) Cutler, M.; Lapkin, A.; Plucinski, P. K., Comparative assessment of technologies for extraction of artemisinin (A summary of report commissioned through Malaria Medicines Ventures MMV). **2006**, 1-17; (f) Lapkin, A. A.; Plucinski, P. K.; Cutler, M.,

- Comparative assessment of technologies for extraction of artemisinin. *J. Nat. Prod.* **2006**, *69* (11), 1653-1664.
95. (a) Price, R. N., Artemisinin drugs: novel antimalarial agents. *Expert Opin. Investig. Drugs* **2000**, *9* (8), 1815-1827; (b) Wiesner, J.; Ortmann, R.; Jomaa, H.; Schlitzer, M., New Antimalarial Drugs. *Angew. Chem. Int.* **2003**, *42* (43), 5274-5293.
96. WHO (World Health Organisation) *World Malaria Report*; Geneva, 2010.
97. Lin, A. J.; Zikry, A. B.; Kyle, D. E., Antimalarial activity of new dihydroartemisinin derivatives .7. 4-(*p*-substituted phenyl)-4(*R* or *S*)- 10(*alpha* or *beta*)-dihydroartemisininoxy butyric acids. *J. Med. Chem.* **1997**, *40* (9), 1396-1400.
98. (a) Ozturk, C.; Kusefoglul, S. H., New polymers from epoxidized soybean oil with pyridine derivatives. *J. Appl. Polym. Sci.* **2011**, *121* (5), 2976-2984; (b) Barrett, L. W.; Sperling, L. H.; Murphy, C. J., Naturally functionalized triglyceride oils in interpenetrating polymer networks *J. Am. Oil Chem. Soc.* **1993**, *70* (5), 523-534; (c) Desroches, M.; Escouvois, M.; Auvergne, R.; Caillol, S.; Boutevin, B., From vegetable oils to polyurethanes: Synthetic routes to polyols and main industrial products. *Polym. Rev.* **2012**, *52* (1), 38-79.
99. Lapkin, A. A.; Plucinski, P. K., 'Engineering factors for efficient flow processes in chemical industries' in *Chemical reactions and processes under flow conditions*. RSC: Cambridge 2010.
100. McPake, C. B.; Murray, C. B.; Sandford, G., Epoxidation of alkenes using HOF<sup>+</sup> MeCN by a continuous flow process. *Tetrahedron Lett.* **2009**, *50* (15), 1674-1676.
101. Kee, S. P.; Gavriilidis, A., Design and performance of a microstructured PEEK reactor for continuous poly-*L*-leucine-catalysed chalcone epoxidation. *Org. Process Res. Dev.* **2009**, *13* (5), 941-951.
102. Mello, R.; Alcalde-Aragones, A.; Olmos, A.; Gonzalez-Nunez, M. E.; Asensio, G., Epoxidation of olefins with a silica-supported peracid in supercritical carbon dioxide under flow conditions. *J. Org. Chem.* **2012**, *77* (10), 4706-4710.
103. Cullen, C. J.; Wootton, R. C. R.; Mello, A. J., Alkene epoxidation with a polystyrene immobilised metal salen catalyst in a continuous-flow microfluidic reactor. *J. Appl. Phys.* **2009**, *105* (10).
104. (a) Venturello, C.; Dalosio, R., Quaternary ammonium tetrakis(diperoxotungsto)phosphates(3-) as a new class of catalysts for efficient alkene epoxidation with hydrogen peroxide *J. Org. Chem.* **1988**, *53* (7), 1553-1557; (b) Venturello, C.; Alneri, E.; Ricci, M., A new effective catalytic-system for epoxidation of olefins by hydrogen peroxide under phase-transfer conditions. *J. Org. Chem.* **1983**, *48* (21), 3831-3833.
105. Csanyi, L. J.; Jaky, K., Peroxo-oxometallate formation under phase-transfer conditions *J. Mol. Catal.* **1990**, *61* (1), 75-84.
106. (a) Yadav, G. D.; Pujari, A. A., Epoxidation of styrene to styrene oxide: Synergism of heteropoly acid and phase-transfer catalyst under Ishii-Venturello mechanism. *Org. Process Res. Dev.* **2000**, *4* (2), 88-93; (b) Yadav, G. D.; Satoskar, D. V., Kinetics of epoxidation of alkyl esters of undecylenic acid: Comparison of traditional routes vs. Ishii-Venturello chemistry. *J. Am. Oil Chem. Soc.* **1997**, *74* (4), 397-407; (c) Duncan, D. C.; Chambers, R. C.; Hecht, E.; Hill, C. L., Mechanism and dynamics in the H<sub>3</sub>PW<sub>12</sub>O<sub>40</sub>-catalysed selective epoxidation of terminal olefins by H<sub>2</sub>O<sub>2</sub> - formation, reactivity, and stability of [PO<sub>4</sub> [WO(O<sub>2</sub>)<sub>2</sub>]<sub>4</sub>]<sup>3-</sup>. *J. Am. Chem. Soc.* **1995**, *117* (2), 681-691.

107. Kozhevnikov, I. V.; Mulder, G. P.; Steverink-de Zoete, M. C.; Oostwal, M. G., Epoxidation of oleic acid catalyzed by peroxy phosphotungstate in a two-phase system. *J. Mol. Catal. A-Chem.* **1998**, *134* (1-3), 223-228.
108. (a) Sherringham, J. A.; Clark, A. J.; Keene, R. T., New chemical feedstock from unsaturated oils. *Lipid Technology* **2000**, *12*, 129 -132; (b) Coles, S. R.; Barker, G.; Clark, A. J.; Kirwan, K.; Jacobs, D.; Makenji, K.; Pink, D., Synthetic mimicking of plant oils and comparison with naturally grown products in polyurethane synthesis. *Macromol. Biosci.* **2008**, *8* (6), 526-532; (c) Clark, A.; Keene, B.; Hignett, R. *Low-Cost Synthesis and Evaluation of Polymers Prepared From Oilseed Rape and Euphorbia Lagascae Oil*; Coventry, 2001; p 32.
109. LaPorte, T. L.; Wang, C., Continuous processes for the production of pharmaceutical intermediates and active pharmaceutical ingredients. *Curr. Opin. Drug Discovery Dev.* **2007**, *10*, 738-745.
110. Newman, D. J.; Cragg, G. M., Natural products as sources of new drugs over the last 25 years. *J. Nat. Prod.* **2007**, *70* (3), 461-477.
111. (a) Klayman, D. L.; Lin, A. J.; Acton, N.; Scovill, J. P.; Hoch, J. M.; Milhous, W. K.; Theoharides, A. D.; Dobek, A. S., Isolation of artemisinin (qinghaosu) from *Artemisia annua* growing in the United States. *J. Nat. Prod.* **1984**, *47* (4), 715-717; (b) Brossi, A.; Venugopalan, B.; Dominguez Gerpe, L.; Yeh, H. J. C.; Flippen-Anderson, J. L.; Buchs, P.; Luo, X. D.; Milhous, W.; Peters, W., Arteether, a new antimalarial drug: synthesis and antimalarial properties. *J. Med. Chem.* **1988**, *31* (3), 645-650.
112. (a) Yoon, N. M., Selective reduction of organic compounds with aluminum and boron hydrides. *Pure Appl. Chem.* **1996**, *68* (4), 843-848; (b) Hudlicky, M., *Reductions in organic chemistry*. John Wiley & Sons: Chichester, 1984; (c) Conant, J. B.; Cutter, H. B., Irreversible reduction and catalytic hydrogenation. *J. Phys. Chem.* **1923**, *28* (10), 1096-1107.
113. (a) Lin, A. J.; Klayman, D. L.; Milhous, W. K., Antimalarial activity of new water-soluble dihydroartemisinin derivatives. *J. Med. Chem.* **1987**, *30* (11), 2147-2150; (b) Brossi, A.; Venugopalan, B.; Dominguez Gerpe, L.; Yeh, H. J. C.; Flippen-Anderson, J. L.; Buchs, P.; Luo, X. D.; Milhous, W.; Peters, W., Arteether, a new antimalarial drug: synthesis and antimalarial properties. *J. Med. Chem.* **1988**, *31* (3), 645-650; (c) Ferreira, J. F. S.; Janick, J., Immunoquantitative analysis of artemisinin from *Artemisia annua* using polyclonal antibodies. *Phytochemistry* **1996**, *41* (1), 97-104; (d) Sy, L.-K.; Hui, S.-M.; Cheung, K.-K.; Brown, G. D., A rearranged hydroperoxide from the reduction of artemisinin. *Tetrahedron* **1997**, *53* (22), 7493-7500; (e) Galal, A. M.; Gui, W.; Slade, D.; Ross, S. A.; Feng, S. X.; Hollingshead, M. G.; Alley, M. C.; Kaur, G.; ElSohly, A. A., Synthesis and evaluation of dihydroartemisinin and dihydroartemisitene acetal dimers showing anticancer and antiprotozoal activity. *Bioorg. Med. Chem.* **2009**, *17* (2), 741-751; (f) Jaziri, M.; Diallo, B.; Vanhaelena, M.; Homèsb, J.; K., Y.; Shimomura, K., Immunodetection of artemisinin in *Artemisia annua* cultivated in hydroponic conditions. *Phytochemistry* **1993**, *33* (4), 821-826; (g) The chemistry and synthesis of qinghaosu derivatives. China Cooperative Research Group on qinghaosu and its derivatives as antimalarials. *J. Tradit. Chin. Med.* **1982**, *2* (1), 9-16.
114. (a) Avery, M. A.; Mehrotra, S.; Johnson, T. L.; Bonk, J. D.; Vroman, J. A.; Miller, R., Structure-activity relationships of the antimalarial agent artemisinin .5. Analogs of 10-deoxoartemisinin substituted at C-3 and C-9. *J. Med. Chem.* **1996**, *39* (21), 4149-4155; (b) Avery, M. A.; Bonk, J. D.; Mehrotra, S., Deuterated antimalarials: Synthesis of trideutero-artemisinin, dihydroartemisinin, and arteether.

- J. Labelled Comp. Radiopharm.* **1996**, *38* (3), 249–254; (c) Posner, G. H.; Paik, I.-H.; Sur, S.; McRiner, A. J.; Borstnik, K.; Xie, S. J.; Shapiro, T. A., Orally active, antimalarial, anticancer, artemisinin-derived trioxane dimers with high stability and efficacy. *J. Med. Chem.* **2003**, *46* (6), 1060–1065.
115. Buzzi, S.; Presser, A.; Freyhold, M. v. *Determining a viable protocol for the derivatisation of artemisinin into dihydroartemisinin*; 2007.
116. (a) Lapkin, A.; Plucinski, P. K., Engineering factors for efficient flow processes in chemical industries. In *Chemical Reactions and Processes under Flow Conditions*, Luis, S. V.; Garcia-Verdugo, E., Eds. RSC: Cambridge, 2010; pp 1-43; (b) Bavykin, D. V.; Lapkin, A. A.; Kolaczowski, S. T.; Plucinski, P. K., Selective oxidation of alcohols in a continuous multifunctional reactor: ruthenium oxide catalysed oxidation of benzyl alcohol. *Appl. Catal. A: Gen.* **2005**, *288*, 165-174; (c) Fan, X.; Plucinski, P. K.; Lapkin, A. A., Liquid phase hydrogenation in a structured compact reactor. *Catal. Today* **2009**, *147S*, S313-S318.
117. Lin, A. J.; Klayman, D. L.; Milhous, W. K., Antimalarial activity of new water-soluble dihydroartemisinin derivatives. *J. Med. Chem.* **1987**, *30* (11), 2147-2150.
118. Bhakuni, R. S.; Jain, D. C.; Sharma, R. P., An improved procedure for the synthesis of ethers of dihydroartemisinin. *Indian J. Chem. Sect B-Org. Chem. Incl. Med. Chem.* **1995**, *34* (6), 529-530.
119. El-Ferally, F. S.; Al-Yahya, M. A.; Orabi, K. Y.; McPhail, D. R.; McPhail, A. T., A new method for the preparation of arteether and its C-9 epimer. *J. Nat. Prod.* **1992**, *55* (7), 878-883.
120. Boehm, M.; Fuenfschilling, P. C.; Krieger, M.; Kuesters, E.; Struber, F., An improved manufacturing process for the antimalaria drug coartem. Part I. *Org. Process Res. Dev.* **2007**, *11* (3), 336-340.
121. Bora, P. P.; Baruah, N.; Bez, G.; Barua, N. C., New method for the synthesis of ether derivatives of artemisinin. *Synth. Commun.* **2012**, *42*, 1218-1225.
122. Lin, A. J.; Miller, R. E., Antimalarial activity of new dihydroartemisinin derivatives. *J. Med. Chem.* **1995**, *38* (5), 764-770.
123. Wei, G.; Liao, X.; Huang, Z.; Cheng, J.; Y, H., Facial One-Pot Conversion and Characterisation of Dihydroartemisinin and Artemether. *J. Nat. Prod.* **2010**, *3*, 161-164.
124. (a) Mol, J. C., Application of olefin metathesis in oleochemistry: an example of green chemistry. *Green Chem.* **2002**, *4* (1), 5-13; (b) Ivin, K. J.; Mol, J. C., *Olefin metathesis and metathesis polymerization*. Academic Press: London, 1997; (c) Astruc, D., The metathesis reactions: from a historical perspective to recent developments. *New J. Chem.* **2005**, *29* (1), 42-56.
125. Banks, R. L.; Bailey, G. C., Olefin Disproportionation. A New Catalytic Process. *Ind. Eng. Chem. Prod. Res. Dev.* **1964**, *3* (3), 170-173.
126. (a) Soufflet, J. P.; Commereu, D.; Chauvin, Y., Catalysis of transformation of olefins by tungsten complexes - possible shape of intermediates. *Comptes Rendus Hebdomadaires Des Seances De L Academie Des Sciences Serie C* **1973**, *276* (2), 169-171; (b) Herisson, J. L.; Chauvin, Y., Transformation catalysis of olefins by tungsten complex, telomerization of cyclic olefins in presence of acyclic olefins. *Makromol. Chem.* **1971**, *141*, 161-176.
127. (a) Guggenberger, L. J.; Schrock, R. R., Tantalum carbyne complex. *J. Am. Chem. Soc.* **1975**, *97* (10), 2935-2935; (b) Wood, C. D.; McLain, S. J.; Schrock, R. R., Multiple metal-carbon bonds. 13. Preparation and characterization of monocyclopentadienyl mononeopentylidene complexes of niobium and tantalum

- including the first details of an  $\alpha$ -abstraction process. *J. Am. Chem. Soc.* **1979**, *101* (12), 3210-3222; (c) Schrock, R. R.; Messerle, L. W.; Wood, C. D.; Guggenberger, L. J., Multiple metal-carbon bonds. 9. Preparation and characterization of several alkylidene complexes,  $M(\eta^5-C_5H_5)_2(alkylidene)X$  ( $M = tantalum$  or  $niobium$ ), and the x-ray structure of  $Ta(\eta^5-C_5H_5)_2(ChC_6H_5)(CH_2C_6H_5)$ . An investigation of alkylidene ligand rotation. *J. Am. Chem. Soc.* **1978**, *100* (12), 3793-3800.
128. Tebbe, F. N.; Parshall, G. W.; Reddy, G. S., Olefin homologation with titanium methylene compounds. *J. Am. Chem. Soc.* **1978**, *100* (11), 3611-3613.
129. (a) Katz, T. J.; Lee, S. J.; Acton, N., Stereospecific polymerizations of cycloalkenes by a metal-carbene. *Tetrahedron Lett.* **1976**, (47), 4247-4250; (b) Kress, J.; Wesolek, M.; Osborn, J. A., Tungsten (IV) carbenes for the metathesis of olefins. Direct observation and identification of the chain carrying carbene complexes in a highly active catalyst system. *J. Chem. Soc. Chem. Commun.* **1982**, (9), 514-516; (c) Katz, T. J.; Sivavec, T. M., Metal-catalyzed rearrangement of alkene-alkynes and the stereochemistry of metallacyclobutene ring opening. *J. Am. Chem. Soc.* **1985**, *107* (3), 737-738; (d) Kress, J.; Agüero, A.; Osborn, J. A., Recent advances in the chemistry of tungsten—carbene complexes. *J. Mol. Catal.* **1986**, *36* (1-2), 1-12.
130. (a) Bielawski, C. W.; Grubbs, R. H., Living ring-opening metathesis polymerization. *Prog. Polym. Sci.* **2007**, *32* (1), 1-29; (b) Armstrong, S. K.; Susan, Ring closing diene metathesis in organic synthesis. *J. Chem. Soc.* **1998**, (2), 371-388; (c) Trnka, T. M.; Grubbs, R. H., The development of  $L_2X_2Ru=CHR$  olefin metathesis catalysts: an organometallic success story. *Acc. Chem. Res.* **2001**, *34* (1), 18-29.
131. (a) Michrowska, A.; Grela, K., Quest for the ideal olefin metathesis catalyst. *Pure Appl. Chem.* **2008**, *80* (1), 31-43; (b) Dias, E. L.; Nguyen, S. T.; Grubbs, R. H., Well-defined ruthenium olefin metathesis catalysts: mechanism and activity. *J. Am. Chem. Soc.* **1997**, *119* (17), 3887-3897.
132. Vougioukalakis, G. C.; Grubbs, R. H., Ruthenium-based heterocyclic carbene-coordinated olefin metathesis catalysts. *Chem. Rev.* **2009**, *110* (3), 1746-1787.
133. Choo, Y.-M.; Ooi, K.-E.; Ooi, I.-H.; Tan, D. H., Synthesis of a palm-based star-shaped hydrocarbon via oleate metathesis. *J. Am. Oil Chem. Soc.* **1996**, *73* (3), 333-336.
134. Bosma, R. H. A.; Van Den Aardweg, G. C. N.; Mol, J. C., Heterogeneous metathesis of unsaturated esters using a rhenium-based catalyst. *J. Organomet. Chem.* **1983**, *255* (2), 159-171.
135. (a) Boeda, F.; Clavier, H.; Nolan, S. P., Ruthenium-indenylidene complexes: powerful tools for metathesis transformations. *Chem. Comm.* **2008**, *24*, 2726-2740; (b) Sibeijn, M.; Mol, J. C., Ethenolysis of methyl oleate over supported Re-based catalysts. *J. Mol. Catal.* **1992**, *76* (1-3), 345-358; (c) Bosma, R. H. A.; van den Aardweg, F.; Mol, J. C., Comethesis of methyl oleate and ethylene; a direct route to methyl dec-9-enoate. *J. Chem. Soc., Chem. Commun.* **1981**, (21), 1132-1133.
136. Forman, G. S.; Bellabarba, R. M.; Tooze, R. P.; Slawin, A. M. Z.; Karch, R.; Winde, R., Metathesis of renewable unsaturated fatty acid esters catalysed by a phoban-indenylidene ruthenium catalyst. *J. Organomet. Chem.* **2006**, *691* (24-25), 5513-5516.
137. Mol, J. C., Industrial applications of olefin metathesis. *J. Mol. Catal. A: Chem.* **2004**, *213* (1), 39-45.

138. Freitas, E. R.; Gum, C. R., Shell higher olefin process. *Chem. Eng. Prog.* **1979**, *75*, 73-76.
139. Holser, R.; Doll, K.; Erhan, S., Metathesis of methyl soyate with ruthenium catalyts. *Fuel* **2006**, *85* (3), 393-395.
140. Nuyken, O.; Pask, S. D., Ring-opening polymerization - An introductory review. *Polymers* **2013**, *5* (2), 361-403.
141. (a) Bingöl, B.; Kroeger, A.; Jannasch, P., Well-defined phosphonated homo- and copolymers *via* direct ring opening metathesis polymerization. *Polymer* **2013**, *54* (25), 6676-6688; (b) Mariconda, A.; Grisi, F.; Granito, A.; Longo, P., Stereoselective ring-opening metathesis polymerization of 7-*tert*-butoxy-bicyclo[2,2,1]hepta-2,5-diene by NHC-ruthenium catalysts. *Macromol. Chem. Phys.* **2013**, *214* (17), 1973-1979; (c) Kalluru, S. H.; Cochran, E. W., Synthesis of polyolefin/layered silicate nanocomposites *via* surface-initiated ring-opening metathesis polymerization. *Macromolecules* **2013**, *46* (23), 9324-9332.
142. (a) Mutlu, H.; de Espinosa, L. M.; Meier, M. A. R., Acyclic diene metathesis: a versatile tool for the construction of defined polymer architectures. *Chemical Society Reviews* **2011**, *40*, 1404-1445; (b) Wagener, K. B.; Boncella, J. M.; Nel, J. G., Acyclic diene metathesis (ADMET) polymerization. *Macromolecules* **1991**, *24* (10), 2649-2657.
143. (a) Sydlik, S. A.; Delgado, P. A.; Inomata, S.; VanVeller, B.; Yang, Y.; Swager, T. M.; Wagener, K. B., Triptycene-containing polyetherolefins *via* acyclic diene metathesis polymerization. *J. Polym. Sci., Part A: Polym. Chem.* **2013**, *51* (8), 1695-1706; (b) Xie, M. R.; Han, H. J.; Jin, O. Y.; Du, C. X., Synthesis of ionic hybrid polymers with polyhedral oligomeric silsesquioxane pendant by acyclic diene metathesis polymerization and characterization. *Acta Chim. Sinica* **2013**, *71* (10), 1441-1445; (c) Abdellatif, M. M.; Nomura, K., Precise synthesis of mmphiphilic multiblock copolymers by combination of acyclic diene metathesis (ADMET) polymerization with atom transfer radical polymerization (ATRP) and click chemistry. *ACS Macro Letters* **2012**, *1* (3), 423-427.
144. (a) Rybak, A.; Meier, M., Acyclic diene metathesis with a monomer from renewable resources: control of molecular weight and one-step preparation of block copolymers. *ChemSusChem* **2008**, *1* (6), 542-547; (b) Biermann, U.; Metzger, J. O.; Meier, M. A. R., Acyclic triene metathesis oligo- and polymerization of high oleic sun flower oil. *Macromol. Chem. Phys.* **2010**, *211* (8), 854-862.
145. Nordin, N. A. M.; Yamin, B. M.; Yarmo, M. A.; Pardan, K.; Alimuniar, A. B., Metathesis of palm oil. *J. Mol. Catal.* **1991**, *65*, 163-172.
146. Hellbardt, S.; Patzschke, H. P., Ullmann's encyclopedia of industrial chemistry. 5th, Ed. 1987; p 55.
147. (a) Boelhouwer, C.; Mol, J. C., Metathesis reaction of fatty-acid esters. *Prog. Lipid Res.* **1985**, *24* (3), 243-267; (b) Van Dam, P.; Mittelmeijer, M.; Boelhouwer, C., Homogeneous catalytic metathesis of unsaturated fatty esters: New synthetic method for preparation of unsaturated mono- and dicarboxylic acids. *J. Am. Oil Chem. Soc.* **1974**, *51*, 389-392.
148. Erhan, S. Z.; Bagby, M. O.; Nelsen, T. C., Drying properties of metathesized soybean oil. *J. Am. Oil Chem. Soc.* **1997**, *74* (6), 703-706.
149. Refvik, M. D.; Larock, R. C.; Tian, Q., Ruthenium-catalyzed metathesis of vegetable oils. *J. Am. Oil Chem. Soc.* **1999**, *76*, 93-98.
150. Borja, G.; Pleixats, R.; Alibes, R.; Cattoen, X.; Man, M. W. C., Organic-inorganic hybrid silica material derived from a monosilylated Grubbs-Hoveyda

- ruthenium carbene as a recyclable metathesis catalyst. *Molecules* **2010**, *15*, 5756-5767.
151. *Software for drop shape analysis*. Kruss GmbH: 2004-2009.
152. Bresson, S.; Rousseau, D.; Ghosh, S.; El Marssi, M.; Faivre, V., Raman spectroscopy of the polymorphic forms and liquid state of cocoa butter. *Eur. J. Lipid Sci. Technol.* **2011**, *113* (8), 992-1004.
153. (a) Williams, D. H.; Fleming, I., *Spectroscopic methods in organic chemistry*. McGraw-Hill Higher Education: 2008; (b) Lambert, J. B.; Shurvell, H. F.; Lightner, D. A.; Cooks, R. G., *Organic structural spectroscopy*. Prentice-Hall, Inc.: New Jersey, 1998; p 568; (c) Bresson, S.; Rousseau, D.; Ghosh, S.; Marssi, M. E.; Faivre, V., Raman spectroscopy of the polymorphic forms and liquid state of cocoa butter. *Eur. J. Lipid Sci. Technol.* **2011**, *113* (8), 992-1004.
154. Barison, A.; Pereira da Silva, C. W.; Campos, F. R.; Simonelli, F.; Lenz, C. A.; Ferreira, A. G., A simple methodology for the determination of fatty acid composition in edible oils through <sup>1</sup>H NMR spectroscopy. *Magn. Reson. Chem.* **2010**, *48* (8), 642-650.
155. *AOCS. Official Methods Ce 1-62*. American Oil Chemists' Society: IL, USA.
156. Lipp, M.; Anklam, E., Review of cocoa butter and alternative fats for use in chocolate - Part A. Compositional data. *Food Chem.* **1998**, *62* (1), 73-97.
157. *CPA202 reaction calorimeter system. Measuring the truth in chemical processes is our obsession.* **2004**.
158. Buzzi, S.; Presser, A.; Freyhold, M. *Determining a viable protocol for the derivatisation of artemisinin into dihydroartemisinin.* available from [www.mmv.org](http://www.mmv.org); 2007.
159. (a) Banta-Wright, S. A.; Steiner, R. D., Tandem mass spectrometry in newborn screening. *J. Perinat. Neonatal. Nurs.* **2004**, *18* (1), 41-58; (b) Starks, C. M.; Liotta, C. L., *Phase Transfer Catalysis, Principles and Techniques*. Academic Press: New York, 1978.
160. Fan, X.; Sans, V.; Yaseneva, P.; Plaza, D. D.; Williams, J.; Lapkin, A., Facile stoichiometric reductions in flow: An example of ertemisinin. *Org. Process Res. Dev.* **2012**, *16* (5), 1039-1042.
161. *Umberto Manual Version 5. ifu Institut fur Umweltinformatik.* ifeu Institut fur Energie- und Umweltforschung, Heidelberg: Hamburg, Germany, 2011.
162. Guinee, J. B. Life Cycle Assessment - An Operational Guideline to the ISO standards - Parts 1-3, Ministry of Housing, Spatial Planning and the Environment and the Center Of Environmental Science. 2001.
163. *Cumulative Energy Demand - Terms, Definitions, Methods of Calculation. VDI Guideline 4600.* Dusseldorf, Germany, 1999.
164. Frischknecht, R.; Jungbluth, N.; Althaus, H. J.; Doka, G.; Heck, T.; Hellweg, S.; Hischier, R.; Nemecek, T.; Rebitzer, G.; Spielmann, M.; Wernet, G., *Overview and methodology. Ecoinvent report No. 1.* . Swiss Centre for Life Cycle Inventories: Dübendorf, 2007.
165. Kreutzer, M. T.; Kapteijn, F.; Moulijn, J. A.; Kleijn, C. R.; Heiszwolf, J. J., Inertial and interfacial effects on pressure drop of Taylor flow in capillaries. *Aiche J.* **2005**, *51* (9), 2428-2440.
166. (a) Ruiz, M. C.; Lermada, P.; Padilla, R., Drop size distribution in a batch mixer under breakage conditions. *Hydrometallurgy* **2002**, *63* (1), 65-74; (b) Mlynek, Y.; Resnick, W., Drop sizes in an agitated liquid-liquid system. *Aiche J.* **1972**, *18* (1), 122-&; (c) Pacek, A. W.; Chamsart, S.; Nienow, A. W.; Bakker, A., The influence of impeller type on mean drop size and drop size distribution in an agitated

- vessel. *Chem. Eng. Sci.* **1999**, *54* (19), 4211-4222; (d) Laso, M.; Steiner, L.; Hartland, S., Dynamic simulation of liquid-liquid agitated dispersions. 1. Derivatation of a simplified model. *Chem. Eng. Sci.* **1987**, *42* (10), 2429-2436; (e) Zhou, G. W.; Kresta, S. M., Correlation of mean drop size and minimum drop size with the turbulence energy dissipation and the flow in an agitated tank. *Chem. Eng. Sci.* **1998**, *53* (11), 2063-2079.
167. Ehrfeld, W.; Hessel, V.; Lowe, H., *Microreactors: New technology for modern chemistry*. Wiley-VCH: Germany, 2000.
168. Perry, R. H.; Green, D. W., *Perry's chemical engineers handbook*. McGraw-Hill: New York, 1997.
169. Fogler, H. S., *Elements Of chemical reaction engineering*. Prentice Hall Professional Technical Reference: 2006.
170. Williams, D. F., I., *Spectroscopic methods in organic chemistry*. McGraw-Hill Education Ltd.: New York, 2008; p 27-48.
171. Darby, R., *Chemical Engineering Fluid Mechanics*. 2 ed.; CRC Press: 2001.
172. Ruhland, T. M.; Groschel, A. H.; Ballard, N.; Skelhon, T. S.; Walther, A.; Muller, A. H. E.; Bon, S. A. F., Influence of Janus Particle Shape on Their Interfacial Behavior at Liquid-Liquid Interfaces. *Langmuir* **2013**, *29* (5), 1388-1394.
173. Sinnott, R. K.; Towler, G., *Chemical Engineering Design: SI edition*. Elsevier Science: 2009.
174. Bocanegra, R.; Gaonkar, A. G.; Barrero, A.; Loscertales, I. G.; Pechack, D.; Marquez, M., Production of cocoa butter microcapsules using an electrospray process. *J. Food Sci.* **2005**, *70* (8), E492-E497.
175. Sinnott, R.; Towler, G., *Chemical Engineering Design*. Butterworth-Heinemann Ltd: 2009; p 1038.
176. [www.surface-tension.de/t](http://www.surface-tension.de/t).
177. Phibbs, M. K.; Giguere, P. A., Hydrogen peroxide and its analogues. I. Density, refractive index, viscosity, and surface tension of deuterium peroxide-deuterium oxide solutions. *Can. J. Chem.* **1951**, *29* (2), 173-183.
178. Vargaftik, N. B.; Volkov, B. N.; Voljak, L. D., International Tables of the Surface-Tension of Water. *J. Phys. Chem. Ref. Data* **1983**, *12* (3), 817-820.
179. Reid, R. C.; Prausnitz, J. M.; Poling, B. E., Diffusion Coefficient. In *The Properties of Gases and Liquids*, Fourth ed.; McGraw-Hill, Inc: 1987; pp 577-626.
180. Reid, R. C.; Prausnitz, J. M.; Poling, B. E., Pressure Volume Temperature Relations of Pure Gases and Liquids. In *The Properties of Gases and Liquids*, McGraw-Hill, Inc.: 1987; Vol. Fourth, pp 53-55
181. Bercic, G.; Pintar, A., The role of gas bubbles and liquid slug lengths on mass transport in the Taylor flow through capillaries. *Chem. Eng. Sci.* **1997**, *52* (21-22), 3709-3719.
182. Bercic, G., Influence of operating conditions on the observed reaction rate in the single channel monolith reactor. *Catal. Today* **2001**, *69* (1-4), 147-152.
183. Cybulski, A.; Edvinsson, R.; Irandoust, S.; Andersson, B., Liquid-phase methanol synthesis - modeling of a monolithic reactor. *Chem. Eng. Sci.* **1993**, *48* (20), 3463-3478.
184. Burns, J. R.; Ramshaw, C., The intensification of rapid reactions in multiphase systems using slug flow in capillaries. *Lab. Chip.* **2001**, *1* (1), 10-15.
185. Waelchli, S.; von Rohr, P. R., Two-phase flow characteristics in gas-liquid microreactors. *Int. J. Multiph. Flow* **2006**, *32* (7), 791-806.

186. Fichtner, M.; Mayer, J.; Wolf, D.; Schubert, A., Microstructured rhodium catalysts for the partial oxidation of methane to syngas under pressure. *Ind. Eng. Chem. Res.* **2001**, *40* (16), 3475-3483.
187. Jin, H. X.; Liu, H. H.; Zhang, Q.; Wu, Y. K., On the susceptibility of organic peroxy bonds to hydride reduction. *J. Org. Chem.* **2005**, *70* (11), 4240-4247.
188. (a) Haynes, R. K.; Chan, H.-W.; Cheung, M.-K.; Chung, S. T.; Lam, W.-L.; Tsang, H.-W.; Voerste, A.; Williams, I. D., Stereoselective preparation of 10 $\alpha$ - and 10 $\beta$ -aryl derivatives of dihydroartemisinin. *Eur. J. Org. Chem.* **2003**, (11), 2098-2114; (b) Boehm, M.; Fuenfschilling, P. C.; Krieger, M.; Kuesters, E.; Struber, F., An improved manufacturing process for the antimalaria drug coartem. Part I. *Org. Proc. Res. Dev.* **2007**, *11* (3), 336-340.
189. Anastas, P. T.; Warner, J. C., *Green chemistry: Theory and practice*. Oxford University Press: Oxford, 1998.
190. Aycocock, D. F., Solvent applications of 2-methyltetrahydrofuran in organometallic and biphasic reactions. *Org. Proc. Res. Dev.* **2007**, *11* (1), 156-159.
191. Trost, B. M., Atom economy - A challenge for organic synthesis: Homogeneous catalysis leads the way. *Angewandte Chemie-International* **1995**, *34* (3), 259-281.
192. WHO (World Health Organisation). Quality requirements for artemisinin as a starting material in the production of antimalarial active pharmaceutical ingredients (APIs). Geneva, Switzerland. **2011**.
193. Suberu, J. O.; Goraka, A. P.; Jacobs, L.; Roepe, P. D.; Sullivan, N.; Barker, G. C.; Lapkin, A. A., Anti-plasmodial polyvalent interactions in *Artemisia annua* L. aqueous extract <sup>13</sup>C possible synergistic and resistance mechanisms. *PLOS ONE* **2013**, *8* (11).
194. Stringham, R. W.; Teager, D. S., Streamlined process for the conversion of artemisinin to artemether. *Org. Proc. Res. Dev.* **2012**, *16*, 764-768.
195. Pinnau, I.; Toy, L. G., Gas and vapor transport properties of amorphous perfluorinated copolymer membranes based on 2,2-bis(trifluoromethyl)-4,5-difluoro-1,3-dioxole/tetrafluoroethylene. *J. Membr. Sci.* **1996**, *109* (1), 125-133.
196. Resnick, P. R.; Buck, W. H., Teflon AF amorphous fluoropolymers. In *Modern Fluoropolymers*, 1997; pp 397-419.
197. Yang, L.; Jensen, K. F., Mass transport and reactions in the Tube-in-Tube reactor. *Org. Process Res. Dev.* **2013**, *17* (6), 927-933.
198. (a) Wilson, B.; Sherrington, D. C.; Ni, X., Butylation of phenylacetonitrile in an oscillatory baffled reactor. *Ind. Eng. Chem. Res.* **2005**, *44* (23), 8663-8670; (b) Wilson, B.; Ni, X.; Sherrington, D. C., On the investigation of a phase-transfer catalysis reaction in an oscillatory baffled reactor. *Ind. Eng. Chem. Res.* **2001**, *40* (23), 5300-5304.
199. Knauer GmbH, H., *Knauer pump 100 manual*. Wissenschaftliche Gerätebau: Berlin, Germany, 2011.
200. Sigma Aldrich, <http://www.sigmaaldrich.com/spectra/fnmr/FNMR000803.PDF>.